5-2014

COMPETITION BETWEEN GRB2 AND PLCγ1 FOR BINDING TO FGFR2 REGULATES PHOSPHOLIPASE AND PTEN ACTIVITY, LEADING TO CELL INVASION AND PROLIFERATION

zahra timsah

COMPETITION BETWEEN GRB2 AND PLCγ1 FOR BINDING TO FGFR2 REGULATES PHOSPHOLIPASE AND PTEN ACTIVITY, LEADING TO CELL INVASION AND PROLIFERATION

A

DISSERTATION

Presented to the Faculty of

The University of Texas Health Science Center at Houston

and

The University of Texas M. D. Anderson Cancer Center

Graduate School of Biomedical Sciences

In Partial Fulfillment the Requirements for

The Degree of

DOCTOR OF PHILOSOPHY

by

Zahra Timsah, B.S., M.S.

Houston, Texas

May 2014

COMPETITION BETWEEN GRB2 AND PLCγ1 FOR BINDING TO FGFR2 REGULATES PHOSPHOLIPASE AND PTEN ACTIVITY, LEADING TO CELL INVASION AND PROLIFERATION

By

Zahra Timsah, B.S., M.S.

APPROVED:

_____
John E. Ladbury, Ph.D. Supervisory Professor

_____
Gary E. Gallick, Ph.D.

_____
John F. Hancock, M.B., B.Chir.,Ph.D.

_____
Elsa R. Flores, Ph.D.

_____
Jeffrey A. Frost, Ph.D.

APPROVED:

_____
Dean, The University of Texas
Graduate School of Biomedical Sciences at Houston

Dedication

This work is dedicated to my mother for being there for me every step of the way supporting my goals lovingly and never doubting my choices. I also dedicate it to Sahar…my best friend, my rock and my inspiration. I cannot wait for “Emilia” to become one of the best selling novels of all time.

Both of you have taught me that ambition knows no boundaries and no obstacles and here I am dreaming big and committing to making every dream come true. Having you in my life is a true blessing.

I also want to thank my siblings Abeer, Jihan, Ali, and Hussain for surrounding me with this much care and love. Being the youngest in such a big family certainly has its perks!

Last but not least, I would like to dedicate it to the loving memory of my father who was a great man with great stories. I wish we had had more time together.

As for my “Poova”, you will always be remembered as the wonderful creature that you truly were. You always knew how to put a smile on my face.

Acknowledgements

One of the thrills of completion is to look over the journey past and remember those who have helped me along this long yet fulfilling road. I would like to express my earnest gratitude to Professor John E. Ladbury whom I consider to be not just my mentor but also a dear friend. I could not have asked for a better role model who is both patient and supportive. I am proud of my academic roots and will do my very best in turn to pass on the research values that he has given to me. I can honestly say that I enjoyed every second I spent in his lab doing what I love and loving what I do.

I would also like to thank my committee members, Professor Gary E. Gallick Professor John F. Hancock, Associate Professor Jeffrey Frost, and Associate Professor Elsa R. Flores who provided encouraging and constructive comments. Reviewing a thesis is not an easy task and I am appreciative of their thoughtful and detailed comments. Also, many thanks to Dr. Mikhail Bogdanov for helping to shape and guide the direction of my work. He has taught me so many techniques and provided me with instructive feedback that pushed me to think outside the box.

Last but not least, I have been surrounded by brilliant lab-mates from whom I learnt a lot. It was and will continue to be an exciting adventure being a member of the “Ladbury Group”.

COMPETITION BETWEEN GRB2 AND PLCγ1 FOR BINDING TO FGFR2 REGULATES PHOSPHOLIPASE AND PTEN ACTIVITY, LEADING TO CELL INVASION AND PROLIFERATION

By Zahra Timsah, Ph.D.

Supervisory Professor: John E. Ladbury, Ph.D.

Fluctuations in the relative concentrations of proteins in non-stimulated cells can lead to aberrant signaling. In a novel interaction, the SH3 domain of Plcγ1 competes with the SH3 domain of Grb2 for binding to FGFR2 in a concentration-dependent manner. Consequently, reduction of cellular concentrations of Grb2 lead to receptor-dependent recruitment of unphosphorylated Plcγ1. Bringing of the phospholipase to the membrane in this way upregulates its activity, resulting in increased PIP_2 turnover to IP_3 and DAG resulting in elevated cellular calcium levels. These signaling events increase cell migration and invasion. A further consequence of the depletion of PIP_2 is the inhibition of PTEN phosphatase activity. Inhibition of PTEN activity leads to the accumulation of PIP_3, which recruits Akt leading to its phosphorylation and activation. Therefore, depletion of Grb2 indirectly leads to activation of the proto-oncogene Akt inducing phenotypic alterations characteristic of tumorigenesis including anchorage-independent cell growth and tumor formation in mice models.

Table of Contents

List of Tables

List of Figures

Chapter One: Introduction

FGFR signaling and its role in cancer

Fibroblast growth factor (FGF) signaling mediates and controls many physiological functions. The FGF family is composed of 18 different ligands that act through 4 conserved receptor tyrosine kinases (RTKs): fibroblast growth factor receptor (FGFR) 1, FGFR2, FGFR3, and FGFR4 (**Fig 1.1**). A fifth receptor, FGFR5, is known to negatively regulate signaling even though it lacks a tyrosine kinase (TK) domain. FGFs are secreted glycoproteins that are sequestered via heparan-sulfate proteoglycans (HPSGs) to the extracellular matrix or cell surface. Heparinases, FGF binding proteins, and proteases release FGFs allowing them to bind to HPSGs (**Fig 1.1**)**.** The specificity of the ligand-receptor interaction is mediated by FGFR alternative splicing and tissue specific expression of both FGFs and FGFRs (1).

FGFRs rely on ligand-dependent dimerization (1) or protein-dependent dimerization, as is the case for FGFR2 (2). Dimerization causes a conformational change that activates the intracellular kinase domain, resulting in the trans-phosphorylation of the intracellular tail and TK domains. Phosphorylated tyrosine residues on the receptor provide binding sites for downstream effectors allowing for a cascade of downstream signals to occur, ultimately influencing mitogenesis and differentiation (1).

In the absence of extracellular stimulation, FGFR2 binds to the C-terminal Src Homology 3 (SH3) domain of growth factor receptor-bound protein 2 (Grb2) (2,3). The Grb2 dimer recruits two molecules of FGFR2 to form a

heterotetramer. In this state 'background' receptor kinase activity is limited to the phosphorylation of tyrosine residues (Y) 653 and 654 in the activation loop of FGFR2. Furthermore, the receptor is unable to recruit downstream effector proteins or initiate signal transduction. Upon extracellular growth factor stimulation, FGFR2 dimerization is stabilized, leading to the upregulation of autophosphorylation. Full activation of the receptor induces phosphorylation of Grb2 on Y209. This results in the release of Grb2, thus allowing other downstream proteins to be recruited to FGFR2 (**Fig 1.2**).

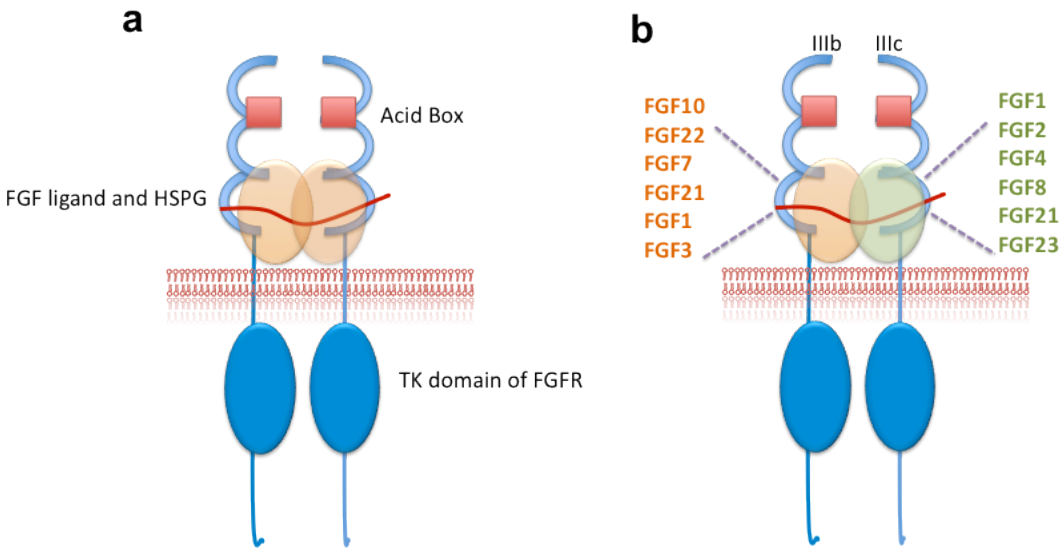

Fig 1.1 FGFR structure and control of ligand specificity. a) The structure of the FGFR complex comprises two receptor molecules, two FGFs, and one HSPG chain. FGFs bind to cell surface HSPGs with low affinity and to FGFRs with high affinity. FGFRs are composed of three extracellular immunoglobulin (Ig) domains, a single transmembrane helix, and an intracellular split tyrosine kinase (TK) domain. The second and third Ig domains form the ligand-binding pocket and have distinct domains that bind both FGFs and HSPGs. Ligand-binding specificity is generated by alternative splicing of the Ig III domain. The first half of Ig III is encoded by an invariant exon (IIIa), which is spliced to either exon IIIb or IIIc.**b**) FGFR2-IIIb and FGFR2-IIIc ligands are shown in orange and green, respectively.

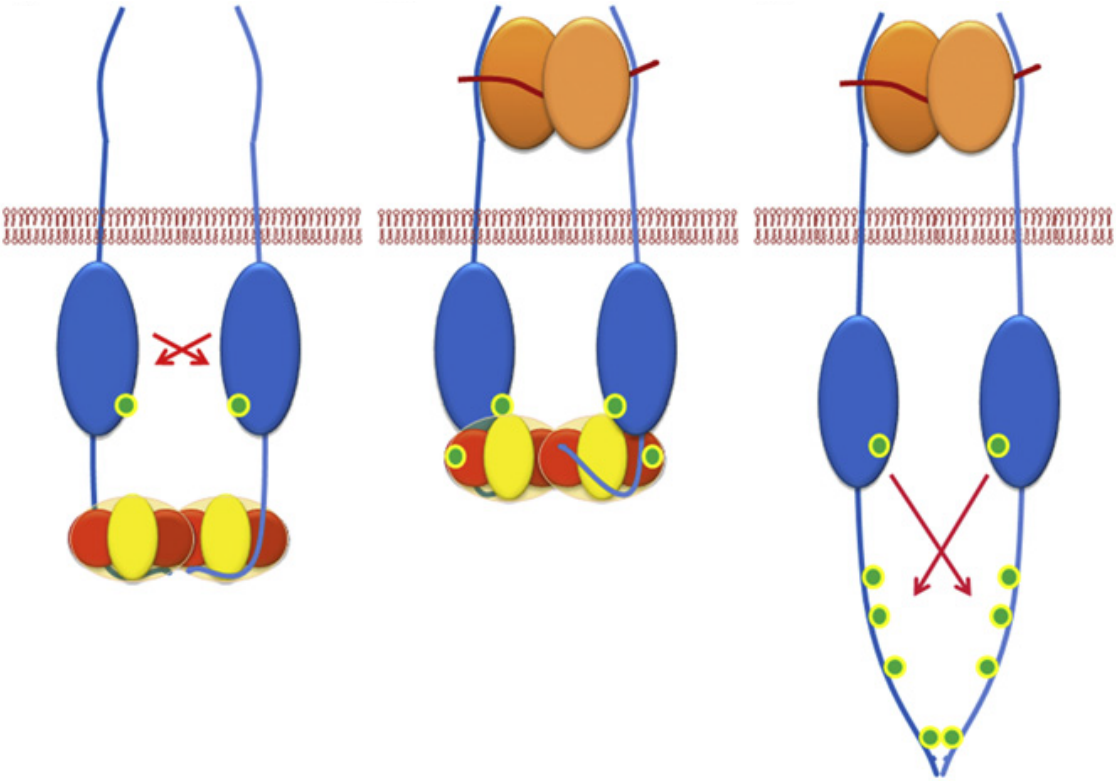

Fig 1.2 Model of the molecular mechanism of Grb2-mediated activation of FGFR2. Dimeric Grb2 (SH3 domains—red; SH2 domain—yellow) is bound via its C-SH3 domain to the C-terminal region of FGFR2 (blue), resulting in the formation of a 2:2 heterotetramer and receptor predimerization. The kinase domains of FGFR2 (blue ovals) permit the phosphorylation of Y653 and Y654. The binding of FGF (orange) and HSPG (red line) to FGFR2 induces a conformational change that results in Grb2 phosphorylation by the FGFR2 kinase domain. Phosphorylated Grb2 is released from the receptor. FGFR2 kinase domains become fully activated and transphosphorylate tyrosine residues formerly buried in the Grb2-receptor interface (adapted from Lin *et al*., 2012 with permission from *Cell*).

In addition to Grb2, many other adaptor proteins bind to FGFRs. For example, fibroblast growth factor receptor substrate 2 (FRS2) binds to the juxtamembrane region of FGFRs through its phosphotyrosine binding (PTB) domains. Phosphorylated FRS2 can recruit son of sevenless (SOS) and in turn activate the mitogen activated protein kinase (MAPK) pathway. FGFRs can directly or indirectly (via adaptor proteins) activate four pathways: rat sarcoma (RAS)/ rapidly accelerated fibrosarcoma (RAF)/MAPK, phosphatidylinositide 3-kinase (PI3K)/-AKR mouse T-cell lymphoma protein (Akt; protein kinase B), signal transducer and activator of transcription (STAT), and phospholipase Cγ1 (Plcγ1) (1).

The significance of FGFR signaling in tumorigenesis was shown by a screen of 1000 somatic mutations in the coding exons of 518 protein kinase genes in 210 cancers (4). For example, bladder cancer has a well-established link to *FGFR* mutations. *FGFR2* mutations, which are usually extracellular and equal to the activating germline mutations found in craniosynostosis syndromes, have been found in 12% of endometrial carcinomas (5). Endometrial cancer-derived cell lines are sensitive to FGFR tyrosine inhibitors,which reflects oncogenic addiction to mutant-activated FGFR.

Protein recruitment to activated FGFR2 usually occurs via the C-terminal region of the receptor. C-terminal sequence splicing leads to the derivation of a major group of isoforms. One should note that perturbation of the amino acid sequence in this region might have pathogenic and tumorigenic outcomes. For example, point mutations in the C-terminal region of FGFR2 have been linked

to melanoma (6), and deletions of the C-terminal sequence, which are found in a majority of human breast carcinoma cells, have enhanced transforming activity (7,8). Deletions in the FGFR2 C-terminal sequence are also found in bladder, stomach, and gastric cancers (9-12).

Grb2: Function and importance

Grb2 is a ubiquitously expressed adaptor protein that is generally considered to play a passive role in RTK signaling because it does not possess intrinsic enzymatic activity. Grb2 consists of a Src Homology 2 (SH2) domain sandwiched between N and C-terminal SH3 domains (**Fig 1.3**). The SH2 domain binds phosphorylated tyrosine residues on docking proteins or receptors. The N and C-terminal SH3 domains recognize proline-rich sites on proteins, such as SOS (13), or receptors, such as FGFR2 (2).

Grb2 is critical for the regulation of mitogen-independent FGFR2 heterotetramer formation (2) and inhibits tyrosine-protein phosphatase non-receptor type 11 (PTPN11 or Shp2)-mediated FGFR2 activation loop tyrosine dephosphorylation (3). Thus, evidence indicates that Grb2 is not a passive adaptor protein but rather a fundamental positive and negative regulator of FGFR2 phosphorylation and downstream signal transduction (3).

Fig 1.3 Grb2 domains. Grb2 consists of one phosphotyrosine (pY)-binding SH2 domain sandwiched between two proline rich motif-binding SH3 domains.

Plcγ1: Function and importance

Mitogen-induced stimulation of various cell surface receptors activates the cytoplasmic lipase phospholipase C gamma **(**Plcγ). The two Plcγ isoforms 1 and 2 act downstream of receptors with and without intrinsic TK activity. The Plcγs are unique amongst the phospholipases in having the split phospholipase domain separated by functional domains. The catalytic domain of phospholipases is composed of X and Y boxes, which are two sequentially discrete regions separated by an extended linker region (X/Y linker).The X/Y linker includes sequentially a split PH domain, two SH2 domains (NSH2 and CSH2, respectively) and an SH3 domain (**Fig 1.4**). Activated Plcγ1 hydrolyzes the membrane lipid phosphatidylinositol 4,5-bisphosphate (PI[4,5]P_2 or PIP_2) to form inositol 1,4,5-trisphosphate (IP_3) and diacylglycerol (DAG). IP_3 mediates Ca^{2+} mobilization, whereas DAG activates protein kinase C (PKC) signaling.

Plcγ1 activation requires membrane translocation. Plcγ1 is phosphorylated on four main tyrosines: 472, 771, 783, and 1254. Phosphorylation on Y783 has been reported to be required for Plcγ1activation.

Fig 1.4 Plcγ1 domains. Schematic illustration of the sequence of Plcγ1 domains. PH: pleckstrin homology domain. EF: EF-hand calcium-binding domain. X and Y: catalytic domains. P and H: split PH domain. NSH2 and CSH2: N-terminal and C-terminal Src homology 2 domains. SH3: Src homology-3 domain. C2: protein kinase C conserved region 2 domain.SH2 (yellow) and SH3 (red) domains shown as circles.

Plcγ1 phosphorylation on Y1254 was shown to be required for maximal growth factor-induced stimulation, whereas phosphorylation on Y771 was proposed to act as a negative regulator. Some studies have also shown that phosphorylation of both Y775 and Y783 play equally important roles in Plcγ1activation (14).

Other studies and as shown in **Fig 1.5** reported that the catalytic domain of this lipase is inhibited by its CSH2 domain. Upon stimulation, NSH2 domain binds to the receptor leading to receptor-mediated Plcγ1 phosphorylation on Y783. This consequently induces a conformational rearrangement that releases the autoinhibition of the enzymatic activity(15).

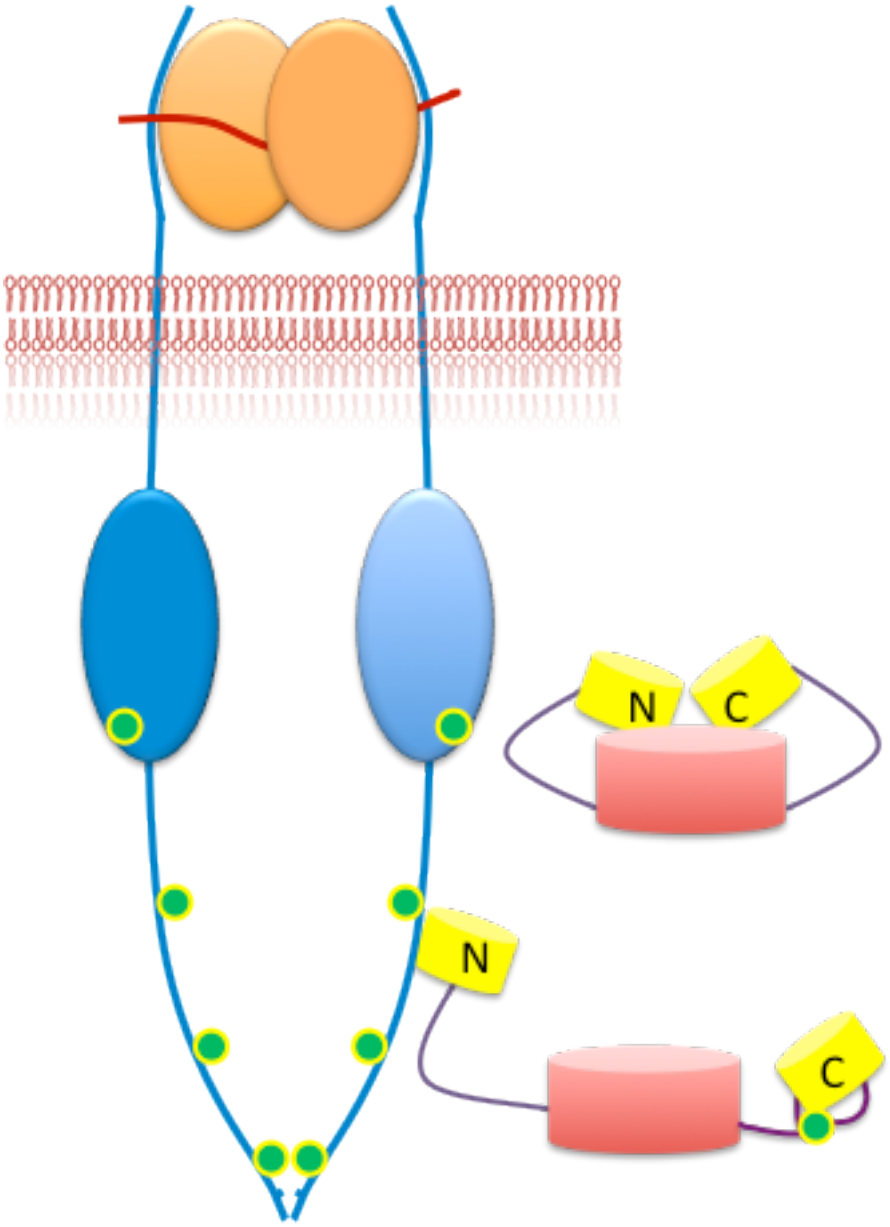

Fig 1.5 Mechanism for phosphorylation-dependent Plcγ1 activation. *In the non-stimulated state, the catalytic domain (*red cylinder*) of Plcγ1 is auto-inhibited by the CSH2 domain (*yellow cylinder*). Receptor activation provides a pY (*green dot*) docking site for the NSH2 domain (*yellow cylinder*) of the lipase, resulting in its translocation to the plasma membrane for site-specific tyrosine phosphorylation by RTKs. Tyrosine phosphorylation of Plcγ1 induces direct interactions with the CSH2 domain. Engagement of the CSH2 domain by phosphorylated tyrosine induces structural rearrangements of the CSH2 domain with respect to the catalytic domain, leading to the release of auto-inhibition.*

Plcγ1 has many important functions in the intracellular transduction of receptor-mediated tyrosine kinase activators. It is also considered to be critical in mediating metastasis. Tumor metastasis is the ability of cancer cells to spread from a primary site and form tumors at distant sites. It is a multistep process that involves local invasion, followed by intravasation and survival, extravasation, initiation, and maintenance of micrometastases at distant sites, and vascularization of resultant tumors (16) (**Fig 1.6**). Cell motility and invasion play an indispensable role in metastasis; therefore, identification of involved proteins and characterization of the underlying mechanisms regulating cell motility are essential to understanding metastasis development.

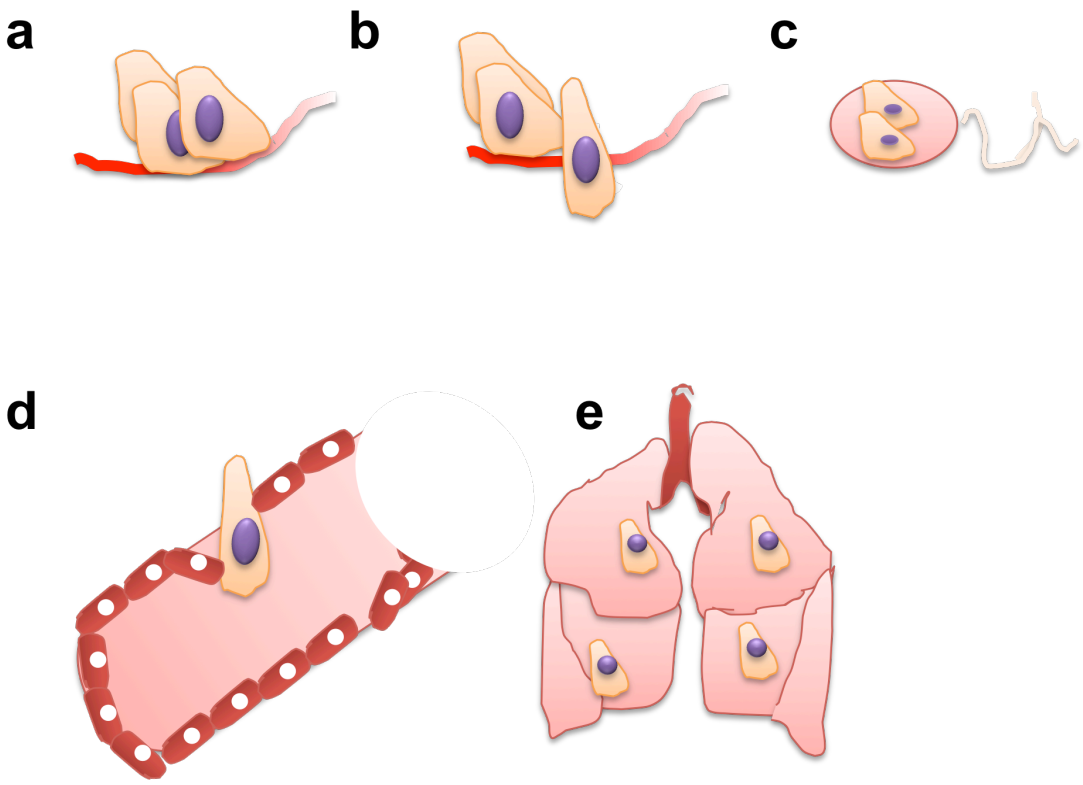

Fig 1.6 A schematic of the metastatic process a) An *in situ* cancer surrounded by an intact basement membrane. **b**) Invasion requires changes in cell–cell and cell–extracellular matrix adherence, destruction of proteins in the matrix and stroma, and motility. Metastasizing cells enter distant tissues by means of **c**) the lymphatics (pink oval) **d**) the circulation (red ovals represent endothelial cells). **e**) This is followed by survival and arrest of tumor cells and extravasation from the circulatory system. Metastatic colonization (here in the lungs) occurs through single cells, which can develop into angiogenic metastases.

Directed cell migration is regulated by growth factors and chemokines that bind and activate specific receptors, such as RTKs, which activate cytoskeleton rearrangement and cellular motility via a network of signaling pathways. Activated Plcγ1 plays a decisive role in both cytoskeletal changes and migratory ability associated with the metastatic process. Plcγ1 is highly expressed in metastatic colorectal cancer and breast carcinomas. Plcγ1 is critical for breast cancer cell migration and invasion, and down-regulation of its lipase activity has

been shown to inhibit the metastasis of human MDA-MB-231 breast cancer cells to lung in an *in vivo* mouse model (17). However, the mechanism by which this lipase induces metastasis or the domains involved require further investigation.

PTEN: Function and importance

Phosphatase and tensin homolog (PTEN) is a phosphatidylinositol phosphate (PIP) phosphatase specific for the 3-position of the inositol ring. PTEN has been shown to have activity towards PIP, $PI(3,4)P_2$, and phosphatidylinositol (3,4,5)-triphosphate ($PI(3,4,5)P_3$ or PIP_3) *in vitro.* However, PIP_3 is the most important substrate *in vivo* (**Fig 1.7**). PIP_3 (generated by PI3K via the phosphorylation of PIP_2) provides a binding site for many PH domain-containing signaling proteins such as Akt and 3-phosphoinositide dependent protein kinase-1 (PDK1). Thus, PTEN via PIP_3 can affect a large variety of physiological processes in both developing and adult organisms. PIP_3 is best known for its promotion of cell proliferation and survival by inducing phosphorylation and activation of Akt kinase.

PTEN is involved in several pathological processes and is inactivated or deleted in many tumor types where the frequency of tumor-associated mutations rivals that of the p53 tumor suppressor (18). Indeed it is considered to be the second most highly mutated oncogene.

The substrate of PTEN, PIP3, is important in chemotaxis. During chemotaxis, PIP_3 localizes sharply to the leading edge of the cell to regulate the direction

and formation of pseudopods at the cell anterior. Such an effect, however, also requires PIP_2-regulated localization of PTEN to the cell posterior (19).

PTEN is regulated by numerous molecular mechanisms generating a continuum of functional PTEN levels in sporadic cancers and inherited syndromes. PTEN function can be compromised by genetic mutations, which result in a heterozygous loss (50%) or a homozygous loss (100%) of function. In addition, several PTEN-interacting proteins can either positively or negatively regulate PTEN function. Furthermore, disruption of competing endogenous RNA (ceRNA) networks, epigenetic silencing, transcriptional repression, microRNA (miRNA) regulation, post-translational modifications, and aberrant localization can lead to subtle or significant changes in PTEN function (20).

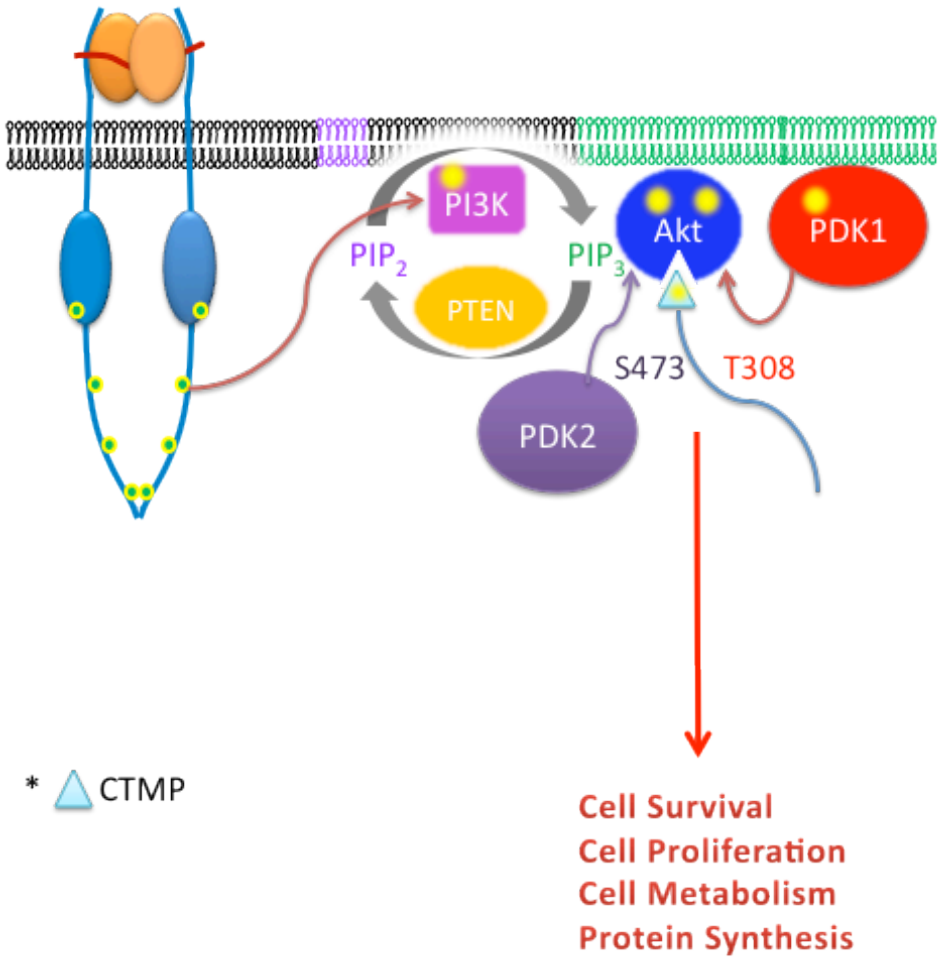

Fig 1.7: PTEN/PI3K/Akt pathway. PTEN opposes PI3K function to inactivate Akt signaling. Following PTEN loss or down-regulation the resulting accumulation of PIP_3recruits the pleckstrin homology (PH) domain-containing proteins Akt and PDK1 to the membrane. Akt is then activated by phosphorylation at threonine 308 (T308) by PDK1 and phosphorylation at serine 473 (S473) by PDK2 (mTORC2; composed of mammalian target of rapamycin [mTOR], DEP domain-containing mTOR-interacting protein [DEPTOR], target of rapamycin complex subunit LST8 [mLST8], mammalian stress-activated protein kinase interacting protein 1 [mSIN1], proline-rich protein 5 [PROTOR], and rapamycin-insensitive companion of mTOR [RICTOR]). At the membrane, association with carboxyl-terminal modulator protein (CTMP) prevents Akt phosphorylation and hence, its full activation. Phosphorylation of CTMP results in the release of Akt and its subsequent phosphorylation. Activated Akt drives cell survival, proliferation, and cellular metabolism through inhibitory/activatory phosphorylation of downstream proteins.

Akt: Function and importance

Akt is a serine/threonine kinase that was originally identified as a homologue of the v-Akt oncogene from a transforming retrovirus in a spontaneous thymoma of a mouse. There are three members of the Akt family (Akt 1, Akt 2, and Akt 3) with certain isoform-specific features. On PI3K activation, the PH domain of Akt binds to $PIP_{3.}$ This leads to the phosphorylation of Akt at threonine 308 and serine 473 and its full activation(**Fig 1.7**).

Activated Akt regulates multiple processes, such as cellular proliferation, apoptosis, and glucose metabolism, through its well-characterized downstream effectors. Akt can be inactivated by CTMP which binds to Akt preventing its phosphorylation and downstream signaling. Moreover, overexpression of CTMP can reverse the phenotype of v-Akt-transformed cells (**Fig 1.7**). Akt is also regulated by its association with heat shock protein 90 (HSP90), which protects it from protein phosphatase 2A (PP2A)-mediated dephosphorylation (21,22).

Chapter Two: SH3 domains of Grb2 and Plcγ1 compete for the same binding site on FGFR2

Background

Recently, Grb2 has been shown to form a kinase-active heterotetramer with two molecules of FGFR2 in non-stimulated cells (2, 3, 23). This causes the phosphorylation of activation loop tyrosine residues, which is inadequate to cause downstream activation of signaling pathways. Grb2 binds FGFR2 through its C-terminal SH3 domain; therefore, this protein complex formation occurs independently of growth factor stimulation and tyrosine phosphorylation. Thus, Grb2 can prevent aberrant downstream signaling by acting as a concentration-dependent control protein.

The physiological importance of maintaining an elevated Grb2 concentration is highlighted through database analysis (**Fig 2.1**). Database analysis showed that FGFR2-expressing tumor tissue samples with low concentrations of Grb2 display concomitant high expression levels of another FGFR2 ligand, Plcγ1. Low Grb2 expression and increased expression of Plcγ1 have been linked with the metastatic potential of many types of cancers. Therefore, investigation of the molecular basis of this inverse relationship between Grb2 and Plcγ1 protein concentrations and its effect on metastatic outcome is likely to be highly important.

To investigate this relationship one should understand the function and molecular basis of activation of both proteins. Upregulation of Plcγ1 activity usually occurs when the NSH2 domain of Plcγ1 binds to a cognate site on FGFR2 (pY769; 24-26). Once bound to the receptor, Plcγ1 becomes

phosphorylated on several tyrosine residues, including Y775 and Y783, within the X/Y linker region (27,28). This is followed by the intramolecular binding of CSH2 to pY783 which activates the Plcγ1 by inducing a gross conformational change that releases the auto-inhibition (15,29-31). Access to plasma membrane-embedded phospholipids is facilitated by the binding of the N-terminal PH domain to PIP_3 (32).

On the other hand, the ubiquitously expressed adaptor protein,Grb2, which does not possess enzymatic activity, is involved in numerous RTK signaling events. This protein is best known for its role in linking activated RTKs to the guanine nucleotide exchange factor SOS to upregulate the downstream MAPK pathway in growth factor-stimulated cells. Also, Grb2 is critical in forming a stable heterotetramer with FGFR2, thus maintaining homeostasis in non-stimulated cells (2,23). Upon FGFR2 stimulation, Grb2 is phosphorylated and is released from the receptor. Thus, it plays a dual regulatory role in FGFR2-mediated signaling in stimulated and non-stimulated cells.

RTK-mediated signal transduction is initiated through provision of cognate, phosphorylated binding sites to downstream signaling targets by the action of growth factor-dependent up-regulation of the receptor kinase. This mechanism represents a level of control that is imposed by the requirement of specific kinase phosphorylation precluding the effects of random binding events and fluctuation of local protein concentrations. Here, we demonstrate that Grb2 constitutively controls the stimulation-independent recruitment of Plcγ1 to FGFR2 and its subsequent membrane localization and activation through direct

inhibition of a mutual binding site on the receptor. Therefore, this interaction is dependent on protein concentration and relative equilibrium binding constants and not phosphorylation status of the proteins of interest.

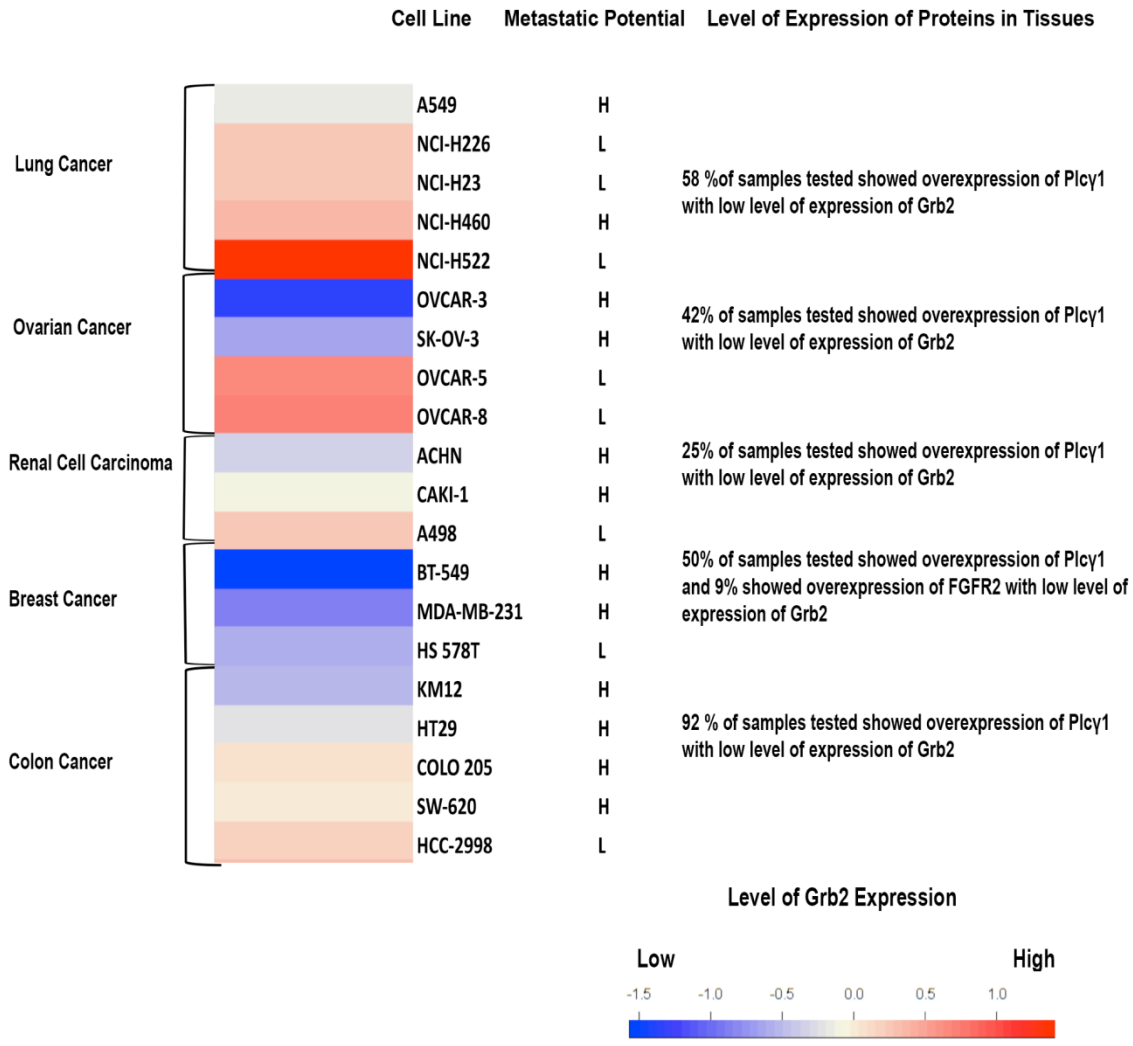

Figure 2.1 Metastatic potential is dependent on expression levels of Plcγ1 and Grb2. The Grb2 expression level in cancer cell lines was based on data extracted from Gene Expression Omnibus (GEO) website (accession number: GSM127198). The heat map was generated using the R Console Statistical Program. The data shown only includes 20 cell lines out of 60 cells lines used in the original proteomic-based profiling. Cancer types were chosen based on the expression of FGFR2 and ability to form macrometastasis. Adherent cell lines were selected for compatibility and comparability with the focus of this work; therefore, central nervous system cancer cell lines, leukemic cell lines, and

melanoma cell lines were not included. Cell lines were classified as having high relative metastatic potential (H) or low relative metastatic potential (L) based on extensive literature search. Plcγ1 and FGFR2 expression levels in tissues were extracted from thehttp://www.proteinatlas.org/website and verified by literature search. The percentage of protein expression in the tissues was based on the level of antibody staining, which can be found in the “Cancer Tissue Summary” provided by the website.

Methods

Cells

Human embryonic kidney 293T (HEK293T), and human squamous carcinoma, A431 epidermoid carcinoma were maintained in Dulbecco’s modified Eagle’s high glucose medium (DMEM). DMEM was supplemented with 10% (vol/vol) fetal bovine serum (FBS) and 1% antibiotic/antimycotic (Lonza) in a humidified incubator at 37°C with 10% CO_2. HEK293T cells stably expressing FGFR2 with a C-terminal GFP fusion (FGFR2-GFP) were produced as previously described and used throughout except in stated experiments in which parental cell lines were adopted (45). Grb2 (G2i), and Plcγ1 (Pγi) knockdown cells were generated by infecting cells Grb2 shRNA and Plcγ1 shRNA lentiviral particles, respectively, followed by selection with 7 μg/ml puromycin. Controls cells (Ci) were infected with scrambled shRNA lentiviral particles. Knockdown of Grb2 and Plcγ1 in surviving cells was confirmed by western blot. Cells were serum starved overnight prior to stimulation with FGF9 for 30 min.

Molecular Cloning

Truncated Plcγ1 polypeptides SH223 (residues 550-848) and SH3 (residues 795-848) were made. For SH223, individual point mutations (R586A and R694A) were generated in NSH2 and CSH2. Tyrosine mutants and double mutants (DM) were generated from full-length human influenza hemagglutin (HA)-tagged Plcγ1. Three individual point mutations were generated in a GST-tagged polypeptide corresponding to the very C-terminal 58 amino acids (P804A, P810A, and P813A). The kinase dead cytoplasmic portion of FGFR2 (residues 413-821) was generated through a point mutation (K517I).

Protein Expression and Purification

6Xhistidine, glutathione S-transferase (GST), HA, green fluorescent protein (GFP), and red fluorescent protein (RFP)-tagged full-length and truncated constructs of FGFR2, Grb2, and Plcγ1 were expressed and purified from *E.Coli* as previously described (28).

For protein purification, the constructs of interest were transformed into competent cells. LB media (1 L) with 50 μg/ml antibiotic (ampicillin or kanamycin) was inoculated with10 ml transformed cells. The culture was grown to an OD_{600} cell density of 0.6 at 37°C with constant shaking. The temperature was dropped down to 20°C before the addition of 300 μM IPTG for the induction of protein expression. After a 12-h growth period, the cells were harvested by centrifugation, resuspended in purification buffer (50 mM Tris lysis buffer pH 8.0, 100 mM NaCl, 1 mM β-mercaptoethanol, and protease inhibitors),

sonicated, and centrifuged (20,000 x *g*) for 45 min at 4°C. The pellet was removed, and the filtered supernatant (cleared extract) was applied to an affinity column equilibrated with purification buffer. Proteins were eluted from the column with 200 mM imidazole or 20mM glutathione. Concentrated proteins (~5 ml) were applied to an equilibirated Superdex SD75 gel filtration column loaded with purification buffer. SDS-PAGE analysis was used to detect purity.

Western Blot Analysis, Immunoprecipitation and GST Pull Down

Cultured cells were grown in 10 cm dishes and serum starved overnight. Cells were either left unstimulated (basal) or stimulated with 20 ng/ml FGF9 (R&D Systems) for 30 min. Cells were lysed with Hepes lysis buffer (50 mM Hepes, pH 7.5, 1% [vol/vol] igepal-C630, 1 mg/ml bacitracin, 1 mM EDTA, 10 mM NaF, 1 mM sodium orthovanadate, 10% [vol/vol] glycerol, 50 mM NaCl, 1 mM PMSF, and Protease Inhibitor Cocktail Set III [EMD Millipore]) as previously described (2). Protein concentration was quantified by Bradford assay, and 50 µg of total proteins was used for every blot. For purified proteins, only 10 ng of protein was utilized for western blot and densitometric analysis via imageJ software (U. S. National Institutes of Health, Bethesda, Maryland, USA, http://imagej.nih.gov/ij/), was performed on the blots. Protein A/G Plus-Agarose (Santa Cruz Biotechnology, Inc) was used for immunoprecipitation experiments. For GST pull down assays, cleared extract from cells expressing GST-tagged proteins or empty GST vector that was incubated for 2 h at room temperature with glutathione sepharose beads that were soaked for 30 min in PBS, washed

four times with PBS, and then resuspended in Tris buffer. The resultant GST-tagged protein bound to the beads was incubated with cell lysates overnight at 4°C before washing three times with PBS to avoid non-specific binding. This was followed by western blot analysis to detect protein-protein complex formation. Antibodies were purchased from the following sources: phosphotyrosine (pY99), FGFR2 (C-17), Grb2 (C-23), anti-goat secondary antibody, and HA-probe (Y-11) (Santa Cruz Biotechnology Inc); anti-GFP (goat) and anti-RFP (mouse) (Rockland Immunochemicals); β-actin, GST, and anti-mouse and anti-rabbit secondary antibodies (Cell Signaling Technology); and THE™ HA-tag (mouse) and Plcγ1 (mouse) (BD Biosciences).

Additional reagents used in experiments were purchased as follows: ATP competitive FGFR2 inhibitor SU 5402, scrambled shRNA, (catalog no. sc-108080), and Grb2 shRNA (catalog no. sc-29335-v) (Santa Cruz Biotechnology, Inc); phalloidin (catalog. no: 8953) (Cell Signaling Technology); Metafectene transfection reagent (Biontex-USA); and puromycin dihydrochloride, selection antibiotic, (Invitrogen).

Cell Fractionation

HEK293T Ci and G2i cells were serum starved overnight. Cells were either left unstimulated, or stimulated with 20 ng/ml FGF9 for 30 min and then washed three times with PBS. Cell fractionation was performed using the Subcellular Protein Fractionation Kit for Cultured Cells (Thermo Scientific). The protein content in the cytoplasmic and membrane extracts was quantified and analyzed

by western blot. FGFR2 and β-actin were used to determine the purity of the membrane and cytoplasmic extracts, respectively.

MTT Assay

A working solution of MTT was prepared by diluting the 5 mg/ml stock solution (Promega) 1:10 in PBS. Cells were seeded in 12-well plates. The medium was aspirated and replaced with 40 µl MTT/well. Cells were then incubated for 3 h at 37°C. The MTT dye was solubilized with 1 ml acidic isopropanol (0.04 M HCl), followed by two 30-min incubation periods in between which the solution was gently mixed. Finally, the dye solution was transferred to a 1.5 ml eppendorf tube and centrifuged at 13,000 rpm for 3 min. The supernatant was pipetted into disposable cuvettes and absorbance was measured at 570 nm with background wavelength subtraction at 650 nm. Results were plotted using Excel (Microsoft) and presented as the mean ± standard deviation of the relative fluorescence units (RFUs) of three independent experiments performed in triplicate.

Surface Plasmon Resonance (SPR)

SPR experiments were performed using a BIAcore T100 instrument with temperature maintained at 25°C in running buffer (50 mM HEPES, pH 7.5, 100 mM NaCl, and 1 mM β-mercaptoethanol). The CSH3 of Grb2 (Grb2CSH3) was immobilized to Series S CM4 Sensor Chips to a final level of ~700-900 resonance units (RU) using the manufacturer's protocol. Synthesized FGFR2 C-terminal peptide (23 amino acids; C23) was diluted in running buffer, and

binding experiments were performed using a flow rate of 30 µl/min with 180 s contact time and 300 s dissociation time. Data analysis was performed using BIAcore evaluation software with data subtraction against blank immobilized, paired flow-cells.

Fluorescence Microscale Thermophoresis (MST)

MST Experiments were performed using a Monolith NT.115 instrument (NanoTemper) with temperature maintained at 25°C. The Plcγ SH3 domain was labeled with primary amine coupling of NT-647 dye according to the manufacturer's protocol and purified using Superdex 25 resin in a buffer containing 50 mM HEPES (pH 7.5), 100 mM NaCl, and 1 mM β-mercaptoethanol. Titration series were made using a 1:1 dilution of synthesized FGFR2 C-terminal peptide (23 amino acids) while maintaining a constant 25 nM NT-647-labeled Plcγ SH3 domain. Thermophoresis was monitored at four separate temperature gradients. MST experiments were performed in triplicate while.

Fluorescence Lifetime Measurement

Fluorescenceresonance energy transfer (FRET) experiments were done to measure complex formation between Alexa Fluor 488-labeled C58 (emitter) and Alexa Fluor 555-labeled Plcγ1SH3 (acceptor). In all experiments, 250 µl of sample was labeled with 10 µM Alexa Fluor (Invitrogen). The sample was then rotated at room temperature for 1 h before quenching with 40µl Tris-Hcl (pH 8).

Labeled sample was separated from free dye using a gel filtration column. C58 and Plcγ1SH3 were incubated at an equimolar concentration of 0.5 μM. Grb2CSH3 concentration was increased sequentially as follows: 0.1 μM, 0.5 μM, and 0.7 μM. Experiments were performed in a spectrofluorometer (QuantaMaster-4-CW; Photon Technology International) at 23°C in 50 mM Tris-HCl, 100 mM NaCl, 1 mM β-mercaptoethanol, and 5% glycerol at pH 8.5. C58 lifetime decay was measured using a pulsed nitrogen laser with an excitation of 488 nm, emission of 510 nm, start delay of 135 ns, and end delay of 150 ns. 200 channels were used with an integration time of 50 μs, 3 averages, 5 shots, and a frequency of 8 Hz. FeliX32 analysis software (Photon Technology International) was used to fit the decay curves and compute the lifetime constants.

Fluorescence Lifetime Imaging Microscopy (FLIM) Analysis

HEK293T cells stably expressing GFP-FGFR2 were transfected with different RFP-tagged Plcγ1 domains or full length HA-Plcγ1 using Metafectene. The efficiency of transfection was confirmed using western blot analysis. Serum starved cells on glass coverslips were either left unstimulated or stimulated with 20 ng/ml of FGF9. Cells were fixed with 4% (wt/vol) paraformaldehyde (pH 8.0) for 20 min. HA-Plcγ1-transfected cells were fixed, washed with PBS, permeabilized with 0.5% (vol/vol) Triton X-100, and blocked with blocking buffer (3% BSA, 0.5% Triton X, and 5% fetal calf serum). Cells were then washed with PBS and incubated overnight with Alexa Fluor 555-labeledanti-HA antibody (Y-

11). Cells were washed with PBS and mounted onto a slide with mounting buffer (0.1% p-phenylenediamine/75% glycerol in PBS). Imaging was performed using a confocal microscope (model SP5; Leica) at 20°C as described previously (2). FLIM data was collected with an inverted advanced confocal microscope system (TCP SP5; Leica) with an internal photomultiplier tube detector. The samples were excited with a tunable fs titanium-sapphire pumped laser (Mai Tai BB; Spectra-Physics). Images were acquired with an oil-immersion objective (NA 1.4) and a line scan speed of 400 Hz, with an image size of 512 × 512 pixels. Pixels used for analysis were 256 x 256. The fluorescence decays were fitted with a single exponential decay model using SPCImage software (Becker & Hickl), and the GFP fluorescence lifetimes were displayed in a false-color histogram. The data shown are representative of three slides prepared from three independent experiments.

Results

Grb2 inhibits the binding of Plcγ1 to FGFR2

We generated Grb2 shRNA knockdown (G2i) and scrambled shRNA control (Ci) A431 cells (**Fig 2.2a**). Immunopreciptiation of Plcγ1 by FGFR2 under non-stimulated conditions showed that the presence of Grb2 in Ci cells inhibited the association of Plcγ1 with the receptor (**Fig 2.2b**). Immunoprecipitation of Plcγ1 by FGFR2 (**Fig 2.2c**) and FGFR2 by Plcγ1 (**Fig 2.2d**) revealed similar inhibitory effects in HEK293T Ci cells stably over-expressing FGFR2. A constitutive

Plcγ1-FGFR2 interaction was observed in G2i cells (**Fig 2.2 b,c,d**). Therefore, the Plcγ1-FGFR2 interaction occurred in the Grb2 knockdown background.

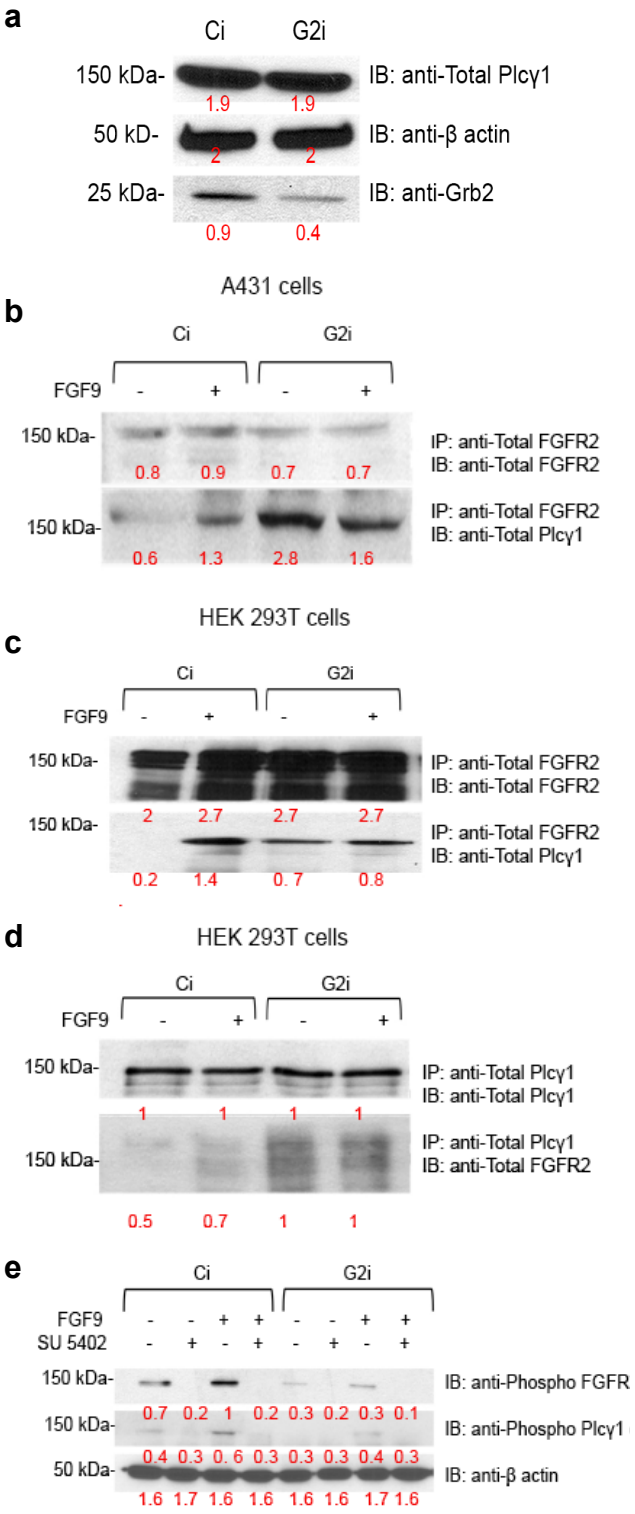

f

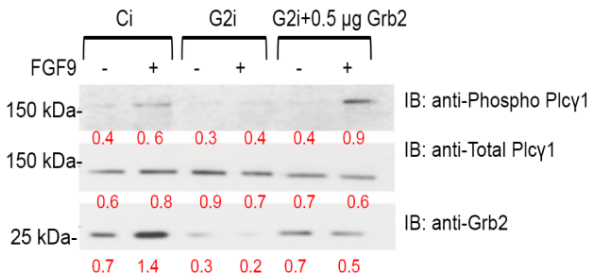
Ci
G2i
G2i+0.5 μg Grb2
FGF9
- + - + - +
150 kDa-
IB: anti-Phospho Plcγ1
0.4 0. 6 0.3 0.4 0.4 0.9
150 kDa-
IB: anti-Total Plcγ1
0.6 0.8 0.9 0.7 0.7 0.6
25 kDa-
IB: anti-Grb2
0.7 1.4 0.3 0.2 0.7 0.5

g

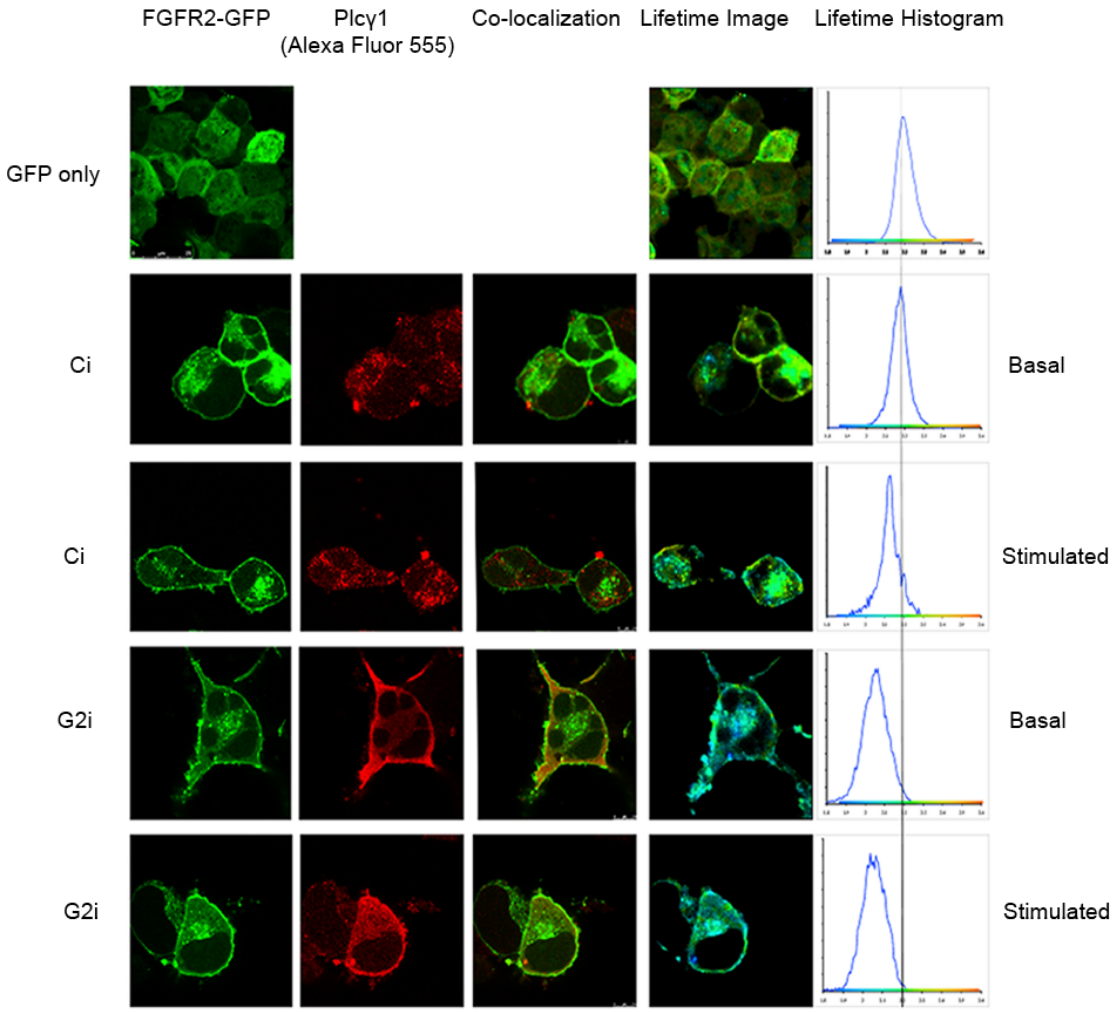
FGFR2-GFP
Plcγ1 (Alexa Fluor 555)
Co-localization
Lifetime Image
Lifetime Histogram
GFP only
Ci
Basal
Ci
Stimulated
G2i
Basal
G2i
Stimulated

Fig2.2 Plcγ1 constitutively binds to FGFR2 in the absence of Grb2.a) Grb2 knockdown in A431 G2i cells was confirmed by western blot. A431 cells transfected with scrambled shRNA were used as a control (Ci cells). Total Plcγ1 and β-actin were used as loading controls.**b**) A431 and **c**) Ci (control) and G2i (Grb2 knockdown) HEK293T cells were serum starved overnight an either left Unstimulated (basal) or stimulated with FGF9. Cell lysates were obtained and immunoprecipitation was performed using FGFR2 antibody. The expression of total FGFR2 and total Plcγ1 in the immunoprecipitates was determined by western blot. Quantification of western blots was done using ImageJ software and presented in arbitrary units.**d**) Lysates obtained from HEK293T Ci and G2i cells that were unstimulated (basal) or FGF9-stimulated were used for immunoprecipitation with Plcγ1 antibody.Immunoprecipitates were analyzed for total Plcγ1 and total FGFR2 by western blot.**e**) In the absence of Grb2, the binding of Plcγ1 to FGFR2 does not induce Plcγ1 phosphorylation. HEK293T Ci and G2i cells were serum starved overnight and either left untreated or treated with 30 μM SU5402 kinase inhibitor for 2 h. Basal or FGF9-stimulated cell lysates were obtained and the expression of phosphorylatedPlcγ1 and phosphorylated FGFR2 was determined by western blot. **f**) Western blot result showing the phosphorylation state of Plcγ1 in unstimulated and FGF9-stimulated HEK293T cells. Cell lysates from serum-starved Ci, G2i, and G2i cells with 0.5 μg Grb2 knocked in were obtained, and western blot was done to determine the expression of phosphorylated Plcγ1, total Plcγ1 (loading control), and Grb2 (efficiency of knockdown/knock in). **g**) HEK293T Ci and G2i cells stably transfected with GFP-tagged FGFR2 were transiently transfected with HA-Plcγ1. Non-transfected cells were used as controls to detect the initial lifetime of GFP using FLIM (top row). Constitutive Plcγ1-FGFR2 interaction does not occur in the presence of Grb2. However, in the absence of Grb2,Plcγ1-FGFR2 complex formation occurs as evidenced by the reduction in emission lifetime of GFP (left shift of the peak in graph; right hand column).

Importantly, Plcγ1 phosphorylation did not occur in HEK293T cells when Plcγ1 was constitutively bound to FGFR2 (**Fig 2.2e**). FGF9-mediated FGFR2 stimulation induced Plcγ1-FGFR2 complex formation as expected. Under these conditions, Grb2 binding was abrogated (1), FGFR2 was tyrosine-phosphorylated, providing a site for the binding of Plcγ1NSH2 (**Fig 2.2b,c,d**), and Plcγ1 wasphosphorylated in Ci cells (**Fig 2.2e**). Knocking Grb2 back into G2i cells restored Plcγ1 phosphorylation in stimulated cells (**Fig 2.2f**).

To confirm that the presence of Grb2 affects Plcγ1-FGFR2 complex formation in a cellular context, we performed FLIM on HEK293T Ci and G2i cells stably over-expressing C-terminally GFP-tagged FGFR2 (FGFR2-GFP) and transfected with HA-Plcγ1 (**Fig 2.2g**). Fluorescence lifetimes were measured between GFP and an Alexa Fluor 555 (AF555)-labeled anti-HA-Plcγ1 antibody. Under non-stimulated conditions in Ci cells, the GFP fluorescence lifetime was unaffected, suggesting the absence of binding between FGFR2and Plcγ1. However, in the absence of Grb2, the GFP fluorescence lifetime was significantly reduced (left shift of lifetime graph; **Fig 2.2g**). This reduction in GFP fluorescence lifetime was due to FRET between GFP (donor) and AF555 (acceptor) as the fluorophores approach to within ~10 nm of one another, suggesting that FGFR2 and Plcγ1 wereclose enough to form a complex. Stimulation of the receptor resulted in clear protein complex formation through the well-characterized binding of Plcγ1 to phosphorylated receptor.

The SH3 domain of Plcγ1 binds to FGFR2

To identify more precisely the FGFR2 site that interacts with Plcγ1, we performed pull down experiments with truncated polypeptides including the protein-binding domains of Plcγ1 (**Fig 2.3a**). Under basal conditions, a GST-tagged polypeptide containing the NSH2, CSH2, and SH3 domains of Plcγ1 (SH223) was able to pull down FGFR2 only in G2i cells (**Fig 2.3b**). Truncating the peptide to isolate the SH3 domain was also effective in pulling down the receptor (**Fig 2.3b**). We confirmed the interaction between the SH3 domain of Plcγ1 (Plcγ1SH3) and FGFR2 with additional pull down experiments using mutant forms of SH223 (**Fig 2.3c**). R586A and R694A mutants (which disable NSH2 and CSH2 binding to pY, respectively) and the DM did not abrogate binding to non-stimulated receptor in G2i cells (**Fig 2.3c**). This suggested that the SH3 domain, but not the SH2 domains, of Plcγ1 interacted with the receptor under non-stimulated conditions.Upon receptor stimulation, Plcγ1-FGFR2 complex formation was observed in R694A SH223-mutated Ci cells, which was consistent with a previous report demonstrating binding of NSH2 to the activated receptor (31).

FLIM was also utilized to assess Plcγ1SH3 binding in a cellular context. In HEK293T cells transfected with GFP-tagged FGFR2 and RFP-tagged Plcγ1SH3, binding was not observed in Ci cells under non-stimulated conditions. However, FGFR2-Plcγ1SH3 complex formation did occur in G2i cells (left shift of lifetime graph compared to isolated RFP; **Fig2.3d**).

Therefore, Plcγ1SH3 binding to FGFR2 occurred only in the absence of Grb2. Similar results were obtained in cells transfected with RFP-tagged SH223 of Plcγ1 (**Fig 2.4a,b,c**).

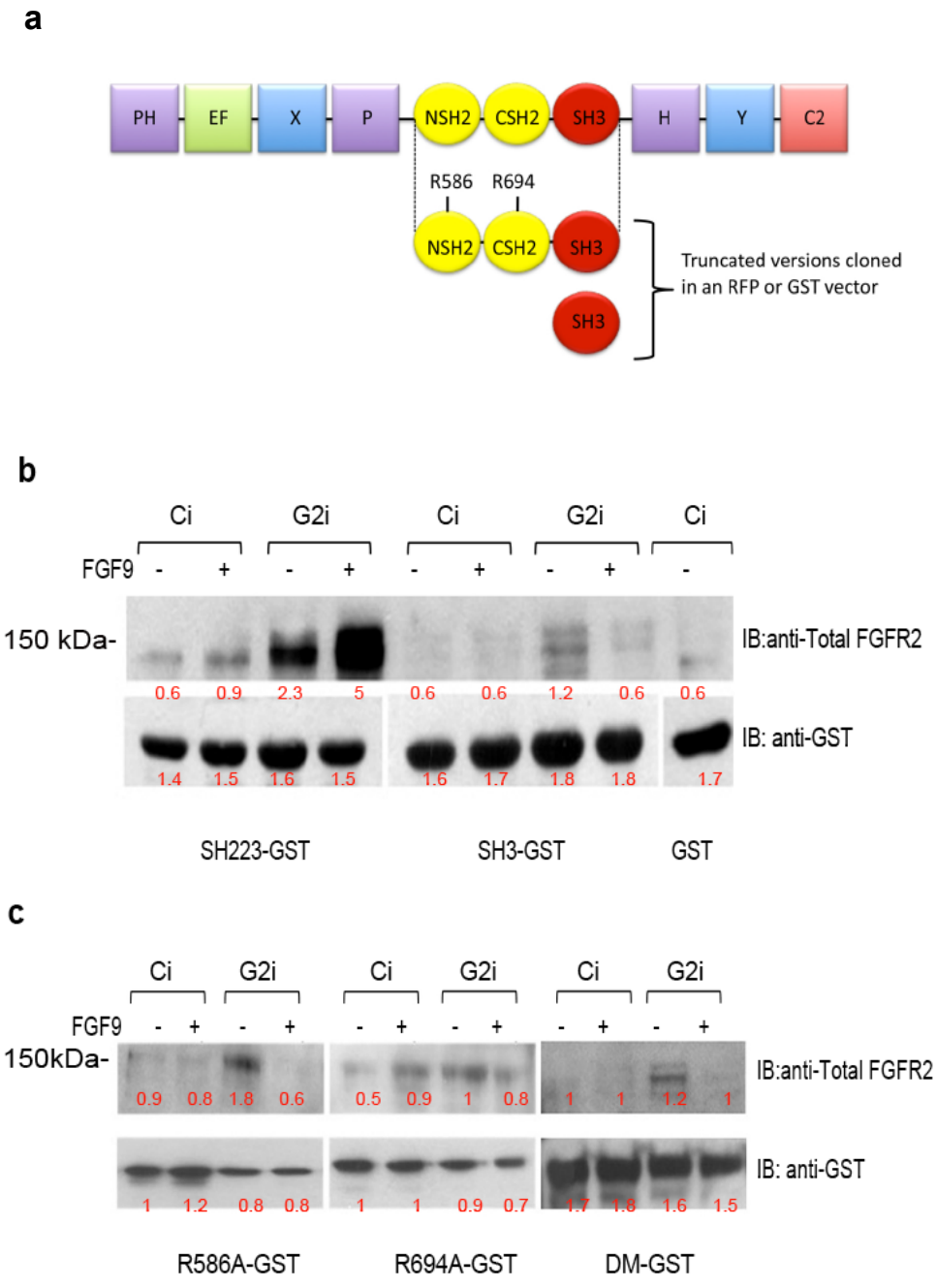

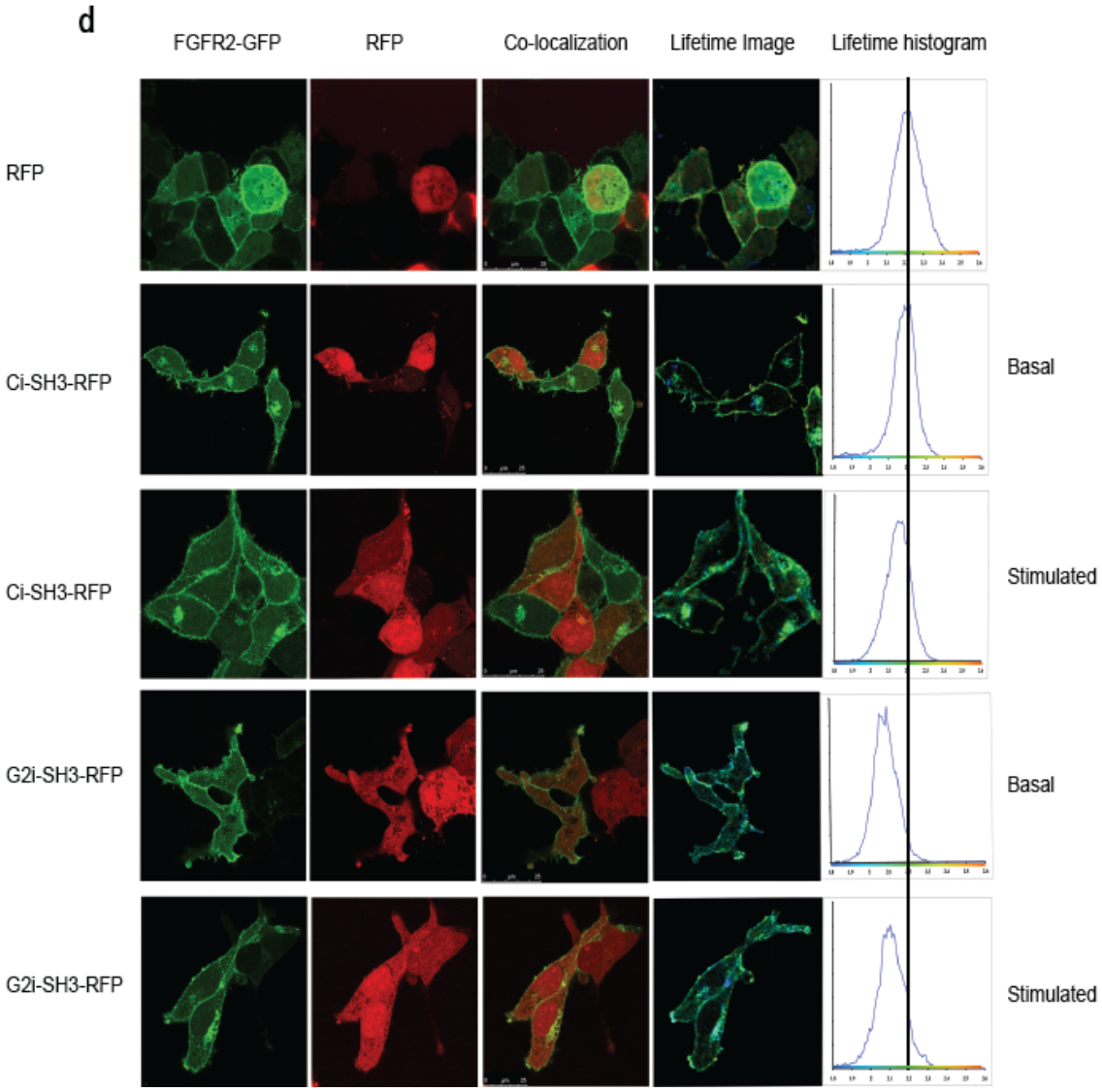

Fig 2.3 The SH3 domain of Plcγ1 binds to FGFR2.a) Schematic illustration of the sequence of Plcγ1 domains. SH223 and SH3 truncated versions shown with the arginine residues (R586 and R694) that were mutated in SH2 domains to abrogate binding topY on FGFR2.**b**) C-terminal GST-tagged polypeptides SH223-GST, SH3-GST, and GST alone (used as a control) on glutathione beads were incubated with cell lysates obtained from basal and FGF9-stimulated Ci and G2i HEK293T cells. Western blot was used to determine total FGFR2 and GST expression.**c**) R586A and R694A mutations were made in the NSH2 and CSH2 of SH223 of Plcγ1, respectively. R586A and R694A mutants and DM of SH223 were used for GST pull down assays of basal and FGF9-stimulated HEK293T whole cell lysates. **d**) RFP-tagged Plcγ1SH3 was transiently transfected in HEK293T cells stably transfected with FGFR2-GFP. Ci and G2i cells were used for FLIM analysis. Graph (right hand column) shows distribution of GFP fluorescence lifetime. Complex formation is shown by a

reduction of the GFP lifetime (left shift of peak). Cells transfected with empty RFP vector were used as a control (top row).

a

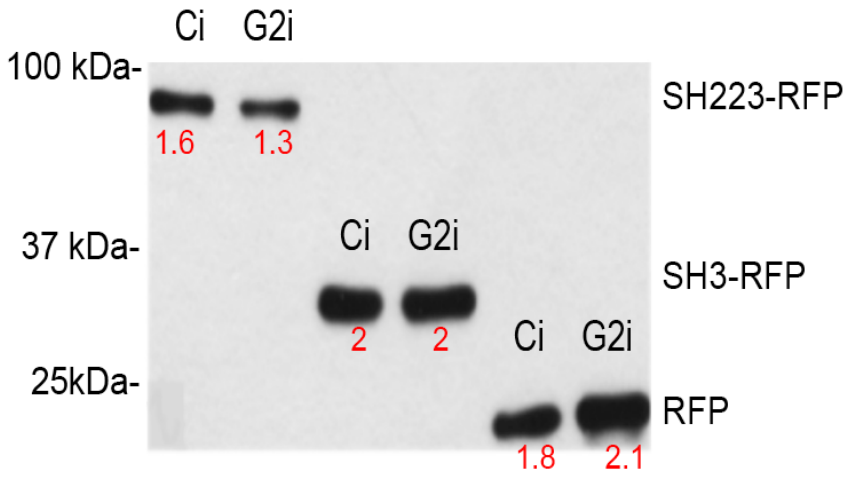

b

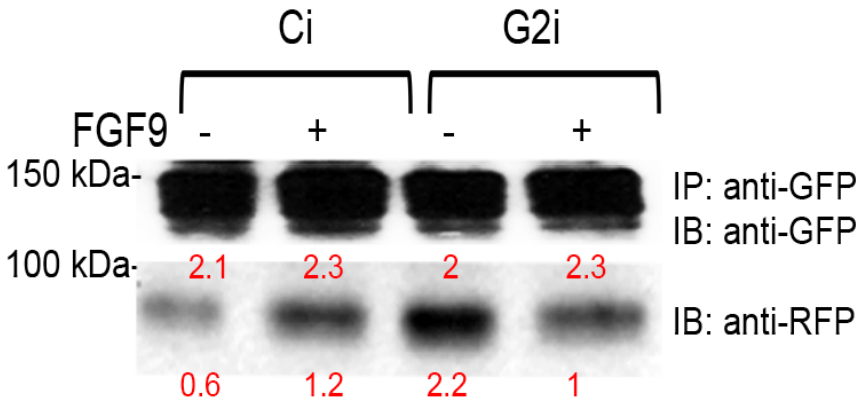

c

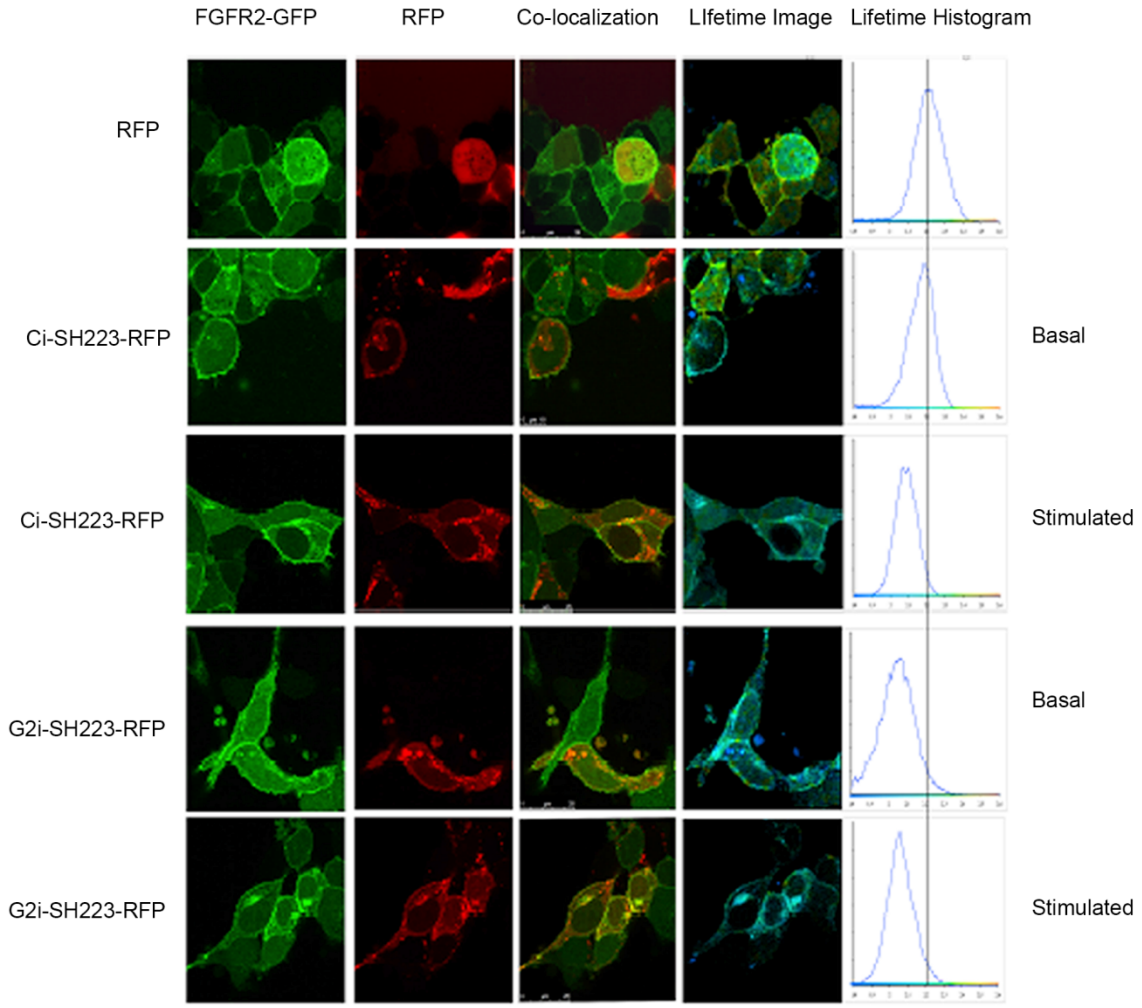

Fig 2.4 Plcγ1 binding to FGFR2 is independent of phosphorylation state.a) Western blot showing the efficiency of transfection of RFP-tagged SH223 and SH3 constructs in HEK293T control (Ci) and Grb2 knockdown (G2i) cells.Cells transfected with RFP empty vector were used as a control.**b**) HEK293T Ci and G2i cells stably expressing FGFR2-GFP were transfected with SH223-RFP, serum starved overnight, and treated with FGF9 for 30 min. Cells were washed and lysed before immunoprecipitation with anti-GFP antibody. Western blot analysis was done to determine the expression of GFP (as a control) and RFP to detect the association of FGFR2 with the Plcγ1 SH223 domain.**c**) Cells transfected with SH223-RFP or RFP alone were used to detect binding to FGFR2-GFP by FLIM. Reduced fluorescence lifetime (left shift of peaks in right hand column) indicates complex formation.

The C-terminal SH3 domain of Grb2 (Grb2CSH3) binds to a peptide corresponding to residues 807-821 of the very C-terminus of FGFR2 (2,3). To determine whether Plcγ1SH3 binds to a similar region on FGFR2, we initially used a C-terminally GST-tagged 58 residue peptide representing the very C-terminal sequence of FGFR2 (C58; residues 764-821). In a GST pull down experiment, Plcγ1 was clearly associated with C58 in non-stimulated G2i HEK293T cells (**Fig 2.5a**). In an *in vitro* experiment, C58 was able to pull down purified Plcγ1; however, this interaction was reduced in the presence of Grb2 (**Fig 2.5b**).

The Grb2CSH3-FGFR2 interface incorporates a cognate sequence including proline residues 810 and 813 on the receptor (2). We confirmed that Plcγ1 binds to the same location as Grb2 in pull down assays of HEK293T cell lysates with C58, in which the binding site was disrupted through mutation of the C-terminal proline residues to alanine (P810A, and P813A; **Fig 2.5c**). P810A and P813A mutations, which are in the defined Grb2CSH3 binding site, induced negligible complex formation in the basal state even in G2i cells. However, in cells with a proline to alanine mutation (P804A), which is just outside the structurally determined binding site for Grb2, Plcγ1 was able to bind to C58 in G2i cells.

To demonstrate that the binding of Plcγ1 is independent of FGFR2 phosphorylation in the non-stimulated state, Y769 on C58-GST was mutated to phenylalanine (Y769F). Complex formation between C58 and Plcγ1 was

observed in the absence of pY769 in G2i cells, which indicated that the Plcγ1 and FGFR2 interaction is mediated by Plcγ1SH3 (**Fig 2.5d**). Conversely, the ability of C58 to pull down Plcγ1 from Ci cell lysates was limited.

We confirmed the binding between Plcγ1SH3 and the C-terminal (residues 799-821; C23) of FGFR2 *in vitro* using MST. The equilibrium dissociation constant (K_d) of this interaction was approximately 40 μM (**Fig 2.5e**). This is similar to the binding affinity of the second FGFR2 molecule to the Grb2 dimer bound to FGFR2 in the formation of the FGFR2-Grb2 heterotetramer (K_d ~ 25 μM) (2). Therefore, it is possible that approximately equimolar concentrations of Plcγ1SH3 and Grb2 would compete equally for binding to FGFR2 in cells (see schematic **Fig. 2.5f**).

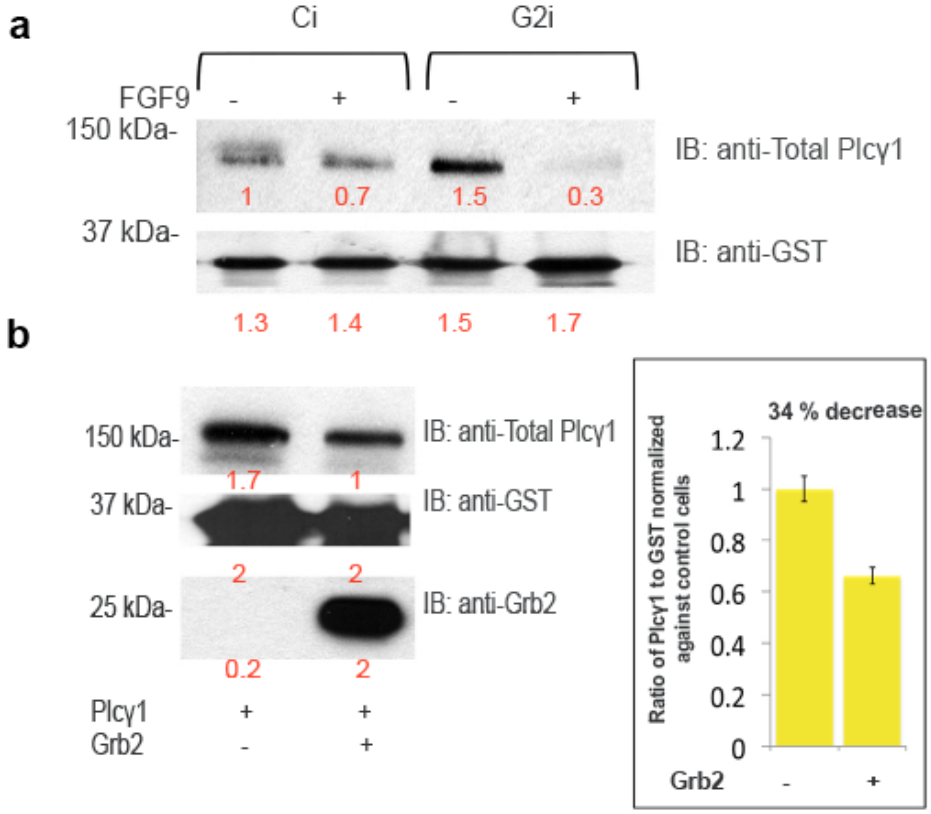
a
Ci
G2i
FGF9
-
+
-
+
150 kDa-
IB: anti-Total Plcγ1
1
0.7
1.5
0.3
37 kDa-
IB: anti-GST
1.3
1.4
1.5
1.7
b
150 kDa-
IB: anti-Total Plcγ1
1.7
1
37 kDa-
IB: anti-GST
2
2
25 kDa-
IB: anti-Grb2
0.2
2
Plcγ1
+
+
Grb2
-
+
34 % decrease
Ratio of Plcγ1 to GST normalized against control cells
1.2
1
0.8
0.6
0.4
0.2
0
Grb2
-
+

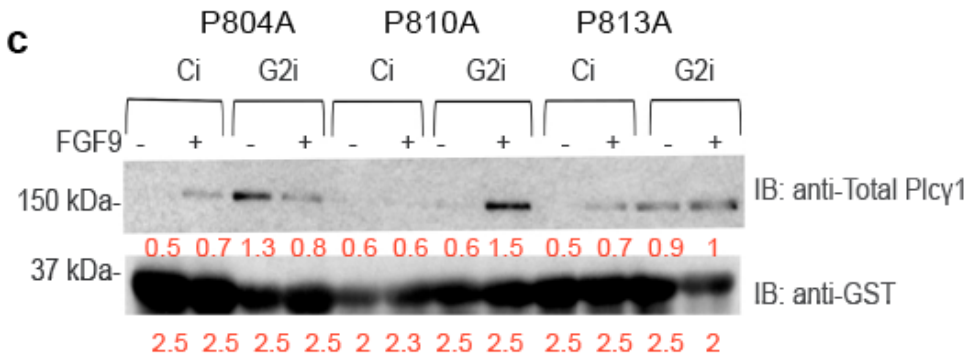
c
P804A
P810A
P813A
Ci
G2i
Ci
G2i
Ci
G2i
FGF9
- + - + - + - + - + - +
150 kDa-
IB: anti-Total Plcγ1
0.5 0.7 1.3 0.8 0.6 0.6 0.6 1.5 0.5 0.7 0.9 1
37 kDa-
IB: anti-GST
2.5 2.5 2.5 2.5 2 2.3 2.5 2.5 2.5 2.5 2.5 2

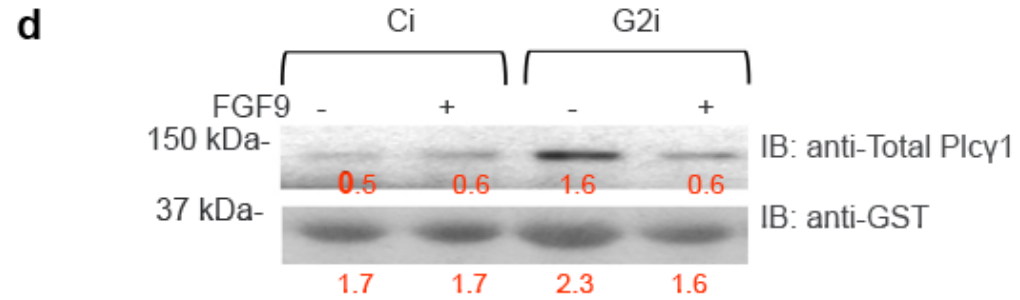
d
Ci
G2i
FGF9 - + - +
150 kDa-
0.5 0.6 1.6 0.6
IB: anti-Total Plcγ1
37 kDa-
IB: anti-GST
1.7 1.7 2.3 1.6

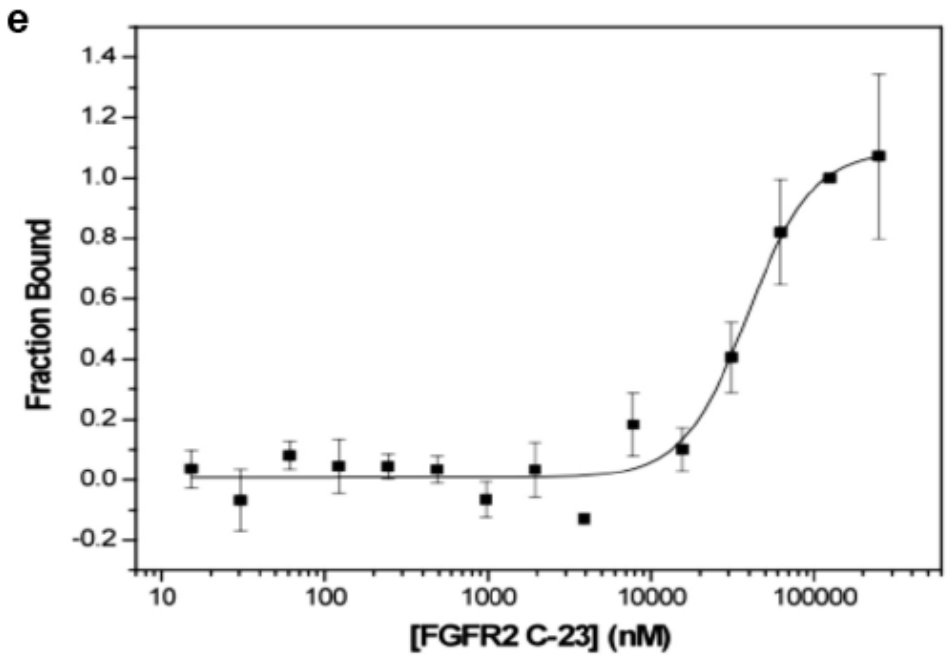
e
Fraction Bound
1.4
1.2
1.0
0.8
0.6
0.4
0.2
0.0
-0.2
10
100
1000
10000
100000
[FGFR2 C-23] (nM)

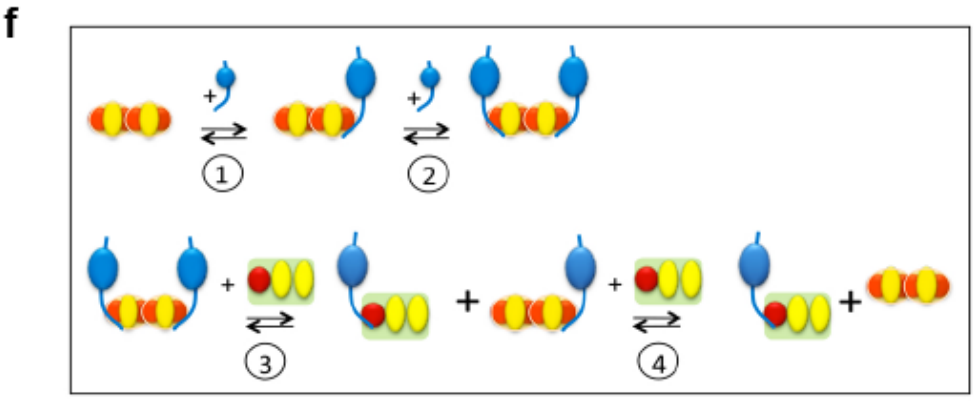
f
1
2
3
4

Fig 2.5 Plcγ1 binds to the C-terminus of FGFR2.a) Plcγ1 binds C58 more effectively in the absence of Grb2. Pull down assays ofcell lysates from basal and FGF9-stimulated HEK293T Ci and G2i cells with C58 were performed to determine whether Plcγ1 binds to the C-terminus of FGFR2.Western blot analysis was done to determine total Plcγ1 and GST expression in the immunoprecipitates.**b**) C58 on glutathione beads was incubated with purified Plcγ1 alone or in combination with Grb2 (equimolar concentration of 10 ng) in a GSTpull down assay. The expression of Plcγ1, GST, and Grb2 was determined by western blot and quantitated by densitometric analysis. The histogram presents the ratio of Plcγ1 to GST following normalization to control cells of 3 independent experiments. Error bars represent standard deviation of the mean (right panel).**c**) P804A, P810A, and P813A-mutatedC58 were used in a GST pull down assay using HEK293T cell lysates. Western blot was done to determine the expression of total Plcγ1 and GST.**d**) C58 with a point mutation Y769F (to which the SH2 domain(s) of Plcγ1 are known to bind) was used in a GST pull down assay of cell lysates from HEK293T cells,followed by western blot analysis. The blot was probed for total Plcγ1 and GST. **e**) MST was used to measure the binding of C23 to Plcγ1SH3. C23 was titrated with 25 nM NT-647-labeled Plcγ1SH3 domain. Binding curve fit to a K_d = 39 μM. **f**) Schematic showing the concentration-dependent equilibrium between Grb2 and Plcγ1 for FGFR2 binding. Top panel: Formation of Grb2-FGFR2 heterotetramer. (1) Binding of first FGFR2 molecule to Grb2 dimer; K_d = 0.1 μM. (2) Binding of second FGFR2 molecule to Grb2 dimer; K_d ~ 25 μM. Bottom panel: Competition between Grb2 and Plcγ1 (only the SH domains are highlighted). (3) Increasing concentrations of Plcγ1 compete to disrupt the Grb2-FGFR2 heterotetramer (K_d ~ 40 μM). (4) Under high Plcγ1 and/or low Grb2 concentrations, Plcγ1 binding to FGFR2 will dominate. SH2 – yellow; SH3 domain – red; FGFR2 – blue; Plcγ1 – green.

Plcγ1 and Grb2 compete for binding to FGFR2

The binding of both Grb2 and Plcγ1 via their respective SH3 domains to an identical region of FGFR2 with similar affinities indicatesthat constitutive Plcγ1 activation relies on a concentration-dependent competition for FGFR2 binding. To confirm this, an *in vitro* competition assay using fluorescence spectrometry was performed to assess whether increasing concentrations of Grb2 could effectively displace Plcγ1 from FGFR2. C58 was labeled with Alexa Fluor 488 (AF488), and Plcγ1SH3 was labeled with AF555. The fluorescence lifetime of

AF488-tagged C58 (green arrow; **Fig 2.6a**) will decrease in the proximity of AF555 through FRET. Mixing of 0.5 μM of both C58 and PlcγSH3 reduced the fluorescence lifetime of AF488 (red arrow) due to PlcγSH3 and C58 complex formation. Subsequent addition of increasing concentrations (0.1-0.7 μM; maroon arrows) of Grb2CSH3 increased AF488 emission lifetimes as the unlabeled Grb2CSH3 replaced PlcγSH3 on C58.

Localization to the plasma membrane is fundamental to Plcγ1 phospholipase lipase function. In the absence of Grb2, a significant concentration of Plcγ1 localizes to the membrane. This was not observed in Ci cells (**Fig 2.6b**). These data are consistent with increased concentrations of Plcγ1 being recruited to the membrane through binding to FGFR2 under non-stimulatory conditions.

In summary, these results show that both proteins are competing for the same binding site on FGFR2 in a concentration dependent manner. Thus, Plcγ1 will replace Grb2 on the receptor only in G2i cells under basal non stimulated conditions.

a

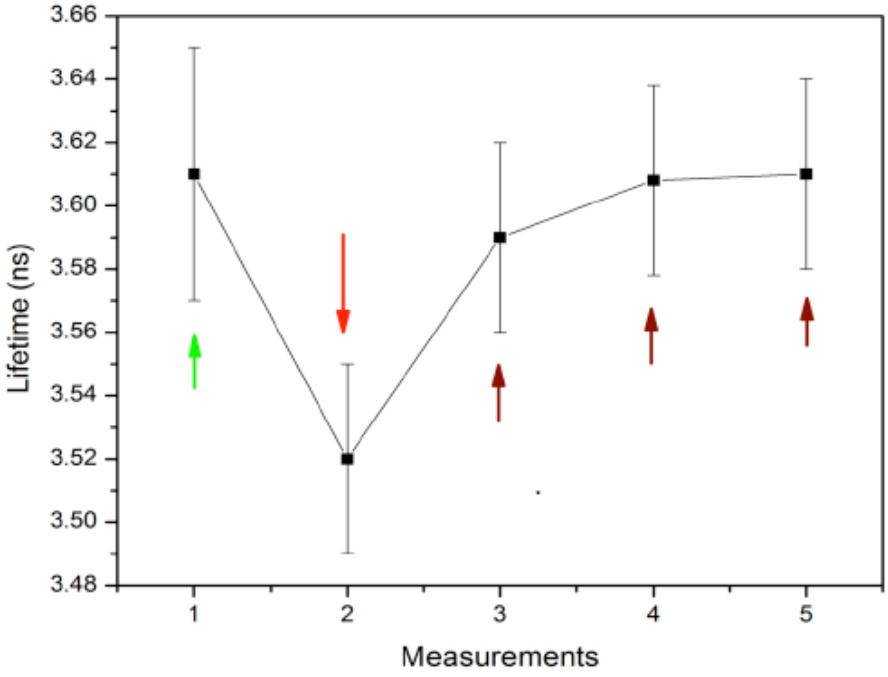
3.66
3.64
3.62
3.60
3.58
3.56
3.54
3.52
3.50
3.48
Lifetime (ns)
1
2
3
4
5
Measurements

b

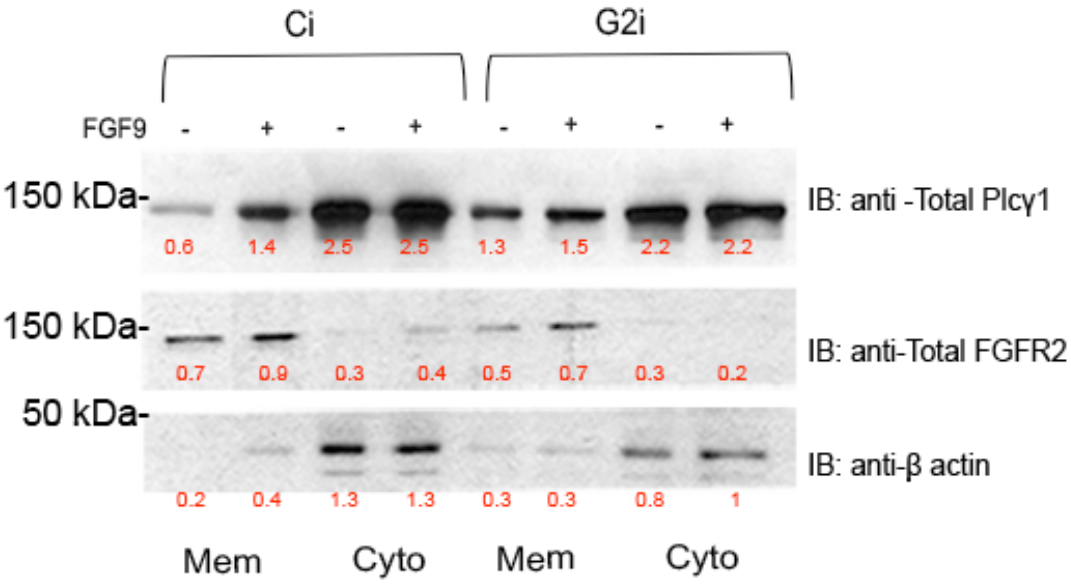
Ci
G2i
FGF9 - + - + - + - +
150 kDa-
0.6 1.4 2.5 2.5 1.3 1.5 2.2 2.2
IB: anti -Total Plcγ1
150 kDa-
0.7 0.9 0.3 0.4 0.5 0.7 0.3 0.2
IB: anti-Total FGFR2
50 kDa-
0.2 0.4 1.3 1.3 0.3 0.3 0.8 1
IB: anti-β actin
Mem
Cyto
Mem
Cyto

Fig 2.6 Plcγ1 and Grb2 compete for binding to FGFR2.a) Fluorescence spectroscopy measurement of AF555 and AF488-labeled Plcγ1SH3 binding to C58 in the presence of Grb2CSH3.The green arrow indicates the lifetime measurement (ns) of C58 (0.5 μM). The red arrow indicates the addition of Plcγ1SH3 (0.5 μM). The maroon arrows indicate the sequential addition of 0.1, 0.5, and 0.7 μM Grb2CSH3 to the C58 and Plcγ1SH3 mixture. **b**) Expression of Plcγ1 in the cellular fractions of HEK293T lysates. Total FGFR2 and β-actin were used to determine the purity of the membrane (Mem) and cytoplasmic (Cyto) fractions, respectively.

Chapter Three: Grb2 and Plcγ1 competition controls lipase mediated cell migration and invasion

Background

When it comes to the activation mechanism of Plcγ1, some features remain speculative. For example, tyrosine phosphorylation may not always be essential or adequate for full activation of Plcγ1 (33). However, phosphorylation and X/Y linker region-mediated intramolecular interactions are required to induce membrane localization and phospholipase activity (34). Thus, the previously described SH3-mediated binding of Plcγ1 to FGFR2 might be critical in placing the lipase in close proximity to its substrate, leading to phosphorylation-independent Plcγ1 activation.

Hydrolysis of the Plcγ1 substrate PIP_2 is known to be required for the development of cellular protrusions, filopodia, and lamellipodia and directional cell migration (35,36). Plcγ1 activity has been implicated in differentiation, cell proliferation, chemotaxis, actin remodeling, and cell migration (37-40). Plcγ1 functions are associated with phosphoinositide metabolism, which directly impacts the actin cytoskeleton (41,42).

Here, we show that SH3-mediated binding of Plcγ1 to FGFR2 under conditions where the law of mass action favors Plcγ1 over Grb2 (i.e., higher intracellular concentration of Plcγ1 vs. Grb2) increases Plcγ1 activity and PIP_2 hydrolysis, thereby inducing cellular invasion and metastasis.

Methods

Cells

Human embryonic kidney 293T (HEK293T), and LoVo colon cancer cells were maintained in Dulbecco's modified Eagle's high glucose medium (DMEM), whereas ROS17/2.8 osteosarcoma cells were grown in phenol red-free DMEM. DMEM was supplemented with 10% (vol/vol) fetal bovine serum (FBS) and 1% antibiotic/antimycotic (Lonza) in a humidified incubator at 37°C with 10% CO_2. Grb2 (G2i), and Plcγ1 (Pγi) knockdown cells were generated by infecting cells Grb2 shRNA and Plcγ1 shRNA lentiviral particles, respectively, followed by selection with 7 μg/ml puromycin. Controls cells (Ci) were infected with scrambled shRNA lentiviral particles. Knockdown of Grb2 and Plcγ1 in surviving cells was confirmed by western blot. Cells were serum starved overnight prior to stimulation with FGF9 for 30 min.

Western Blot Analysis, and inhibitors

Western blot analysis method is the same as that of the previos chapter. Antibodies utilized are also mentioned in the "Methods" section of the previous chapter. Additional reagents used in this part were purchased as follows: Plc inhibitor U73122 (Sigma Aldrich); and Plcγ1 shRNA (catalog no. sc-29452-v) (Santa Cruz Biotechnology, Inc); phalloidin (catalog. no: 8953) (Cell Signaling Technology).

In vitro Plcγ1 Reconstitution Assay to Measure [^{3}H] PI(4,5)P_2 Hydrolysis.

Synthetic 1,2-dioleoyl-sn-glycero-3-phosphoethanolamine, 1,2-dioleoyl-sn-glycero-3-phospho-L-serine, and 1,2-dioleoyl-sn-glycero-3-phospho-(1'-myo-inositol-4',5'-bisphosphate) (100 µg of each) (Avanti Polar Lipids) were combined in chloroform:methanol (2:1) in a molar ratio of 1:1:1 with 0.6 µCi of [2-^{3}H(N)] PtdIns (4,5)P_2 (Perkin Elmer Life Science). Mixed phospholipid vesicles were created by drying the mixture under vacuum using a Savant Speed Vac Concentrator, resuspending the dried lipid mixture, and dispersing on ice by sonication using a probe sonicator at amplitude 15% for 1 min (Branson Digital Sonifier) in 1 ml of 20 mM Hepes pH 7.4, 20 mM NaCl, 4 mM EGTA, 8 mM $MgCl_2$, 220 mM KCl, and 0.15 mM $CaCl_2$. Sodium cholate was added to achieve a final concentration of 0.1% and dissolved by vortexing. To perform the assay, a radiolabeled substrate was provided as mixed phospholipid vesicles (100 µl), which were complemented with cholate (as described above) and combined with an equal volume of cell lysate. The purified proteins were utilized in experiments to determine enzyme activity and potential regulation by kinase dead FGFR2, Grb2, and Plcγ1CSH3 (100 µl). Full-length Plcγ1 was purchased from EMD Millipore. Cell lysates were derived from HEK293T cells. Assays were performed for 2 h at 37°C and terminated by the addition of 0.75 ml of chloroform/methanol/HCl (20:40:1), followed by the addition of 0.25 ml chloroform and 0.25 ml of 0.1 M HCl. Samples were vigorously vortexed for 1 min and then centrifuged for 1 min.

Aliquots (100µl) of the upper aqueous (containing the PIP_2 hydrolysis product IP_3) and bottom (containing the Plcγ1 substrate PIP_2) phases were collected, dried on GF/F glass microfiber filter, quantitated by liquid scintillation spectrometry, and normalized to protein concentration. To demonstrate that other proteins were not involved in the phospholipid turnover in our study, controls consisting of buffers and purified proteins were assayed for PIP_2 turnover (**Fig 3.1**).

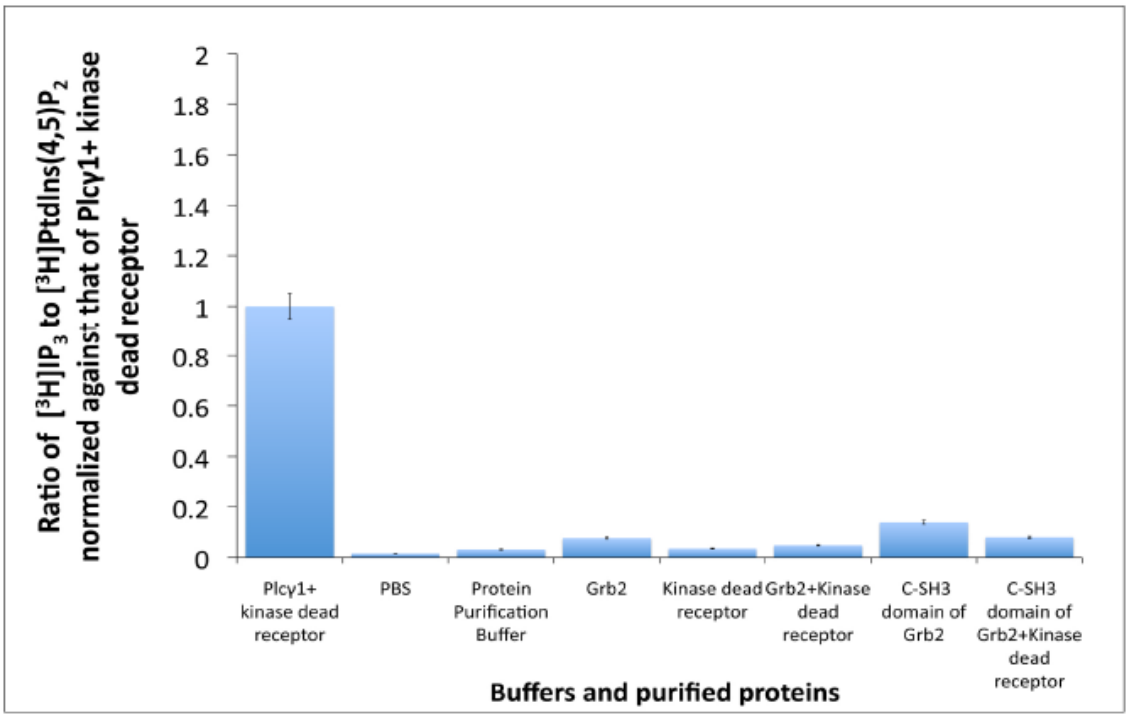

Fig 3.1 Controls for phospholipase *in vitro* reconstitution assays. The ratio of $[^3H]IP_3$ to $[^3H]PIP_2$ was determined and normalized to Plcγ1 plus kinase dead receptor. Values shown represent the mean ± standard deviation of three independent experiments.

Assay of Plcγ1 Activity in Whole Cells

Cellular Plcγ activity was estimated from the measurement of the steady-state level of PIP_2 in [^{3}H]myo-inositol uniformly radiolabelled cells because the PI3K pathway utilizes only a very small fraction of the $PI(4,5)P_2$ pool compared with that hydrolyzed by Plc, and the contribution of reutilization of dephosphorylated [^{3}H]inositol released from PIP_2 is negligible (43).

To measure cellular amounts of phosphoinositides, HEK293T cells were pre-labeled with myo-[2-^{3}H(N)]inositol (1 μCi/ml) (Perkin-Elmer) for 24 h in inositol-free, FBS-free DMEM medium. Cells were then incubated for 30 min with 20 ng/ml FGF9 and washed with PBS. After labeling, cells were harvested, washed, and subjected to lipid extraction and thin layer chromatography (TLC) analysis.

Lipid Extraction and TLC Analysis

Lipid extraction and TLC analysis was performed using the Bligh Dyer method (44) with some important modifications. The HEK293T cell pellet was resuspended in 0.2 ml of 0.5 M NaCl in 0.1 M HCl, and then 0.6 ml of chloroform:methanol (1:2) was added and vigorously vortexed for 30 min. An additional 0.2 ml of 0.5 M NaCl in 0.1 M HCl was added and vortexed for 10 min. After a 5-min centrifugation in an Eppendorf Table Centrifuge, the upper water-methanol phase (containing IP_3) was discarded, and the lower chloroform lipid phase (containing PIP_2) was carefully transferred to a new eppendorf tube. The lipid extract (10 ml) was dried on a GF/F glass microfiber filter and counted

in a scintillation counter. Lipid extracts were immediately analyzed by TLC. To ensure that the same volumes were used in the TLC analysis, the 25,000 cpm aliquots were diluted with chloroform when necessary. Prior to silica gel TLC analysis, $PI(4,5)P_2$ and $PI(3,5)P_2$ were separated by one-dimensional TLC on potassium oxalate-impregnated silica gel plates using a highly polar solvent system containing chloroform/methanol/ammonium hydroxide/water (57:50:4:11, vol/vol/vol/vol) (45). High-performance Partisil LK5 silica gel-precoated TLC plates (20 cm) with a concentration-zone (Whatman Inc. Clifton, NJ) were impregnated for 1 min in 1.2 % (wt/vol) potassium oxalate in methanol-water (2:3). After air drying for 15 min, the plates were desiccated at 100°C for 60 min before use. Radiolabeled lipids were visualized and quantified using a Personal Molecular ImagerTM FX (Bio-Rad Laboratories). Stored images were processed and quantified using Quantity One software for scanning and analysis of the captured Phosphor images (Bio-Rad Laboratories). Phospholipid content was expressed as mol% of total phospholipid based on the pixel intensity of the captured signal on Phosphor screen generated by the radiolabeled spots on the TLC plate. Phospholipids were identified based on their retardation factor (R_f) using different phosphoinositides as standards.

Intracellular Calcium

The intracellular calcium concentration was measured with use of the Fura-2AM fluorescent indicator. Data was obtained as described previously (46,47).

Briefly, HEK293T cells were incubated with 5μM Fura-2AM (Calbiochem) at room temperature for 1 h in the dark and washed with MBSS solution (140mM NaCl, 5.4mM KCl, 0.5 mM $MgCl_2$, 0.4 mM $MgSO_4$, 3.3 mM $NaHCO_3$, 2 mM $CaCl_2$, 10 mM HEPES, and 5.5 mM glucose at pH 7.4). Imaging was performed with use of an InCyt Im Imaging workstation (Intracellular Imaging, Inc.), Nikon Eclipse TS 100 inverted microscope, and a 12-bit CCD camera (Pixel Fly, Cooke). Fura-2-loaded cells were excited alternately at 340 and 380 nm, and the fluorescence emission at 510 nm was measured. The F340/F380 emission ratio was used as an index of intracellular calcium.

For each experiment, the responses of 20-30 cells were monitored and their fluorescence emission ratios averaged at the end of recording. Ratios were converted to an intracellular calcium concentration ($[Ca^{2+}]i$) using the equation: $[Ca^{2+}]i = K_d\beta(R-R_{min})/(R_{max}-R)$, where K_d is the Ca^{2+} dissociation constant of Fura-2, β is the ratio of the fluorescence emission intensity of 380 nm excitation in Ca^{2+}-depleting and Ca^{2+}-saturating conditions, R is the ratio at any time, R_{min} is the minimum ratio in Ca^{2+}-depleting conditions (measured in the presence of 0 mM extracellular Ca^{2+}, 5 μM EGTA, and 2 μM ionomycin), and R_{max} is the maximum ratio in Ca^{2+}-saturating conditions (measured in the presence of 10 mM extracellular Ca^{2+} and 2 μM ionomycin)(51).

Wound Healing Assay

HEK293T Ci, G2i, and Pγi cells were left untreated or transiently transfected with the appropriate construct. Briefly, cells were seeded into a 12-well plate

until they reached full confluency. After overnight serum starvation, the surface of the cells was scratched with a pipette tip. Cells were washed three times with PBS and then incubated in 1% serum for 6 h with or without U73122 (for Ci and G2i cells). Images were taken using a confocal microscope (model SP5; Leica) after 0 h and 6 h. The average distance traveled by the cells between six arbitrarily chosen points along the wound was quantified in three independent experiments. The percentage of wound closure was calculated in each experiment and normalized to that of controls. Values are presented as the mean ± standard deviation.Differences in the percentage of wound closure were evaluated using theStudent's t-test.

Invasion Assay

Matrigel Invasion Chambers in two 24-well plates with 8.0 μm pores were purchased from BD Biosciences. Briefly, cells were counted via a hemocytometer using trypan blue to exclude dead cells. Following rehydration of the chambers, 5 x 10^4 cells in 0.5 ml serum-free medium were seeded into the upper chamber. Serum-containing (1%) medium (0.75 ml) was added to the lower chamber. After incubation for 6 to 24 h in a humidified incubator at 37°C with 10% CO_2, non-invasive cells were scraped off the membrane with cotton swabs, and invasive cells were fixed and stained using the Hema 3 Stat Pack (Fisher Scientific). After drying, membranes at the bottom of each chamber were pealed, mounted onto a slide with mounting buffer (0.1% p-phenylenediamine/75% glycerol in PBS), and covered with a glass cover slip.

Images were taken using a Leica inverted microscope. The number of invasive cells were counted in four different microscopic fields and are presented as the mean ± standard deviation of triplicate samples. Differences in the number of invasive cells were compared using the Student's t-test. It is important to note that metastatic LoVo cells exhibit slower growth and migratory properties compared with HEK293T cells. Also, ROS cells were larger in size and hence, the number of cells counted per field was lower. Therefore, relative comparisons of invasion were not performed between cell lines.

Flow Cytometry and Imaging of Actin Polymerization

HEK293T Ci and G2i cells were seeded in 6-well plates at equal confluency. Serum-starved cells were detached and treated with 1% serum to detect any early signaling related to changes in actin polymerization. Cells were then detached again with versene (Lonza), suspended in DMEM, and centrifuged for 5 min at 1000 rpm. The supernatant was aspirated, and the pellet was suspended in 1 ml of cold PBS. Cells in suspension were then pipetted with gentle vortexing into 2.5 ml of pure ice cold-ethanol to achieve a final ethanol concentration of 70%. Suspended cells were incubated at -20°C overnight. Cells were pelleted at 1500 rpm for 5 min and incubated in 500 µl phalloidin solution diluted in PBS containing 0.05% Triton X-100, and 0.1 mg/ml RNase for 60 min at 37°C.The solution was transferred to a 5-ml round bottom polystyrene tube for flow cytometry. The Gallios Flow Cytometer (Beckman Coulter) was used. GFP^-/$phalloidin^-$, GFP^+/$phalloidin^-$, and GFP^-/$phalloidin^+$ cells

were used as controls, and GFP^+/$phalloidin^+$ cells were gated. The geometrical Y-mean value was used as a measure of actin polymerization. Values were normalized to control cells and presented as the mean ±standard deviation of triplicate samples.

For actin imaging, detached cells in 1% serum on coverslips were fixed with paraformaldehyde, permeabilized, blocked as previously described, and treated with Hoescht for 15 min at a dilution of 1:10,000. Cells were then washed with PBS, incubated with phalloidin solution, mounted onto coverslips, and imaged using aconfocal microscope (model SP5; Leica).

Data Base Analysis

All analyses were performed in R (version 3.0.1) (http:///www.r-project.org/). Clinical information was downloaded, and CEL (Affymetrix U133Plus2) array files supplied with the paper from reference 48. justRMA was used to compute expression values.

Clinical information and level2 Affymetrix (Affymetrix U133 Array Plate Set) gene expression data publicly available from the Cancer Genome Atlas Project (TCGA; http://tcga-data.nci.nih.gov/) for ovarian serous cystadenocarcinoma were also downloaded. Homogeneity between cohorts is important for valid comparisons. Therefore, tumors of low malignant potential, non-serous tumors, and tumors other than ovarian or peritoneum were excluded. Samples from patients who received chemotherapy were also excluded.

For each cohort (TCGA, reference 48), the relationship between FGFR2/Plcγ1/Grb2 expression and overall survival was evaluated. To do this, patients were grouped into percentiles according to mRNA expression. The Log-rank test was employed to determine the association between mRNA expression and survival, and the Kaplan-Meyer method was used to generate survival curves. Cut-off points to significantly split (log-rank test p-value <0.05) the samples into low/high mRNA groups were recorded. The cut-off to optimally separate the patients in both data sets (smallest p-value in each of the cases) was chosen. In each cohort, we added second and third expression levels to gain further insight into the association between FGFR2/Plcγ1/Grb2 expression and overall survival.Therefore,in the second expression level, the cohort was divided into four groups according to low/high gene1 expression and low/high gene2 expression.To do this,the optimal cut-off levels for gene1 and gene2 were determined as described above.Survival rates between the low FGFR2/high Plcγ1 and high FGFR2/low Plcγ1 groups were compared with the low FGRF2/low Plcγ1 and high FGRF2/high Plcγ1. Similar comparisons were made for the FGFR2/Grb2 groups. Larger differences in median survival times were observed when the expression levels of two genes was included in the analysis instead of single gene expression. Furthermore, significantly larger differences in median survival times were observed with the addition of the third expression level compared with the second expression level.

Results

Competition between Plcγ1 and Grb2 dictates signaling response

To demonstrate the competition between Grb2 and Plcγ1 in non-stimulated conditions, HEK293T Ci and G2i cells were transfected with 0.5 µg of HA-Plcγ1 or left untransfected (**Fig 3.2a**) and serum starved overnight. Cell lysates were obtained and incubated with radioactive substrate either for 2 h (**Fig 3.2b**) or overnight (**Fig 3.2c**). In Ci cells, an increase in Plcγ1 lipase activity was observed with increased Plcγ1 expression, suggesting that Plcγ1 can displace Grb2 from FGFR2 binding (**Fig 3.2b**). Increased expression of Plcγ1 in the absence of Grb2 also increased phosphoinositide turnover, presumably due to the additional availability of FGFR2 for complex formation with Plcγ1.

In a similar experiment, the competitive binding between Plcγ1 and Grb2 was demonstrated under non-stimulated conditions in Grb2-overexpressing cells (**Fig 3.2c**). As expected from previous experiments, G2i cells showed elevated IP_3 production compared with Ci cells (**Fig 3.2d**). Increasing the expression of Grb2 (0.5 µg and 1 µg plasmid) in G2i cells resulted in Grb2-mediated displacement of Plcγ1 bound to FGFR2 with a concomitant reduction in IP_3: PIP_2 ratio. These findings highlight that the concentration-dependent competition between Grb2 and Plcγ1 for FGFR2 binding controls basal cellular phospholipase activity.

a

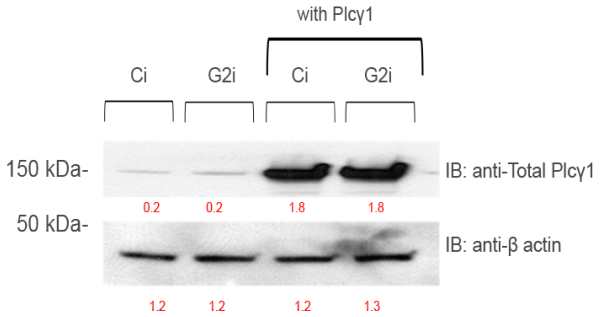
with Plcγ1
Ci
G2i
Ci
G2i
150 kDa-
IB: anti-Total Plcγ1
0.2
0.2
1.8
1.8
50 kDa-
IB: anti-β actin
1.2
1.2
1.2
1.3

b

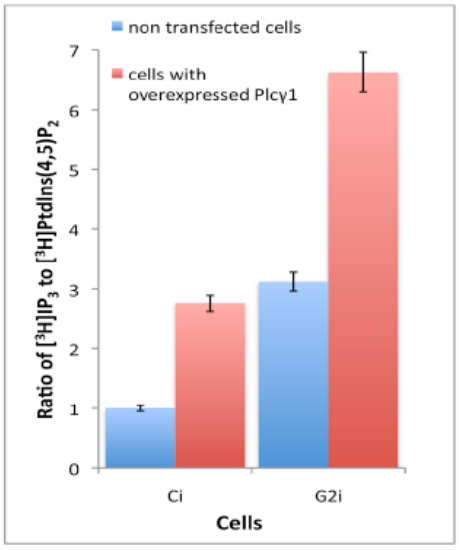
non transfected cells
cells with overexpressed Plcγ1
Ratio of [3H]IP3 to [3H]PtdIns(4,5)P2
0
1
2
3
4
5
6
7
Ci
G2i
Cells

c

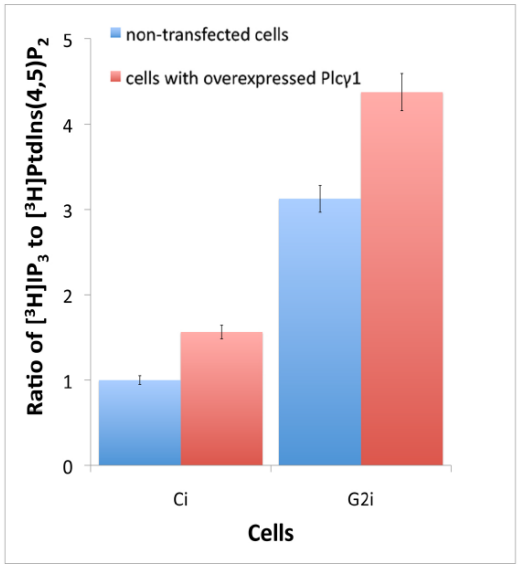
non-transfected cells
cells with overexpressed Plcγ1
Ratio of [3H]IP3 to [3H]PtdIns(4,5)P2
0
1
2
3
4
5
Ci
G2i
Cells

d

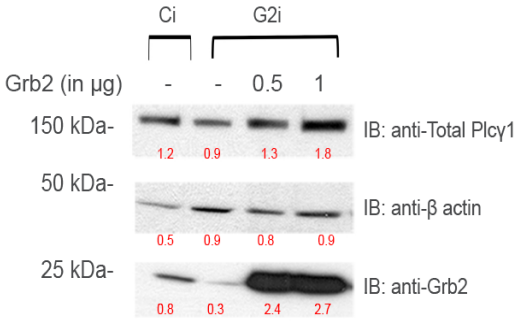
Ci
G2i
Grb2 (in µg)
-
-
0.5
1
150 kDa-
IB: anti-Total Plcγ1
1.2
0.9
1.3
1.8
50 kDa-
IB: anti-β actin
0.5
0.9
0.8
0.9
25 kDa-
IB: anti-Grb2
0.8
0.3
2.4
2.7

e

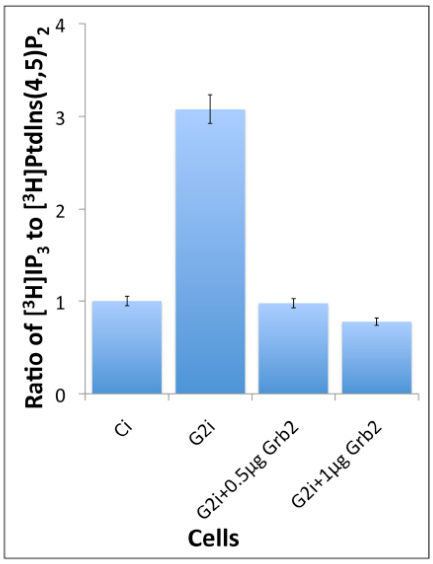

Fig 3.2 Competition between Plcγ1 and Grb2 dictates signaling response. **a**) HEK293T Ci and G2i cells were either left untransfected or transfected with 0.5 µg of Plcγ1 and serum starved overnight. Cell lysates were obtained, andthe expression of total Plcγ1 and β-actin (loading control) was determined by western blot. **b**) Phospholipase assay was done to determine the ratio of $[^3H]IP_3$ to $[^3H]PtdIns(4,5)P_2$ (PIP_2) in untransfected and HA-Plcγ1-transfected HEK293T Ci and G2i cells. Cells were incubated with $[^3H]PtdIns(4,5)P_2$ substrate for 2 h. Values shown represent the mean ± standard deviation of three independent experiments.**c**) Phospholipase assay was performed on untransfected and HA-Plcγ1-transfected serum-starved HEK293T Ci and G2i cells that were incubated with $[^3H]PtdIns(4,5)P_2$substrate for 24 h.The ratio of $[^3H]IP_3$ to $[^3H]PtdIns(4,5)P_2$ was calculated after scintillation counting. Values shown represent the mean ± standard deviation of three independent experiments. **d**) Serum-starved HEK293T Ci cells were left untransfected andG2i cells were either untransfected or transfected with increasing amounts of myc-tagged Grb2 (0.5 µg and 1 µg). Cell lysates were obtained and western blot analysis was performed to determine the expression of Grb2 and the loading controls total Plcγ1 and β-actin.**e**) Grb2 downregulates Plcγ1 activity. Cellular phospholipase assay was used to determine the activity of Plcγ1 in untransfected and myc-Grb2-transfected G2i HEK293T cells (0.5 µg and 1 µg). Five independent measurements were made for each experiment. The data was normalized to control cells, and normalized data were used to calculate the standard deviation.

Plcγ1 is constitutively active upon FGFR2 binding

To establish whether Plcγ1 recruitment to FGFR2 is sufficient to promote enzyme activity, the steady-state level of PIP_2 substrate was determined in HEK293T Ci and G2i cells. To do this, cells were incubated overnight under serum starvation conditions with radioactive myo-[2-^{3}H] inositol. Lipids were extracted, separated, and identified by TLC. Quantification of TLC bands showed that PIP_2 concentration was ~50% lower in G2i cells compared with Ci cells (**Fig 3.3a**). Therefore, a higher concentration of PIP_2 was turned over in the absence of Grb2 under non-stimulated conditions. We confirmed this observation by measuring phosphoinositide turnover in total cell lysates of equal protein concentration prepared from Ci and G2i cells incubated with radiolabeled PIP_2 for 2 h. After phase separation, the IP_3 product and remaining PIP_2 substrate were quantified using scintillation counting, and the IP_3 to PIP_2 ratio was calculated (**Table 3.1**). In the G2i background, a dramatic increase in phospholipase activity as measured by PIP_2 turnover was observed in the non-stimulated state (**Fig 3.3b**).

Further confirmation of the constitutive upregulation of Plcγ1 activity in the absence of Grb2 was provided by the dramatic increases in basal $[Ca^{2+}]i$ and F340/F380 emission ratio in G2i cells compared with Ci cells (**Fig 3.3c**). Basal $[Ca^{2+}]i$ was increased approximately five-fold and 2.5-fold in G2i cells compared with Ci cells, respectively ($[Ca^{2+}]i$,~55 nM vs. ~250 nM; F340/F380 ratio, 0.2 vs. 0.5; **Fig 3.3d**). Addition of ionomycin (a Ca^{2+} ionophore) resulted in the expected increase in calcium concentration, which confirmed that the cells were

functional (see arrows **Fig 3.3c,e**). The low $[Ca^{2+}]$I in parental HEK293T cells, which have negligible FGFR2 expression, demonstrated that the increasein Plcγ1 activity was due to FGFR2 recruitment and not to non-specific binding to the lipid membrane (**Fig 3.3e,f,g**). Furthermore, overexpression of HA-Plcγ1 in parental cells failed to increase $[Ca^{2+}]$i to the levels observed in the presence of FGFR2 in G2i cells (**Fig3.3e,f**).

a

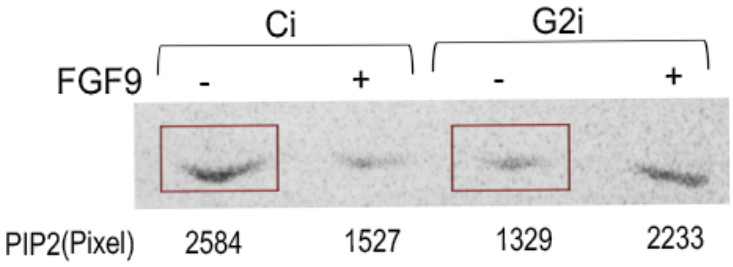
Ci
G2i
FGF9
-
+
-
+
PIP2(Pixel)
2584
1527
1329
2233

b

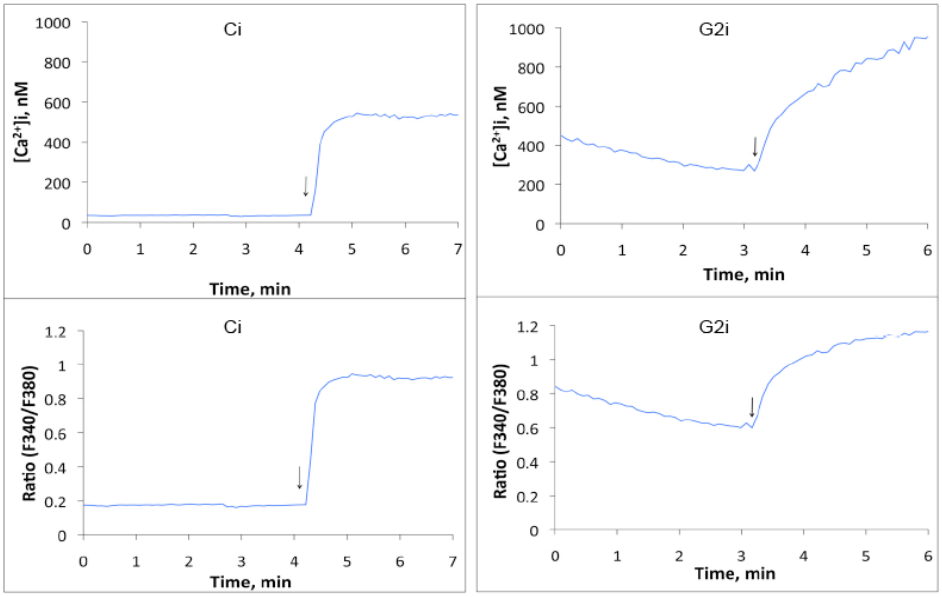
Ci
G2i
[Ca2+]i, nM
Ratio (F340/F380)
Time, min

c

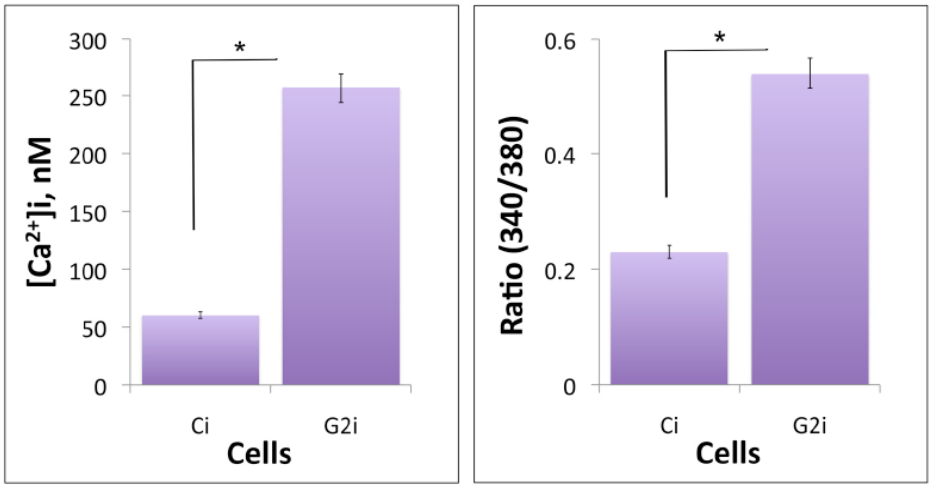
[Ca2+]i, nM
Ratio (340/380)
Ci
G2i
Cells
*

d

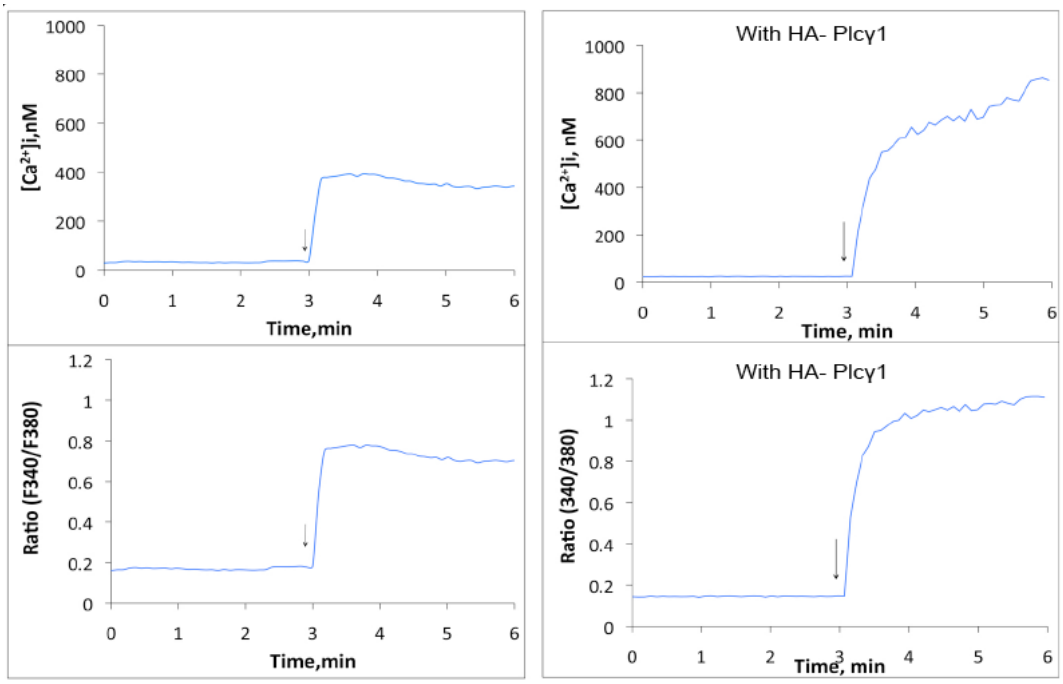
[Ca2+]i,nM
Time,min
With HA- Plcγ1
[Ca2+]i, nM
Time, min
Ratio (F340/F380)
Time,min
With HA- Plcγ1
Ratio (340/380)
Time, min

e

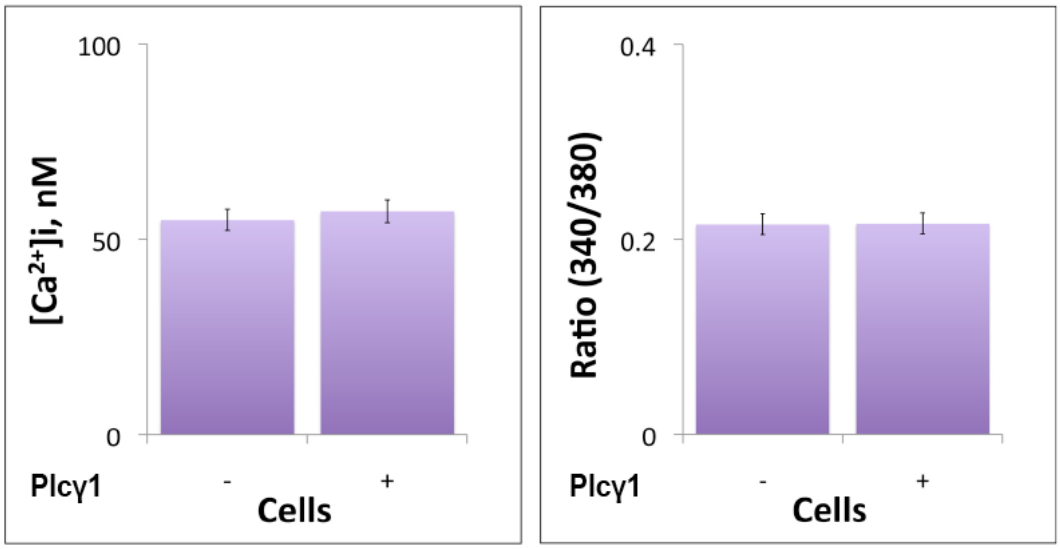
[Ca2+]i, nM
Plcγ1
-
+
Cells
Ratio (340/380)
Plcγ1
-
+
Cells

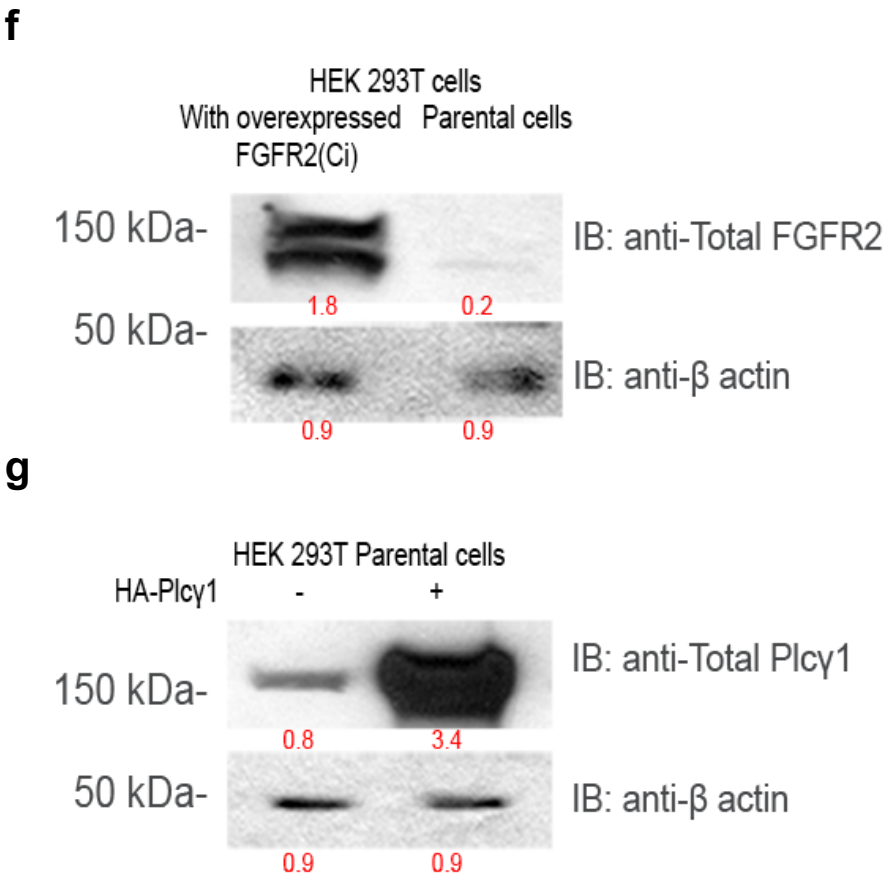

Fig 3.3 Plcγ1 is constitutively active in the absence of Grb2.a) HEK293T Ci and G2i cells were labeled with radioactive myo-[2^{-3}H]inositol overnight and then serum starved. Cells were left untreated or stimulated with FGF9. Lipids were extracted, separated by TLC, and PIP_2 and PIP_3 were identified. PIP_2 bands are shown. **b**) HEK293T Ci and G2i cells were loaded with Fura 2-AM. [Ca^{2+}]i, and F340/F380 emission ratio were plotted after calibrating the measurements to detect their specificity and sensitivity for Fura 2-AM. Ionomycin was added to detect effective transfer of Ca^{2+} across cell membranes. Arrows indicate the timepoint of ionomycin addition. **c**) [Ca^{2+}]i and F340/F380 emission ratio were determined from 0 to 2 min in Ci and G2i cells. Values shown represent the mean ± standard deviation of three independent experiments.*Student's t-test (p value ≤ 0.05). **d**) Parental HEK293T cells, which have low endogenous FGFR2 expression, were left untreated or transfected with 0.5 µg of Plcγ1. Cells were loaded with Fura 2-AM, and [Ca^{2+}]i and F340/F380 ratio were plotted. Arrows indicate the timepoint of ionomycin addition. **e**) [Ca^{2+}]i and F340/F380 ratio from 0 to 2 minutes were determined in parental cells. Values shown represent the mean ± standard deviation of three independent experiments. **f**) Western blot was performed on cell lysates from Ci cells and parental HEK293T cells to show the negligible level of FGFR2 expression in parental cells (upper panel). **g**) Western blot showing the efficiency of HA-Plcγ1 transfection in serum-starved parental cells (lower panel). The expression of total FGFR2, total Plcγ1, and β-actin in **f**) and **g**) was determined in non-transfected and HA-Plcγ1-transfected parental cells.

a

Example of counts obtained with cell lysates (2 hours incubation)	Ci	Ci + U73122	Ci + HA-Plcγ1	Ci + DM	Ci + TM	G2i	G2i + U73122	G2i + HA-Plcγ1	G2i + DM	G2i + TM	G2i + 0.5 µg Grb2	G2i + 1 µg Grb2
CPM in upper phase ($[^3H]IP_3$)	229	94	201	186	201	236	98	325	250	1224	118	57
CPM in lower phase ($[^3H]$Ptdlns(4,5)IP_2	1952	1581	704	323	499	616	507	320	265	1603	513	745
Ratio	0.11	0.05	0.28	0.57	0.40	0.38	0.19	1.01	0.94	0.76	0.23	0.07
Released($[^3H]IP_3$) in pmol	0.38	0.16	0.34	0.31	0.34	0.40	0.16	0.55	0.42	2.07	0.20	0.096

b

Example of counts obtained with purified proteins (2 hours incubation)	PBS	Potein purification buffer	Grb2	C-SH3 domain of Grb2	Kinase dead receptor	Grb2+ Kinase dead receptor	C-SH3 domain of Grb2 + Kinase dead receptor	Plcγ1 + Kinase dead receptor	Plcγ1 + Kinase dead receptor+ Grb2	Plcγ1 + Kinase dead receptor + C-SH3 domain of Grb2
CPM in upper phase($[^3H]IP_3$)	370	174	544	130	341	99	170	1117	886	212
CPM in lower phase($[^3H]$Ptdlns (4,5)IP_2	4808	4333	4069	747	3554	1978	1000	2254	3306	632
Ratio	0.07	0.04	0.13	0.17	0.07	0.05	0.17	0.49	0.27	0.33
Released($[^3H]IP_3$) in pmol	0.62	0.29	0.92	0.22	0.58	0.17	0.28	1.89	1.50	0.36

Table 3.1 Examples of the upper phase and lower phase counts (prior to averaging) from the 2-h lipase assay in a) cell lysates and b) purified proteins. The calculated ratio of $[^3H]IP_3$ to $[^3H]$Ptdlns(4,5)$P_2$and $[^3H]IP_3$ release in pmol are shown. $[^3H]IP_3$ release was calculated based on the initial cpm value of substrate used and converted to pmol: (cpm of $[^3H]$ IP_3 x 7.5)/4415.

Grb2 knockdown results in Plcγ1 recruitment to FGFR2 and positively regulates Plcγ1 activity in the non-stimulated state. We showed that these events are mutually dependent by adopting an *in vitro* reconstitution assay to assess whether the binding of isolated Plcγ1 to FGFR2 can activate phospholipase

PIP_2 turnover in the presence and absence of Grb2. To ensure that the receptor and Plcγ1 remained unphosphorylated, a kinase dead FGFR2 ($FGFR2_{KD}$) was generated by K517I point mutation. Unphosphorylated Plcγ1 and $FGFR2_{KD}$ (10 μM) were incubated for 2 h with radioactive PIP_2, and the ratio of IP_3 to PIP_2 was calculated (**Fig 3.4a**). In the presence of $FGFR2_{KD}$, Plcγ1 exhibited a high level of *in vitro* phospholipase activity. Addition of either Grb2 or Grb2CSH3 to the Plcγ1 and $FGFR2_{KD}$ mixture significantly reduced phospholipase activity (**Fig 3.4a**).This strongly suggested that the binding of Plcγ1 to unphosphorylated FGFR2 is sufficient to upregulate phospholipase activity and that Grb2 inhibits this interaction.

To show that the increase in phospholipase activity is independent of Plcγ1 phosphorylation, lipid turnover was measured in two Plcγ1 mutants: Plcγ1TM, all tyrosines in the X/Y linker region (Y771F, Y775F, Y783F) and C-terminal (Y977F, Y1253F) were mutated to phenylalanine (**Fig 3.4b**) and Plcγ1DM, both SH2 domains were disabled with R586A and R694A mutations (**Fig 3.4b**). Overexpression of both Plcγ1TM and Plcγ1DM increased phospholipase activity (**Fig 3.4c**).

a

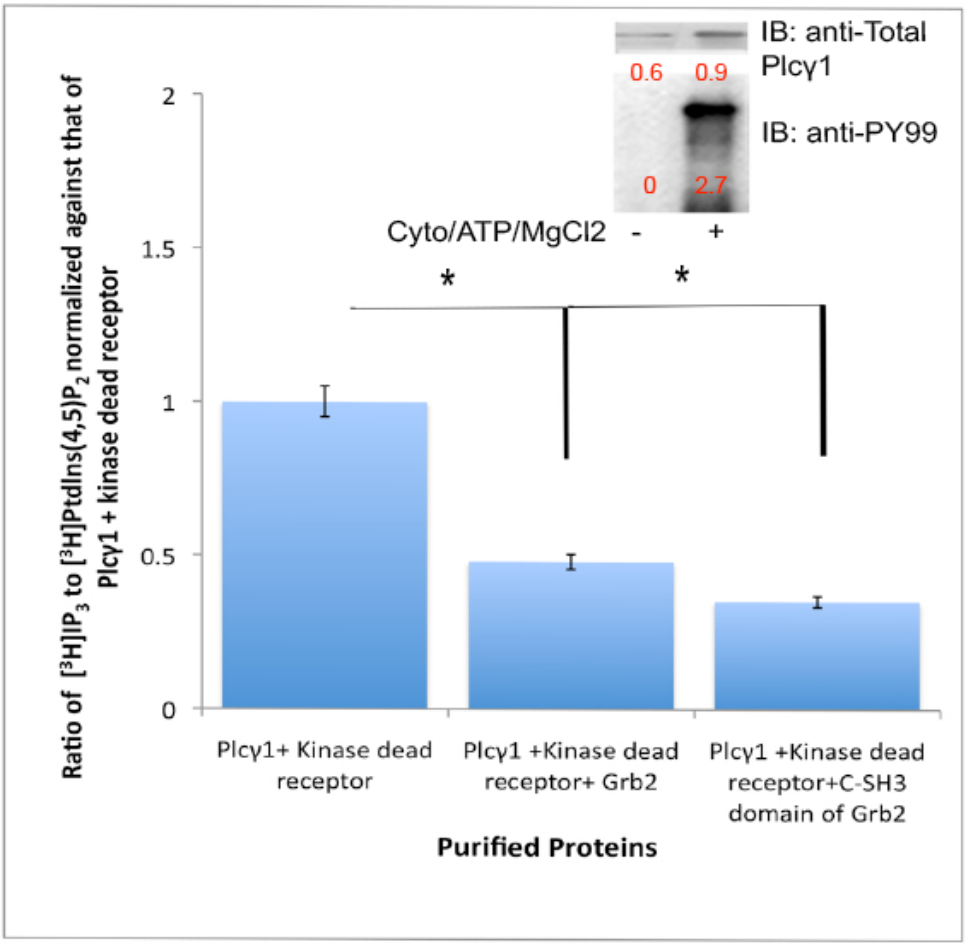
IB: anti-Total Plcγ1
IB: anti-PY99
0.6
0.9
0
2.7
Cyto/ATP/MgCl2 - +
*
*
Ratio of [³H]IP₃ to [³H]PtdIns(4,5)P₂ normalized against that of Plcγ1 + kinase dead receptor
2
1.5
1
0.5
0
Plcγ1+ Kinase dead receptor
Plcγ1 +Kinase dead receptor+ Grb2
Plcγ1 +Kinase dead receptor+C-SH3 domain of Grb2
Purified Proteins

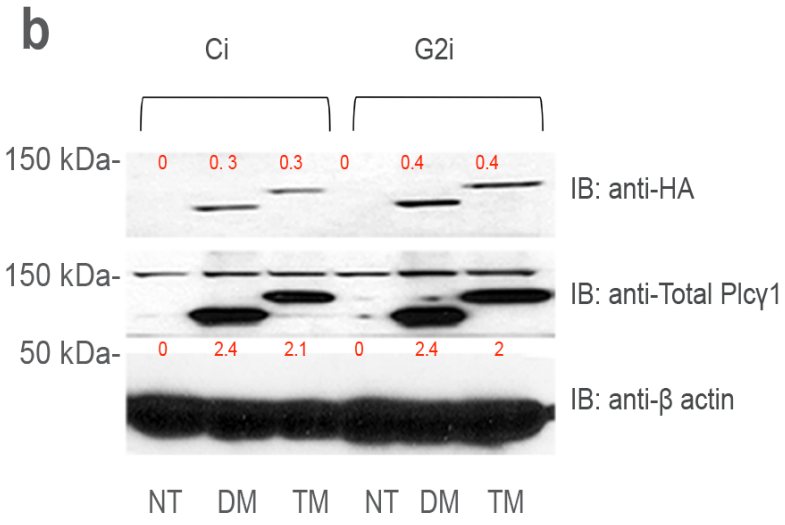
b
Ci
G2i
150 kDa-
0
0. 3
0.3
0
0.4
0.4
IB: anti-HA
150 kDa-
IB: anti-Total Plcγ1
50 kDa-
0
2.4
2.1
0
2.4
2
IB: anti-β actin
NT
DM
TM
NT
DM
TM

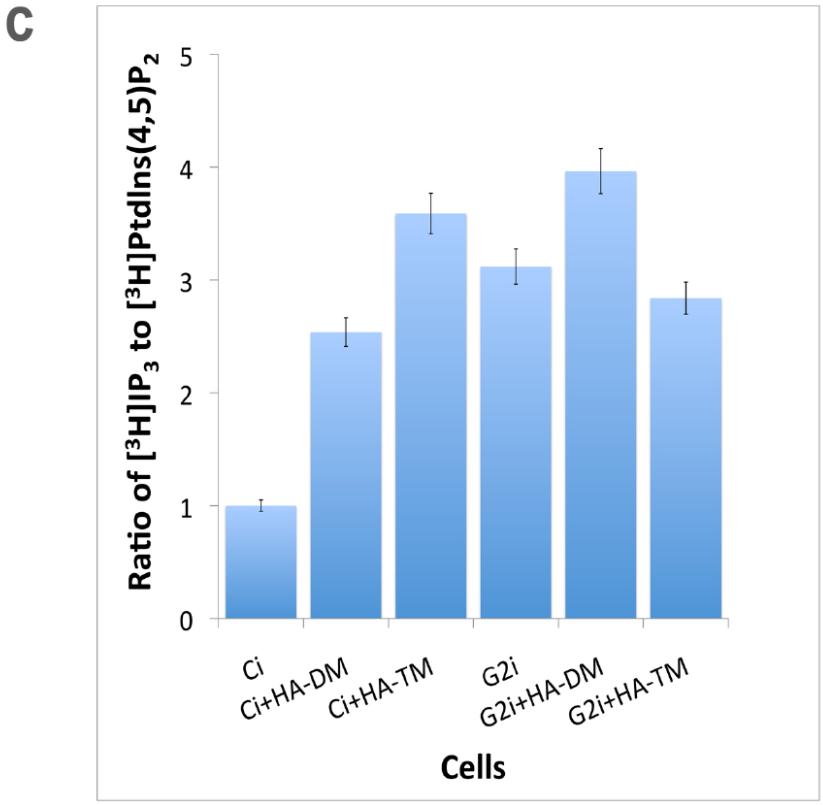
c
Ratio of [3H]IP3 to [3H]PtdIns(4,5)P2
5
4
3
2
1
0
Ci
Ci+HA-DM
Ci+HA-TM
G2i
G2i+HA-DM
G2i+HA-TM
Cells

Fig 3.4 Plcγ1 SH3-mediated phospholipase activity is concentration dependent and phosphorylation independent. a) *In vitro* reconstitution assay showing the inhibitory effect of full-length Grb2 andGrb2CSH2 on Plcγ1 activity. The ratio of [^{3}H]IP_3 to [^{3}H]PIP_2 was computed, and values shown represent the mean ± standard deviation of three independent experiments. *Student's t-test (p value ≤ 0.05). Insert: Western blot demonstrating that the Plcγ1 used in these experiments was unphosphorylated (left lane). Incubation of Plcγ1 with the cytoplasmic portion of FGFR2, ATP, and $MgCl_2$ induced Plcγ1 phosphorylation - positive control (right lane). The blot was probed with anti-pY (showing phosphorylated protein; lower panel) and anti-Plcγ1.**b**) Plcγ1 is active in the absence of phosphorylation and intramolecular SH2 domain interactions. Five point mutations where made in full-length HA-Plcγ1 (Y771F, Y775F, Y783F, Y977F, and Y1253F; TM; http://www.phosphosite.org). Two point mutations were made in the CSH2 and NSH2 of full-length HA-Plcγ1 (R586A and R694A; DM). Serum-starved HEK 293T cells were transiently transfected with DM, TM, or left untransfected (NT). Western blot analysis was done to detect the efficiency of transfection. The membrane was probed with the following antibodies: anti-HA, anti-total Plcγ1, and anti-β-actin (loading control). **c**) Cellular lipase assay was performed on cell lysates obtained from untransfected, DM-transfected, and TM-transfected serum-starved HEK293T cells. [^{3}H]IP_3 to [^{3}H]PtIdIns(4,5)P_2 ratios were normalized tocontrol cells. Error bars represent the standard deviation. Both TM and DM are able to turnover lipid. Elevated concentrations of the Plcγ1 mutants are capable of outcompeting endogenous Grb2 for binding to FGFR2. In G2i cells, the difference in lipid turnover was less dramatic, presumably because the competition for FGFR2 binding is reduced in the absence of Grb2.

Competition between Plcγ1 and Grb2 dictates cell migration and invasion

Previous reports have demonstrated that upregulation of Plcγ1 activity increases cellular motility and metastasis (17). Grb2 and Plcγ1 compete for binding to FGFR2; therefore, in situations where the respective concentrations of the proteins favor Plcγ1 binding, we would expect an increase in cell motility and invasion. We used a wound healing assay to investigate the physiological outcome of the competition between Plcγ1 and Grb2 for FGFR binding. Motility was increased in G2i basal cells compared with Ci basal cells (**Fig 3.5a,b**). A dramatic increase in cell motility in the absence of Grb2 was observed by

monitoring the wound healing assay over a 24-h period using time lapse microscopy (videos are not included in this report). Our findings are consistent with previous reports demonstrating that upregulation of Plcγ1 phospholipase activity in the absence of Grb2 increases cell motility by increasing cellular calcium concentrations (14,49,50). To demonstrate that the competition between Plcγ1 and Grb2 dictates cell migration response, we overexpressed Plcγ1DM in Ci cells. Plcγ1DM is incapable of binding to pY on FGFR2 and, thus any effect of Plcγ1 activity will be due to SH3-mediated recruitment. Cell motility and $[Ca^{2+}]i$ were greater in Plcγ1DM Ci cells than in untransfected Ci cells (**Fig 3.5c,d,e,f**). MTT assay confirmed that cell viability was unaffected by transfection of DM (**Fig 3.5 g**). Ci and G2i cells treated with the phospholipase inhibitor U73122 and HEK293T Pyi cells stably overexpressing FGFR2 induced negligible wound healing capability (**Fig 3.5 h,i**), confirming that the observed wound healing was due to Plcγ1. Also, MTT assay demonstrated that the observed wound healing was not due to reduced cell viability (**Fig 3.5 j**). Plcγ1 knockdown in Pyi cells was confirmed by western blot (**Fig 3.5 k**).

a

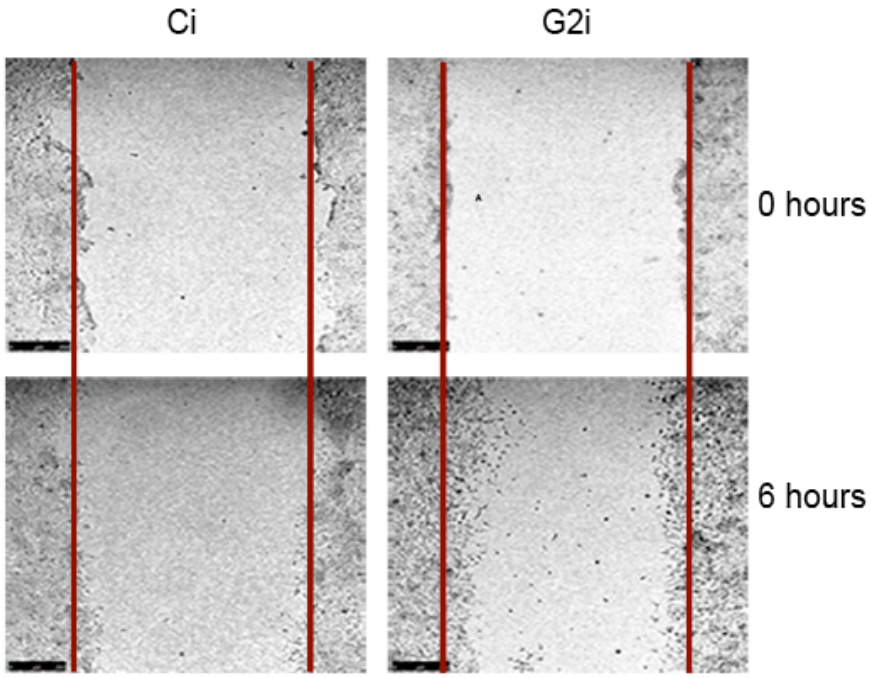
Ci
G2i
0 hours
6 hours

b

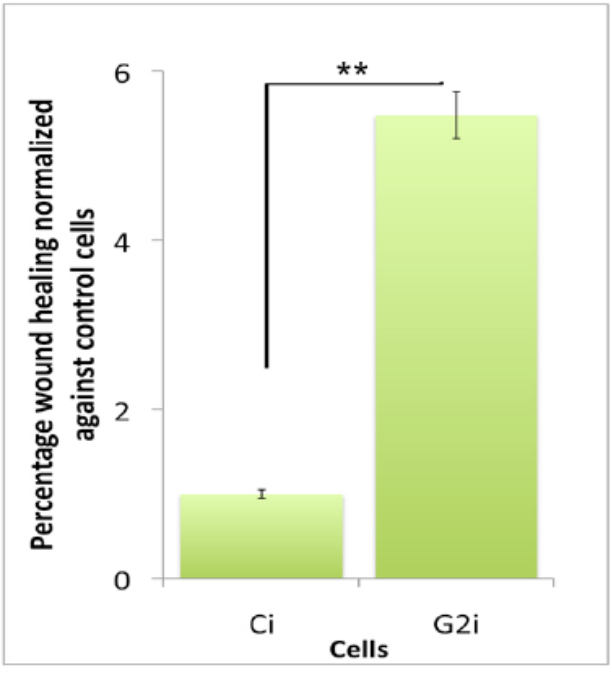
Percentage wound healing normalized against control cells
6
4
2
0
**
Ci
G2i
Cells

c

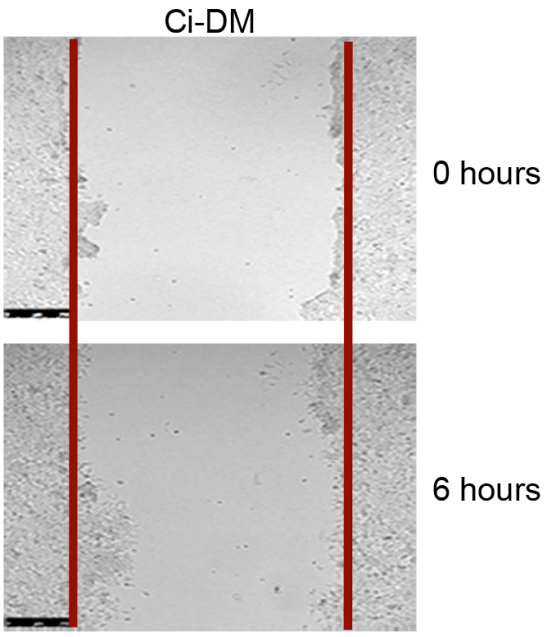
Ci-DM
0 hours
6 hours

d

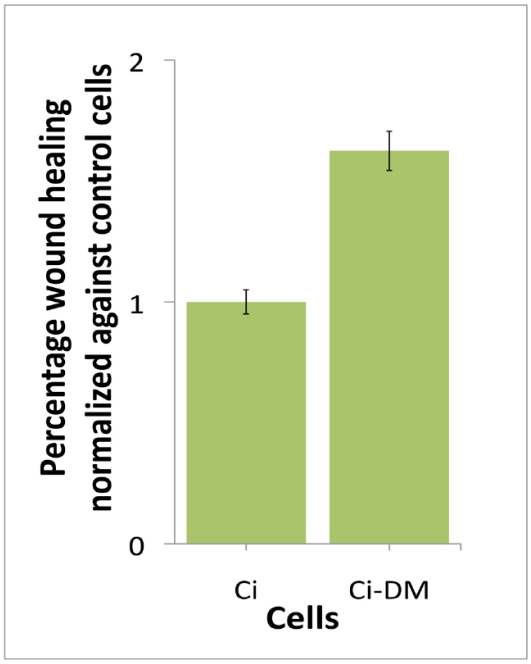
Percentage wound healing normalized against control cells
2
1
0
Ci
Ci-DM
Cells

e

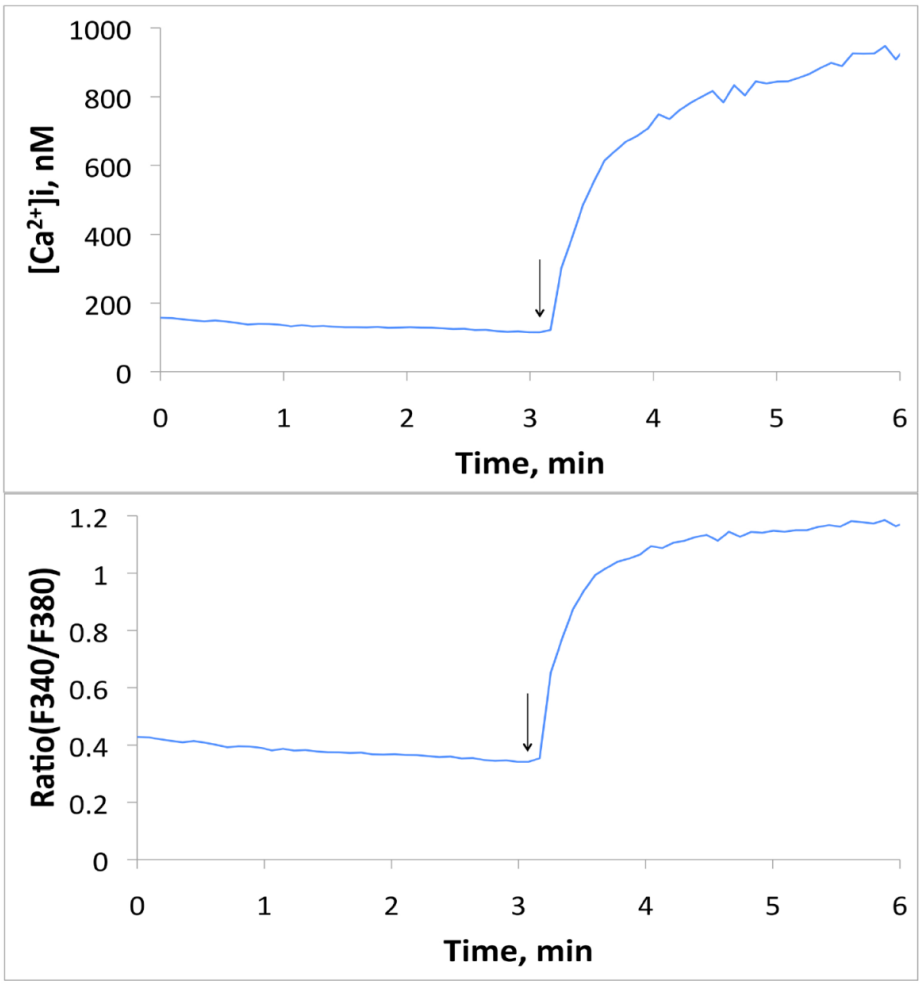
1000
800
600
400
200
0
[Ca2+]i, nM
0
1
2
3
4
5
6
Time, min
1.2
1
0.8
0.6
0.4
0.2
0
Ratio(F340/F380)
0
1
2
3
4
5
6
Time, min

f

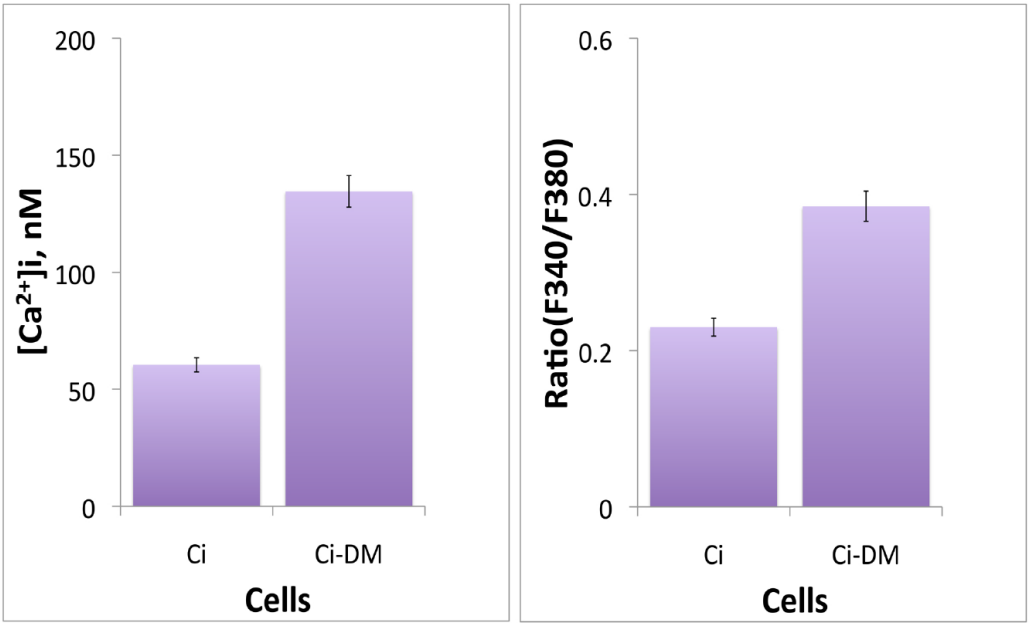
200
150
100
50
0
[Ca2+]i, nM
Ci
Ci-DM
Cells
0.6
0.4
0.2
0
Ratio(F340/F380)
Ci
Ci-DM
Cells

g

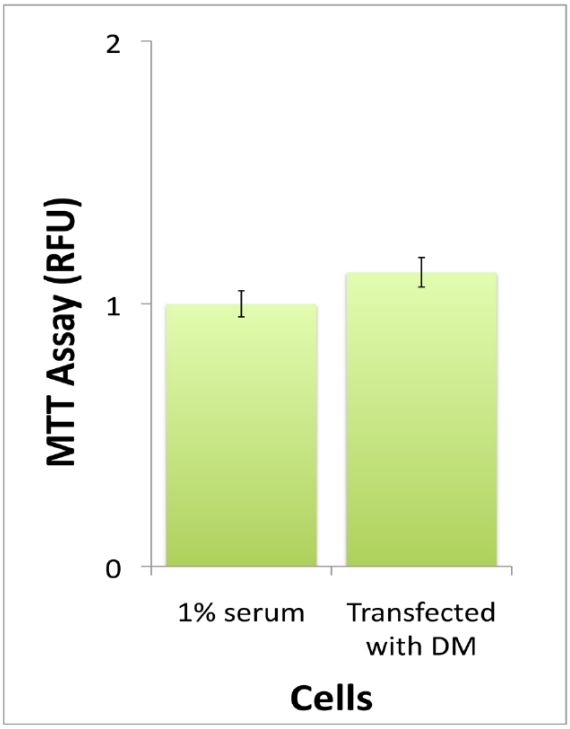
2
1
0
MTT Assay (RFU)
1% serum
Transfected with DM
Cells

h

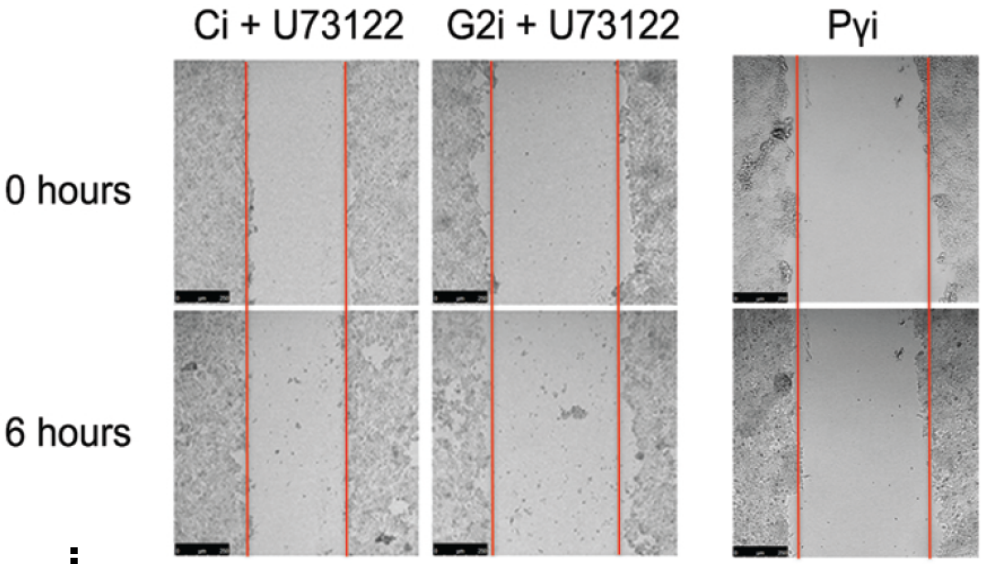
Ci + U73122
G2i + U73122
Pγi
0 hours
6 hours

i

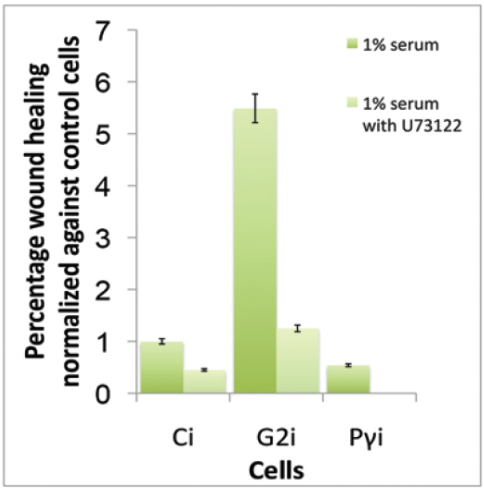
Percentage wound healing normalized against control cells
7
6
5
4
3
2
1
0
1% serum
1% serum with U73122
Ci
G2i
Pγi
Cells

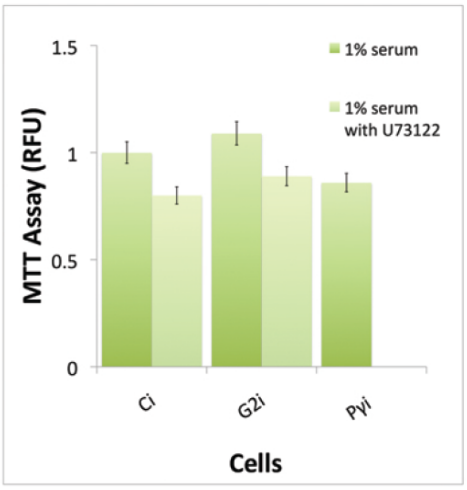
MTT Assay (RFU)
1.5
1
0.5
0
1% serum
1% serum with U73122
Ci
G2i
Pγi
Cells

j

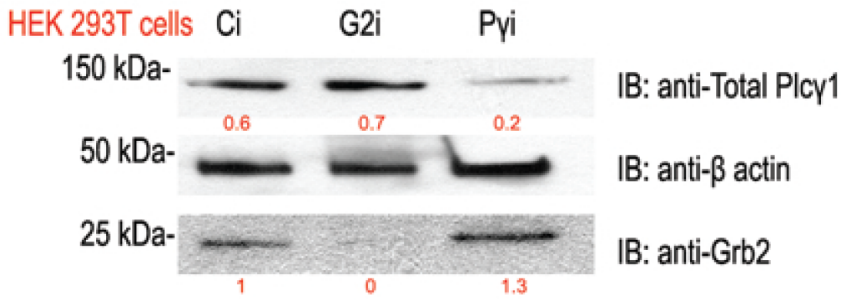

Fig 3.5 Plcγ1 activity increases cell motility in the absence of Grb2. a) Wound healing assays were performed in triplicate on HEK293T Ci and G2i cells treated with 1% serum for 6h. Images were taken at the beginning of the experiment (0 h) and at 6 h. **b**) Distance traveled by HEK293T Ci and G2i cells was quantified in three independent experiments. The percentage of wound closure was calculated, averaged, and normalized against control cells. Values shown represent the mean ± standard deviation. *Student's t-test (p value ≤ 0.01).**c**) Untransfected and DM-transfected Ci cells were used in a scratch wound healing assay. Cells were treated with 1% serum. Images were taken at 0 h and 6 h. **d**) The percentage of wound closure was measured, averaged, and normalized against control cells. Values shown represent the mean ± standard deviation of three independent experiments. **e**) DM-transfected HEK293T Ci cells were loaded with Fura 2-AM in Hanks' buffer, and basal calcium release was determined by measuring $[Ca^{2+}]i$ and F340/380 emission ratios. Ionomycin was added to detect effective transfer of Ca^{2+} across cell membranes. Arrows indicate the time ofionomycin addition. **f**) Calcium release was compared between untransfected and DM-transfectedHEK293T Ci cells. Calcium release was determined by measuring $[Ca^{2+}]i$ and F340/380 emission ratiofrom 0 to 2 min. Values shown represent the mean ± standard deviation of three independent experiments. **g**) MTT assay was performed on untransfected and DM-transfected Ci cells. Values shown represent the mean ± standard deviation ofthreeindependent experiments. **h**) Wound healing assay was performed on HEK293T Ci and G2i cells treated with 1% serum containing 9 μM U73122 and Plcγ1 knockdown (Pγi) cells. Images were taken at the beginning of the experiment and at 6 hours.**i**) Distance traveled by untreated and U73122-treated cells was quantified, and the normalized percentage of wound closure was calculated. Values shown represent the mean ±standard deviation of three independent experiments.**j**) MTT assays were performed to demonstrate the lack of effect of Grb2 and Plcγ1 knockdown, scrambled shRNA transfection,

and U73122 treatment on cell viability.**k**) Western blot showing the efficiency of Grb2 and Plcγ1 knockdown in G2i and Pyi HEK293T cells, respectively.

We also determined whether the competition between Plcγ1 and Grb2 affects cell invasion properties (**Fig 3.6a,b**). At 6 and 24 h, G2i cells had an increased invasive capacity compared with Ci cells. This can be specifically attributed to Grb2 knockdown because invasion decreased with increasing Grb2concentrations in HEK293T cells (**Fig 3.6c,d**). Similar results were obtained in LoVo metastatic human colon adenocarcinoma cells, which express low levels of Grb2 and high levels of FGFR2 (top panel, **Fig 3.6g**) (51). After 24 h in the presence of increasing concentrations of Grb2, the number of invaded LoVo cells was reduced (**Fig 3.6c,d,e**).

The inhibitory effect of Grb2 on invasion was further confirmed in Ci and G2i cells generated from the Rat osteosarcoma ROS17/2.8cell line, which expresses endogenous levels of FGFR2 (**Fig 3.6h**). Inhibition of Plcγ1 by U73122 treatment or knockdown decreased the invasive ability of HEK293T, LoVo, and ROS cells (**Fig 3.6f,i**). Downregulation of Plcγ1 expression in LoVo and ROS Pyi cells was confirmed by western blot (**Fig3.6g[bottom panel],h**) The inhibitory effect of Plcγ1 downregulation was not due to decreased cell viability as confirmed by MTT assay (**Fig 3.6j**).

a

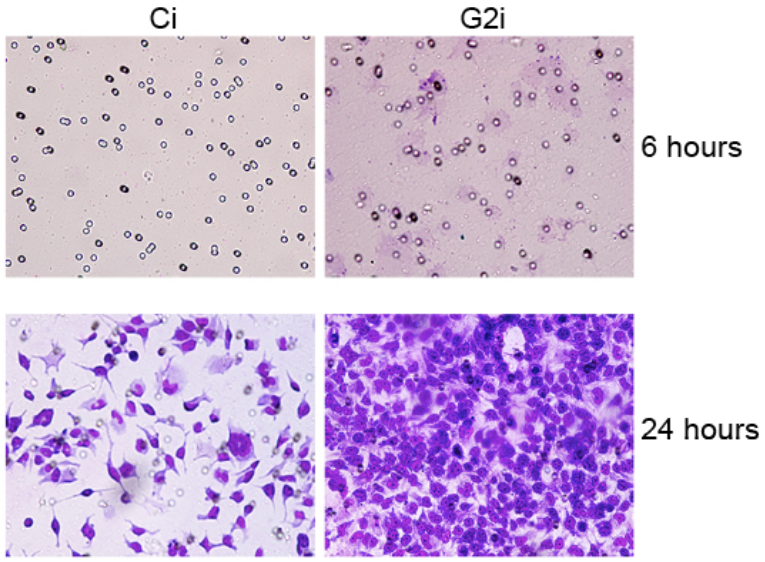
Ci
G2i
6 hours
24 hours

b

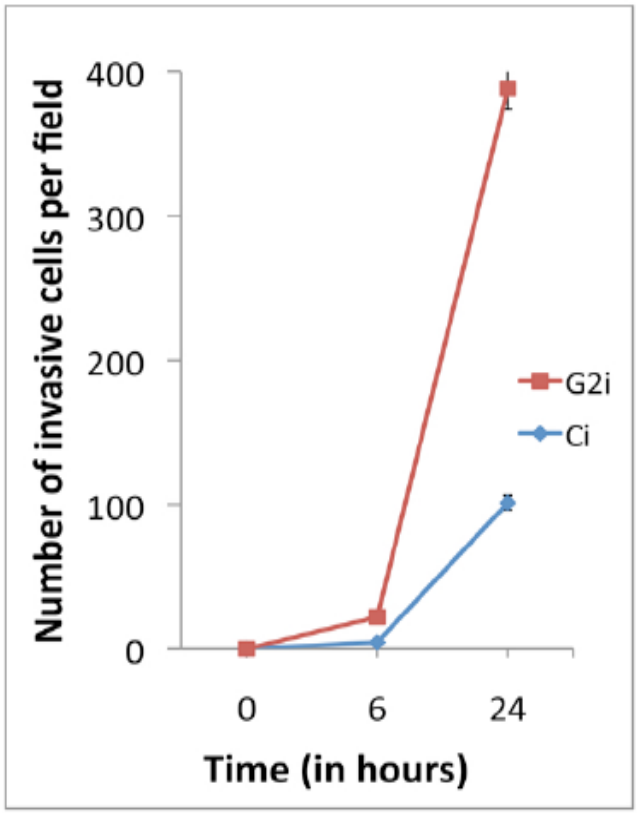
Number of invasive cells per field
400
300
200
100
0
0
6
24
Time (in hours)
G2i
Ci

c

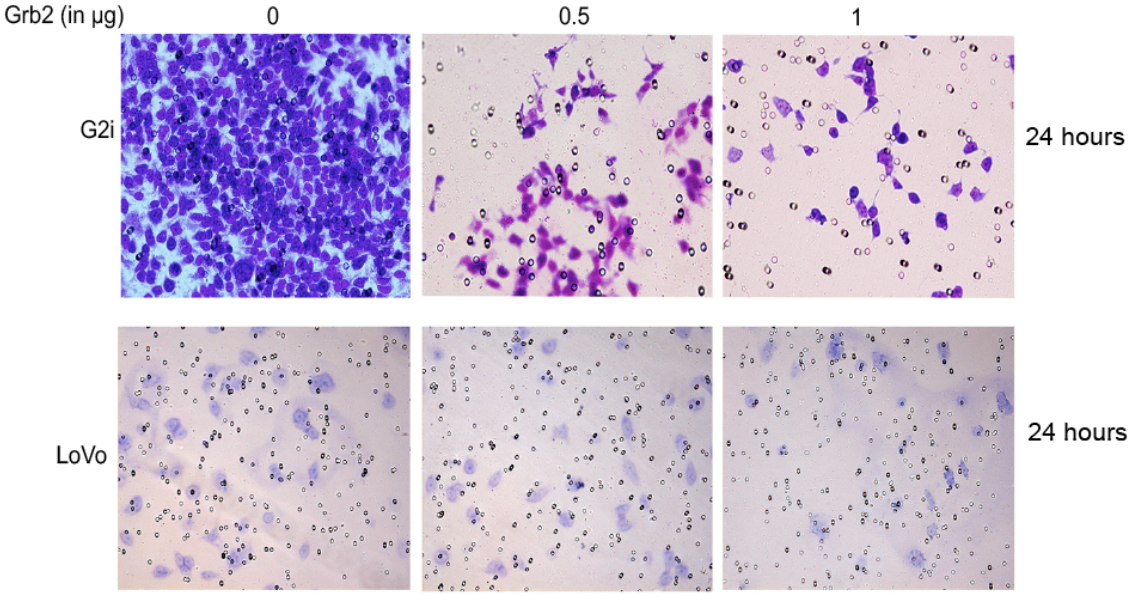
Grb2 (in µg)
0
0.5
1
G2i
24 hours
LoVo
24 hours

d

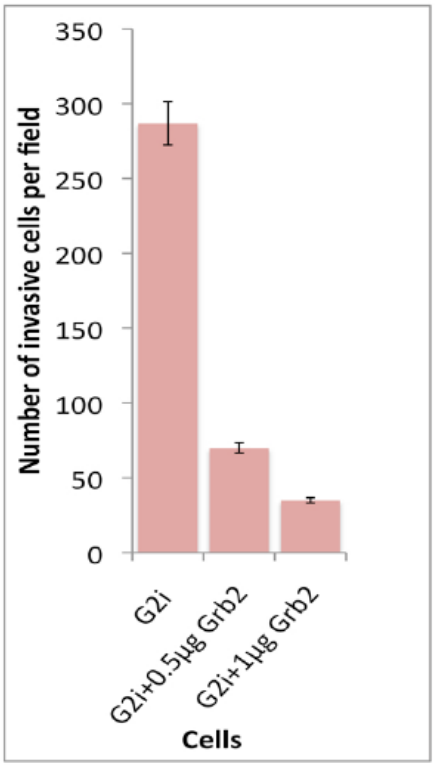
Number of invasive cells per field
350
300
250
200
150
100
50
0
G2i
G2i+0.5µg Grb2
G2i+1µg Grb2
Cells

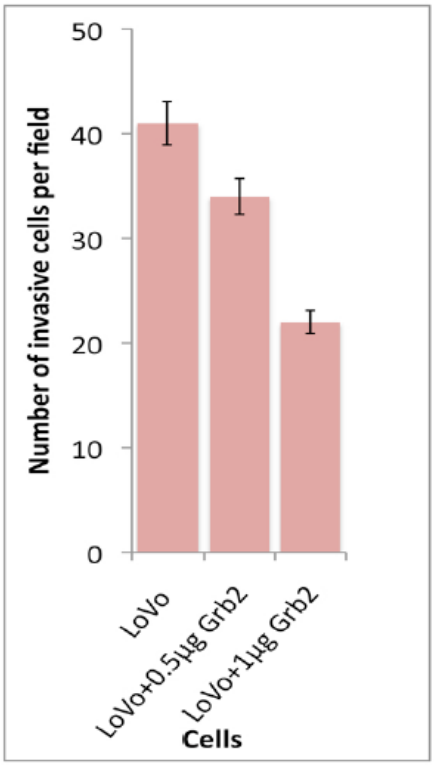
Number of invasive cells per field
50
40
30
20
10
0
LoVo
LoVo+0.5µg Grb2
LoVo+1µg Grb2
Cells

e

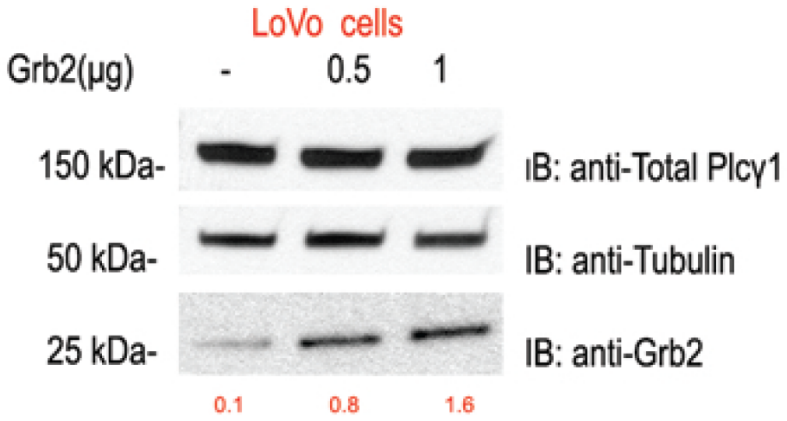
LoVo cells
Grb2(μg)
-
0.5
1
150 kDa-
IB: anti-Total Plcγ1
50 kDa-
IB: anti-Tubulin
25 kDa-
IB: anti-Grb2
0.1
0.8
1.6

f

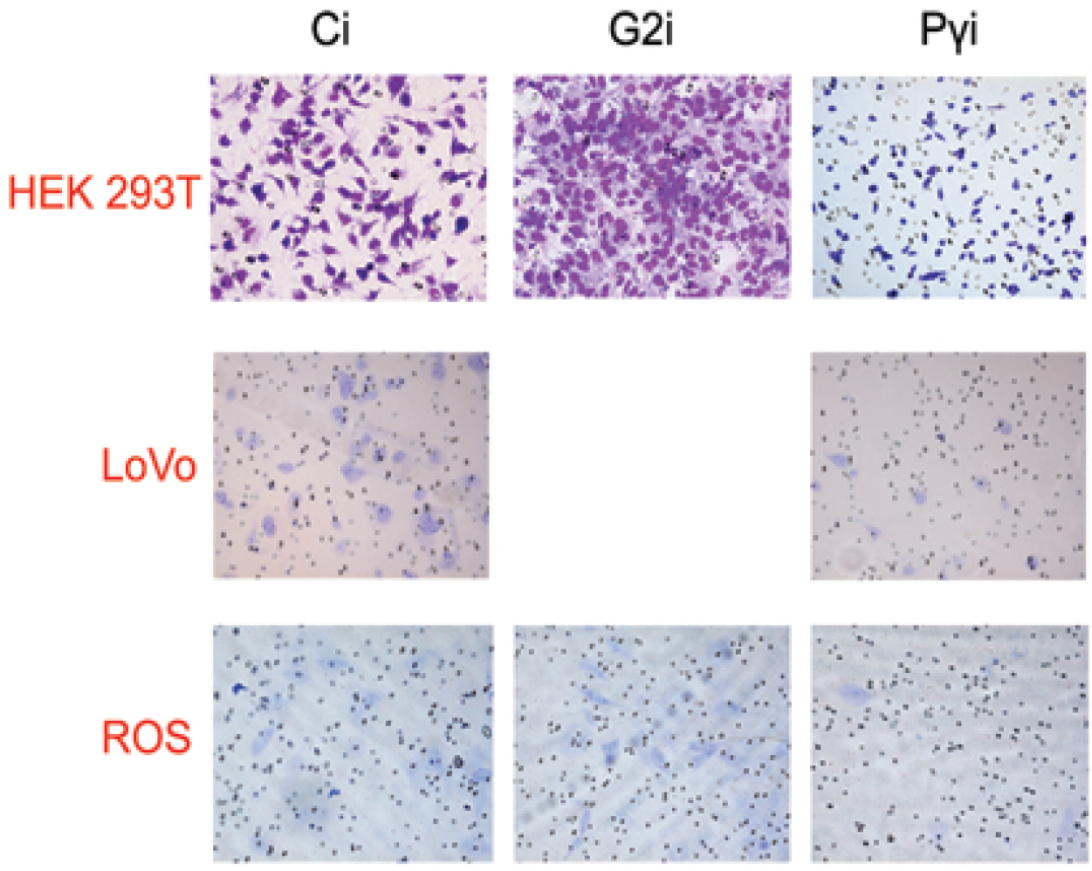
Ci
G2i
Pγi
HEK 293T
LoVo
ROS

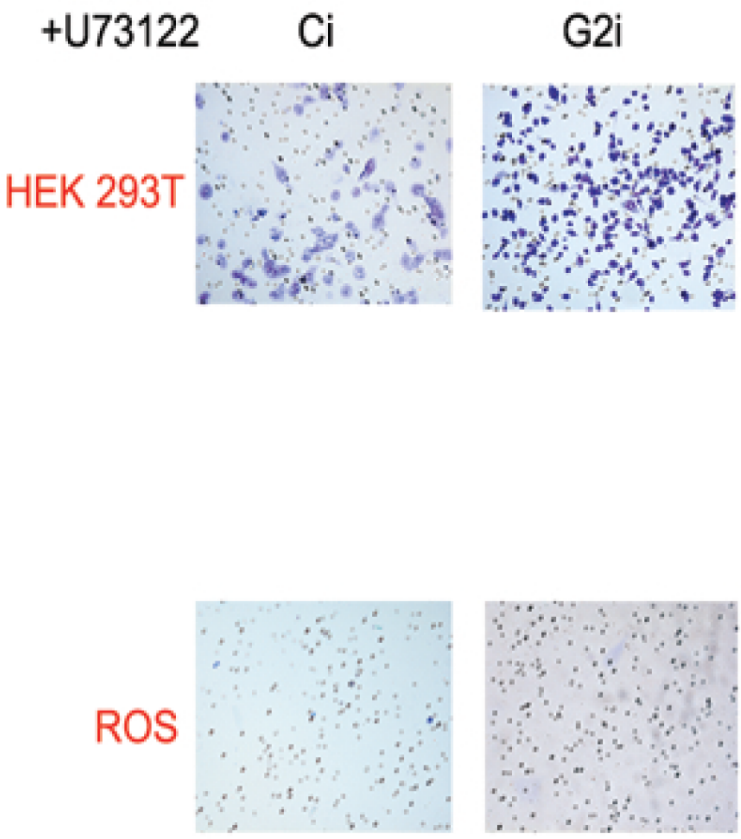
+U73122
Ci
G2i
HEK 293T
ROS
LoVo (untransfected with shRNA)
U73122
-
+

g

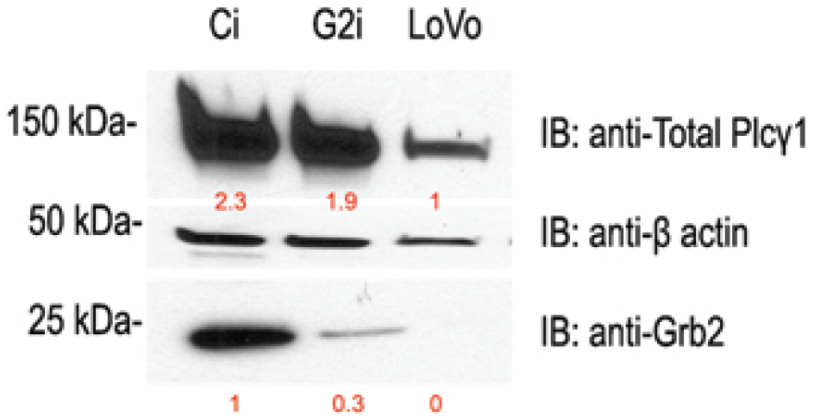
Ci
G2i
LoVo
150 kDa-
50 kDa-
25 kDa-
IB: anti-Total Plcγ1
IB: anti-β actin
IB: anti-Grb2
2.3
1.9
1
1
0.3
0
LoVo cells
Ci
Pγi
150 kDa-
50 kDa-
1.2
0.4
IB: anti-Total Plcγ1
IB: anti-β actin

h

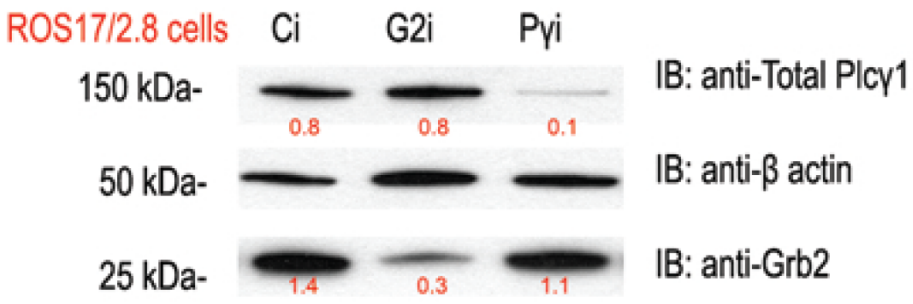
ROS17/2.8 cells
Ci
G2i
Pγi
150 kDa-
50 kDa-
25 kDa-
IB: anti-Total Plcγ1
IB: anti-β actin
IB: anti-Grb2
0.8
0.8
0.1
1.4
0.3
1.1

i

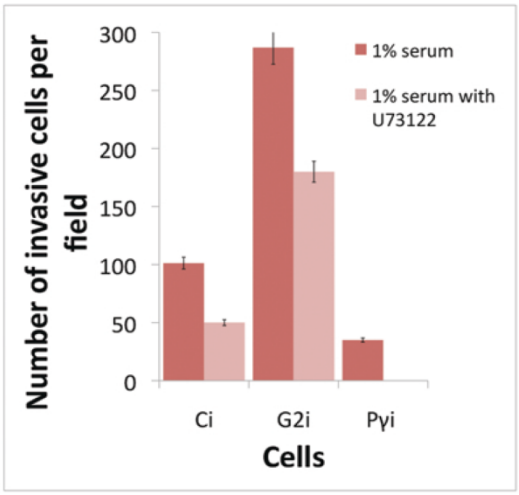
Number of invasive cells per field
300
250
200
150
100
50
0
1% serum
1% serum with U73122
Ci
G2i
Pγi
Cells

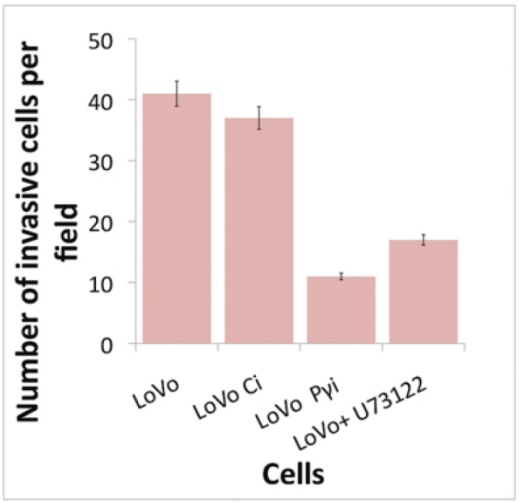
Number of invasive cells per field
50
40
30
20
10
0
LoVo
LoVo Ci
LoVo Pγi
LoVo+ U73122
Cells

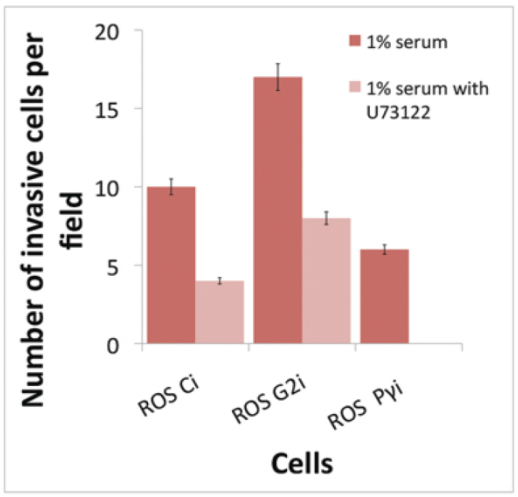
Number of invasive cells per field
20
15
10
5
0
1% serum
1% serum with U73122
ROS Ci
ROS G2i
ROS Pγi
Cells

j

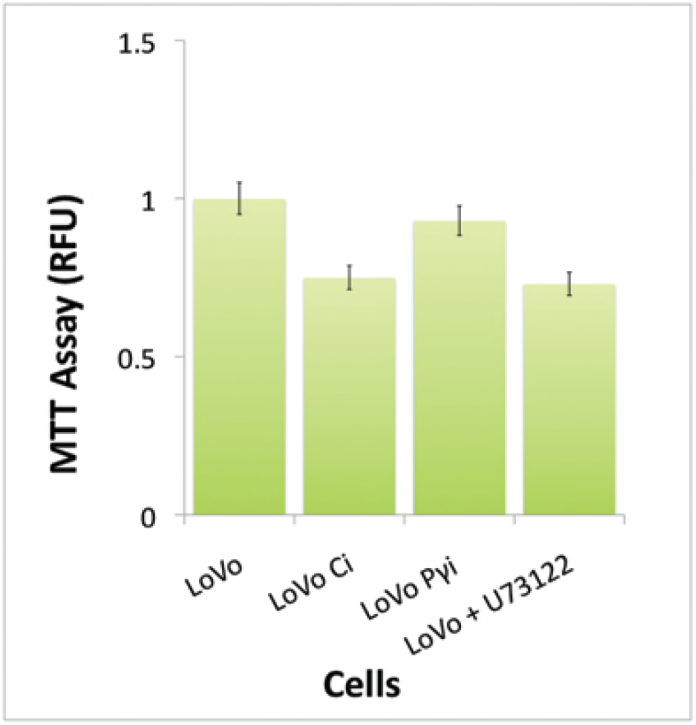
1.5
1
0.5
0
MTT Assay (RFU)
LoVo
LoVo Ci
LoVo Pyi
LoVo + U73122
Cells

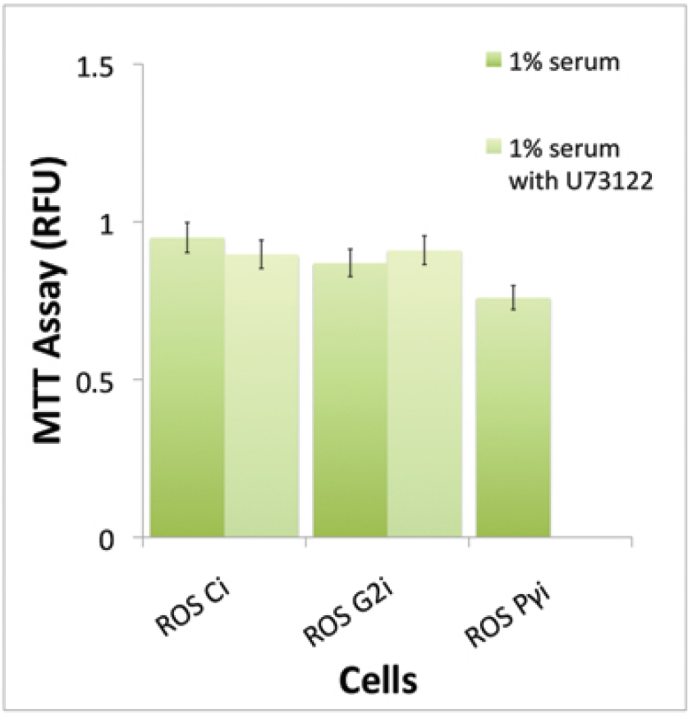
1.5
1
0.5
0
MTT Assay (RFU)
1% serum
1% serum with U73122
ROS Ci
ROS G2i
ROS Pyi
Cells

Fig 3.6 Plcγ1 activity increases invasive behavior in the absence of Grb2.a) Matrigel invasion assays were used to determine whether the competition between Plcγ1 and Grb2 dictates invasion. HEK293T Ci and G2i cells were placed in the upper chamber in serum starvation medium, and 1% serum was placed in the lower chamber. Images were taken after 6 h and 24 h. G2i cells are more invasive than Ci cells at both timepoints. **b**) The number of invasive cells was counted in four microscopic fields for each sample. Values shown represent the mean ± standard deviation of triplicate samples.**c**) Invasion assay was performed on HEK293T G2iand LoVo cells transfected with increasing concentrations of Grb2 (0.5 µg and 1 µg). Images were taken after 24h. G2i (*left*) and LoVo (*right*) cells transfected with 0.5 and 1 µg Grb2. **d**) The number of invasive cells was counted in 4 microscopic fields. Values shown represent the mean ± standard deviation of triplicate samples.**e**) LoVo cells were left untransfected or transfected with myc-tagged Grb2 (0.5 µg, and 1 µg). Cells were serum starved overnight. Cell lysates were obtained, and the efficiency of Grb2 transfection was determined by western blot analysis. Total Plcγ1 and tubulin were used as loading controls. **f**) (*Top panel*) Invasion assays were performed on Ci, G2i, and Pγi HEK293T;Ci, G2i, and Pγi ROS cells; and Ci and Pγi LoVo cells. LoVo cells have a relatively low level of endogenous Grb2 expression. (*Middle panel*) Invasion assays were performed on untreated U73122-treated HEK293T and ROS Ci and G2i cells. U73122 wasadded tothe upper and lower chambers ata final concentration of 9 µM. (*Bottom panel*)Invasion assays were performed on LoVo cells (untransfected with shRNA)that were left untreated or treated with U73122. In all cases, cells were incubated for 24 h, fixed, stained, mounted onto microscopic slides, and imaged at 20X magnification.**g**) (*Top panel*)Western blot was performed to determine total Plcγ1 and Grb2 expression incell lysates obtained from serum-starved HEK293T Ci and G2i cells and LoVo cells. β-actin was used as loading control.(*Middle panel*)Western blot results showing the efficiency of Plcγ1 knockdown in LoVo Pyi cells. The membrane was probed for total Plcγ1, Grb2, and β-actin. **h**) Western blot showing the efficiency of Grb2 and Plcγ1 knockdown in ROS G2i and Pyi cells, respectively. Ci cells were used as controls. The membrane was probed for total Plcγ1, Grb2, and β-actin.**i**) The number of invasive cells was counted in four microscopic fields and presented as the mean ± standard deviation of triplicate samples.**j**) MTT assays were performed to confirm that the inhibitory effects of Grb2 and Plcγ1 downregulation were not due to adverse effects oncell viability. Values are expressed as relative fluorescent units (RFUs) and presented as the mean ± standard deviation of three independent measurements.

To test whether the Plcγ1-dependent invasive potential requires FGFR2, parental HEK293T cells, in which FGFR2 expression is negligible, were transfected with scrambled shRNA, Grb2 shRNA, and Plcγ1 shRNA to generate PCi, PG2i, and PPYi cell lines, respectively (**Fig 3.7a**). After 24 h, PPYi cells exhibited limited invasive ability (**Fig 3.7b,c**) compared with PG2i cells. Cell viability was confirmed by MTT assay (**Fig 3.7d**).

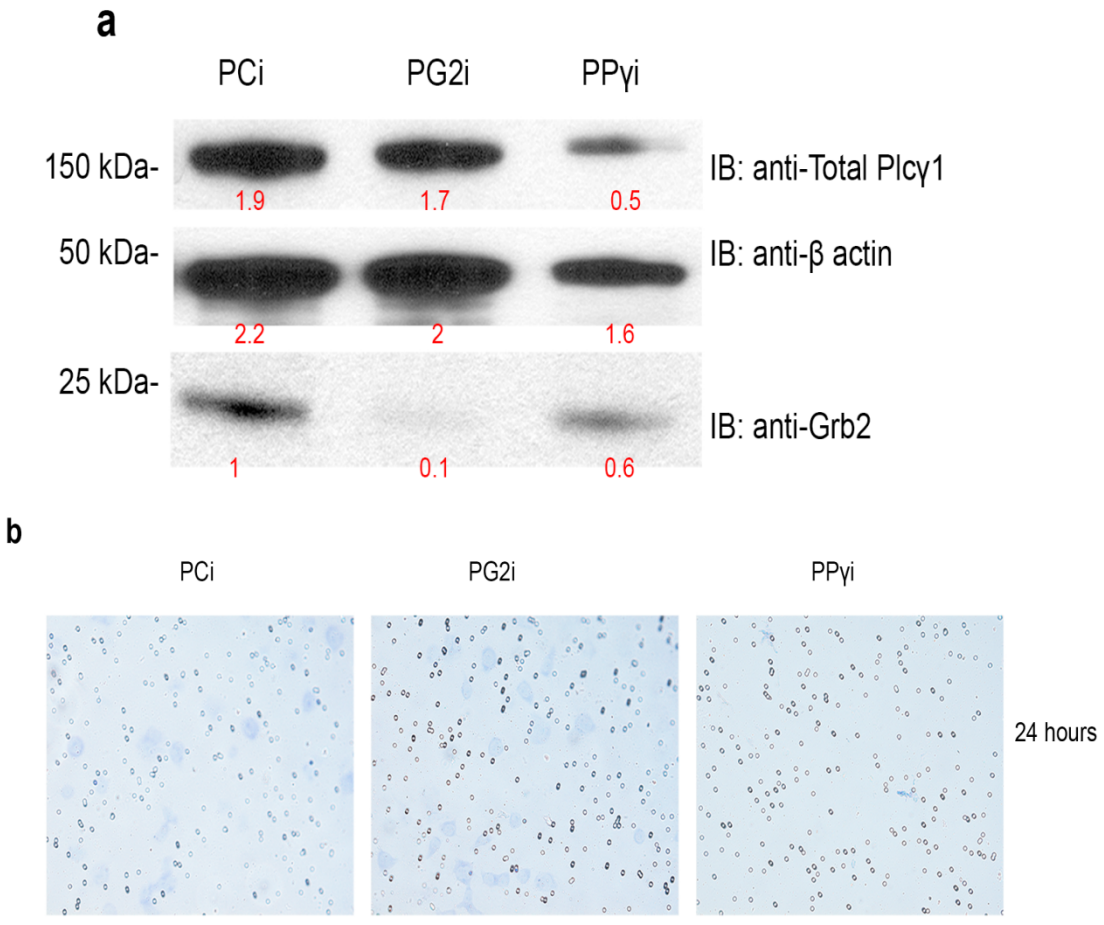

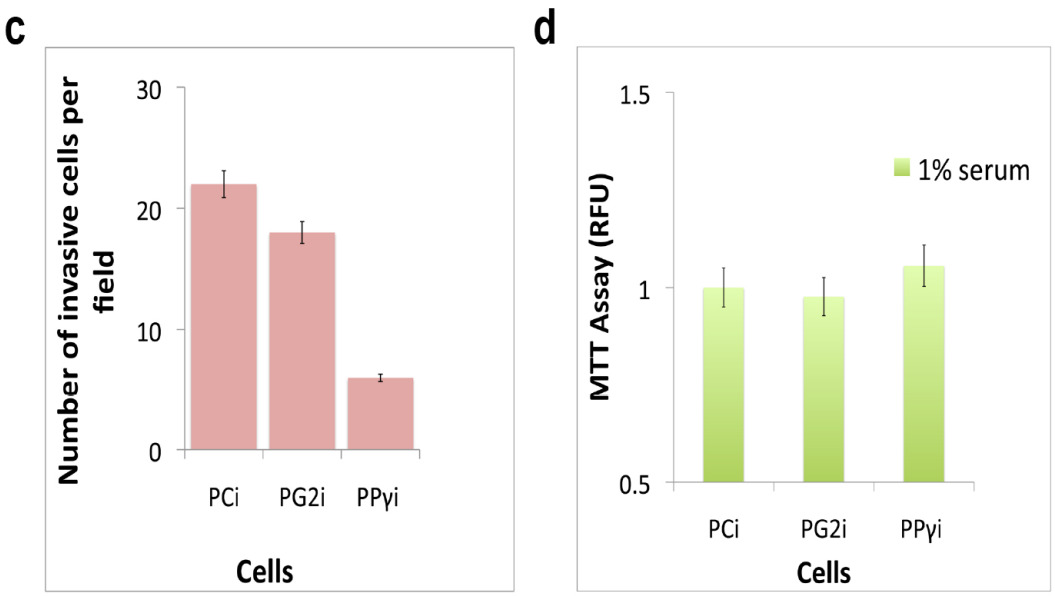

Fig 3.7 Invasive behavior in cells is FGFR2 dependent. a) HEK293T parental cells, which express low levels of FGFR2 were used to generate stable Grb2 (PG2i) and Plcγ1 (PPγi) knockdowns. Cells transfected with scrambled shRNA (PCi) were used as a control. Western blot analysis was done to determine the efficiency of the Grb2 and Plcγ1knockdown. β-actin was used as a loading control. **b**) PCi, PG2i, and PPγi cells were used in a 24-h invasion assay. **c**) The number of invasive PCi, PG2i, and PPγi cells was counted in four microscopic fields and presented as the mean ± standard deviation of three independent experiments performed in triplicate. **d**) Cell viability of PCi, PG2i, and PPγi cells was determined by MTT assay. Data shown represent the mean ±standard deviation of three independent experiments.

Next, we evaluated the effect of Plcγ1 on morphological changes associated with invasive behavior, including actin polymerization. Changes in the actin cytoskeleton precede cell migration and invasion. Therefore, phalloidin staining was used to detect changes in actin polymerization in HA-Plcγ1-transfected Ci and G2i cells. Under basal conditions, Plcγ1 was localized on migratory structures in G2i cells compared withCi cells (**Fig 3.8a**). Furthermore, G2i cells

were larger and had more spread cell morphology and extensions compared with Ci cells (**Fig 3.8b**).

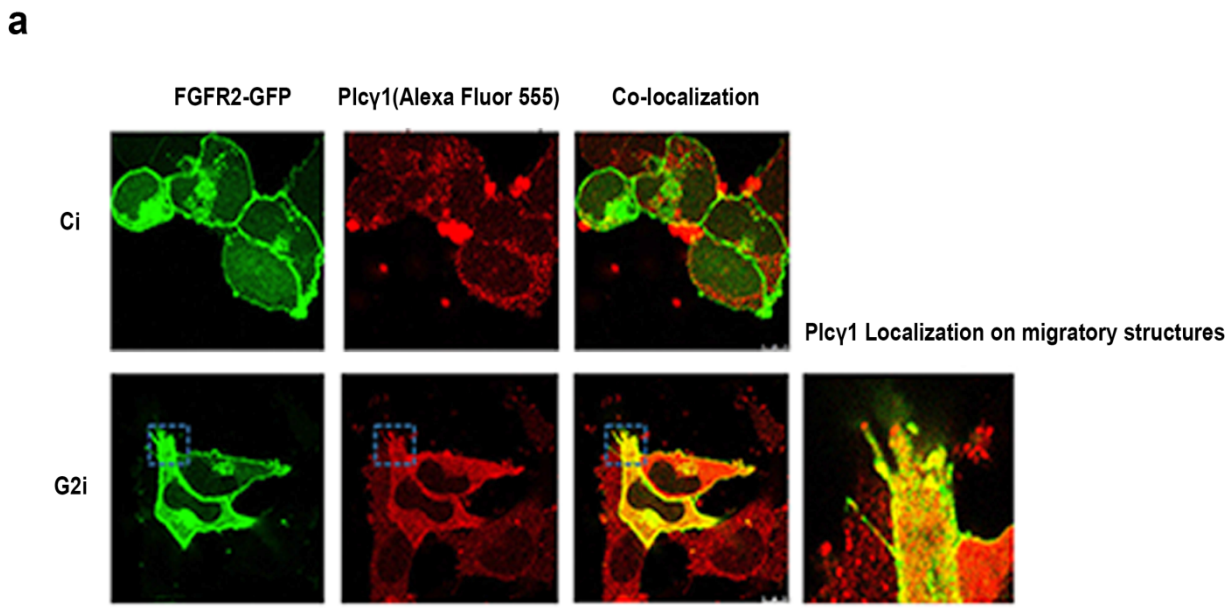

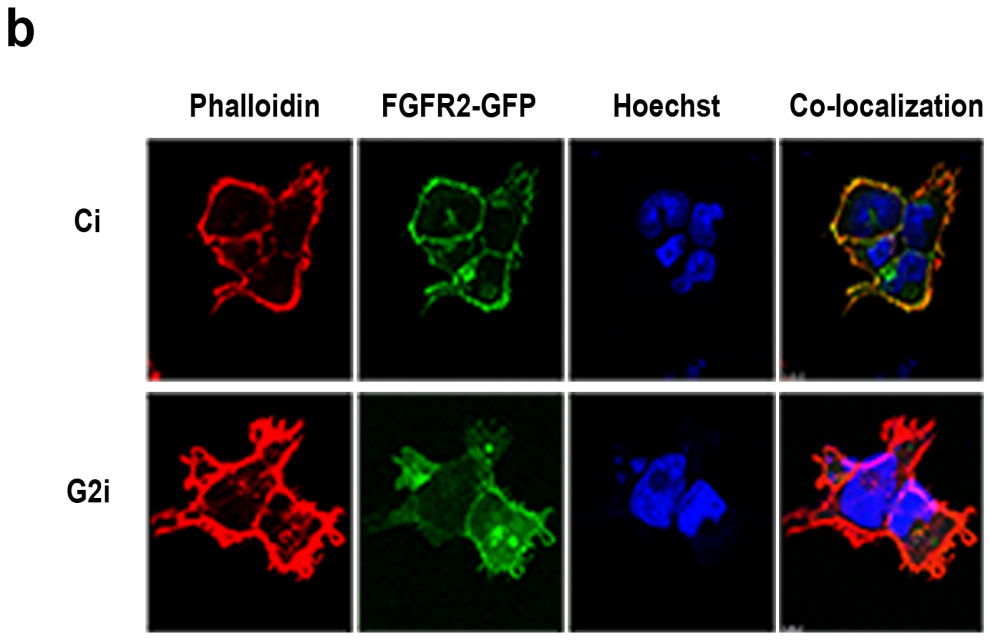

Fig 3.8 Plcγ1 localizes on migratory structures in G2i cells. a) HEK293T Ci and G2i cells stably expressing FGFR2-GFP were transiently transfected with HA-Plcγ1. Serum-starved cells were treated with Alexa Fluor 555-labeled HA-antibody.Microscopy was used to detect Plcγ1 and FGFR2 colocalization (*yellow*).High magnification view of Plcγ1 and FGFR2 colocalization on migratory structures (*lower far right panel*)**. b**) HEK293T Ci and G2i cells were detached and treated with 1% serum for 2 h. Cells were stained with phalloidin to detect actin polymerization and counterstained with Hoechst (nuclear stain). Actin polymerization was induced in G2i, but not Ci, cells as evidenced by phalloidin staining intensity and morphological changes.

Flow cytometric analysis further confirmed the induction of actin polymerization by Plcγ1 activation in the absence of Grb2. Cells with both GFP and phalloidin were counted in Ci and G2i (knockdown cells) samples (**Fig 3.9a,b**). Following quantification and normalization to Ci cells, a ~36% increase in actin polymerization was observed in G2i cells (**Fig 3.9c**).

a

HEK 293T control cells with GFP-FGFR2

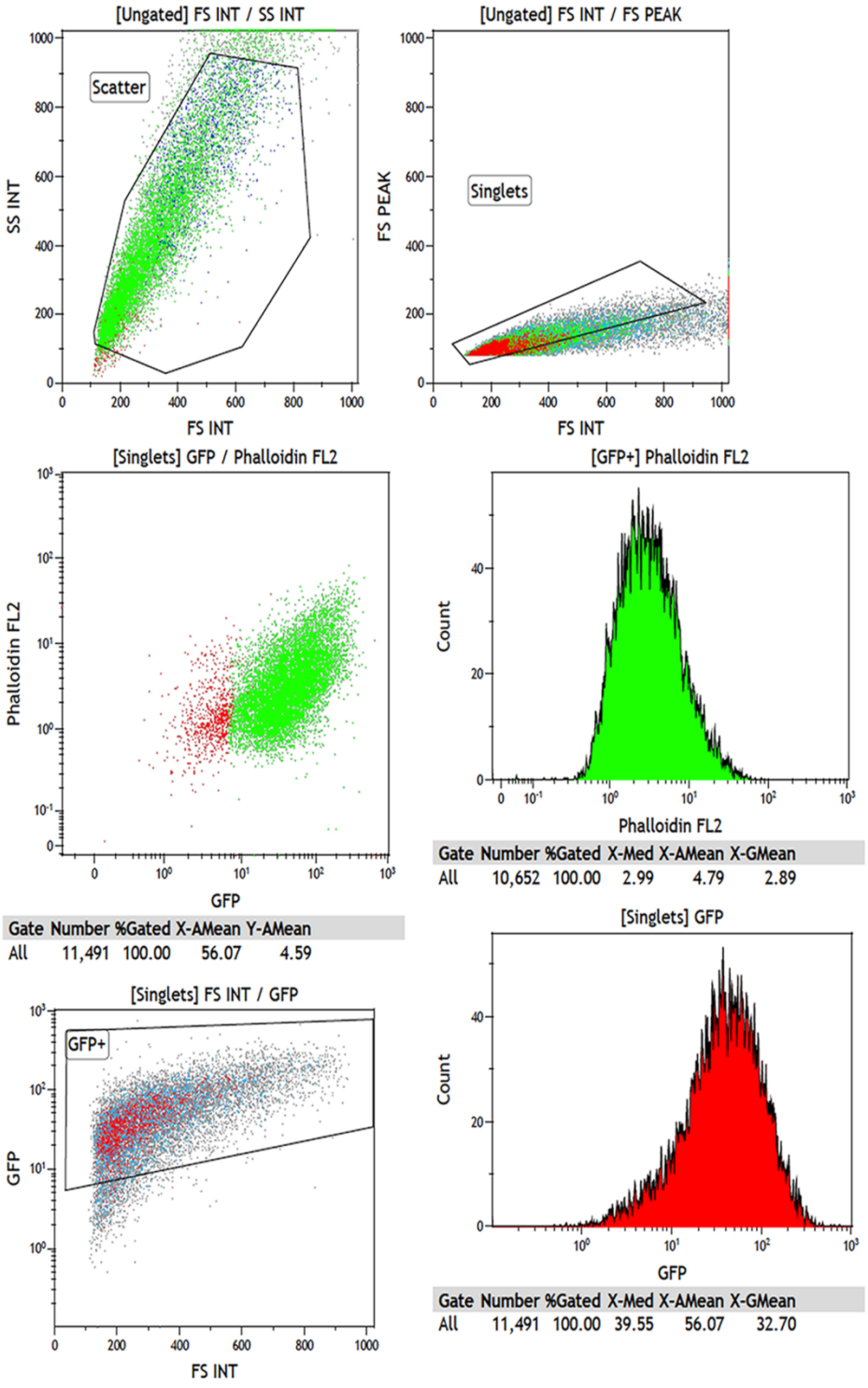

b

HEK 293T knockdown cells with GFP-FGFR2

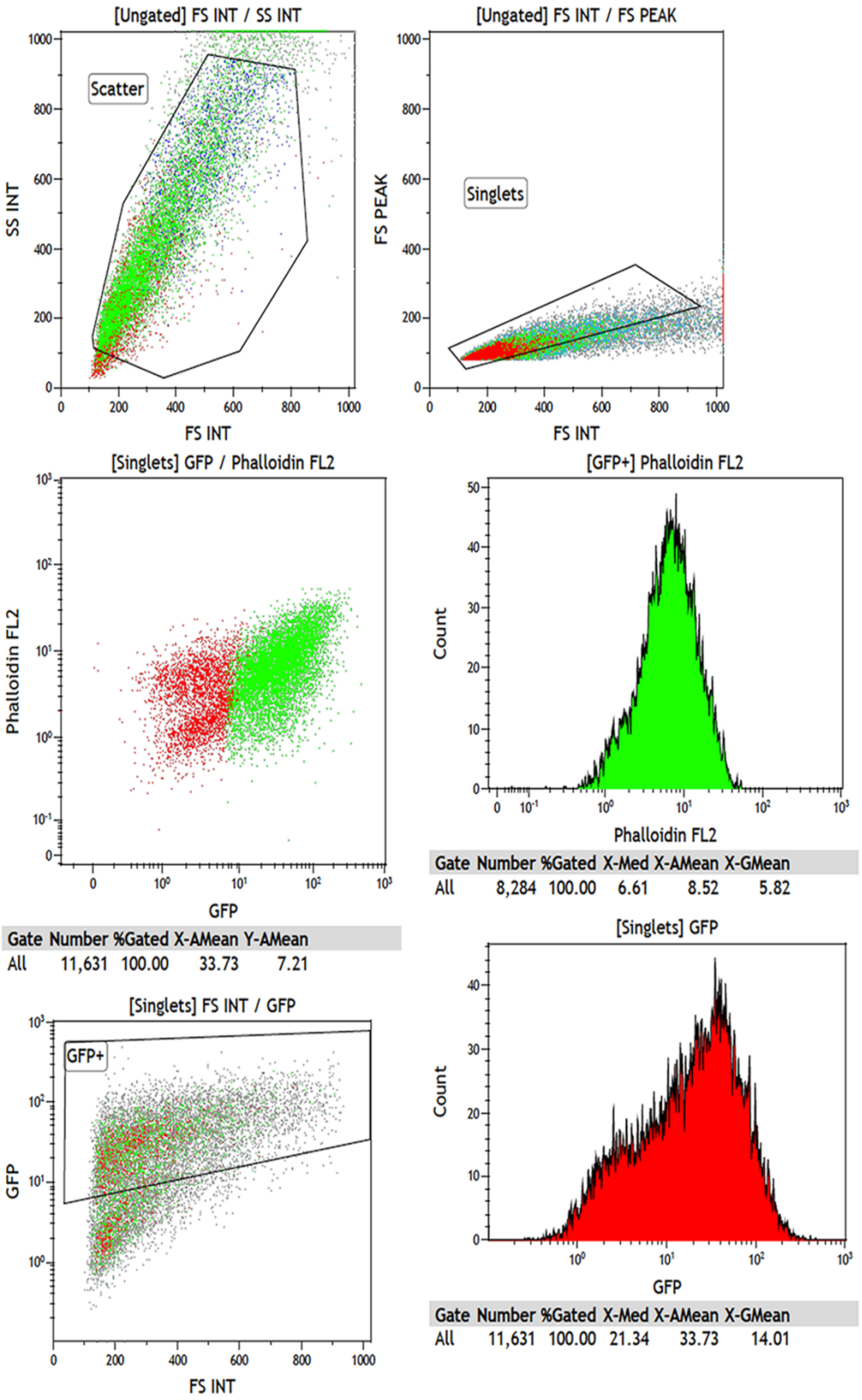

c

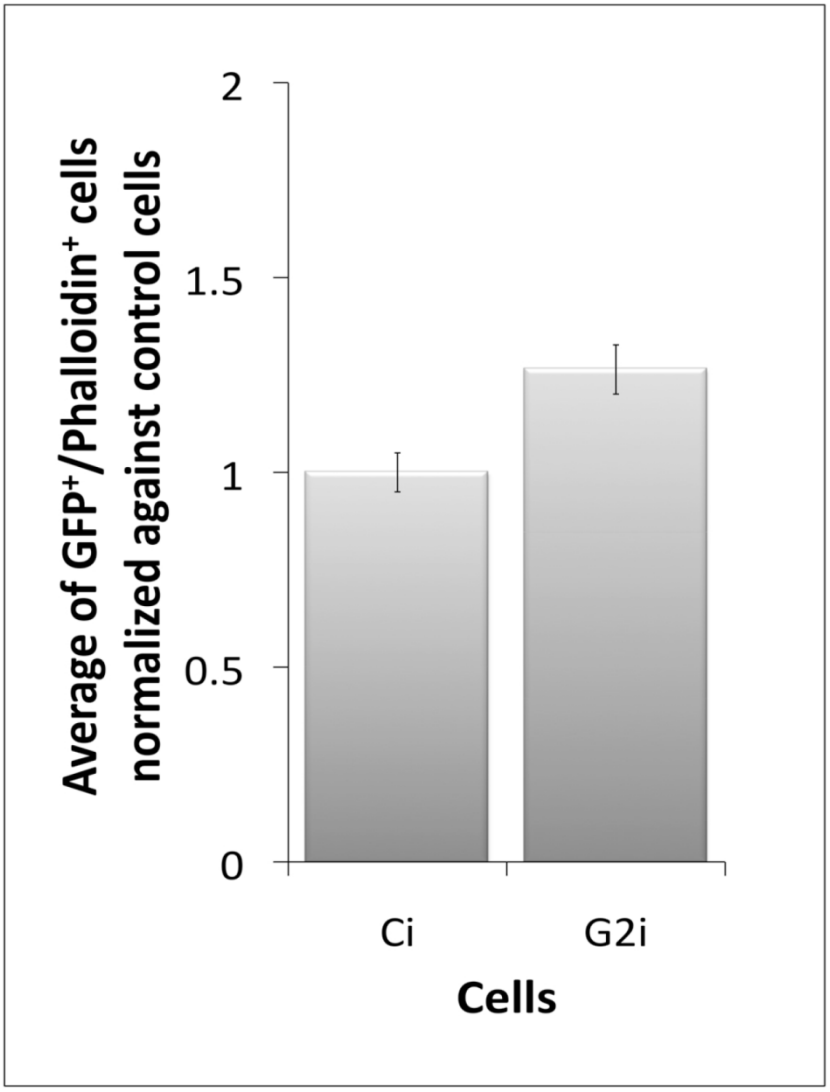

Fig 3.9 Actin polymerization is higher in G2i cells compared withCi cells. **a**), **b**) HEK293T Ci and G2i cells were treated with 1% serum for 2 h,counted, fixed, and stained with phalloidin. Flow cytometricanalysis of phalloidin staining was doneto quantify actin polymerization. **c**) Flow cytometry data was normalized to Ci cells and presented as the mean ±standard deviation of three independent experiments.

Plcγ1 and Grb2 expression influence survival outcome in ovarian cancer patients

Having shown that Plcγ1 and Grb2 competition for FGFR2 binding dictate cell invasion and migration, we next investigated the effect of this competition on the survival outcome of cancer patients. Kaplan-Meier survival curves generated from ovarian cancer patients revealed that high level of FGFR2/Plcγ1 was associated with worse survival compared with low level of FGFR2/Plcγ1, respectively. Also, high Grb2 /low FGFR2 /low Plcγ1 level profile was associated with better survival in ovarian cancer patients compared to low Grb2 /high FGFR2 /high Plcγ1 level profile (**Fig 3.10**).

In summary, Plcγ1 binding to FGFR2 when the Grb2 concentration is low increases cell motility and invasion, which are prerequisites to metastasis. Therefore, Grb2 and Plcγ1 protein concentrations may dictate metastatic potential, which may impact patient survival outcome.

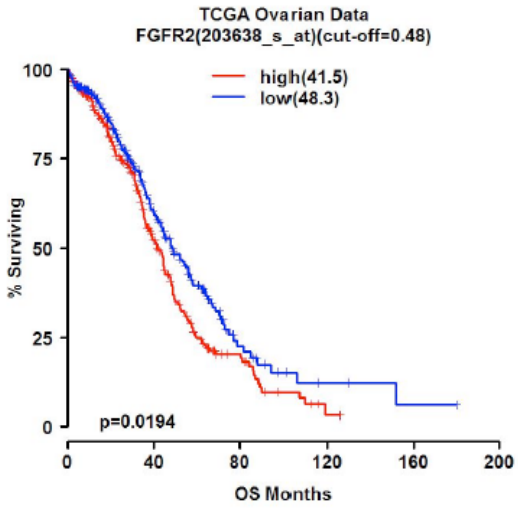
TCGA Ovarian Data
FGFR2(203638_s_at)(cut-off=0.48)
high(41.5)
low(48.3)
% Surviving
p=0.0194
OS Months

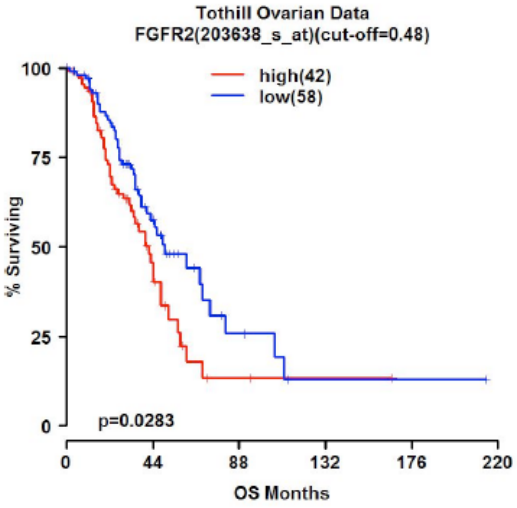
Tothill Ovarian Data
FGFR2(203638_s_at)(cut-off=0.48)
high(42)
low(58)
% Surviving
p=0.0283
OS Months

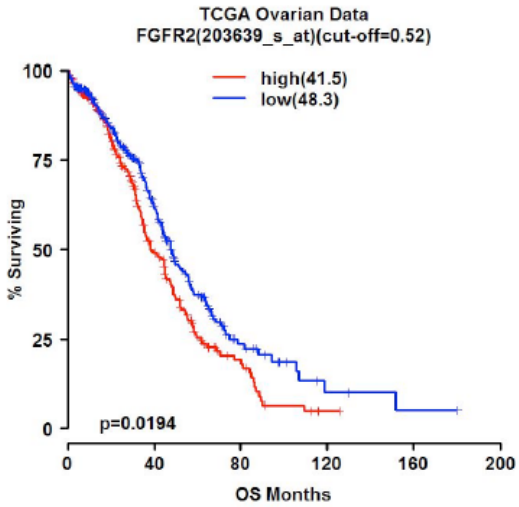
TCGA Ovarian Data
FGFR2(203639_s_at)(cut-off=0.52)
high(41.5)
low(48.3)
% Surviving
p=0.0194
OS Months

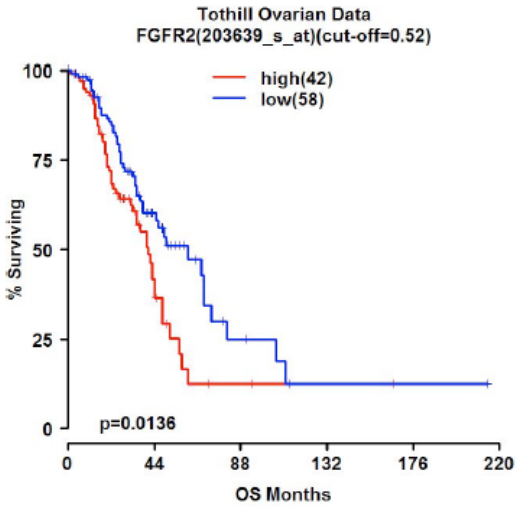
Tothill Ovarian Data
FGFR2(203639_s_at)(cut-off=0.52)
high(42)
low(58)
% Surviving
p=0.0136
OS Months

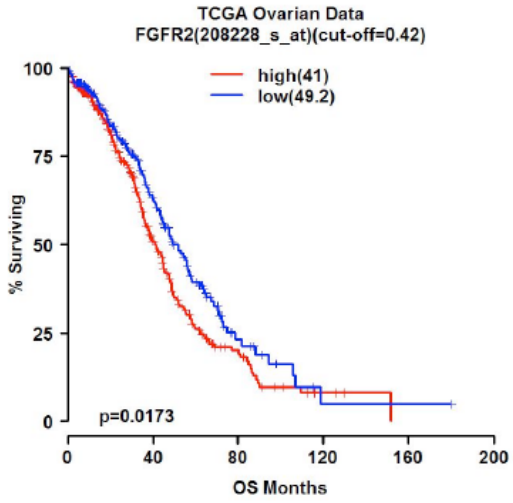
TCGA Ovarian Data
FGFR2(208228_s_at)(cut-off=0.42)
high(41)
low(49.2)
% Surviving
p=0.0173
OS Months

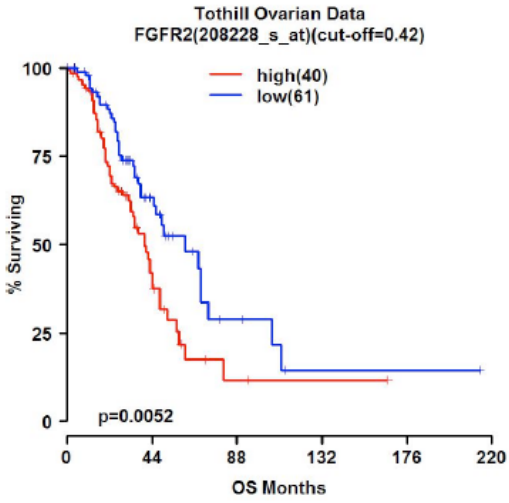
Tothill Ovarian Data
FGFR2(208228_s_at)(cut-off=0.42)
high(40)
low(61)
% Surviving
p=0.0052
OS Months

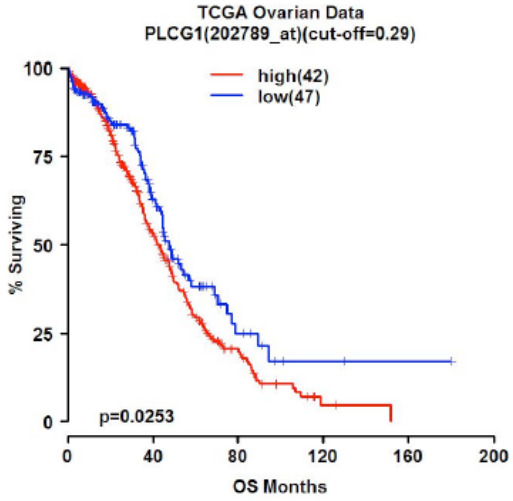
TCGA Ovarian Data
PLCG1(202789_at)(cut-off=0.29)
high(42)
low(47)
% Surviving
p=0.0253
OS Months

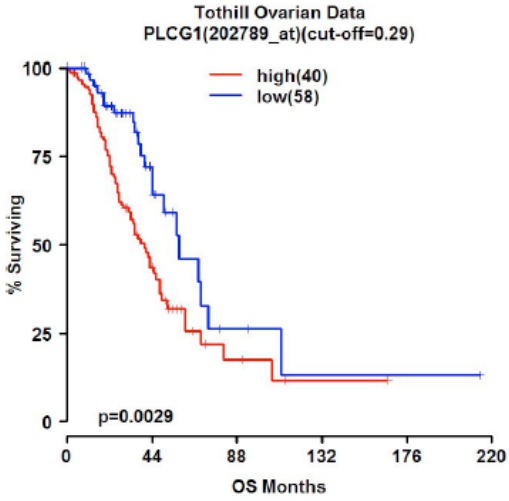
Tothill Ovarian Data
PLCG1(202789_at)(cut-off=0.29)
high(40)
low(58)
% Surviving
p=0.0029
OS Months

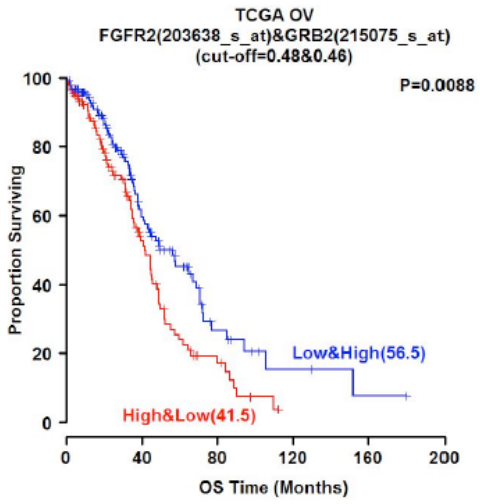
TCGA OV
FGFR2(203638_s_at)&GRB2(215075_s_at)
(cut-off=0.48&0.46)
P=0.0088
Proportion Surviving
Low&High(56.5)
High&Low(41.5)
OS Time (Months)

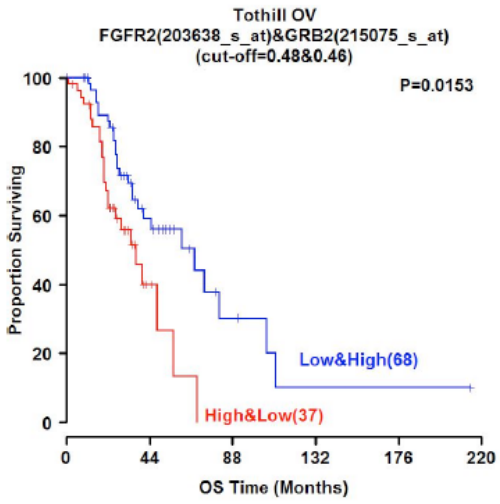
Tothill OV
FGFR2(203638_s_at)&GRB2(215075_s_at)
(cut-off=0.48&0.46)
P=0.0153
Proportion Surviving
Low&High(68)
High&Low(37)
OS Time (Months)

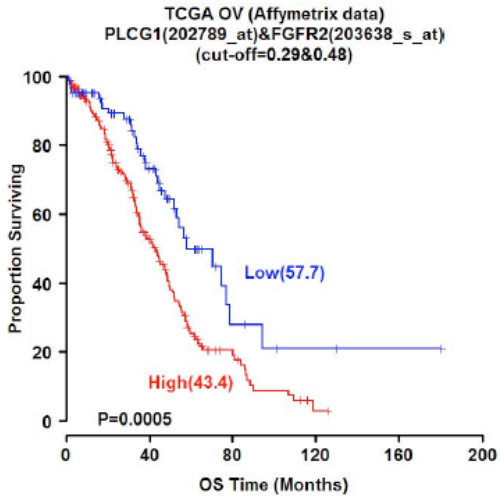
TCGA OV (Affymetrix data)
PLCG1(202789_at)&FGFR2(203638_s_at)
(cut-off=0.29&0.48)
Proportion Surviving
Low(57.7)
High(43.4)
P=0.0005
OS Time (Months)

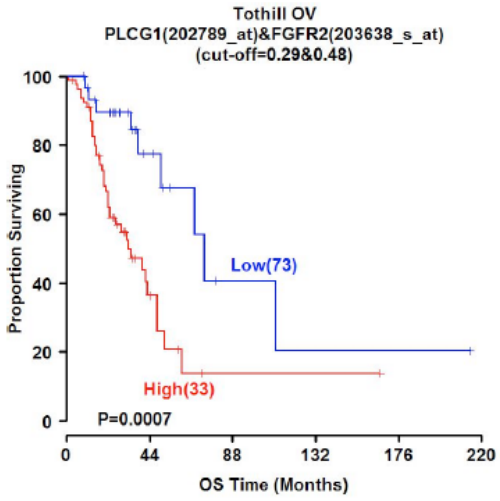
Tothill OV
PLCG1(202789_at)&FGFR2(203638_s_at)
(cut-off=0.29&0.48)
Proportion Surviving
Low(73)
High(33)
P=0.0007
OS Time (Months)

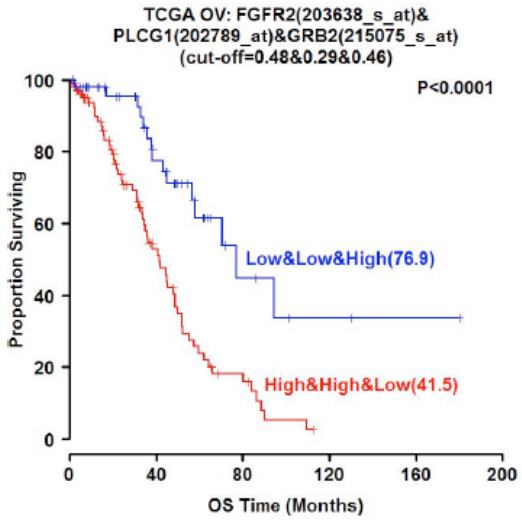
TCGA OV: FGFR2(203638_s_at)&
PLCG1(202789_at)&GRB2(215075_s_at)
(cut-off=0.48&0.29&0.46)
P<0.0001
Proportion Surviving
OS Time (Months)
Low&Low&High(76.9)
High&High&Low(41.5)

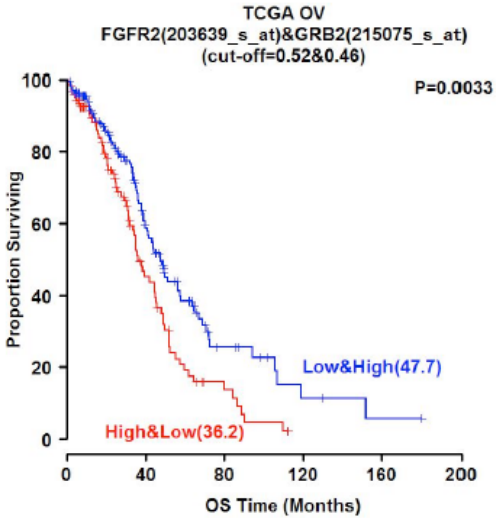
TCGA OV
FGFR2(203639_s_at)&GRB2(215075_s_at)
(cut-off=0.52&0.46)
P=0.0033
Proportion Surviving
OS Time (Months)
Low&High(47.7)
High&Low(36.2)

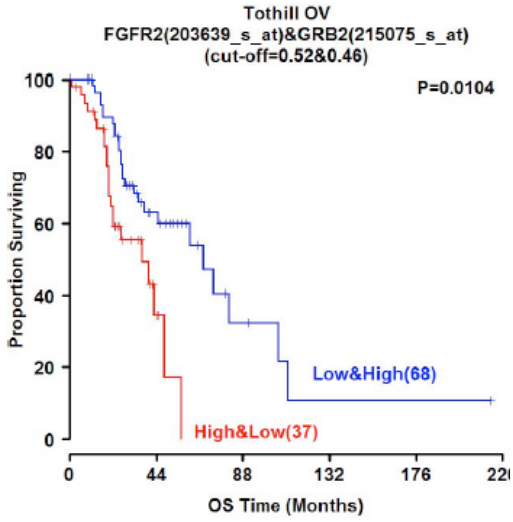
Tothill OV
FGFR2(203639_s_at)&GRB2(215075_s_at)
(cut-off=0.52&0.46)
P=0.0104
Proportion Surviving
OS Time (Months)
Low&High(68)
High&Low(37)

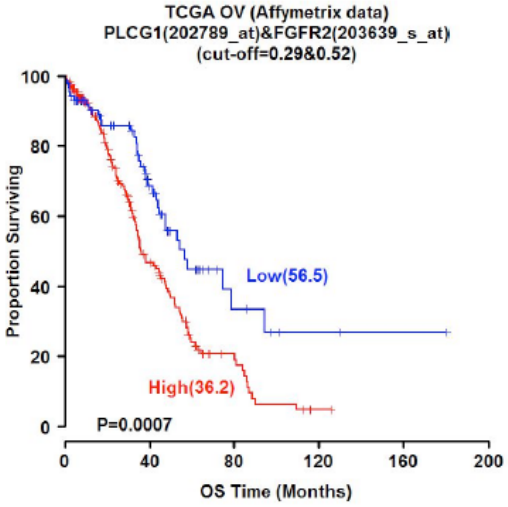
TCGA OV (Affymetrix data)
PLCG1(202789_at)&FGFR2(203639_s_at)
(cut-off=0.29&0.52)
Proportion Surviving
OS Time (Months)
Low(56.5)
High(36.2)
P=0.0007

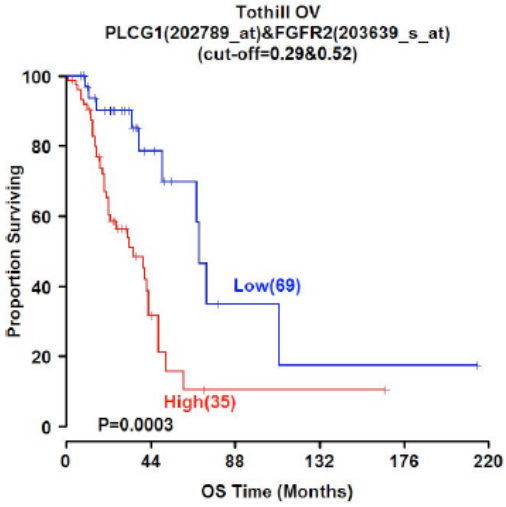
Tothill OV
PLCG1(202789_at)&FGFR2(203639_s_at)
(cut-off=0.29&0.52)
Proportion Surviving
OS Time (Months)
Low(69)
High(35)
P=0.0003

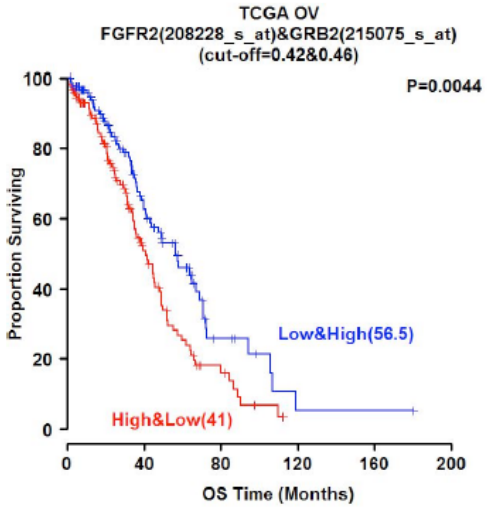
TCGA OV
FGFR2(208228_s_at)&GRB2(215075_s_at)
(cut-off=0.42&0.46)
P=0.0044
Proportion Surviving
OS Time (Months)
Low&High(56.5)
High&Low(41)

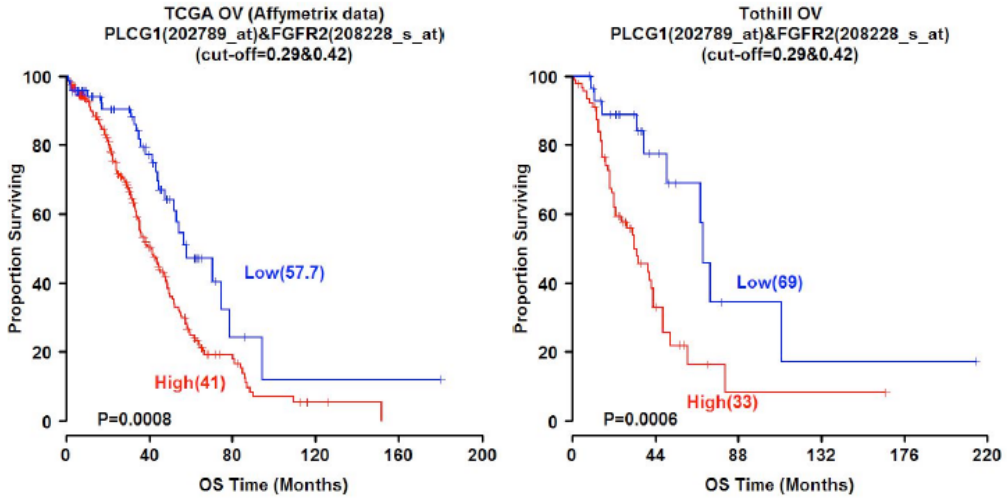

Fig 3.10 High Grb2 and low FGFR2 and Plcγ1 expression profile is associated with better survival in ovarian cancer. Data from online TCGA and Tothill databases was used to generate Kaplan-Meier overall survival (OS) curves of patients with ovarian cancer. mRNA levels of FGFR2, Plcγ1, and Grb2 (presented individually or in different combinations) were determined from microarray studies. Cut-off values and statistical significance determined by Student's t-test are shown for each survival curve.

Chapter Four: PTEN-mediated Akt activation is dictated by Grb2 expression level

Background

The Akt pathway is an important oncogenic pathway that promotes cell growth, survival, and glucose metabolism (22). The activity of this pathway is dependent on plasma membrane phospholipid constituents. Class I PI3Ks phosphorylate plasma membrane-localized PIP_2 to produce PIP_3. PIP_3 binds to Akt to induce Akt activation (52,53). Akt activity is counteracted by PTEN, a lipid phosphatase that hydrolyzes PIP_3 to PIP_2 (54,55). The balance of PI3K and PTEN activity in controlling the abundance of phospholipids is important in cellular response.

It is important to note that PTEN activation is only possible in the presence of a subset of PIPs such as PIP and PIP_2. Recent studies have established that the binding of PIP_2 to the N-terminus of PTEN (56) induces a conformational change (18) that upregulates phosphatase activity (57). PTEN phosphorylation leads to a closed conformation that inhibits phosphatase activity (58).

In the previous chapters, the expression level of Grb2 in cells was shown to have a profound effect on Plcγ1 activity in non-stimulated cells. In cells depleted of Grb2 (G2i cells), Plcγ1 binding to FGFR2 results in Plcγ1 activation and subsequent PIP_2 turnover.

In this chapter, Plcγ1-mediated reduction in PIP_2 concentration due to depleted Grb2 concentration is shown to down-regulate PTEN activity, resulting in PIP_3 accumulation. This leads to membrane-recruitment and activation of the Akt signaling pathway, which enhances cell proliferation (Fig 4.1). Thus, fluctuations in the concentrations of two competing non-phosphorylated proteins via their SH3 domains can affect cell fate by modulating PIP_2 level.

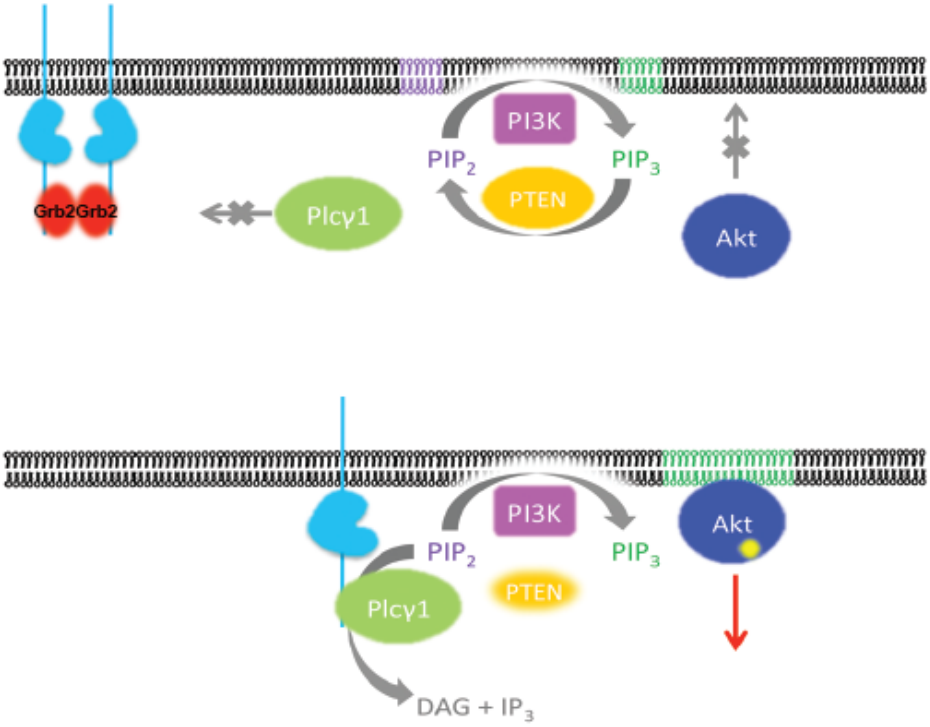

Fig 4.1 Basal stage competition between Grb2 and Plcγ1 controls PTEN-mediated Akt activation. (*top*) In cells with high levels of Grb2, Plcγ1 is unable to bind to FGFR2 and thus, membrane-localized PIP_2 is not depleted. PIP_2 stabilizes PTEN activity. (*bottom*) In the absence of Grb2, Plcγ1 is able to bind to FGFR2. Activated Plcγ1 hydrolyzes PIP_2. Depletion of PIP_2 destabilizes PTEN activity. Loss of PTEN function leads to the accumulation of PIP_3, which binds to Akt to increase its phosphorylation and activity.

Methods

Reagents

FGFR2 (C-17) and Grb2 (C-23) antibody and scrambled shRNA, Grb2 shRNA, and Plcγ1 shRNAs were purchased from Santa Cruz Biotechnology. Anti-GFP and anti-RFP rabbit antibodies were purchased from Rockland Immunochemicals. U0126 (MEK1/2 inhibitor), phospho(Ser^{241})-PDK1, wortmannin (PI3K inhibitor), β-actin antibody, anti-mouse and anti-rabbit secondary antibodies, Akt, phospho(Ser^{473})-Akt, phospho(Thr^{308})-Akt, phospho-PTEN, and phospho($Ser^{21/9}$)-GSK-3α/β (37F11) were purchased from Cell Signaling Technology. Plcγ1 mouse antibody was purchased from BD Biosciences. Puromycin dihydrochloride, selection antibiotic, was purchased from Invitrogen. Metafectene transfection reagent was purchased from Biontex-USA. The Plc inhibitor U73122 was purchased from Sigma-Aldrich. The PTEN inhibitor SF 1670 was purchased from Echelon Biosciences.

Cell culture

Parental and FGFR2-overexpressing HEK293T cells were cultured in DMEM supplemented with 10% (vol/vol) FBS and 1% antibiotic/antimycotic (Lonza) in a humidified incubator at 37°C with 10% CO_2. Ci, G2i, and Pγi cells were established as described in Chapter Two.

Western Blot Analysis

Cultured cells were grown in 10-cm dishes and serum starved overnight. Cells were left untreated or treated with 9 μM U73122, 1 μm wortmannin, or 10 μM U0126 for 2 h. Cells were also treated with 500 nM SF 1670 for 30 min. Cells were lysed with Hepes lysis buffer (50 mM Hepes, pH 7.5, 1% [vol/vol] igepal-C630, 1 mg/ml bacitracin, 1 mM EDTA, 10 mM NaF, 1 mM sodium orthovanadate, 10% [vol/vol] glycerol, 50 mM NaCl, 1 mM PMSF, and Protease Inhibitor Cocktail Set III (EMD Millipore) . Protein concentration was quantified at 595 nm, and 50 μg of total proteins was used for every blot.

Kinase Assay

Cell lysates were collected and incubated with total Akt antibody overnight. Protein A/G Plus-Agarose (Santa Cruz Biotechnology) was used for immunoprecipitation experiments according to the manufacturer's instructions. Cell lysate bound to immobilized antibody waswashed with 3x lysis buffer , suspended in 50μl 1x kinase buffer (Cell Signaling Technology), and incubated with 10 mM ATP (1 μl)and Akt substrate (1 μl;purified GSK-3 fusion protein [Cell Signaling Technology]) for 30 min at 30°C.The reaction was terminated by adding sample loading buffer and heating the samples. Samples (20 μl) were loaded onto a gel and subjected to western blot analysis.

Soft Agar Assay

One milliliter of 1% FBS DMEM containing 0.75% agar was used as the bottom layer. 0.6 x10^4 of indicated cells were cast in agar as a single cell suspension in 1 ml DMEM (upper layer). Cells were left to grow for 8 days. 500 ml of DMEM with 1% FBS (with or without inhibitors (4 μM U73122/100 nM Wortmannin/5 μM U0126/150 nM SF 1670) was added to the wells once a week.

Drugs of interest were added to the underlay and overlay agar medium, as well as the liquid top layer which was initiated one day after seeding the cells. Concentrations were optimized so as to avoid cell death over the prolonged period of 8 days. Every experiment was performed in triplicates. Colonies were counted and averaged in different microscopic fields then normalized against control cells in serum starvation medium. Error bars on the graph represent the standard deviation calculated.

Phosphatase Assay

PIP_2 and Ptdser (both from Avanti Polar Lipids,INC) were prepared to a final concentration of 2 mg/ml and 5 mg/ml respectively in chloroform:methanol: 10mM HCl (20:9:1). The resuspension buffer was composed of 20 mM HEPES (pH 7.5), 1mM $MgCl_2$, and 1 mM EGTA. Kinase buffer consisted of 400 mM HEPES (pH 7.8), 100mM $MgCl_2$, and 20 mM EGTA.

For substrate preparation, 16.8 μl PIP_2 stock and 6 μl Ptdser stock were mixed, evaporated, resuspended in 500 μl resuspension buffer, sonicated for 1 min at

15% on ice. Eighteen microliters water, 2 µl cold ATP, 5 µl purified PI3K (Echelon), 50 µl PIP_2/Ptdser, and 20 µl γ^{32}P-ATP were mixed and incubated at room temperature overnight. The reaction was stopped by adding 100 µl of 1M HCl and 10 µl Ptdser.Ptdser was preparing the carrier lipid at a concentration of 5 mg/ml,drying out 40 µl , then resuspending in 400 µl resuspension buffer and sonicating)+ chloroform:methanol (1:2) + 0.5N NaCl in 0.1 N HCl. The obtained ratio was: 0.1:0.3:0.1.

The reaction was vortexed and centrifuged for 5 min at 10,000 x *g*. The bottom layer was dried and resuspended in 500 µl of lipid resuspension buffer. 145 µl of obtained solution was added to cell lysates or 55 µl was added to purified proteins reaction. In each case, 30 µl of substrate was utilized. This was followed by 2-h incubation at 37°C.

For cell lysate reaction,1M HCl, Ptdser, Chloroform:Methanol, 0.5N NaCl in 0.1 HCl were added as: 85 µl,40 µl, 900 µl, 300 µl.For purified protein reaction, 55 µl,10 µl, 450 µl, 150 µl of each reagent was used. Bottom phase was used for TLC.

PI3K Assay

2 mg/ml of cold PIP_2 and 5 mg/ml of Ptdser were each dissolved in chloroform:methanol: 10 mM HCl (20:9:1). 20 µl of Ptdser mixed with 50 µl PIP_2 were mixed, evaporated, and resuspended in 300 µl of resuspension buffer then sonicated for 1 minute at 15% on ice. 200 µl of kinase buffer was added, along with 32 µl cold 2.5 mM ATP (to a final concentration of 160 µM) and 1 µl

γ^{32}P ATP. 100 µl substrate was mixed with 100 µl of cell lysate and incubated for 2 hours at 37°C. Reaction was stopped by adding 5 µl Ptdser (made by preparing the carrier lipid at a concentration of 5 mg/ml,drying out 40 µl , then resuspending in 1000 µl resuspension buffer and sonicating). For each reaction,1M HCl, chloroform:methanol, 0.5N NaCl in 0.1 HCl were added as: 100 µl, 900 µl, 300 µl. Reaction was centrifuged for 3 minutes. Bottom phase was used for TLC analysis.

Microscopy

HEK293T cells (Ci and G2i) stable expressing GFP-FGFR2 were transfected with an empty mCherry vector or Akt-PH-mcherry using metafectene fllowing manufacturer's instructions. Success of transfection was detected via western blot analysis. Serum starved cells on glass coverslips were fixed with 4% (wt/vol) paraformaldehyde, pH 8.0 for 20 minutes when transfected with the domains. Cells were then washed with PBS, to be mounted onto a slide with mounting buffer (0.1% p-phenylenediamine/75% glycerol in PBS). Imaging was performed using a confocal microscope (model SP5; Leica) to detect colocalization between mcherry tagged construct and GFP used as a membrane marker to indicate membrane localization of the domain.

RPPA Analysis and Heat Map Generation

Cell lysates (Ci and G2i cells in triplicates) were submitted to the RPPA core facility. Based on the technical information provided by the facility, "the samples

were two-fold-serial diluted for 5 dilutions and arrayed on nitrocellulose-coated slide in 11x11 format. Samples were probed with antibodies by CSA amplification approach and visualized by DAB colorimetric reaction. Slides were then scanned on a flatbed scanner to produce 16-bit tiff image. Spots from tiff images were identified and the density was quantified by MicroVigene. Relative protein levels for each sample were determined by interpolation of each dilution curves from the "standard curve" (supercurve) of the slide (antibody). Supercurve is constructed by a script in R written by Bioinformatics. These values (given as Log^2 values) are defined as Supercurve Log2 (Raw) value". All the data points were normalized for protein loading and transformed to linear value designated as "Linear after normalization". The linear values were used for "bar graph" generation were the error bars indicate the calculated standard deviation. Heatmaps for an Unsupervised Hierarchical cluster (unsupervised on both antibodies and samples (data not shown)) and an antibody unsupervised but samples in order were provided. The heatmap included was generated in Cluster 3.0 (http://www.eisenlab.org/eisen/) as a hierarchical cluster using Pearson Correlation and a center metric. The resulting heatmap was visualized in Treeview {http://www.eisenlab.org/eisen/) and presented as a high resolution .bmp format."

Cell fractionation

HEK293T cells (Ci and G2i) were serum starved overnight and then washed 3X with PBS. Subcellular Protein Fractionation Kit for Cultured Cells (Thermo

SCIENTIFIC) was used according to manufaturer's instructions. Following protein quantification, western blot analysis was performed where FGFR2 was used as a membrane marker, and β-actin as cytoplasmic marker.

TCGA analysis

We downloaded and analyzed data publicly available from the Cancer Genome Atlas Project (TCGA; http://tcga-data.nci.nih.gov/) for eleven tumor types: bladder urothelial carcinoma (BLCA), breast invasive carcinoma (BRCA), colon adenocarcinoma (COAD), glioblastoma multiforme (GBM), head and neck squamous cell carcinoma (HNSC), kidney clear cell carcinoma (KIRC), lung adenocarcinona (LUAD), lung squamous cell carcinoma (LUSC), ovarian serous cystadenocarcinoma (OV), thyroid carcinoma (THCA), uterine corpus endometrial carcinoma (UCEC). Level 3 Illumina RNASeq (versions 1 and 2), respectively RPPA data were used to extract mRNA and protein expression levels. Analyses were performed in R (version 2.14.2) (http:///www.r-project.org/) and the statistical significance was defined as a p-value less 0.05. The Spearman's rank-order correlation test was applied to measure the strength of the association between mRNA and RPPA levels across tumor types. A box-and-whisker plot was used to visualize RPPA levels across tumor types.

Molecular cloning

Empty mCherry vector was used in the experiments along with Akt-PH domain cloned in mCherry vector. The kinase dead cytoplasmic portion of FGFR2 (residues 413-821) was generated through a point mutation (K517I) in the catalytic region. Grb2 was also cloned in a myc tagged pCDNA3.1 mammalian expression vector.

Protein expression and purification

6Xhistidine-tagged constructs of FGFR2, and Grb2 were expressed and purified from *E. coli* as previously described (3).

Measurement of PIP_3 level in whole cells

Measurement of steady-state content of phosphatidylinositol 3,4,5-bisphosphate (PtdIns(3,4,5)P_3) was performed in [^{3}H]myo-inositol uniformly radiolabelled cells. HEK293T cells were prelabeled with myo-[2-^{3}H(N)]inositol (1µCi/ml) (Perkin-Elmer) for 24 h in inositol and serum-free DMEM medium and then washed with PBS. After labeling, the cells were harvested, washed, and subjected to lipid extraction and TLC analysis.

Lipid extraction and TLC Analysis

The cell pellet was resuspended in 0.2 ml of 0.5 N NaCl in 0.1 N HCl and 0.6 ml chloroform: methanol (1:2) was added and the suspension was vigorously

vortexed for 30 min. 0.2 ml of 0.5 N NaCl in 0.1 N HCl was added followed by vortexing for 10 min. After 5 min of centrifugation on Eppendorf Table Centrifuge, upper water-methanol phase was discarded and lower chloroform lipid phase was transferred to an Eppendorf tube.

Lipids extracts were used in thin layer chromatography (TLC) analysis. 25,000 cpm aliquots were brought to same volume with chloroform. The phospholipids were analyzed by silica gel TLC after separation by one-dimensional TLC on potassium oxalate impregnated silica gel plates using a solvent system containing chloroform/methanol/ammonium hydroxide/water (57:50:4:11, v/v/v/v) to separate PtdIns(4,5)P_2, PtdIns(3,5)P_2 , and PtdIns(3,4,5)P_3 from one another.

20 cm high-performance Partisil LK5 silica gel precoated TLC plates with a concentration-zone (Whatman Inc. Clifton, NJ) were impregnated for 1 min in 1.2 % (w/v) potassium oxalate in methanol-water (2:3). After air drying, the plates were desiccated at 100°C for 60 min before use. Radiolabeled lipids were visualized and quantified using a Personal Molecular ImagerTM FX (Bio-Rad Laboratories). Stored images were processed and quantified using Quantity One software for scanning and analysis of the captured Phosphor images (Bio-Rad Laboratories). Phospholipid content is expressed as mol% of total phospholipid based on the pixel intensity of the captured signal on Phosphor screen generated by the radiolabeled spots on the TLC plate.

Xenograft mouse model and magnetic resonance imaging (MRI)

Adult female nude mice were injected with 0.5 x10^6 PCi, PG2i, PPγi, Ci, G2i , and Pγi cells in PBS (4 mice per group). Injections were done subcutaneously in the right flank of the animal. After 60 days and for MRI imaging, mice were scanned on a 4.7T Biospec USR47/40 small animal imaging system (Bruker Biospin MRI, Inc., Billerica, MA) with a 35-mm linear volume resonator and 60-mm micro-imaging gradients. A three-plane FLASH imaging sequence was used to confirm animal positioning, and coronal and axial T2-weighted RARE images (TE/TR 57/3000ms, FOV 4cm × 3cm, matrix 256 × 192, RARE factor 12) were used for tumor localization and volume measurement.

For tumor volume calculation ROI was created in imageJ software that surrounds tumors in the axial sections (for every slice). The areas of the ROIs is in mm^2. ROI areas were then summed up and multiplied by the slice thickness (0.75 mm for all of the scans). This is the volume of tumor within the image slices. To account for the slice gap between adjacent slices (0.25 mm for all of the scans), the mean of the ROI areas for each pair of adjacent slices was computed then the sum of these means is multiplied by 0.25 mm to get an estimate of the tumor volume between slices. The tumor volume estimates were then added within slices and between slices to get the total tumor volume in mm^3. Tumor volumes for mice in each group were averaged.

Following imaging, mice were sacrificed, tumors were weighed and weights were averaged in each group and plotted as bar graph where the standard

deviation of the mean is denoted by error bars. Half of each tumor was used for western blot analysis and the other half for immunohistochemistry (IHC). Proteins used in western blot analysis were extracted via sonication up to 30 minutes on ice at low setting (to efficiently separate the lipid fraction found on top of protein layer). This was followed by centrifugation at 13000 rpm for 15 minutes at 4°C. The supernatant containing the proteins was transfered to a new tube. IHC was performed on paraffin embedded tumors sectioned at 5 μm. Hematoxylin and eosin staining along with pAkt (serine 473) antibody staining were performed on rehydrated samples followed by visualization. This was done using automated Leica Bond III- autostainer (Department of Veterinary Medicine & Surgery at MD Anderson Cancer Center). For that, slides were baked at 60ºC for 30 minutes then the temperature was increased to 72ºC. Slides were then rinsed 3 times with Bond Dewax followed by absolute alcohol and Bond Wash. Temperature was then increased to 100ºC, and Bond ER Solution 1 (ph6) was applied and incubated for 30 minutes. Slides were rinsed with Bond Wash and temperature was allowed to come down to room temperature. Antibody Phospho-Akt (Ser473) (D9E) XP Rabbit mAb #4060 (Cell Signaling Technology) was applied at 1:50 dilution and incubated for 15 minutes at room temperature followed by rinsing with Bond Wash. Post Primary was applied and incubated for 8 minutes then slides were again rinsed with Bond Wash. Bond Polymer was applied and incubated for 8 minutes followed by rinsing with Bond Wash 2 times then DIH_2O. Peroxide Block was applied and incubated for 5 minutes then rinsed with Bond Wash 4 times then with DIH_2O.

DAB was applied and incubated for 10 minutes then rinsed with DIH_2O 3 times. Hematoxylin was applied and incubated for 7 minutes then rinsed with Bond Wash. Slides were then removed from Leica Bond III and rinsed with DIH_2O 4 times. They were then dehydrated in graded alcohols and xylene then coverslipped with ClearMount from American MasterTech using Leica CV5030 coverslipper.

Results

Grb2 depletion increases cell proliferation

In non-stimulated FGFR2-over-expressing HEK293T G2i cells, the number and size of anchorage-independent colonies was dramatically increased compared with Ci cells (**Figure 4.2a,b,c,d**). Furthermore, colony formation was abrogated in parental HEK293T cells, which express low levels of endogenous FGFR2 (**Figure 4.2a,e**). Therefore, colony formation was associated with constitutive Grb2-FGFR2 complex formation (2), which inhibits protein recruitment to the receptor C-terminus (59). Anchorage-independent growth was independent of the MAPK pathway as evidenced by the lack of effect of the potent MAPK inhibitor U0126 on colony formation (**Figure 4.2b,c** and **Fig4.3a,b**).

Because Grb2 is a key component of the RTK-mediated up-regulation of the MAPK pathway, which is linked to proliferative response, increased colony growth in the absence of Grb2 was a surprising observation. The absence of a MAPK proliferative signal strongly implicated PI3K/Akt pathway activation in the observed colony formation.

FGFR2-mediated anchorage-independent growth was dependent on Plcγ1 because colony formation was largely abrogated in G2i cells treated with the phospholipase inhibitor U73122 (**Figure 4.2b,c**). Furthermore, Plcγ1 knockdown in GFP-FGFR2-over-expressing HEK293T (Pγi) cells and parental cells stably transfected with empty GFP vector (PPγi) inhibited colony formation (**Fig4.3c-f**). Thus, anchorage-independent growth was specifically dependent on high FGFR2, low Grb2, and high Plcγ1 expression levels.

a

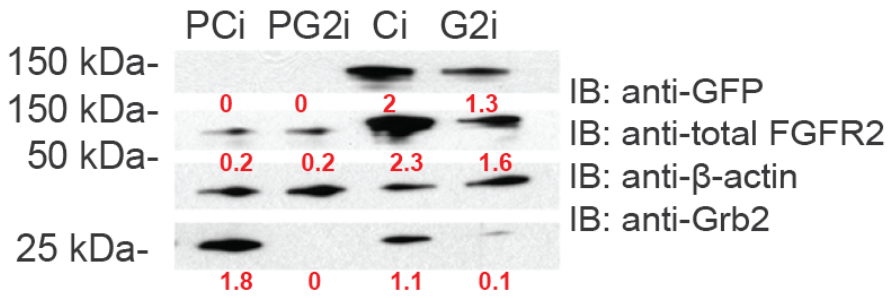
PCi
PG2i
Ci
G2i
150 kDa-
150 kDa-
50 kDa-
25 kDa-
0
0
2
1.3
0.2
0.2
2.3
1.6
1.8
0
1.1
0.1
IB: anti-GFP
IB: anti-total FGFR2
IB: anti-β-actin
IB: anti-Grb2

b

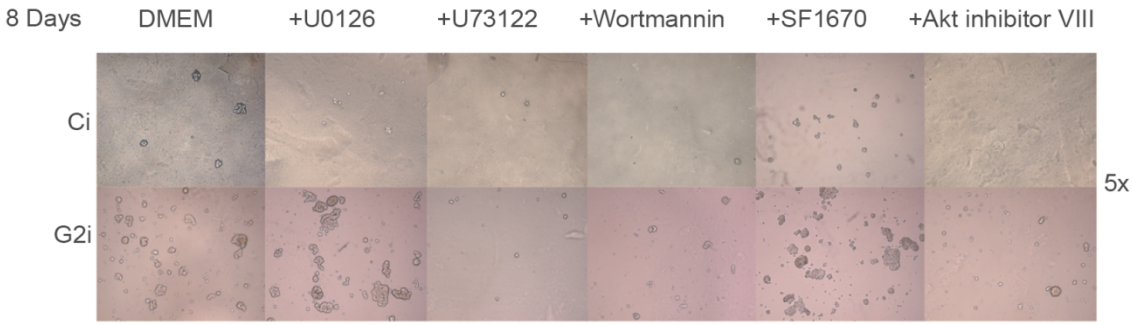
8 Days
DMEM
+U0126
+U73122
+Wortmannin
+SF1670
+Akt inhibitor VIII
Ci
G2i
5x

c

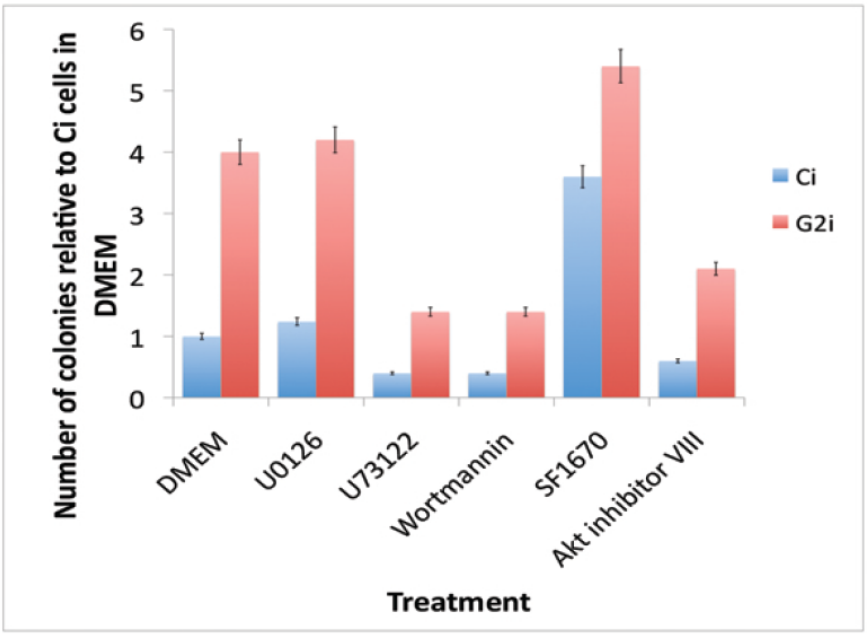
Number of colonies relative to Ci cells in DMEM
0
1
2
3
4
5
6
DMEM
U0126
U73122
Wortmannin
SF1670
Akt inhibitor VIII
Treatment
Ci
G2i

d

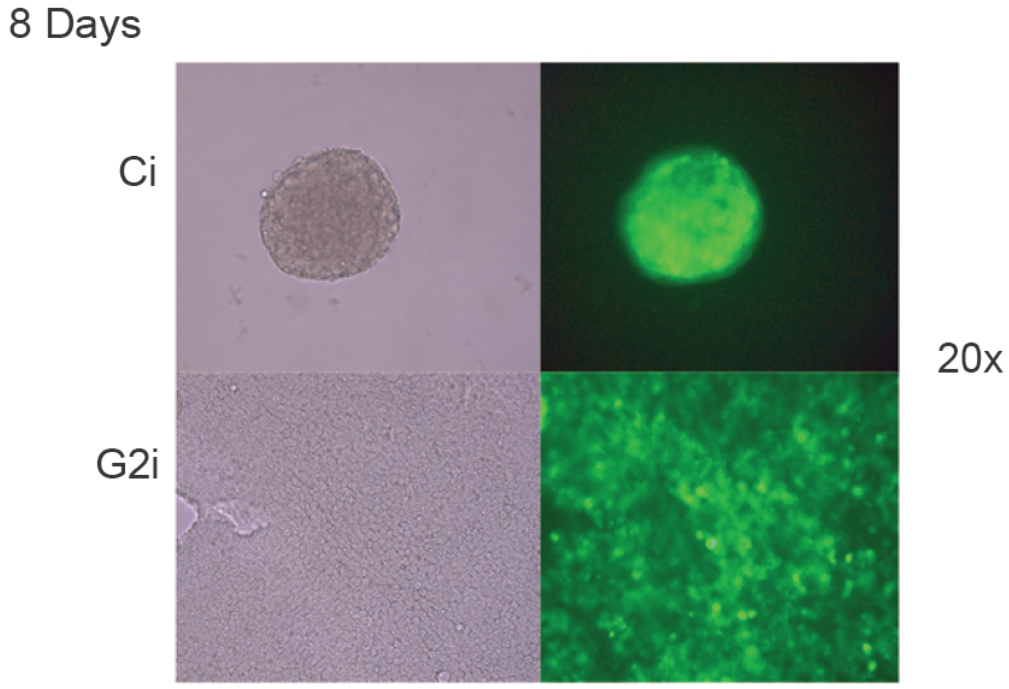
8 Days
Ci
G2i
20x

e

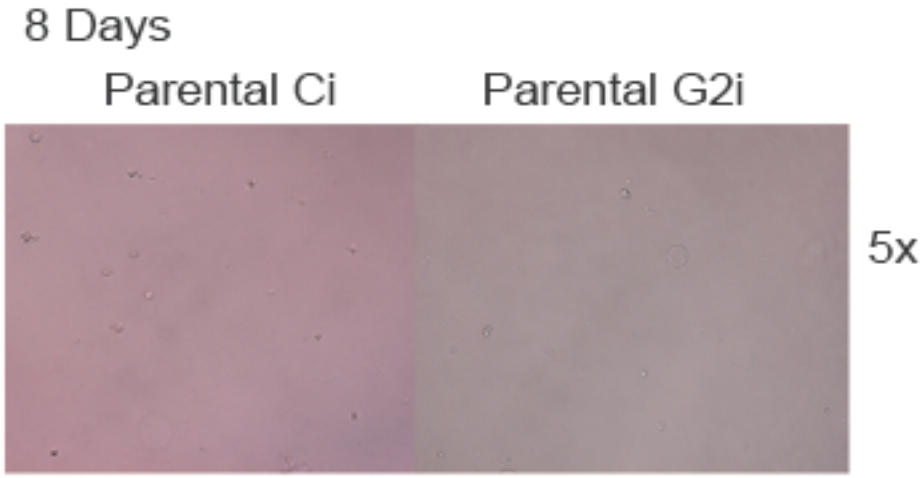

Fig 4.2: FGFR2 is required for Akt-dependent colony formation in Grb2 knockdown cells.a) Parental and FGFR2-overexpressing HEK293T cells were transfected with scrambled and Grb2 shRNAs to generate PCi and PG2i and Ci and G2i cell lines, respectively. Western blot analysis was done to determine the efficiency of FGFR2 transfection and Grb2 knockdown. Arbitrary numbers on the blot represent densitometric analysis performed via Image J software.**b**) Soft agar assay was used to determine anchorage-independent growth in Ci and G2i cells. The lower layer consisted of DMEM/agar containing 1% FBS. The upper layer consisted of a single cell suspension (0.6 $x10^4$)in serum-free DMEM/agar.Colony formation was determined after 8 d. DMEM containing 1% FBS with or without the indicated inhibitors was added to the wells once a week. **c**) The number of colonies was counted in different microscopic fields and normalized to Ci cells in serum-free DMEM. Values shown represent the mean ± standard deviation of three independent experiments. **d**) Magnification of colony formation in GFP-FGFR2-overexpressing Ci andG2i cells.**e**) Anchorage-independent growth was determined in parental HEK293Tcells using soft agar assay as described in **b**.

a

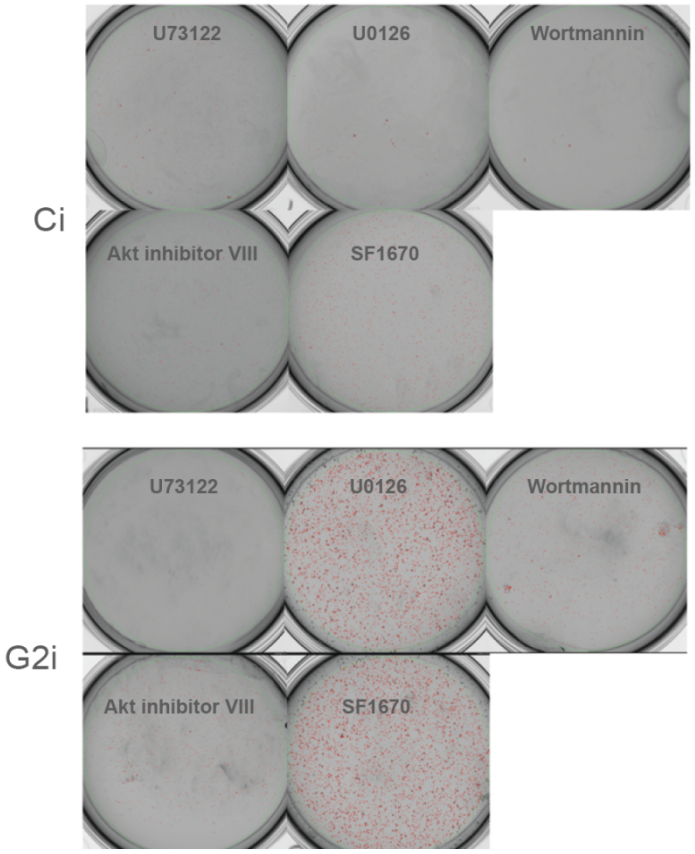
Ci
U73122
U0126
Wortmannin
Akt inhibitor VIII
SF1670
G2i
U73122
U0126
Wortmannin
Akt inhibitor VIII
SF1670

b

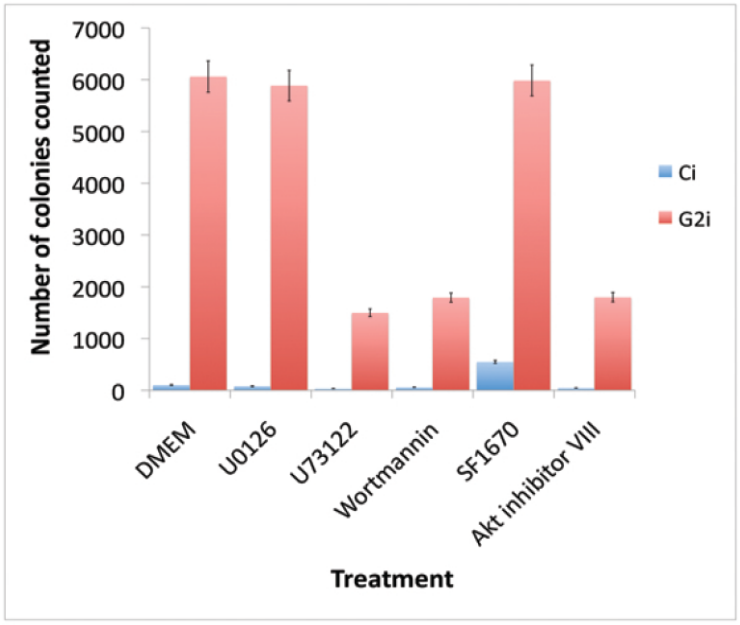
Number of colonies counted
7000
6000
5000
4000
3000
2000
1000
0
Ci
G2i
DMEM
U0126
U73122
Wortmannin
SF1670
Akt inhibitor VIII
Treatment

c

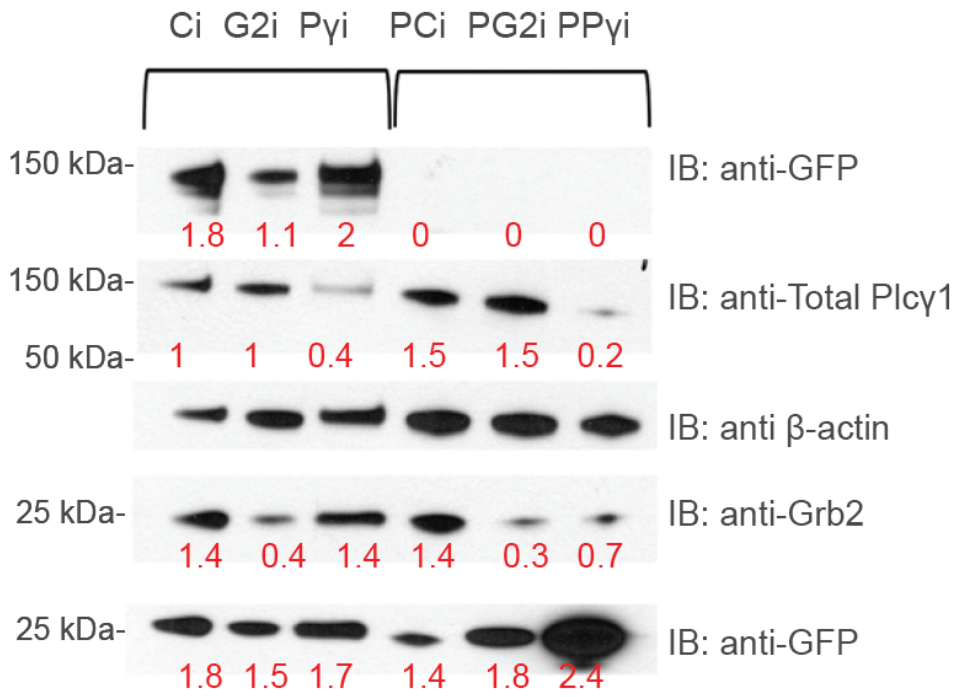
Ci G2i Pγi PCi PG2i PPγi
150 kDa-
IB: anti-GFP
1.8 1.1 2 0 0 0
150 kDa-
IB: anti-Total Plcγ1
50 kDa-
1 1 0.4 1.5 1.5 0.2
IB: anti β-actin
25 kDa-
IB: anti-Grb2
1.4 0.4 1.4 1.4 0.3 0.7
25 kDa-
IB: anti-GFP
1.8 1.5 1.7 1.4 1.8 2.4

d

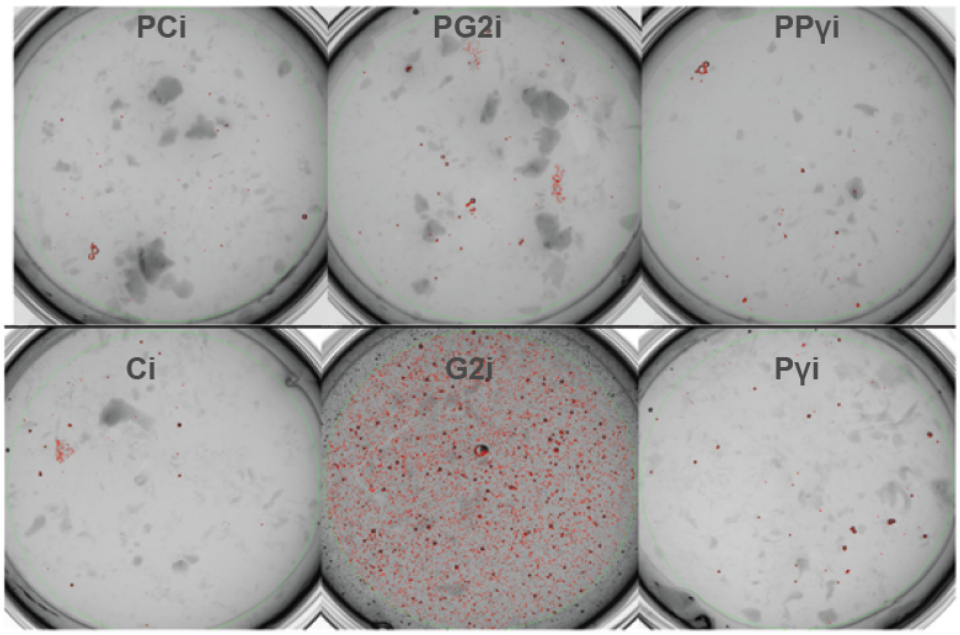
PCi
PG2i
PPγi
Ci
G2i
Pγi

e

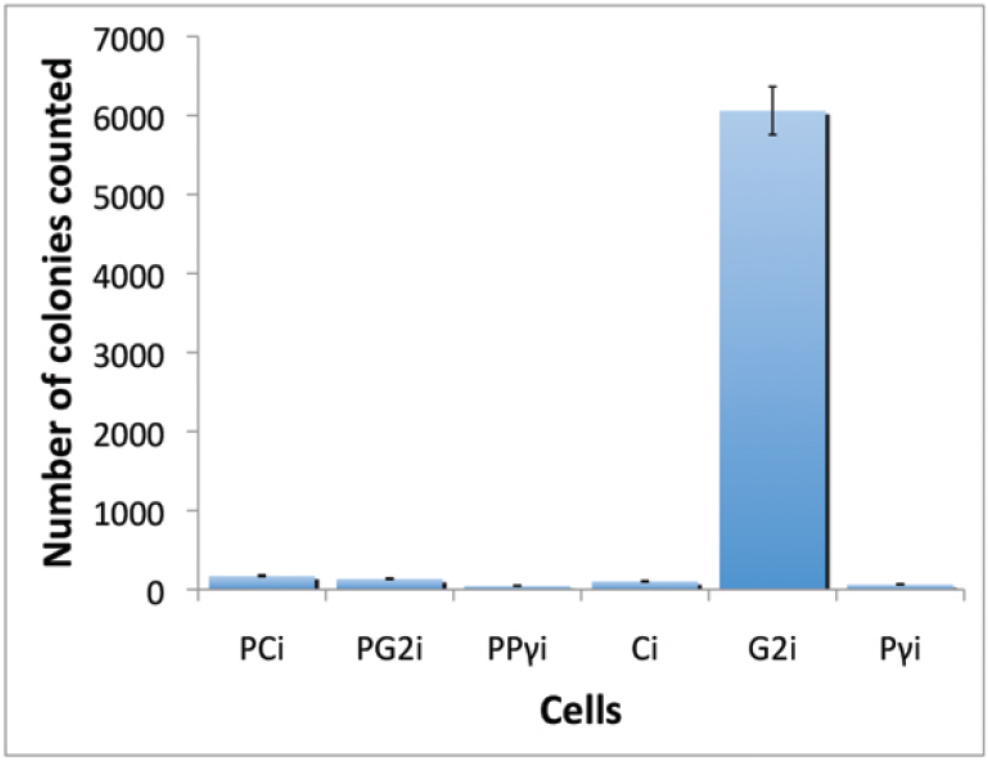
Number of colonies counted
7000
6000
5000
4000
3000
2000
1000
0
PCi
PG2i
PPγi
Ci
G2i
Pγi
Cells

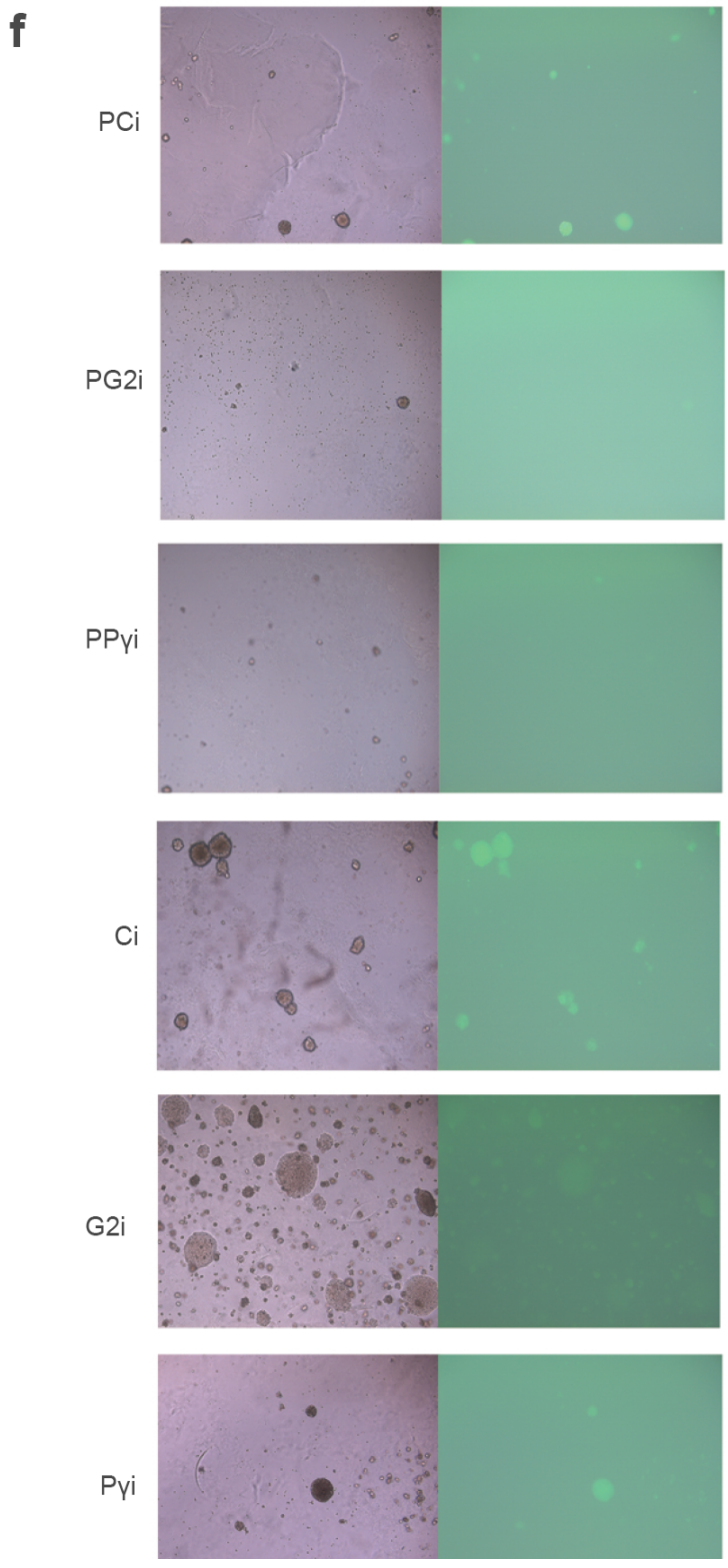
f
PCi
PG2i
PPγi
Ci
G2i
Pγi

Fig 4.3: Plcγ1 is required for FGFR2 to induce Akt-dependent colony formation. a) Soft agar assay was used to evaluate anchorage-independent growth in Ci and G2i cells. The lower layer consisted of DMEM/agar containing 1% FBS. The upper layer consisted of a single cell suspension (0.6 $x10^4$) in serum-free DMEM/agar. After 8 days, DMEM containing 1% FBS with or without the indicated inhibitors was added to the wells once a week. Pictures of the entire well were taken.**b**)The number of colonies was counted and normalized to Ci cells in serum-free DMEM. Values shown represent the mean ± standard deviation of three independent experiments.**c**) Parental and FGFR2-overexpressing HEK293T cells were transfected with scrambled, Grb2 and Plcγ1 shRNAs to generate PCi, PG2i, and PPγi and Ci, G2i, and Pγi cell lines, respectively. The efficiency of Grb2 andPlcγ1 knockdown and FGFR2 transfection was confirmed by western blot analysis.**d**) Soft agar assay was done to evaluate anchorage-independent growth in Ci, G2i, Pγi, PCi, PG2i, and PPγi cells as described in a.**e**) The number of colonies wascounted and normalized to PCi cells in DMEM containing 1% serum. Values shown represent the mean ± standard deviation of three independent experiments.**f**) Magnification (5x) of colony formation in one microscopic field for Ci, G2i, Pγi, PCi, PG2i, and PPγi cells.

PI3K activity is unaffected in Grb2-depleted cells

We previously reported that Grb2 depletion in non-stimulated cells up-regulated Plcγ1, leading to turnover of plasma membrane PIP_2 (59). In addition to Plcγ1, cellular PIP_2 concentration of is regulated by PI3K and PTEN. Therefore, we determined whether PI3K and PTEN were involved in the proliferative cellular response in non-stimulated G2i cells.To do this, reverse phase protein array (RPPA) was used to assess the expression and/or phosphorylation of select proteins and effectors of the PI3K and PTEN pathways in non-stimulated Ci and G2i cells (**Fig 4.4a)**. A comprehensive heat map is shown in **Fig 4.5** and**Table 4.1**. The expression level of the p85 and p110 subunits of PI3K were not appreciably changed between G2i and Ci cell lines (**Fig 4.4b**). The addition of the PI3K inhibitor wortmannin reduced colony formation in Ci and G2i cells, suggesting the presence of constitutive PI3K activity in both cell lines (**Fig 4.2**

b,c). PI3K converts PIP_2 to PIP_3; therefore, the constitutive PI3K activity in G2i cells suggested that the combined activities of Plcγ1 and PI3K deplete the pool of PIP_2 to reduce the PIP_2/PIP_3 ratio (see schematic in **Fig 4.1**).

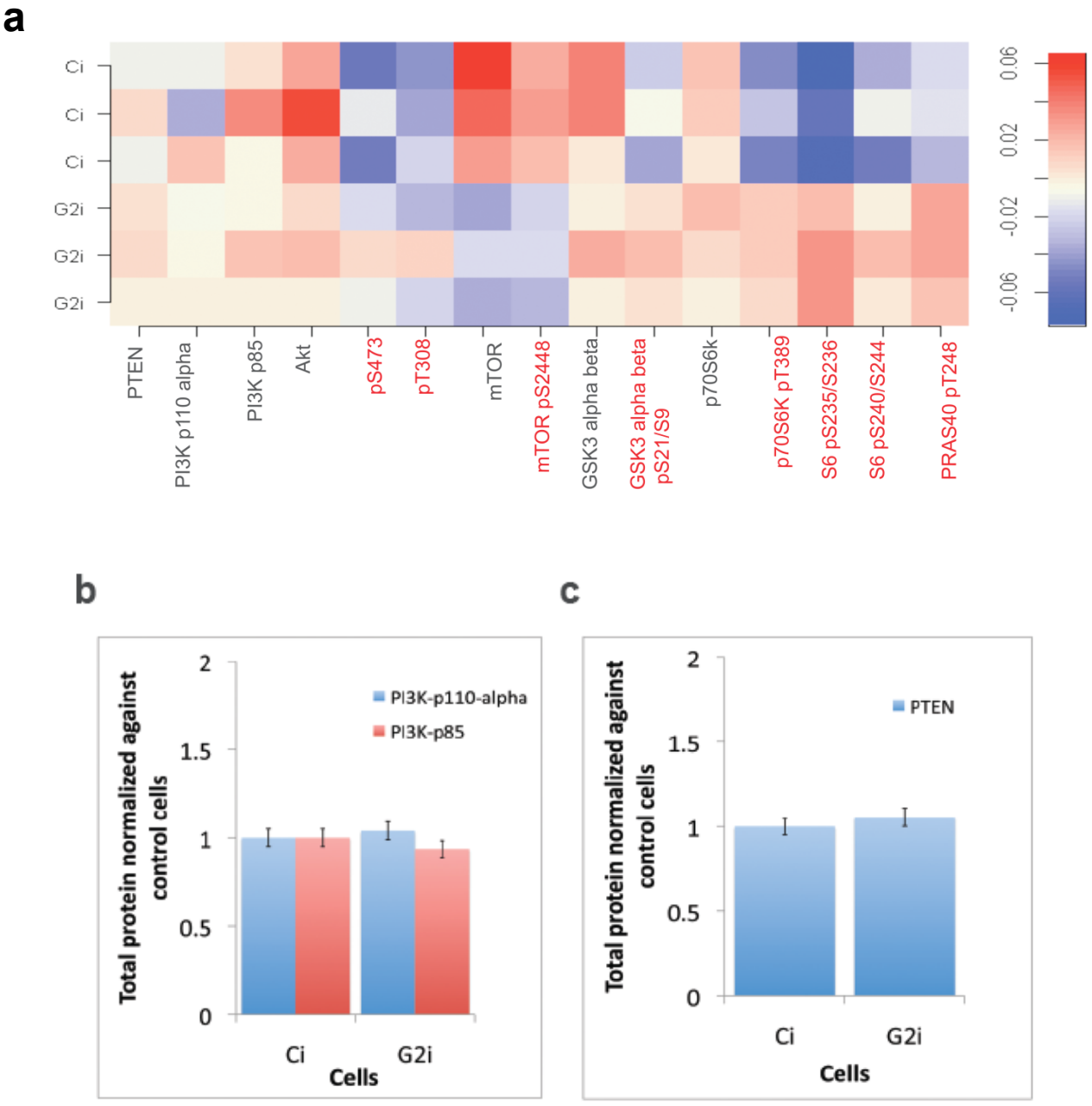

d

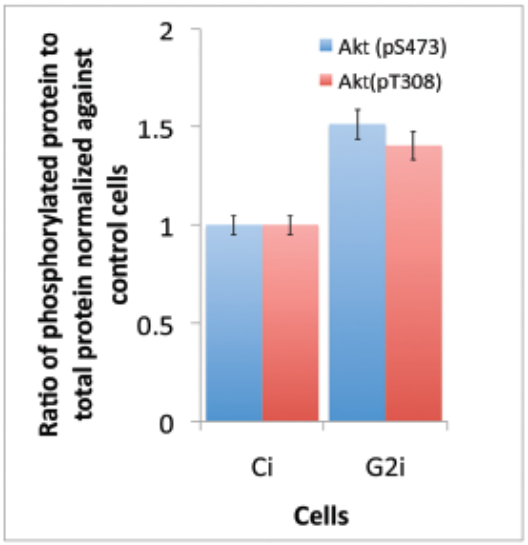
Ratio of phosphorylated protein to total protein normalized against control cells
2
1.5
1
0.5
0
Akt (pS473)
Akt(pT308)
Ci
G2i
Cells

e

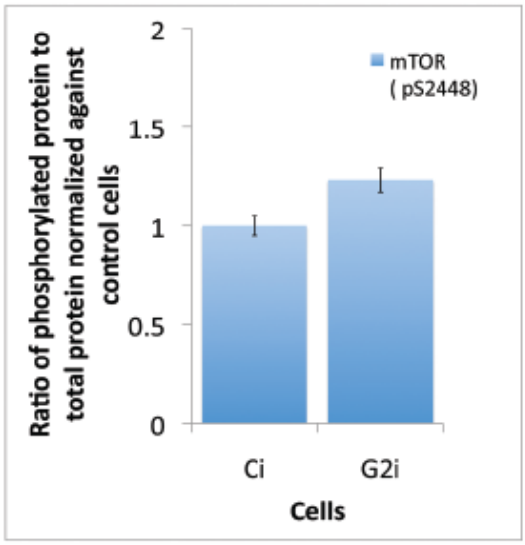
Ratio of phosphorylated protein to total protein normalized against control cells
2
1.5
1
0.5
0
mTOR
(pS2448)
Ci
G2i
Cells

f

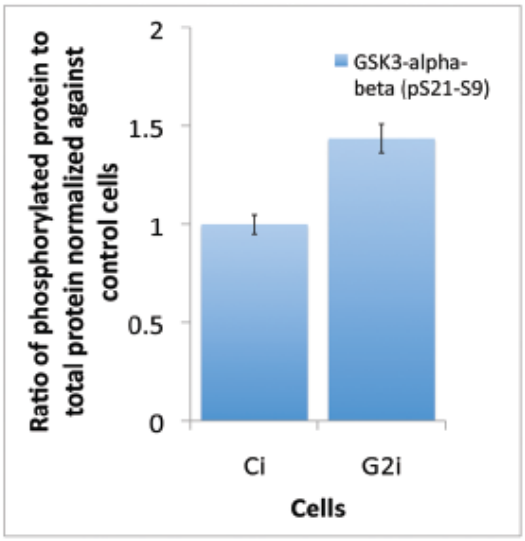
Ratio of phosphorylated protein to total protein normalized against control cells
2
1.5
1
0.5
0
GSK3-alpha-beta (pS21-S9)
Ci
G2i
Cells

g

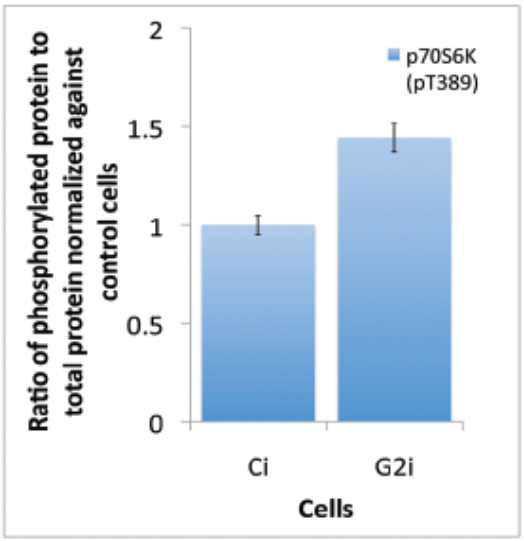
Ratio of phosphorylated protein to total protein normalized against control cells
2
1.5
1
0.5
0
p70S6K
(pT389)
Ci
G2i
Cells

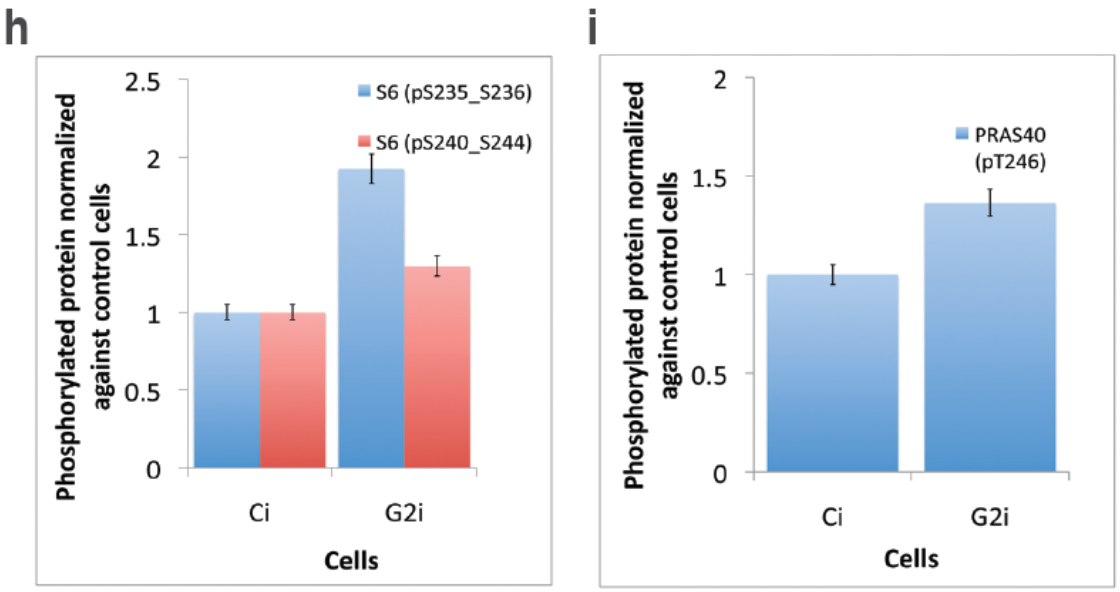

Fig 4.4 Increased phosphorylation of Akt in G2i cells is independent of PI3K and PTEN expression. a) Heat map of the $\log^2$ values of triplicate samples from Ci and G2i cells. The heat map was generated from the original heat map provided by the facility using theR console statistical package.**b-i**) Linear values normalized to control cells were used to construct bar graphs of the ratios of phosphorylated protein to total protein, phosphorylated protein to actin, and total protein to actin.

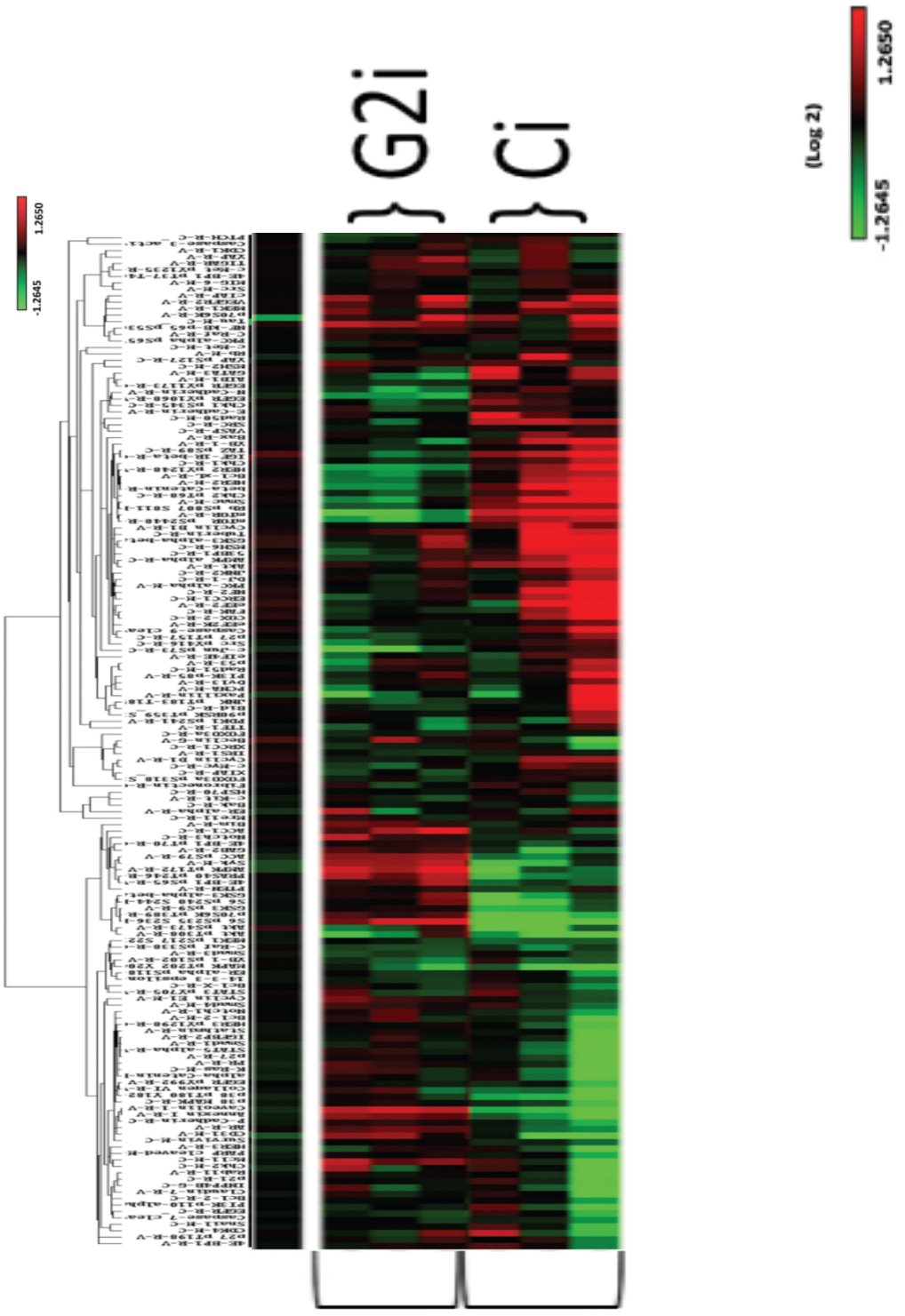

Fig 4.5 Phosphorylation levels of Akt and its downstream effectors is higher in G2i cells compared with Ci cells. RPPA heat map showing the phosphorylation levels of Akt and its downstream effectors in G2i and Ci cells.

	Total PTEN	PI3K-p110-alpha	PI3K-p85	Total Akt	Phosphorylated Akt (Serine 473)	Phosphorylated Akt (Threonine 308)
Ci	1.090579834	0.436649343	2.335569201	3.007820043	0.909052249	0.654950297
Ci	1.22995059	0.367177654	2.924489743	3.620852242	1.224699291	0.6806049
Ci	1.09463821	0.521441928	2.230116403	2.919400685	0.919297713	0.775685497
G2i	1.209501032	0.450361852	2.204692876	2.604253717	1.173441465	0.710449412
G2i	1.228035122	0.458361052	2.539196004	2.816735023	1.401224118	0.961625242
G2i	1.163679211	0.469542887	2.271266121	2.458209744	1.235440329	0.775212965

	Total mTOR	Phosphorylated mTOR (Serine 2448)	Total GSK3-alpha-beta	Phosphorylated GSK3-alpha-beta (Serine 21/9)	Total p70S6K	Phosphorylated p70S6K (Threonine 389)	Phosphorylated S6 (Serine235/236)	Phosphorylated S6 (Serine240/244)	Phosphorylated PRAS40 (Threonine 246)
Ci	9.878680022	1.92269853	5.64098236	1.992227398	3.1777385	1.767151144	2.093519588	2.024540878	1.496991695
Ci	8.648820605	1.981774535	5.637970293	2.236976555	3.097315484	2.04281989	2.399091706	2.404274402	1.544884497
Ci	7.697418793	1.847918229	4.30959441	1.794813431	2.899587442	1.761170659	2.239527709	1.793370155	1.364858516
G2i	4.778102227	1.386060631	4.25648855	2.450103001	3.247006853	2.690817512	4.030998347	2.567469178	2.052589438
G2i	5.493817656	1.419087584	5.130953123	2.695067443	3.014280701	2.697923616	4.447246735	2.908008957	2.067048089
G2i	4.887267389	1.287394207	4.242939227	2.42391246	2.812191854	2.564749685	4.473220993	2.600325589	1.892220984

Table 4.1 Linearized values obtained from the RPPA analysis of G2i and Ci cells. Linearized values of the expression and/or phosphorylation of PTEN and Akt and their downstream effectorsfrom the RPPA analysis of G2i and Ci cellsare shown. Linear values were averaged, normalized tocontrol cells, and used to generate bar graphs.

In Ci cells, the pool of PIP_2 is not as severely affected because Plcγ1 is inhibited in the presence of Grb2. Addition of the PI3K-specific inhibitor wortmannin reduced PIP_3 production in Ci cells; therefore, PI3K contributed in part to PIP_2 depletion (**Fig 4.6a,b**). Intracellular level of PIP_3 in myo-[2-^{3}H(N)]inositol-labeled Ci and G2i cells was also measured in **Fig 4.6c** and it appeared to increase upon knocking down Grb2.

a

b

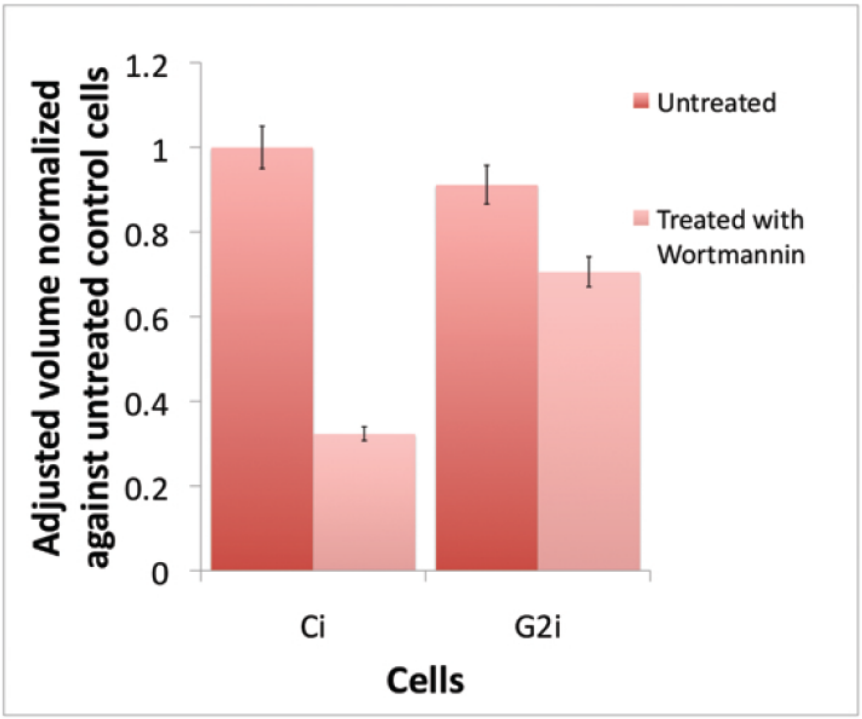

c

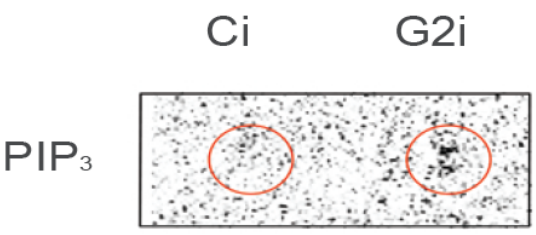

Pixel value 10412 14090

Fig 4.6 PIP_3 to PIP_2 ratio is higher in G2i cells compared with Ci cells and is independent of PI3K p85 phosphorylation level and activity. a) PI3K kinase assay was performed on cell lysates obtained from untreated andwortmannin-treated Ci and G2i cells. Cell lysates were incubated^{32}P-labeled ATP and unlabeled PIP_2, PI3K substrate. PIP_3 product and remaining PIP_2 substrate were separated by TLC. **b**) PI3K kinase assay data was volume adjusted (pixel percentage and normalized to untreated control cells were obtained in duplicates visualized and quantified for adjusted volume. **c**) Lipid was extracted from cell lysates obtained from myo-[2-^{3}H(N)]inositol-labeled Ci and G2i cells . PIP_3 was identified by TLC based on the *Rf* value and quantified at the pixel level.

PTEN activity is down-regulated in Grb2-depleted cells

The effect of PI3K on PIP_3 production is reversed by PTEN phosphatase activity, which restores membrane PIP_2 concentrations. Incubation of G2i cell lysates with ^{32}P-PIP_3 inhibited the ability of PTEN to restore $PI(4,5)P_2$ levels, resulting in a dramatic reductioninPIP$_2$/PIP$_3$ratio (**Fig 4.7a**). RPPA analysis showed that PTEN expression was not significantly different between G2i and Ci cells (**Fig 4.4c**). Because PTEN binding to PIP_2 is required to induce its activity, the reduction in the PIP_2 pool resulting from combined Plcγ1 and PI3K activitiesin G2i cells may affect the ability of PTEN to turnover PIP_3. In other words, PIP_2 depletion negatively regulates PTEN, resulting in the accumulation of PIP_3.To demonstrate that the increase in PIP_3 in G2i cells is dependent on PTEN, cells were treated with the PTEN inhibitor SF1670. PTEN inhibition using SF1670 reduced PIP_2/PIP_3 ratio (**Fig4.7a**). Furthermore, inhibition of Plcγ1 using U73122 reduced PIP_2 concentration and PIP_2/PIP_3 in G2i cells to that of Ci cells (**Fig 4.7a**). To determine whether Plcγ1 affects PTEN phosphatase, Ci cells were either left untransfected or transfected with wild-type Plcγ1. PTEN activity was lower in Plcγ1-transfected Ci cells than in

untransfected Ci cells (**Fig 4.7b**). Together, these findings indicated that Plcγ1-mediated PIP_2 depletion disables PTEN activity.

a

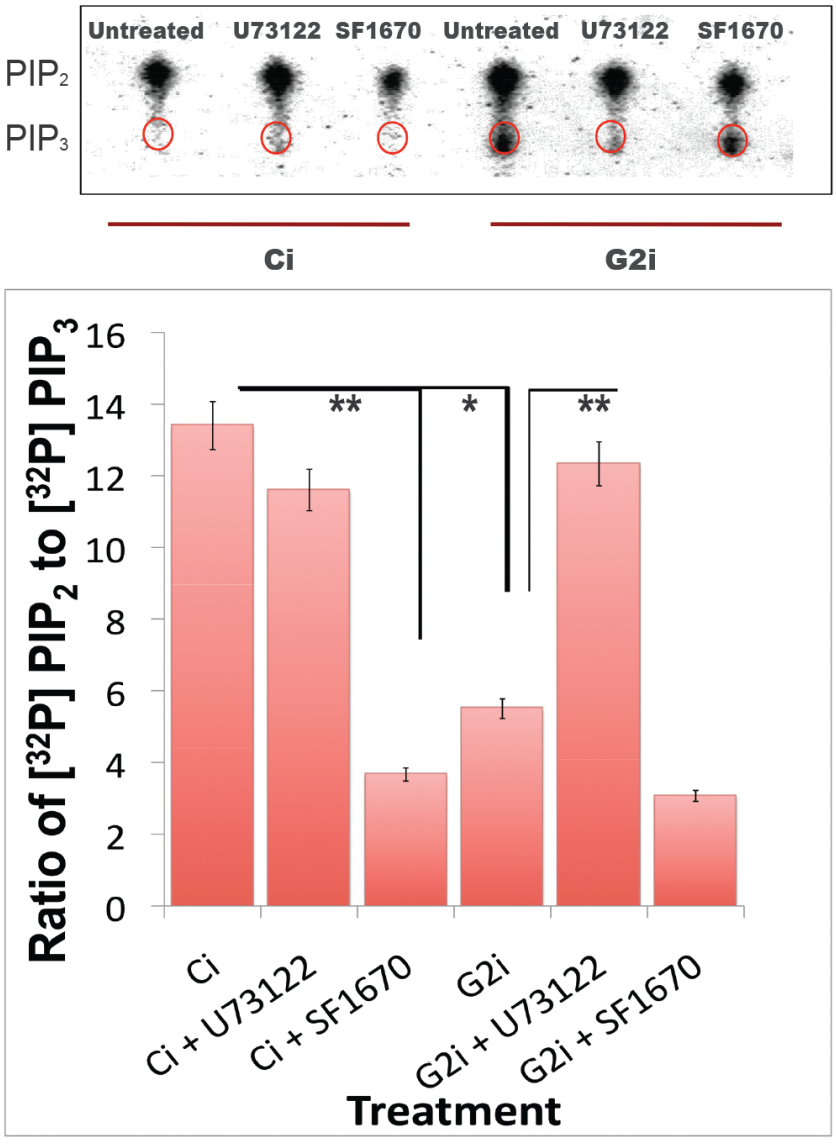

b

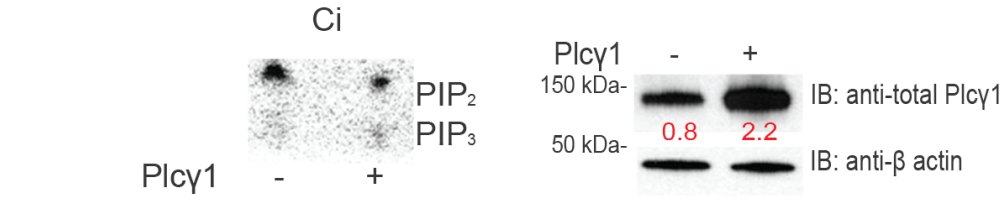

Plcγ1	-	+
PIP_2 pixel value	3778	1495
PIP_3 pixel value	512	531
Ratio	**7**	**3**

c

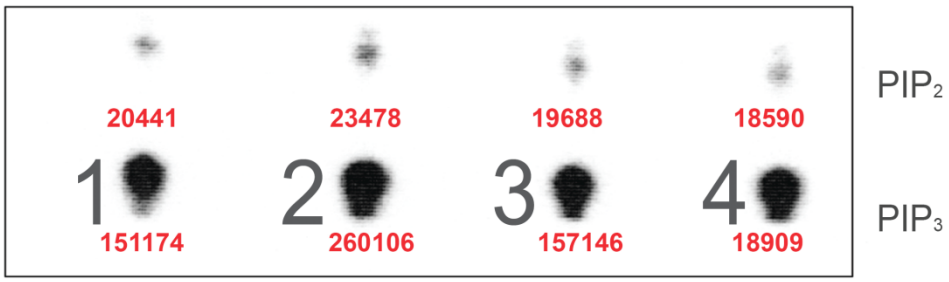
20441
23478
19688
18590
1
2
3
4
151174
260106
157146
18909
PIP2
PIP3

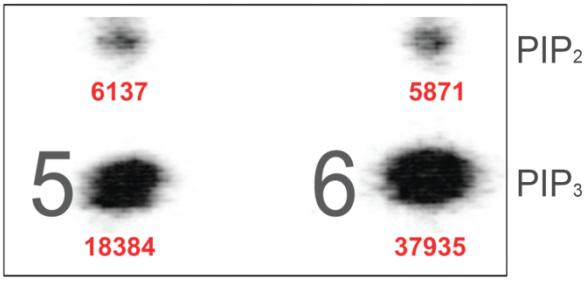
6137
5871
5
6
18384
37935
PIP2
PIP3

d

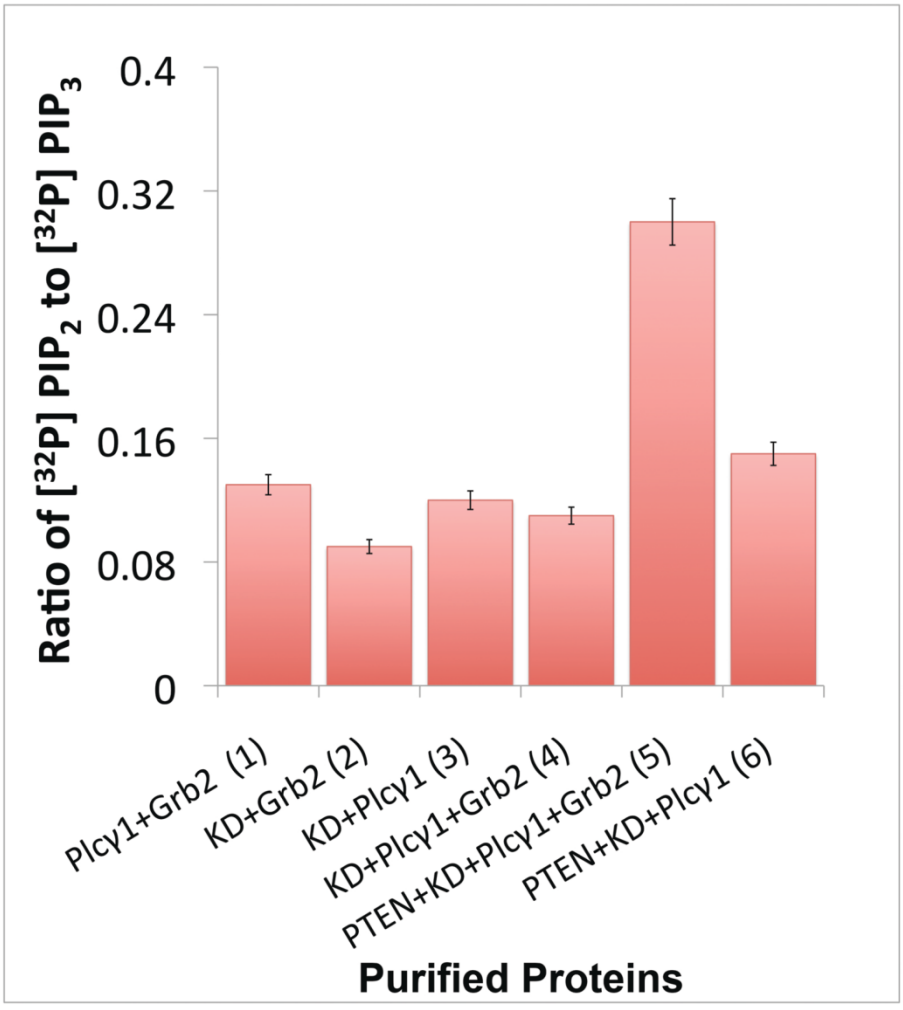
Ratio of [32P] PIP2 to [32P] PIP3
0.4
0.32
0.24
0.16
0.08
0
Plcγ1+Grb2 (1)
KD+Grb2 (2)
KD+Plcγ1 (3)
KD+Plcγ1+Grb2 (4)
PTEN+KD+Plcγ1+Grb2 (5)
PTEN+KD+Plcγ1 (6)
Purified Proteins

e

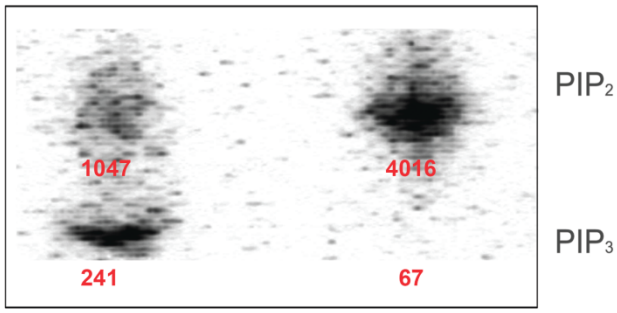
PIP2
PIP3
1047
4016
241
67

f

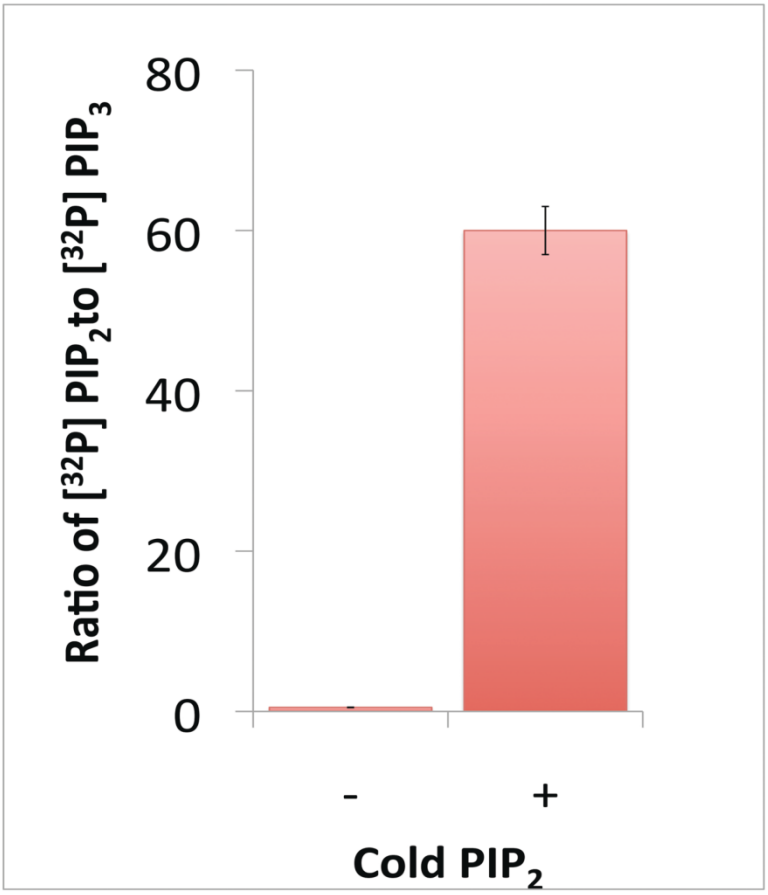
Ratio of [32P] PIP2 to [32P] PIP3
80
60
40
20
0
-
+
Cold PIP2

Fig 4.7 Plcγ1-mediated PIP2 depletion negatively regulates PTEN activity in G2i cells.a) Cell lysates were obtained from cells treated with the Plcγ1 inhibitor U73122 or the PTEN inhibitor. Cell lysates from untreated cells served as a control. Cell lysates were incubated with ^{32}P-labeled PIP_3, and TLC was used to separate and identify PIP_2 and PIP_3 (*top panel*). PIP_2/PIP_3ratioswere generated from the pixel data and are presented as the mean ± standard deviation of three independent experiments (*bottompanel*). *p ≤ 0.05 and **p≤ 0.01 (Student's t-test).(**b**) Ci cells were left untransfected or transfected with Plcγ1.Cell lysates were incubated with ^{32}P-labeled PIP_3, followed by TLC analysis and PIP_3/PIP_2 ratio quantification as described in **a**. **c**,**d**) Various combinations of purified proteins including Plcγ1, Grb2, PTEN, and kinase dead (KD) FGFR2wereincubated with ^{32}P-labeled PIP_3, followed by TLC analysis and PIP_3/PIP_2 ratio quantification as described in **a**. Values shown represent the mean ± standard deviation of triplicatesamples. **e,f**) Purified PTEN was incubated with Ptdser and [^{32}P]-PI (3,4,5)P_3 in the presence or absence of 33 µg/µl cold PIP_2. ^{32}P-PIP_2 and PIP_3 were separated by TLC, visualized, and quantified at the pixel level (*top panel*). PIP_2/PIP_3 ratios were generated from the pixel data and are presented as the mean ± standard deviation of two independent experiments (*bottom panel*).

Inhibition of PTEN using SF1670 slightly increased colony formation in G2i cells (**Fig 4.2b,c and Fig 4.3a,b**). As expected, the effect of PTEN inhibition on colony formation was more dramatic in Ci cells. This is because the suppressive activity of PTEN is abrogated in Ci cells. Our finding corroborates the fact that, in normal cells, constitutive PTEN activation restores plasma membrane PIP_2.

To further examine the relationship between Plcγ1 and PTEN *in vivo*, we utilized purified proteins in an *in vitro* reconstitution assay. KD FGFR2 and Plcγ1 were added to PTEN in the presence and absence of Grb2. PIP_3 accumulation was more dramatic in the absence of Grb2 compared with the presence of Grb2 (**Fig4.7c, d**) Thus, the increased turnover of PIP_2 by Plcγ1 in

the absence of Grb2 decreases PTEN activity and results in the accumulation of PIP_3.

To confirm that $PI(4,5)P_2$ is needed for the stabilization of PTEN activity, purified PTEN was incubated with ^{32}P-PIP_3 and Ptdser in the absence and presence of cold PIP_2.The activity of PTEN was dramatically enhanced in the presence of PIP_2 (**Fig4.7e,f**).

Akt is upregulated in Grb2-depleted cells

The inactivity of PTEN in G2i cells results in the accumulation of PIP_3, on which Akt binds. Upon binding to the membrane, Akt is phosphorylated and downstream signaling ensues. Accumulation of PIP_3 with respect to PIP_2 in the absence of Grb2 is reflected in the increased expression of phosphorylated Akt (pAkt) (Fig **4.3a,d**) and its downstream effectors including mtor glycogen synthase kinase 3 (Gsk3; Ser21; **Fig 4.3f**), p70 S6 kinase (p70S6K; Thr389, Ser235, and Ser240; **Fig 4.3g**), S6 ribosomal protein (Ser235/236 and Ser240/244; **Fig 4.3h**), and proline-rich Akt substrate 40 (Pras; Thr246; **Fig 4.3i**) in G2i cells compared with Ci cells. Thus, Plcγ1 activation in the absence of Grb2 indirectly increased Akt activation and downstream signaling in non-stimulated HEK293T cells.

Elevated levels of pAkt (S473 and T308) were observed in G2i cells compared with Ci cells (**Fig 4.8a**). Treatment of G2i cells with the PTEN inhibitor SF1670 increased Akt phosphorylation.Furthermore, Akt phosphorylation was inhibited by the forced expression of Grb2 in G2i cells (**Fig 4.8b**). Together, these

findings demonstrated that Akt phosphorylation was dependent on PTEN. Interestingly, PTEN phosphorylation was increased in G2i cells compared with Ci cells, whereas Grb2 overexpression decreased PTEN phosphorylation in G2i cells (**Fig 4.8b**).

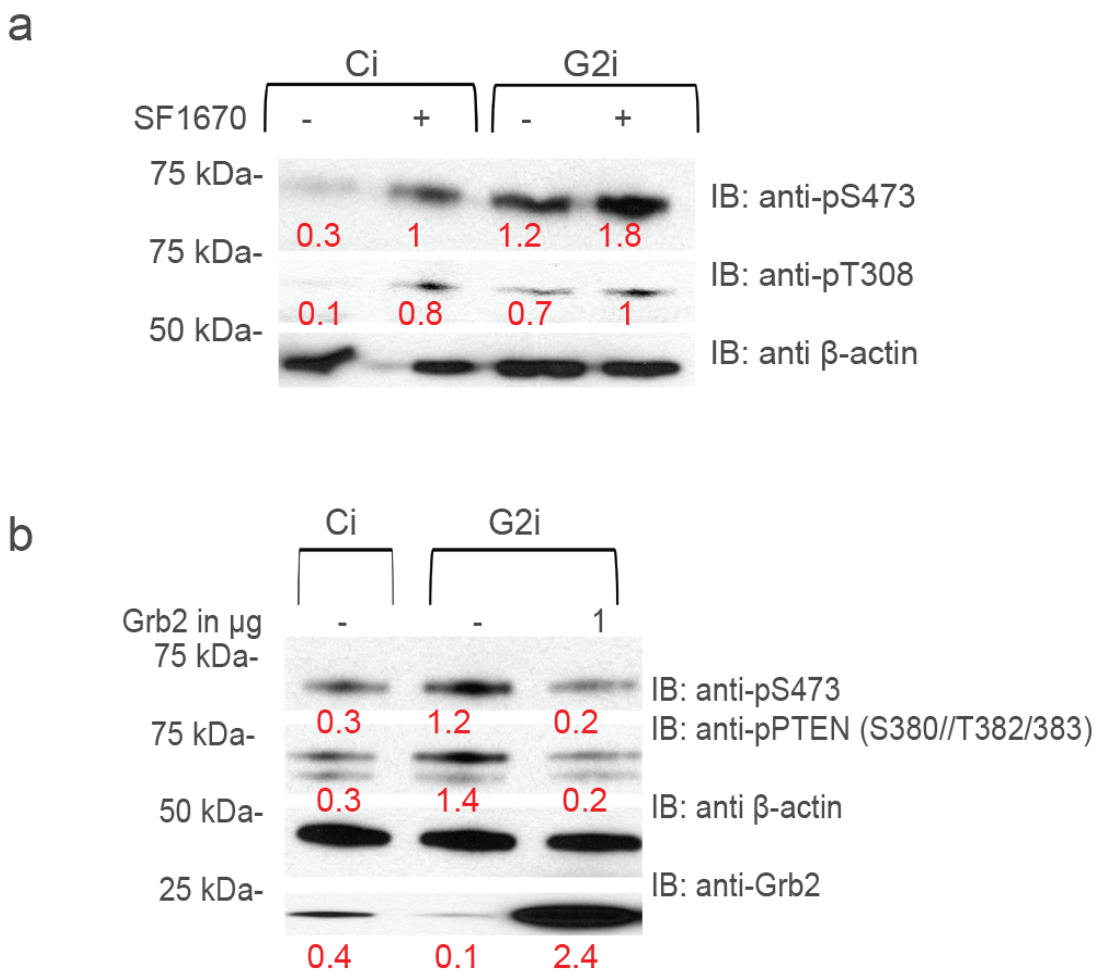

c

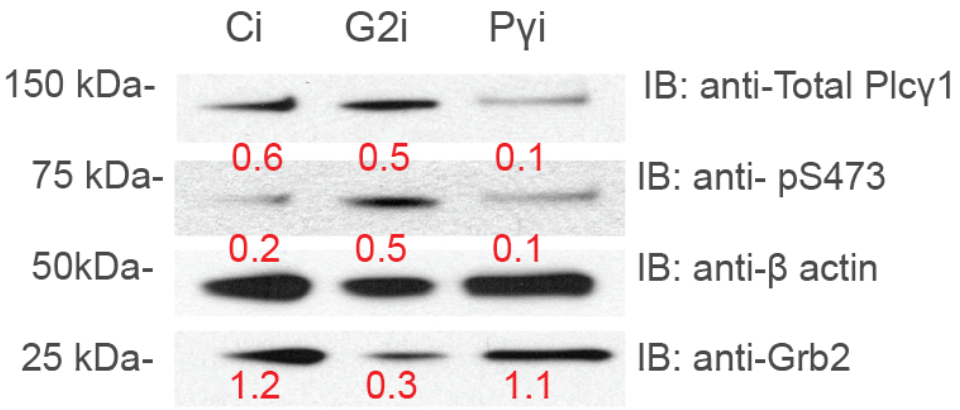
Ci
G2i
Pγi
150 kDa-
IB: anti-Total Plcγ1
0.6
0.5
0.1
75 kDa-
IB: anti- pS473
0.2
0.5
0.1
50kDa-
IB: anti-β actin
25 kDa-
IB: anti-Grb2
1.2
0.3
1.1

d

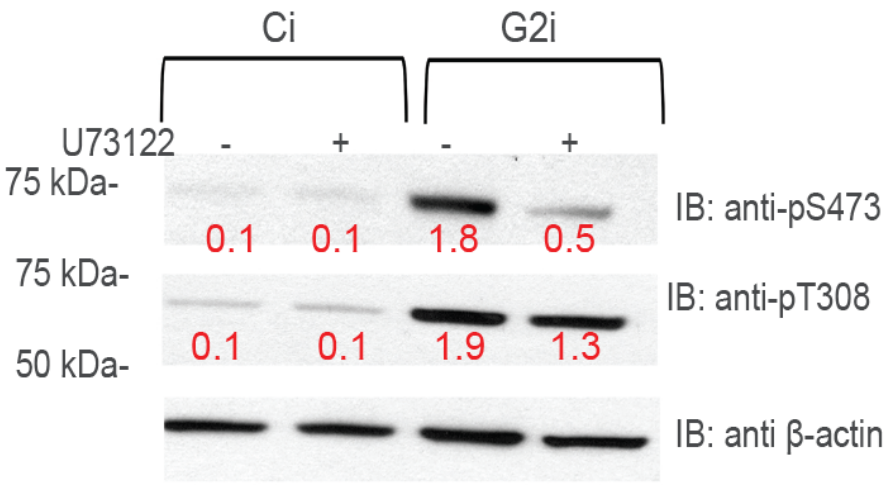
Ci
G2i
U73122
-
+
-
+
75 kDa-
IB: anti-pS473
0.1
0.1
1.8
0.5
75 kDa-
IB: anti-pT308
50 kDa-
0.1
0.1
1.9
1.3
IB: anti β-actin

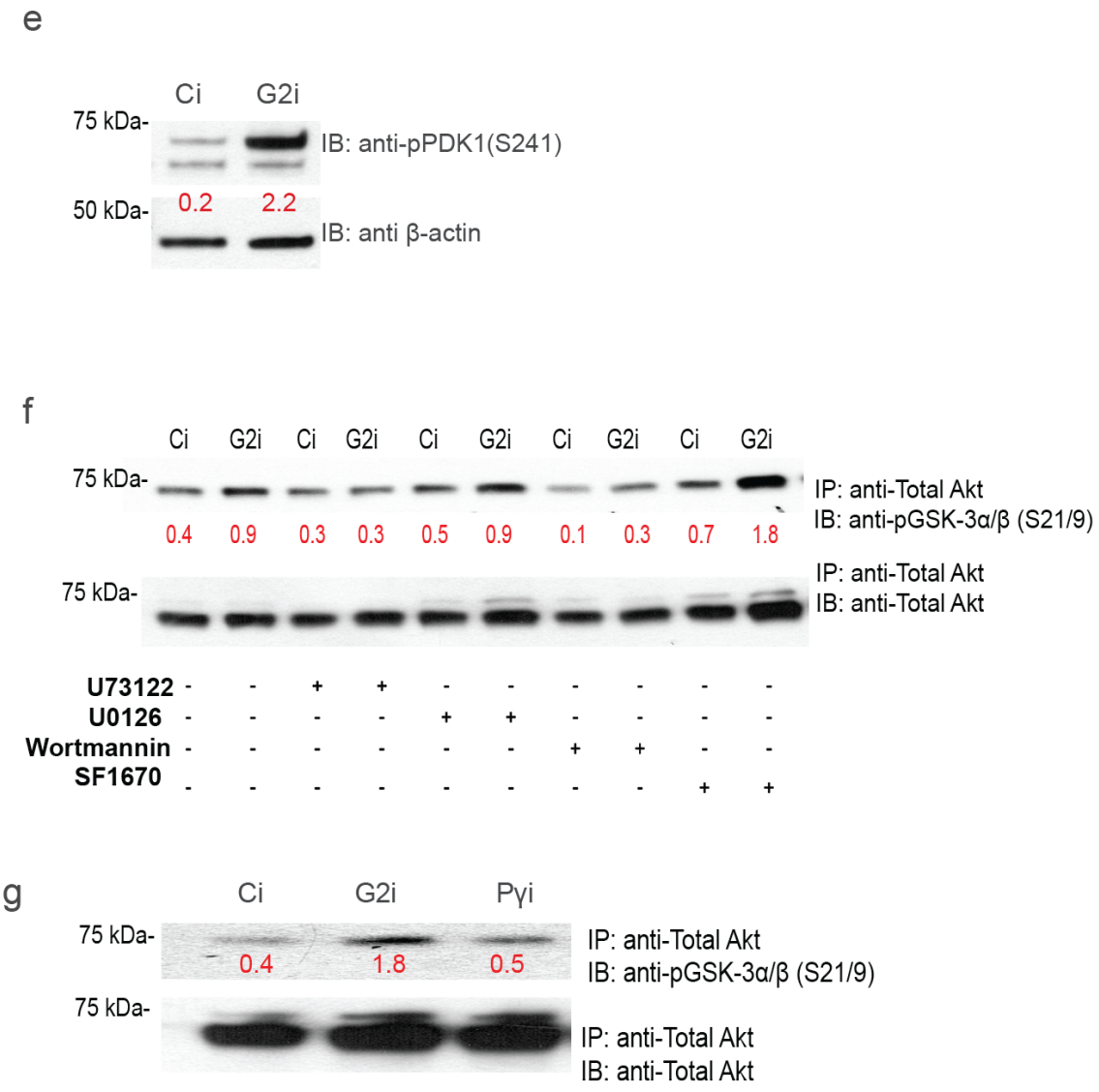

Fig 4.8 PTEN-mediated Akt phosphorylation and activity is dependent on Grb2 and Plcγ1 concentrations. a)Western blot analysis was done to determine the expression of pAkt (Ser473 and T308) in cell lysates obtained from untreated and SF1670-treated Ci and G2i cells.**b**) Western blot analysis was done to determine the expression of pAkt (Ser473) and phosphorylated PTEN (S380/T382/383) in cell lysates obtained from Ci, G2i, and Grb2 knock in G2i cells.**c**) Western blot analysis was done to determine the expression of total Plcγ1, Grb2, and pAkt (Ser473) in Ci, G2i, and Pγi cells.**d**) Western blot analysis was done to determine the expression of pAkt (Ser473 and T308) in cell lysates obtained fromuntreated and U73122-treated Ci and G2i cells.**e**) Western blot analysis was done to determine the expression of phosphorylated

PDK1 (Ser241) in cell lysates obtained from Ci and G2i cells.**f**) Ci and G2i cells were left untreated or treated with the indicated inhibitors. Akt kinase assay was performed on the cell lysates. Western blot analysis was used to detect the effect of the inhibitors on kinase activity.**g**) Akt kinase assay was performed on Ci, G2i, and Pγi cell lysates. In all western blot analyses, β-actin was used as a loading control.

Phosphorylation of PTEN inhibits its phosphatase activity, thereby facilitating PIP_3 accumulation and Akt recruitment. Inhibition of Akt using Akt inhibitor VIII reversed the Grb2-dependent Akt phosphorylation (**Fig 4.9a**) and inhibited colony formation (**Fig 4.2b,c** and **Fig 4.3a,b**).In addition, we demonstrated that Akt phosphorylation in G2i cells was linked to PI3K activity because, in the presence of wortmannin, pAkt was decreased (**Fig 4.9b**) even though PI3K activity wassimilar between Ci and G2i cells. Conversely, Akt phosphorylation was independent of MAPK pathway activation as demonstrated by the negligible effect of the MEK inhibitor U0126 on pAkt levels (**Fig 4.9c**).

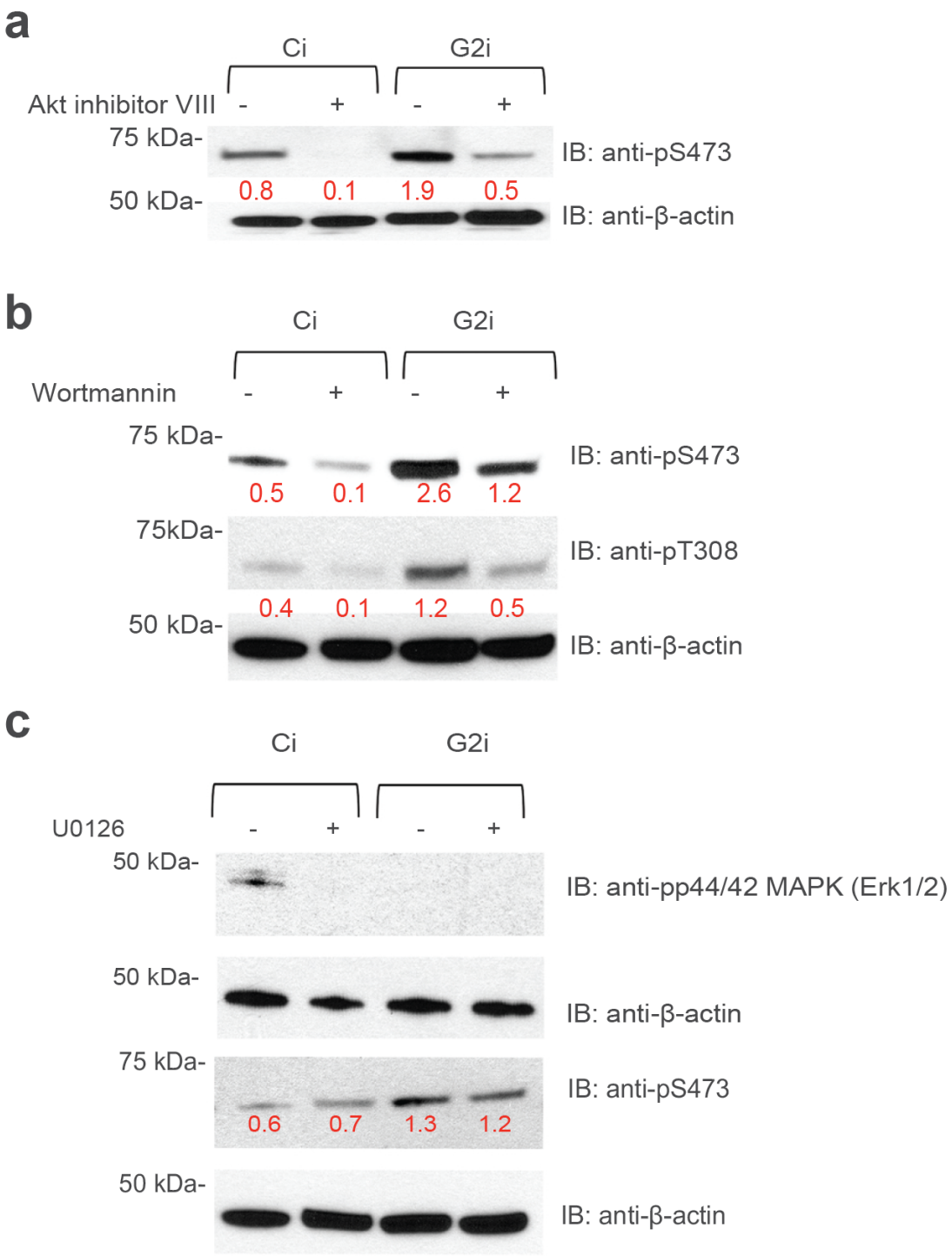
a
Ci
G2i
Akt inhibitor VIII
-
+
-
+
75 kDa-
IB: anti-pS473
0.8
0.1
1.9
0.5
50 kDa-
IB: anti-β-actin
b
Ci
G2i
Wortmannin
-
+
-
+
75 kDa-
IB: anti-pS473
0.5
0.1
2.6
1.2
75kDa-
IB: anti-pT308
0.4
0.1
1.2
0.5
50 kDa-
IB: anti-β-actin
c
Ci
G2i
U0126
-
+
-
+
50 kDa-
IB: anti-pp44/42 MAPK (Erk1/2)
50 kDa-
IB: anti-β-actin
75 kDa-
IB: anti-pS473
0.6
0.7
1.3
1.2
50 kDa-
IB: anti-β-actin

Fig 4.9 Akt phosphorylation is PI3K dependent and MAPK independent in Ci and G2i cells. a) Western blot analysis was done to determine the expression of pAkt (Ser473) in cell lysates obtained from untreated andAkt inhibitor VIII-treatedCi and G2i cells. **b**) Western blot analysis was done to determine the expression of pAkt (Ser473 and T308) in cell lysates obtained from untreated and wortmannin-treated Ci and G2i cells.**c**) Western blot analysis was done to determine the expression of phosphorylated Erk1/2 and pAkt (S473) in untreated and U0126 (MEK1/2 inhibitor)-treated Ci and G2i cells.β-actin was used as a loading control in all western blot analyses.

To demonstrate that Akt phosphorylation was dependent on Plcγ1, Plcγ1 was inhibited using Plcγ1 knockdown (Pγi) cells and U73122. Akt phosphorylation was decreased in Pγi cells (**Fig 4.8c**) and U73122-treated cells (**Fig 4.8d**). These data further support that the reduction in PIP_2 concentration as a result of Plcγ1 activity inactivates PTEN, resulting in Akt activation.

Since PDK1 protein which phosphorylates Akt on T308 also binds to PIP_3 resulting in phosphorylation and activation, we decided to study its phosphorylation status in Ci and G2i cells (**Fig 4.8e**). As expected, its phosphorylation level is higher in G2i cells compared to Ci cells.

To confirm that the increase in Akt phosphorylation level is accompanied by an increase in its activity, we immobilized total Akt from Ci and G2i cells on A/G agarose beads and incubated them with purified GSK (Akt substrate) in the presence of ATP. This kinase assay (**Fig 4.8f, 4.8g**) showed an increase in Akt activity in G2i cells compare to Ci and Pγi cells. U73122, and Wortmannin decreased the activity of Akt but U0126 had little or no effect unlike SF1670, which enhanced the activity. These results match the ones obtained for the

phosphorylation status of this kinase. Thus, Plcγ1 dependent decrease in PTEN activity in G2i cells is reflected in a decrease in the activity of Akt.

To confirm that the constitutive activation of Akt is dependent on the recruitment of the kinase to the plasma membrane in G2i cells we used HEK293T cells over-expressing N-terminally GFP-tagged FGFR2. Since in non-stimulated cells FGFR2 is membrane localized this provides a clear marker for the cell membrane.

We also expressed the PH domain of Akt (Akt-PH) with a mCherry fluorescent fusion protein tag (an empty mCherry vector was used as a control; **Fig 4.10a**). The PH domain has previously been reported to be responsible for the recruitment of Akt to the membrane on stimulation. In Ci cells there is no co-localization of the fluorescent tags reflecting the lack of recruitment of Akt-PH to the membrane (**Fig 4.10b**), however in the G2i cells clear co-localization of Akt-PH to the membrane is observed. This is consistent with the observation that Akt translocates to the PIP_3-rich plasma membrane to be phosphorylated in G2i cells.

We confirmed these results by performing a fractionation experiment in Ci and G2i cells where actin was used as a cytoplasmic marker and FGFR2 as a membrane marker (**Fig 4.10c**). A larger population of Akt was found in the membrane in G2i cells compared to Ci cells. This is consistent with the increased pool of PIP_3 observed in G2i cells serving to recruit Akt.

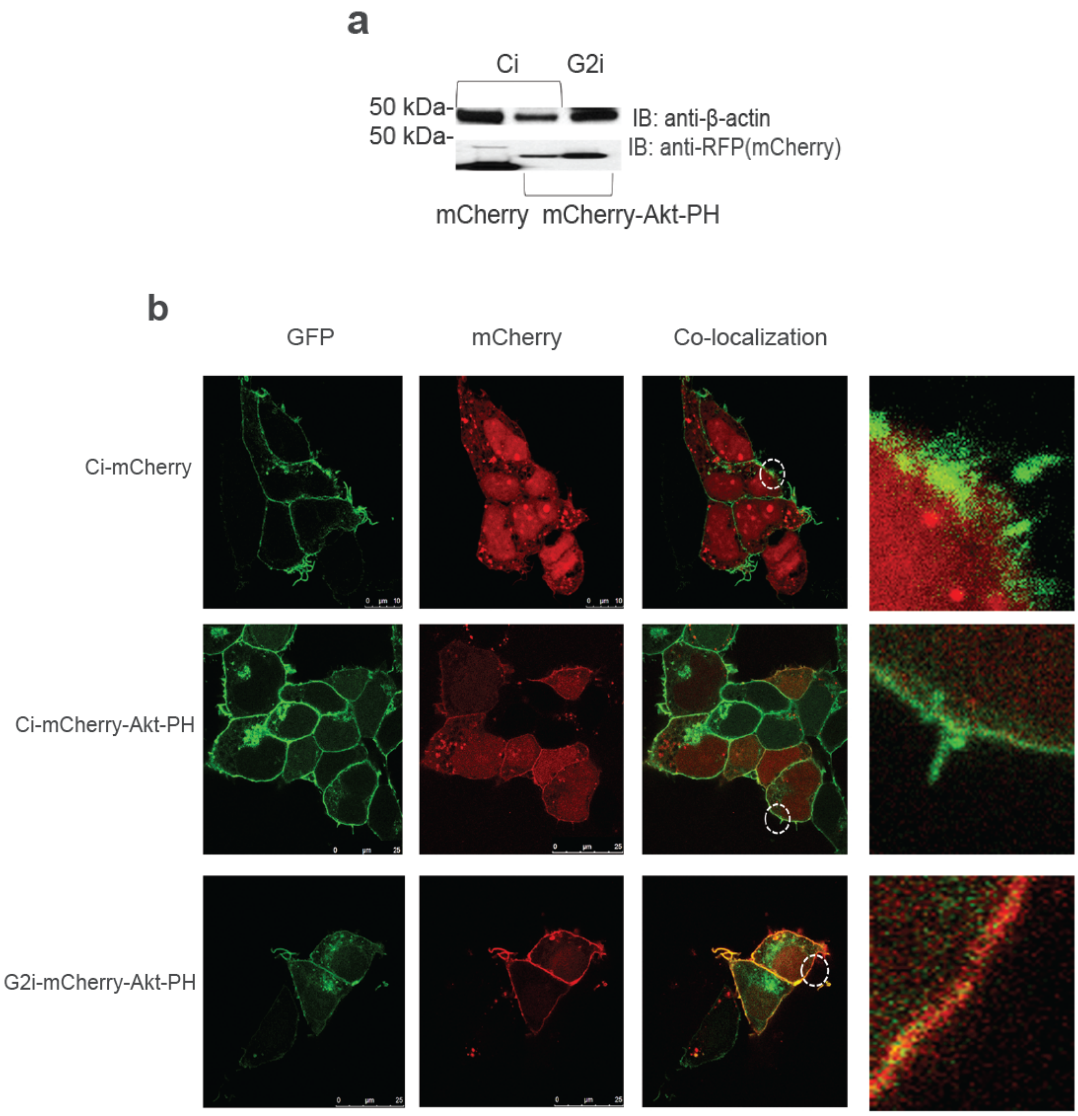
a
Ci
G2i
50 kDa-
50 kDa-
IB: anti-β-actin
IB: anti-RFP(mCherry)
mCherry
mCherry-Akt-PH
b
GFP
mCherry
Co-localization
Ci-mCherry
Ci-mCherry-Akt-PH
G2i-mCherry-Akt-PH

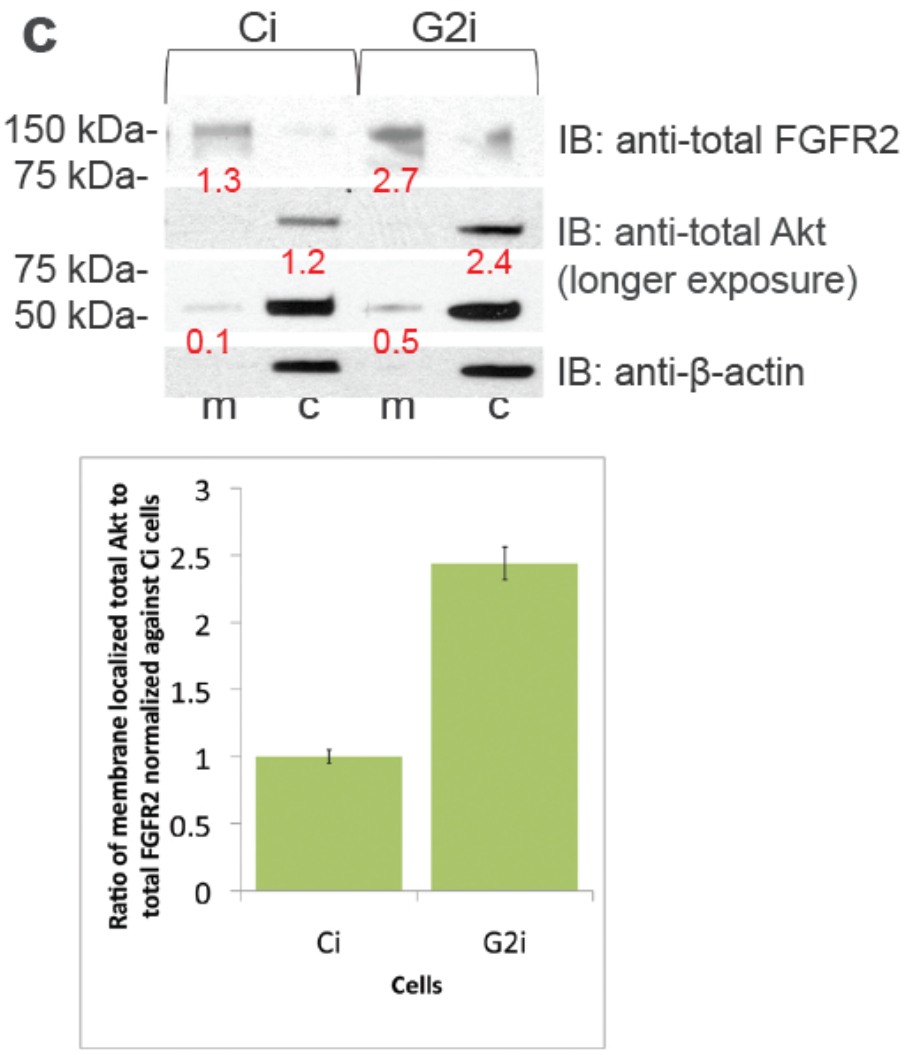

Fig 4.10 Membrane localization of lipid binding Akt-PH domain is higher in G2i cells compared to Ci cells.a) Ci and G2i cells transfected with an empty mCherry vector or mCherry-Akt-PH vector were serum starved, lysed and used for western blot analysis where the blots were probed with the indicated antibodies.**b**) Ci and G2i cells transfected with an empty mCherry vector or mCherry-Akt-PH vector were serum starved and used for microscopy as explained in the Materials and Methods section. FGFR2-GFP was used as a membrane marker to show co-localization of the lipid binding PH domain on the membrane bound FGFR2.**c**) Serum starved Ci and G2i cells were fractionated

into membrane and cytoplasmic portions, lysed and used for western blot analysis then probed with the indicated antibodies.

Akt phosphorylation is concomitant with reduced Grb2 and increased Plcγ1 concentrations in uterine corpus epithelial cancer (UCEC)

According to our data depletion of Grb2, concomitant up-regulation of Plcγ1 and subsequent phosphorylation of Akt should be manifest in cancer. We would expect that cells expressing FGFR2 accompanied by low Grb2 and high Plcγ1 concentrations would exhibit higher oncogenic prevalence. To confirm the physiological relevance of our observations we performed a comprehensive analysis using “The Cancer Genome Atlas” database.

RPPA data on PI3K/PTEN/Akt expression and/or phosphorylation levels in different types of patient tumor samples were extracted. Inverse correlation between the Grb2 concentration and phosphorylation of Akt (on both S473 and T308) were observed in several tumor-types (**Fig 4.11a** (S473), **4.11b** (T308)). Furthermore, pAkt was also seen in several tumor-types with high Plcγ1 expression (**Fig 4.11c** (S473), **4.11d** (T308)). Uterine corpus endometrial carcinoma (UCEC) which is one of the most common cancers of the female reproductive system showed a particularly strong correlation between pAkt with low Grb2 and high Plcγ1 concentrations.

This is consistent with our observations in the HEK293T model cell line reported herein. The RPPA results for tumor types for both S473 and T308 are shown in **Fig 4.11e, 4.11f**.

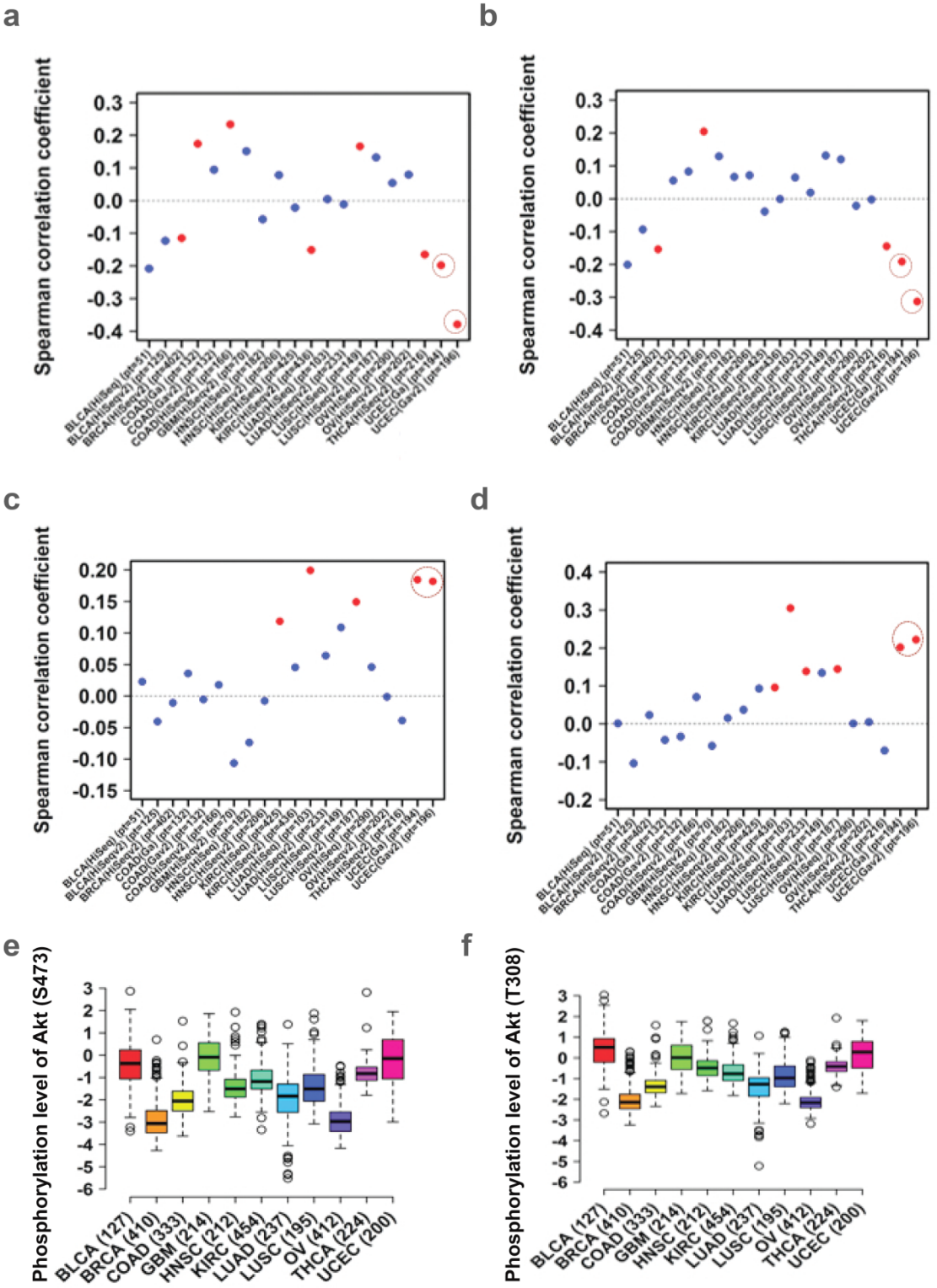
a
b
c
d
e
f
Spearman correlation coefficient
Phosphorylation level of Akt (S473)
Phosphorylation level of Akt (T308)
BLCA (127)
BRCA (410)
COAD (333)
GBM (214)
HNSC (212)
KIRC (454)
LUAD (237)
LUSC (195)
OV (412)
THCA (224)
UCEC (200)

Fig 4.11 Akt phosphorylation level is among the highest in UCEC and it negatively correlates with Grb2 expression but positively correlates with Plcγ1 expression. a),**b**),**c**),**d**) Data was downloaded from TCGA website for eleven tumor types as described in the materials and methods section. Level 3 Illumina RNASeq versions 1 and 2 RPPA data were used for mRNA and protein expression level. Statistical analysis was performed in R (version 2.14.2) where p-value > 0.05 is considered to be significant and is shown in red. p-value< 0.05 is shown in blue. The Spearman's rank-order correlation test was performed to measure the strength of the association between Grb2 mRNA and pS473/pT308 RPPA levels in **a**) and **b**) respectively and also between Plcγ1 and pS473/pT308 RPPA levels in **c**) and **d**) respectively across different tumor types. **e**),**f**) A box-and-whisker plot was used to visualize RPPA levels across tumor types following TCGA database analysis.

Grb2 depletion results in enhanced tumor formation in xenograft mouse model with increased Akt phosphorylation level

PCi, PG2i, PPγi, Ci, G2i, and Pγi cells were used in the generation of a xenograft mouse model where 0.5 x 10^6 cells were subcutaneously injected in the right flank of adult female nude mice (4 mice per group). After 60 days, mice were subjected to MRI scanning as explained in the method section to determine tumor volume in every case. As can be seen in the first panel in **Fig 4.12a** , which corresponds to the coronal section, mice injected with G2i cells showed drastic increase in tumor size and also the development of multiple tumors in the vicinity of the primary one compared to mice injected with Ci and PG2i cells. PCi injection failed to develop noticeable tumors as in the case of Pγi and PPγi (results not shown).

These results are clear in the second panel and also in the third panel which corresponds to the axial sections. Tumor weight and volume (**Fig 4.12b**) are also higher in G2i tumors compared to Ci and PG2i tumors. This outcome is

consistent with the one obtained in colony formation assay where G2i cells were relatively unique in their ability to form multiple colonies of increased size.

Ci and G2i tumors were used in western blot analysis as shown in **Fig 4.13a**. As expected, G2i tumors expressed a higher level of Akt phosphorylation compared to Ci tumors. Total Akt and actin were used as loading controls in both cases.

Morphologically, the G2i tumor cells have a higher grade of malignancy than Ci tumor cells (**Fig 4.13b**). Ci tumor appears to be composed of densely cellular and poorly differentiated neoplastic cells that have small/minimal amount of eosinophilic cytoplasm and oval or pleomorphic nuclei. The nuclei have hyperchromatic, coarse or stippled chromatin and prominent one or two nucleoli. The tumor has delineated margins and is surrounded partially by a fibrous capsule. There is a high mitotic rate of approximately 60-70 mitotic figures per 400x magnification field. Numerous apoptotic cells are present. The tumor has a few small areas of necrosis representing approximately 5-10% of the entire tumor. G2i tumor is composed of similar type of neoplastic cells, but more anaplastic or higher degree of cellular pleomorphism. These neoplastic cells have lower amount of cytoplasm. The nuclei are markedly pleomorphic and have severely coarse, stippled or clumped hyperchromatic chromatin, and prominent multiple nucleoli. A similar high number of nuclear mitotic figure are present. There is increased number of apoptotic cells and large areas of necrosis affecting approximately 60-70% of the entire tumor. The margins of the tumor are indistinct and there is infiltration of tumor cells into the fibroadipose

tissue at the periphery of tumor. As shown in **Fig 4.13c** Ci tumor cells stained negative for pAkt (serine 473) antibody. There is only a minimal nonspecific background staining. Also, the necrotic areas of tumor have nonspecific/false staining. In the G2i sample, there is positive staining of these tumor cells. The staining is more intense in the tumor cells from the perivascular regions. Nonspecific/false background staining of the necrotic areas is also present.

a

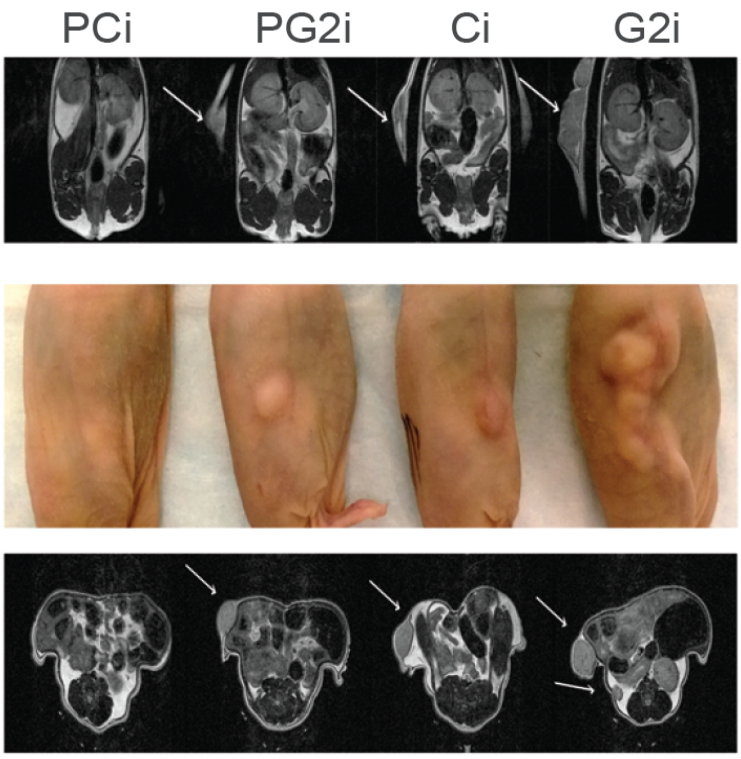
PCi
PG2i
Ci
G2i

b

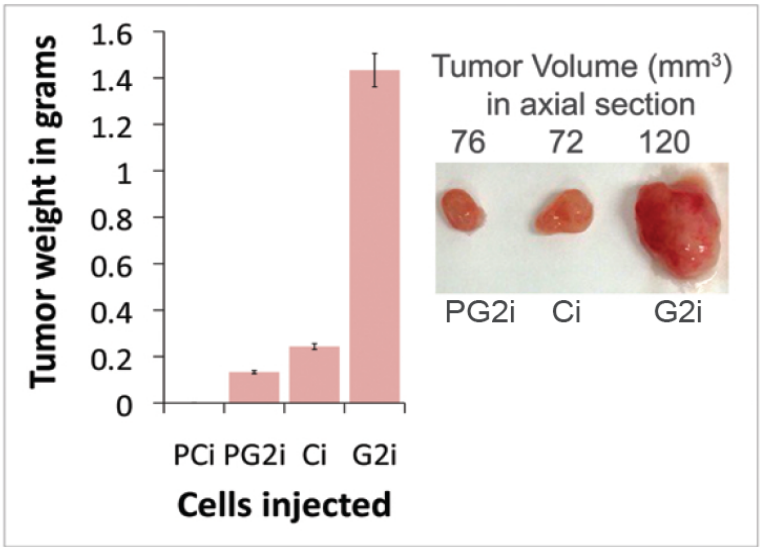
Tumor weight in grams
1.6
1.4
1.2
1
0.8
0.6
0.4
0.2
0
PCi PG2i Ci G2i
Cells injected
Tumor Volume (mm³) in axial section
76 72 120
PG2i Ci G2i

Fig 4.12 Tumor formation is drastically enhanced in mice injected with Grb2 knockdown cells in a background of FGFR2 expression a) First panel: Coronal MRI images of PCi, PG2i, Ci, G2i injected mice following 60 days of subcutaneous injections. Arrows indicate the tumors formed. Second panel: Sample from each group showing absence of tumor (PCi injected mice) or size/number of tumors formed in every group. Third panel. Axial MRI images of PCi,PG2i,Ci,G2i injected mice following subcutaneous injections. Arrows indicate the tumors formed. **b**) Tumors from every group were weighed and averaged. Bar graphs were plotted and error bars denote standard deviation of the mean. Tumor volumes were calculated for mice in every group as explained in details in the methods section.

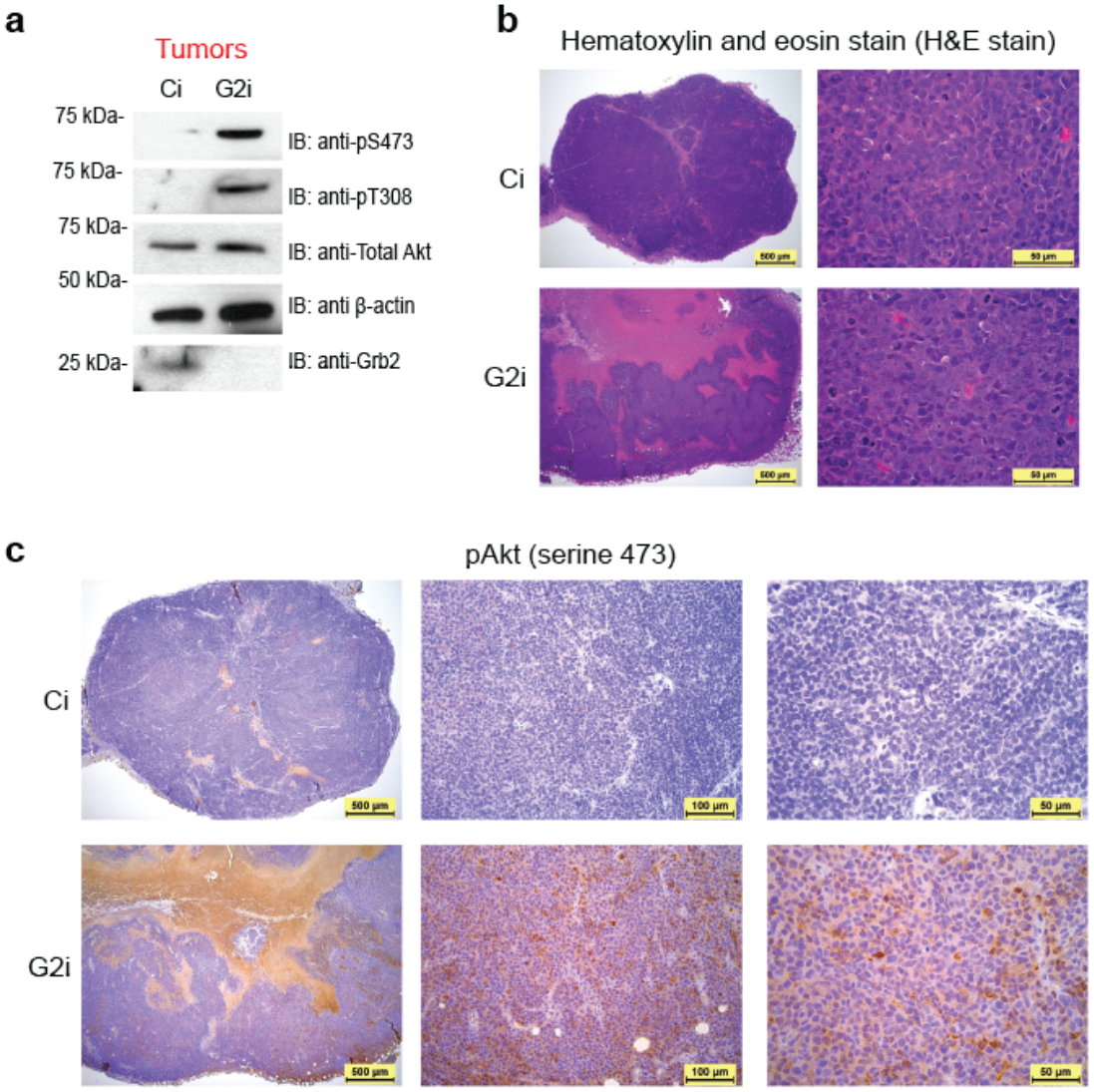

Fig 4.13 G2i cells form tumors of a higher grade of malignancy compared to Ci tumors and have a higher level of Akt phosphorylation a) Tumor sections were sonicated and proteins were extracted and used for western blot analysis where the blots were probed with the indicated antibodies. **b**) H & E staining of Ci and G2i tumors taken at 40x and 600x. **c**) pAkt staining of Ci and G2i tumors taken at 40x, 200x,and 400x.

In summary, competition between Plcγ1 and Grb2 for binding to FGFR2 controls membrane levels of PIP_2 which in turn affects the phosphatase activity of PTEN.Consequenly the phosphorylation statuts and activity of Akt can be modulated accordingly where high levels of Akt phosphorylaion is evident in G2i tumors (tumors formed in xenograft models following the injection of Grb2 knockdown cells in mice).

Chapter Five: Discussion

SH3 domains of Grb2 and Plcγ1 compete for the same binding site on FGFR2

The novel results presented in Chapter 2 represent a critical principle in FGFR2-dependent cancer signaling, specifically that signal transduction-mediated oncogenic outcome can be based entirely on the competition of non-phosphorylated ligands (namely Grb2 and Plcγ1) for a non-phosphorylated protein binding site.

The measured K_Ds for the SH3 domains of both Grb2 and Plcγ1 binding to FGFR2 is similar which means that the receptor binding site could be occupied equally by either Grb2 or Plcγ1 under equimolar conditions.

In normal cells the Grb2 concentration is assumed to be greater than that of Plcγ1 since it is a critical adaptor protein required for the activation of several pathways and thus under non-stimulated conditions Grb2-FGFR2 complex will prevail.

This complex formation leads to the inhibition of the lipase activity of Plcγ1. Nevertheless, any fluctuation in protein concentrations like a decrease in Grb2 (G2i cells) or increase in Plcγ1 and/or FGFR2 will allow the phospholipase to out-compete the inhibitor causing an induction of constitutive and uncontrolled phospholipase activity.

Since tyrosine kinase-mediated signal transduction is typically constrained by stimuli mediated receptor activation/deactivation, the concentration-dependent activation of the lipase seems to be under much looser regulation. The

implications for disease can thus be mediated by protein concentration fluctuations (**Fig 2.1**).

The described process of the SH3 domain-mediated activation of Plcγ1 can be considered an additional mechanism to that which occurs upon the binding of the lipase on pY769 following extracellular stimulation

The dynamics of such SH3 domain mediated basal state binding to the C-terminus of FGFR2 can possibly be dependent on a conformational change in the structure of the lipase mimicking the previously well-established activation caused by NSH2 domain binding. Plcγ1SH3 domain forms an interface with the CSH2-SH3 linker region (residues 759-791) possibly playing a significant role in stabilizing the auto-inhibited state (31). This interaction can in part occlude the canonical proline-rich motif-binding site on Plcγ1SH3 thus basal state binding to FGFR2 will destabilize the auto-inhibitory potential of the CSH2 domain by disrupting the intramolecular SH3 interaction.

Also, it has been previously reported that isolation of the lipase SH3 domain has negligible effect on the enzymatic activity (16), however deletion of the domain does not replicate the effect of binding to FGFR2 and the consequent conformational change. Interestingly, the CSH2 domain has been shown to have some affinity to the CSH2-SH3 linker region in a phosphorylation independent manner (31). Thus, the possible conformational perturbation accompanying the Plcγ1SH3-FGFR2 interaction would expose the CSH2-SH3 linker region and the interaction of CSH2 with the linker will serve to reverse the auto-inhibition. This is plausible especially after taking into consideration a

similar mechanism where the split PH domain of Plcγ2 is critical and sufficient for the activation of the lipase (60-64).

Grb2 and Plcγ1 competition controls lipase mediated cell migration and invasion

Grb2 binds and interacts with several proteins thus depleting it would have significant effects that could affect Plcγ1 activity and/or phospholipid turnover. In this case cellular migratory and invasive potential could be influenced by the fluctuation of protein concentrations via a mechanism independent of the one described here. However, there are many critical points that should be taken into consideration before making such an assumption. So far, this project has provided evidence that the adaptor protein directly affects Plcγ1 lipase activity by the following:

1) Grb2 and Plcγ1 compete for a binding site on FGFR2. When this receptor is absent, like in HEK 293T parental cell line which express negligible levels of FGFR2, the constitutive phospholipase activity is absent.

2) Depletion (via knockdown) or inhibition (via U0122) of Plcγ1 eliminates the cellular effects observed, while knocking in the lipase rescues the phenotype.

3) Plcγ1 activity in other signaling pathways is evident only under conditions of stimulation dependent receptor up-regulation. Here, FGFR2 was left un-stimulated, and therefore was incapable of phosphorylating the lipase.

4) Both Grb2 and Plcγ1 bind to the protein Sos which initiates and activates the downstream MAPK pathway (65). Knocking down Grb2 could result in the

observed phenotype by increasing the influence of the lipase on MAPK signaling. This hypothesis is unlikely since MAPK response is absent on Grb2 knock down (2).

5) Plcγ1 can get activated by non tyrosine kinases (NTKs). When Grb2 is depleted (via knockdown), NTKs like Src Family kinases (SFKs) could become up regulated and hence activate the lipase. In this case, the cells are under basal conditions and NTKs are up regulated solely on stimulation by activated receptors thus activity toward the lipase is improbable.

6) Grb2 mediates the downstream phosphorylation of PIP_2 to PIP_3 via PI3K. So, in the absence of the former there can be an increase in the relative concentration of PIP_2. But since there is an obvious depletion of PIP_2 in G2i cells and a simultaneous increase in intracellular calcium levels, down-regulation of PI3K activity cannot justify the observed phenotype.

It is also critical to analyze the reasons behind the evolution of the Plcγ1SH3 domain mediated constitutive interaction and activation of the lipase alongside the previously well-established SH2 binding to activated FGFR2. The SH3-dependent activation mechanism is highly plausible since it is based on the concentration of the lipase where control of the intracellular level is a “housekeeping” activity critical for the maintenance of membrane constitution homeostasis and the subsequent intracellular calcium mobilization.

For example, there is growing evidence from a number of tissues like vascular smooth muscle, that tyrosine phosphorylation is crucial yet inadequate to fully activate the lipase. It might instead be critical for the translocation of Plcγ1 from

the cytosol to the actin cytoskeleton (66). Also, it has been shown that in *Xenopus* oocytes the binding of the SH3 domain to Sos induces pY783-independent background phospholipase activity (67).

It is important to note that controlling intracellular signaling via the law of mass action makes the cells more sensitive to fluctuations in protein concentrations. As Plcγ1 expression level increases, it can contribute to oncogenesis and metastasis by outcompeting Grb2 for the FGFR2 binding site. For example, it has been previously shown that over-expression of Plcγ1 induces transformation of NIH3T3 fibroblasts (68,69).

Plcγ1 expression is also significantly high in colorectal cancer and colon carcinoma cell lines compared with normal tissue (70). Additionally, several breast carcinoma tissues have an elevated level of expression of non-phosphorylated Plcγ1 (71). For instance, certain breast cancer cell lines like MDA-468 have high levels of membrane-associated non-phosphorylated Plcγ1 before stimulation; i.e. 69% of Plcγ1 is membrane bound under basal non-stimulated conditions compared to 4% in MCF-7 cells (72). Those cells also express high levels of FGFR2 (73) and upon epidermal growth factor (EGF) stimulation there is an insignificant increase in Plcγ1 membrane localization. Therefore, in MDA-468 metastatic breast cancer cell line it is considered possible that there is an up-regulation in the activity of the lipase upon receptor mediated recruitment to the membrane.

A similar effect on oncogenesis and metastatic outcome can be observed in the context of reduced cellular Grb2 concentration. By examining the data from

ovarian cancer patient samples, there was a clear relationship between reduced levels of Grb2 expression and metastasis. In those samples there was a concomitant increase in the expression level of both Plcγ1 and FGFR2.

Thus, Grb2-mediated control of FGFR2 activity is imperative in maintaining cellular homeostasis under basal non-stimulated conditions. Nevertheless, FGFR2-Grb2 heterotetrameric complex formation through CSH3 interaction, which has a weak affinity to the receptor, can leave the complex open to competing SH3 domain binding which might result in an oncogenic outcome.

PTEN-mediated activation of Akt is dictated by Grb2 expression levels

Plcγ1 has been previously shown to be up regulated upon Grb2 depletion in a background of FGFR2 expression (59). Here the competition between Grb2 and Plcγ1 for binding to FGFR2 in a concentration dependent manner appears to cause a perturbation of membrane lipid concentration balance. This effect tends to modulate PTEN activity and consequently Akt membrane localization, phosphorylation and activation.

Thus, the novel results presented in Chapter 4 emphasize the importance of Grb2-Plcγ1 competition in controlling the level of PIP_2 critical for PTEN's association with the membrane. Previous studies have revealed that a truncated version of this tumor suppressor gene missing the PIP_2 binding motif failed to associate with the membrane (74). PIP_2 has also been shown to be required for the induction of a conformational change in the structure of PTEN by binding to the N-terminal domain of the latter. Even mutations in the N-terminus of PTEN have been shown to severely reduce the activity of PTEN by possibly blocking the protein from binding PIP_2 (75). Thus PTEN is suggested to remain cytosolic in an inactive conformation where the catalytic domain is masked by PIP_2-binding domain. When PTEN binds on PIP_2 on the membrane a conformational change is induced that activates the phosphatase activity of PTEN (76,77).

These studies provide strong *in vitro* and cell biological proof yet are lacking to a certain level in the conditions and functional effects of PTEN/PIP_2 interaction.

Chapter 4 presents substantial evidence supporting the importance of PIP_2 in regulating PTEN activity *in vivo* and *in vitro*. It also shows how fluctuations in the concentration of two non-phosphorylated proteins interacting with a receptor via their SH3 domains can have drastic effect not only on migration, invasion, and possibly metastasis but also on tumor development by controlling cellular proliferation through PTEN, which in turn modulates Akt activity (**Fig 5.1**). One can thus argue in favor of the importance of this mechanism where cellular PIP_2 concentration regulates PTEN activity and a decrease in the level of this lipid leads to loss of PTEN function mimicking the effects of tumor-derived mutations identified in PIP_2 binding motif—such as K13E, found in glioblastoma and endometrial carcinoma, and S10N, found in lymphoma (78,79).

Akt (the read out for PTEN activity) has a higher level of membrane localization, and phosphorylation under conditions where Plcγ1 outcompetes Grb2 for FGFR2 binding or upon PTEN inhibition like in G2i cells or SF1670 treated cells respectively. Also, it is important to note that under *in vivo* or *in vitro* conditions (cell lysate based assays and *in vitro* reconstitution assays) where Plcγ1 replaces Grb2 on FGFR2 via its SH3 domain, PTEN is inactive. This is shown to be a direct effect of the depletion of PIP_2 required for the activity and membrane localization of the phosphatase. Hence the end point of fluctuation of Plcγ1/Grb2 concentration in cells and possibly tumors like UCEC is the modulation of Akt activity via PTEN where Akt shows a negative correlation with Grb2 and a simultaneous positive correlation with Plcγ1.

As for the effect of such a mechanism on cellular function, the experiments are based on the concept that in the multistep metastatic process, cancer cells at a certain stage need to grow in an anchorage-independent manner and thus survive without interacting with the cell's substratum. Akt regulates such a process where the inhibition of the Akt pathway leads to the formation of fewer colonies in soft agar (21).

Colony formation is enhanced upon knocking down Grb2 but not Plcγ1 in a background of FGFR2 expression compared to Ci/Pγi cells with FGFR2 and endogenous levels of Grb2 and parental cells that express negligible levels of FGFR2. Also, inhibiting PTEN increases the number of colonies formed, which is an opposite effect to that observed with PI3K or Plcγ1 inhibition.

The soft agar assay results were validated in a xenograft mouse model, where tumor formation seems to be enhanced in G2i cells compared to parental cells ,with negligible levels of FGFR2, and Ci cells. G2i tumor cells express higher level of phosphorylated Akt (western blot and IHC results) compared to Ci cells. Thus, the competition between Grb2 and Plcγ1 can be a critical factor in Akt mediated tumor formation by controlling the levels of PTEN activation.

All of this, along with the effect seen upon inhibiting Akt, leads to the conclusion that cellular proliferation is a direct result of Akt protein activation. These observations are of great significance since they reveal the importance of Grb2 as a global regulator protein affecting several pathways. Also, they show that in cancer development protein-protein competition could be as important as genetic aberration and fluctuations in protein expression levels.

Thus, SH3 domains, which have received little attention especially under non-stimulated conditions, have proven to be essential for normal cell function where any shift in their concentration can tip the balance towards uncontrolled cell proliferation and invasion.

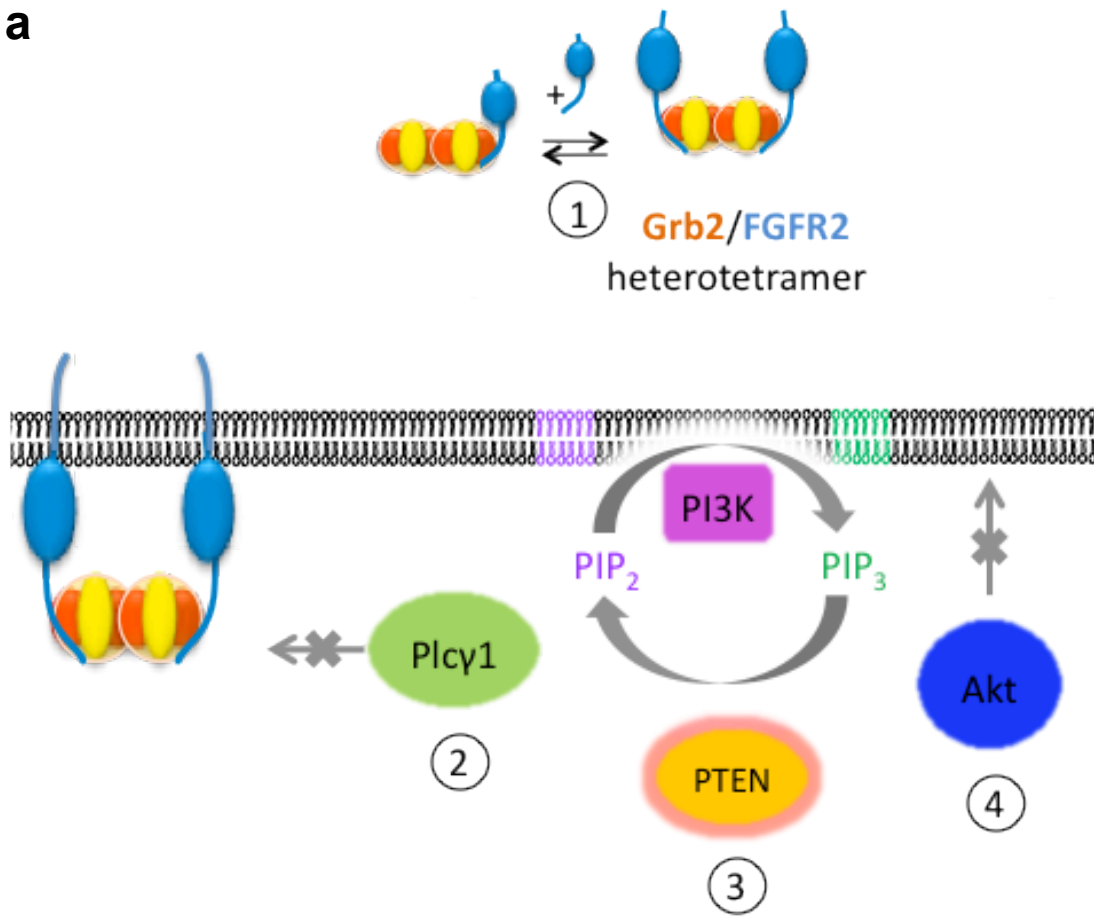

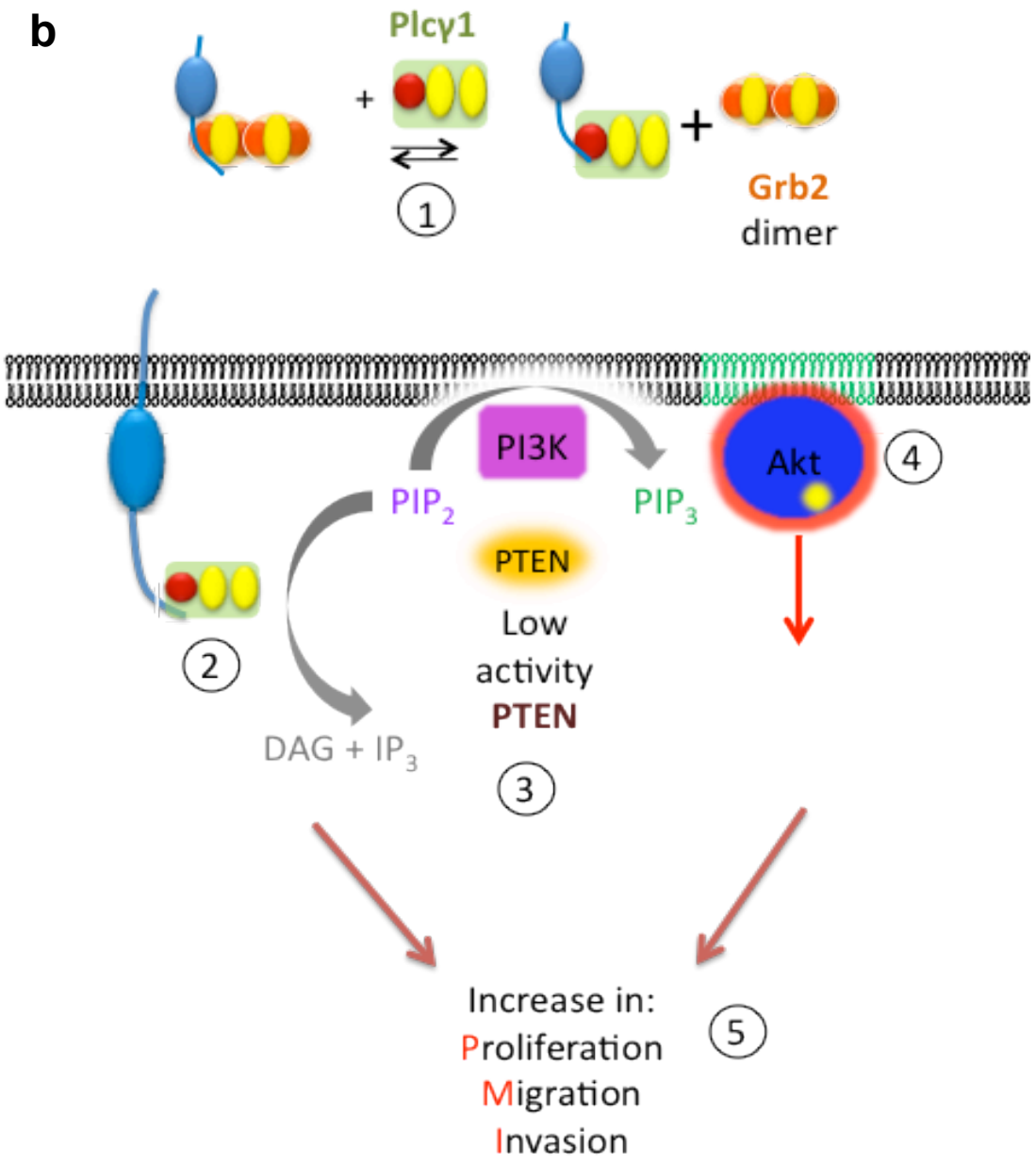
b
Plcγ1
+
1
+
Grb2
dimer
PI3K
PIP2
PIP3
Akt
4
PTEN
Low
activity
PTEN
2
DAG + IP3
3
Increase in:
Proliferation
Migration
Invasion
5

Fig 5.1 Grb2-Plcγ1 competition for binding to the C-terminus of FGFR2 regulates cell proliferation, migration and invasion.a) (1)Dimeric Grb2 binds to two molecules of FGFR2 forming a heterotetramer. (2) Grb2 binding to FGFR2 blocks the access of Plcγ1 to the receptor. (3) Steady state levels of PI3K and PTEN activity and lack of activity of Plcγ1 maintains a normally low level of PIP_3. (4) Akt, which binds on PIP_3 to get phosphorylated and subsequently activated, cannot localize on the membrane efficiently. **b**) (1) When the cellular level of Plcγ1 increases compared to Grb2, it replaces the latter on FGFR2. (2) Receptor binding leads to the constitutive activation of Plcγ1 lipase activity thus hydrolyzing PIP_2 to IP_3 and DAG depleting the membrane of PIP_2. (3) PIP2 is required for the stabilization and membrane localization of PTEN thus PTEN activity is severely dampened while PI3K has a steady state activity. Lack of activity of PTEN, which dephosphorylates PIP3 back to PIP2, causes a buildup of PIP_3. (4) Accumulation of PIP_3 induces a surge in the activity of Akt following its membrane localization. (5) Increase in Plcγ1 and Akt activity amplifies cellular proliferation, migration and invasive potential.

Chapter Six: Conclusion, Significance and Future Directions

Grb2 and Plcγ1 SH3 domain mediated competition for the same binding site on FGFR2 regulates cell migration and invasion

Grb2-mediated control of FGFR2 activity is critical in maintaining cellular homeostasis under basal non-stimulated conditions. This is achieved by the formation of a heterotetrameric complex through Grb2CSH3 interactions (2). Nonetheless the modest affinity of this complex leaves it vulnerable to competing SH3 domain binding. Thus, under appropriate cellular conditions Plcγ1 replaces Grb2 on FGFR2. The lipase in this case becomes constitutively active leading to the depletion of PIP_2 and a surge in intracellular calcium level (59).

This concept is of great significance since it proposes a mechanism for a phosphorylation-independent control of cell membrane constituency and calcium flux leading to the phenotypic response of increased cell motility, which has the potential to lead to metastasis in cancer cells.

In order to establish the solid connection between the intracellular balance between Grb2 and Plcγ1 and metastasis, Ci, G2i and Pγi cells (containing a luciferase vector to monitor metastasis via imaging and MRI) need to be injected in an animal model (like nude mice). In this case, it is possible that G2i cells will show a higher level of metastatic potential compared to Ci cells. If Plcγ1 is indeed responsible for the metastatic outcome then knocking it down will inhibit the metastatic process.

Thus, dependence of this phenotype on the relative intracellular concentrations of Grb2 and Plcγ1 in a FGFR2 background suggests that the expression levels

of these proteins could provide reliable markers for metastatic outcome in patients. This is critical when studying and testing drugs that aim at targeting Grb2 (80-87) since the factor of Grb2/Plcγ1/FGFR2 concentration should be taken into consideration or else the metastatic potential of the primary tumor will be enhanced by shifting the balance towards Plcγ1 and allowing for its constitutive binding to FGFR2 and the consequent uncontrollable up-regulation of its activity.

Also, since Grb2 in this case is acting as a controlling factor that to some extent reduces cell migration and invasion, then manipulating its level of expression can potentially be of great significance in inhibiting metastasis. This rationale can be employed in performing a database search to further investigate the Grb2 specific micro RNAs (miRNA) and their role in silencing Grb2 gene expression.

Prospective candidates and specifically in ovarian cancer can be considered oncogenic and targeting them in cell lines to begin with can open the door for the investigation of a novel therapeutic cancer type dependent anti-metastatic agent.

PTEN-mediated activation of Akt is dictated by Grb2 expression levels

It appears that through the resultant perturbation of the phospholipid constitution of the plasma membrane, depletion of Grb2 has an oncogenic outcome. In this work we investigate the combined effects of enzyme-regulated concentrations of PIP_2 and PIP_3 on Akt signal transduction and demonstrate that these can be directly linked to cellular Grb2 concentration.

Thus, this work provides a novel entrée in understanding the conditions triggering an anomalous Akt response. This provides groundwork for future studies in animal models to show that fluctuating the concentration of Grb2 SH3 domain instead of full length protein (as shown in this work) can control for Plcγ1-FGFR2 association and the subsequent effect on PIP_2 level. This can be the basis of therapeutic agents that mitigate the aberrant Akt oncogenic signaling pathway that drives many cancers, and can become an alternative or adjunctive (secondary) approach to the use of numerous kinase inhibitors, many of which are toxic, and can be highly non-specific when used to dampen the aberrant hyperactivation of Akt. It can also be exploited as a diagnostic tool especially that it is becoming more crucial to develop methods to identify those patients with tumors driven by Akt-based molecular abnormalities (88,89) or when other means of Akt pathway inhibition can be used to enhance the effect of radiation or traditional chemotherapeutic drugs (90-95).

Taken together, the current findings offer a novel concept namely:“The role of SH3 domains competition in tumor development and metastasis” that has the potential to become the foundation of several intervention strategies in PTEN-mediated disease treatment modalities like the pharmacotherapy of cancer.

Bibliography

1. Turner, N., & Grose, R. Fibroblast growth factor signalling: from development to cancer. *Nat Rev Cancer* **10**, 116-129 (2010).

2. Lin, C.-C., Melo, F.A., Ghosh, R., Suen, K.M., Stagg, L.J., Kirkpatrick, J., Arold, S.T., Ahmed, Z. & Ladbury, J.E. Inhibition of basal FGF receptor signaling by dimeric Grb2. *Cell* **149**, 1514-1524 (2012).

3. Ahmed, Z., George, R., Lin, C.-C., Suen, K.M., Levitt, J.A., Suhling, K. & Ladbury, J.E. Direct binding of Grb2 SH3 domain to FGFR2 regulates SHP2 function. *Cell Signal*.**22**, 23–33 (2010).

4. Greenman, C., Stephens, P., Smith, R., Dalgliesh, G. L., Hunter, C., Bignell, G., ...& Cole, J. Patterns of somatic mutation in human cancer genomes. *Nature* **446***,* 153-158 (2007).

5. Dutt, A., Salvesen, H.B., Chen, T.H., Ramos, A.H., Onofrio, R.C., Hatton, C., Nicoletti, R., Winckler, W., Grewal, R., Hanna, M., Wyhs, N., Ziaugra, L., Richter ,D.J., Trovik, J., Engelsen, I.B., Stefansson, I.M., Fennell, T., Cibulskis, K., Zody ,M.C., Akslen, L.A., Gabriel, S., Wong, K.K., Sellers, W.R,, Meyerson,

M.&Greulich, H. Drug-sensitive FGFR2 mutations in endometrial carcinoma." *Proc Natl Acad Sci.* **105**, 8713-8717 (2008).

6. Gartside, M.G., Chen, H., Ibrahimi, O.A., Byron, S.A., Curtis, A.V., Wellens, C.L., Bengston, A., Yudt, L.M., Eliseenkova, A.V., J. Ma., Curtin, J.A., Hyder, P., Harper, U.L., Riedesel ,E., Mann, G.J., Trent ,J.M., Bastian, B.C., Meltzer, P.S., Mohammadi, M.& Pollock ,P.M. Loss-of-function fibroblast growth factor receptor-2 mutations in melanoma. *Mol. Cancer Res*. **7**, 41–54 (2009).

7. Cha, J. Y., Lambert, Q. T., Reuther, G. W. & Der, C. J. Involvement of fibroblast growth factor receptor 2 isoform switching in mammary oncogenesis. *Mol. Cancer Res*. **6**, 435-445 (2008).

8. Cha, J.Y., Maddileti, S., Mitin, N., Harden, T.K. & Der, C.J. Aberrant receptor internalization and enhanced FRS2-dependent signaling contribute to transforming activity of the fibroblast growth factor receptor 2 IIIb C3 isoform. *J. Biol. Chem*. **284**, 6227–6240 (2009).

9. Hattori, Y., Itoh, H., Uchino, S., Hosokawa, K., Ochiai, A., Ino, Y., Ishii, H., Sakamoto, H., Yamaguchi, N., Yanagihara, K., Hirohashi, S., Sugimura, T. & Terada, M. Immunohistochemical detection of K-sam protein in stomach cancer. Clin.*Cancer Res*. **2***,* 1373-1381 (1996).

10. Itoh, H., Hattori, Y., Sakamoto, H., Ishii, H., Kishi, T., Sasaki, H., Yoshida, T., Koono, M., Sugimuro,T. & Terada, M. Preferential alternative splicing in cancer generates a K-sam messenger RNA with higher transforming activity. *Cancer Res*. **54**, 3237-3241 (1994).

11. Ishii, H., Yoshida, T., Oh, H., Yoshida, S. & Terada, M. A truncated K-sam product lacking the distal carboxyl-terminal portion provides a reduced level of autophosphorylation and greater resistance against induction of differentiation. *Mol. Cell. Biol.***15**, 3664–3671 (1995).

12. Katoh, M. Cancer genomics and genetics of FGFR2 (Review). *IntI Oncol*.**33**, 233-237 (2008).

13.Li, N., Batzer, A., Daly, R., Yajnik, V., Skolnik, E., Chardin, P., Bar-Sagi,D., Margolis, B. &Schlessinger, J. Guanine-nucleotide-releasingfactor hSos1 binds to Grb2 and links receptor tyrosine kinases to Rassignalling. *Nature* **363**, 85-88 (1993).

14. Serrano, C.J., Graham, L., DeBell, K., Rawat, R., Veri, M.C., Bonvini, E., Rellahan, B.L. & Reischl, I.G. A new tyrosine phosphorylation site in PLCγ1: the role of tyrosine 775 in immune receptor signaling. *J. Immunol*. **174**, 6233-6237 (2005).

15. Gresset, A., Hicks, S.N., Harden, T.K. & Sondek, J. Mechanism of phosphorylation-induced activation of phospholipase C-gamma isozymes. *J. Biol. Chem*. **285**, 35836–35847 (2010).

16. Steeg, P.S. Metastasis suppressors alter the signal transduction of cancer cells. *Nat Rev Cancer.* **3**, 55-63 (2003).

17. Sala, G., Dituri, F., Raimondi, C., Previdi, S., Maffucci, T., Mazzoletti, M., Rossi, C., Iezzi, M., Lattanzio, R., Piantelli, M., Iacobelli, S., Broggini, M. & Falasca, M. Phospholipase Cγ1 is required for metastasis development and progression. *Cancer Res.* **68**, 10187-10196 (2008).

18. Redfern, R. E., Redfern, D., Furgason, M. L., Munson, M., Ross, A. H., & Gericke, A. (2008). PTEN phosphatase selectively binds phosphoinositides and undergoes structural changes. *Biochemistry*, **47**, 2162-2171 (2008).

19.Iijima, M., Huang, Y. E., Luo, H. R., Vazquez, F., & Devreotes, P. N. Novel mechanism of PTEN regulation by its phosphatidylinositol 4, 5-bisphosphate binding motif is critical for chemotaxis. *J Biol Chem. **279***, 16606-16613 (2004).

20.Song, M. S., Salmena, L., & Pandolfi, P. P. (2012). The functions and regulation of the PTEN tumour suppressor.*NatRevMolCell Biol*.**13**, 283-296 (2012).

21. Nakanishi, K., Sakamoto, M., Yasuda, J., Takamura, M., Fujita, N., Tsuruo, T., Todo, S.&Hirohashi, S.Critical involvement of the phosphatidylinositol 3-kinase/Akt pathway in anchorage-independent growth and hematogeneous intrahepatic metastasis of liver cancer. *Cancer Res*.**62**, 2971-2975 (2002).

22. Vivanco, I., & Sawyers, C. L. The phosphatidylinositol 3-kinase–AKT pathway in human cancer.*Nat Rev Cancer*, ***2***, 489-501 (2002).

23. Ahmed, Z., Lin, C.-C., Suen, K.M., Melo, F.A., Levitt, J.A., Suhling, K. & Ladbury, J.E. Grb2 controls phosphorylation of FGFR2 by inhibiting receptor kinase and Shp2 phosphatase activity. *J. Cell. Biol*. **200**, 493-504 (2013).

24. Peters, K.G., Marie, J., Wilson, E., Ives, H.E., Escobedo, J., Del Rosario, M., Mirda, M. & Williams, L.T. Point mutation of an FGF receptor abolishes phosphatidylinositol turnover and Ca^{2+} flux but not mitogenesis. *Nature***358**, 678-681 (1992).

25. Mohammadi, M., Honegger, A.M., Rotin, D., Fischer, R., Bellot, F., Li, W., Dionne, C.A., Jaye, M., Rubinstein, M. & Schlessinger, J. A tyrosine-phosphorylated carboxy-terminal peptide of the fibroblast growth factor receptor (Flg) is a binding site for the SH2 domain of phospholipase C-gamma 1. *Mol. Cell. Biol*. **11**, 5068-5078 (1991).

26. Bae, J. H., Lew, E. D., Yuzawa, S., Tomé, F., Lax, I. & Schlessinger, J. The selectivity of receptor tyrosine kinase signaling is controlled by a secondary SH2 domain binding site. *Cell* **138**, 514-524 (2009).

27. Kim, H.K., Kim, J.W., Zilberstein, A., Margolis, B., Kim, C.K., Schlessinger, J. & Rhee, S.G. PDGF stimulation of inositol phospholipd hydrolysis requires PLC-g phosphorylation on resides 783 and 1254. *Cell* **65***, 435*–441 (1991).

28. Braiman, A., Barda-Saad, M., Sommers, C. L., & Samelson, L. E. Recruitment and activation of PLCγ1 in T cells: a new insight into old domains. *EMBO J.**25***, 774-784 (2006).

29. Harden, T.K. & Sondek, J. Regulation of phospholipase C isozymes by ras superfamily GTPases. *Annu. Rev. Pharmacol. Toxicol*. **46**, 355-379 (2006).

30. Hicks, S.N., Jezyk, M.R., Gershburg, S., Seifert, J.P., Harden, T.K. & Sondek, J. General and versatile autoinhibition of PLC isozymes. *Mol. Cell*.**31**, 383-394 (2008).

31. Bunney, T.D., Esposito, D., Mas-Droux, C., Lamber, E., Baxendale, R.W., Martins, M., Cole, A., Svergun, D., Driscoll, P.C. & Katan, M. Structural and functional integration of the PLCγ interaction domains critical for regulatory mechanisms and signaling deregulation. *Structure***20**, 2062–2075 (2012).

32. Falasca, M., Logan, S.K., Lehto, V.P., Baccante, G., Lemmon, M.A. & Schlessinger, J. Activation of phospholipase Cγ by PI 3-kinase-induced PH domain-mediated membrane targeting. *EMBO J*. **17***,* 414-422 (1998).

33. Rhee, S.G. Inositol phospholipids-specific phospholipase C: interaction of the gamma 1 isoform with tyrosine kinase. *Trends Biochem.Sci*. **16**, 297-301 (1991).

34. Rellahan, B. L., Graham, L. J., Tysgankov, A. Y., DeBell, K. E., Veri, M. C., Noviello, C., & Bonvini, E. A dynamic constitutive and inducible binding of c-Cbl by PLCγ1 SH3 and SH2 domains (negatively) regulates antigen receptor-induced PLCγ1 activation in lymphocytes. *ExpCell Res.* **289**, 184-194 (2003).

35. Mouneimne, G., Soon, L., DesMarais, V., Sidani, M., Song, X., Yip, S.C., Ghosh, M. Eddy, R., Backer, J.M.& Condeelis, J. Phospholipase C and cofilin are required for carcinoma cell directionality in response to EGF stimulation.*J Cell Biol*.**166**, 697-708 (2004).

36. van Rheenen, J., Song, X., van Roosmalen, W., Cammer, M., Chen, X., Desmarais, V., Yip, S.C., Backer, J.M., Eddy, R.J.& Condeelis ,J.S. EGF-induced PIP2 hydrolysis releases and activates cofilin locally in carcinoma cells. *J Cell Biol*.**179**, 1247-1259 (2007).

37. Rebecchi, M.J. & Pentyala, S.N. Structure, function and control of phosphoinositide-specific phospholipase C. *Physiol. Rev.***80**, 1291-1335 (2000).

38. Rhee, S.G. Regulation of phosphoinositide-specific phospholipase C. *Annu. Rev. Biochem.* **70**, 281-312 (2001).

39. Kölsch, V., Charest, P.G. & Firtel, R.A. The regulation of cell motility and chemotaxis by phospholipid signaling. *J. Cell. Sci*.**121**, 551-559 (2008).

40. Hao, J. J., Liu, Y., Kruhlak, M., Debell, K. E., Rellahan, B. L. & Shaw, S. Phospholipase C–mediated hydrolysis of PIP2 releases ERM proteins from lymphocyte membrane. *J. Cell. Biol*. **184**, 451-462 (2009).

41. Lymn, J.S. & Hughes A.D. Phospholipase C Isoforms, Cytoskeletal organization, and vascular smooth muscle differentiation. *News Physiol. Sci.***15**, 41-45 (2000).

42.Logan, M. R., & Mandato, C. A. Regulation of the actin cytoskeleton by PIP2 in cytokinesis. *Biol Cell*. **98**, 377-388 (2006).

43. Chilvers, E.R., Batty, I.H., Challiss, R.A., Barnes, P.J. & Nahorski, S.R. Determination of mass changes in phosphatidylinositol 4, 5-bisphosphate and evidence for agonist-stimulated metabolism of inositol 1, 4, 5-trisphosphate in airway smooth muscle. *Biochem. J.* **275**, 373-379 (1991).

44. Bligh, E.G. & Dyer, W.J. A rapid method of total lipid extraction and purification.*Can. J. Biochem.Physiol*. **379**, 11-917 (1959).

45. König, S., Hoffmann, M., Mosblech, A. & Heilmann, I. Determination of content and fatty acid composition of unlabeled phosphoinositide species by thin-layer chromatography and gas chromatography. *Anal.Biochem*. **378**, 197-201 (2008).

46. Jin, M., Wu, Z., Chen, L., Jaimes, J., Collins, D., Walters, E.T. & O'Neil, R.G. Determinants of TRPV4 activity following selective activation by small molecule agonist GSK1016790A. *PloS one*. **6***,* e16713 (2011).

47. Berrout, J., Jin, M., Mamenko, M., Zaika, O., Pochynyuk, O. & O'Neil, R.G. Function of transient receptor potential cation channel subfamily V member 4 (TRPV4) as a mechanical transducer in flow-sensitive segments of renal collecting duct system. *J. Biol. Chem*. **287**, 8782-8791 (2012).

48. Tothill, R.W., Tinker, A.V., George, J., Brown, R., Fox, S.B., Lade, S., Johnson, D.S., Trivett, M.K., Etemadmoghadam. D., Locandro. B., Traficante. N., Fereday, S., Hung, J.A., Chiew, Y.E., Haviv, I.; Australian Ovarian Cancer Study Group, Gertig, D., DeFazio, A. & Bowtell, D.D. Novel molecular subtypes of serous and endometrioid ovarian cancer linked to clinical outcome. *Clin Cancer Res.* **14**, 5198-5208 (2008).

49. Carloni, V., Romanelli, R.G., Pinzani, M., Laffi, G. & Gentilini, P.Focal adhesion kinase and phospholipase C gamma involvement in adhesion and migration of human hepatic stellate cells. *Gastroenterology* **112**, 522-531 (1997).

50. Thapa, N. & Anderson, R.A. PIP_2 signaling, an integrator of cell polarity and vesicle trafficking in directionally migrating cells. *Cell. Adh. Migr*.**6**, 409-412 (2012).

51. Matsuda, Y., Ishiwata, T., Yamahatsu, K., Kawahara, K., Hagio, M., Peng, W. –X. Yamamoto, T., Nakazawa, N., Seya, T., Ohaki, Y. & Naito, Z. Overexpressed fibroblast growth factor receptor 2 in the invasive front of colorectal cancer: a potential therapeutic target in colorectal cancer. *Cancer Lett*. **309**, 209-219 (2011).

52. Vanhaesebroeck, B., Leevers, S. J., Ahmadi, K., Timms, J., Katso, R., Driscoll, P. C., Woscholski, R., Parker, P.J & Waterfield, M. D.Synthesis and function of 3-phosphorylated inositol lipids. *Annu Rev Biochem.***70**, 535-602 (2001).

53.Tzenaki, N., Andreou, M., Stratigi, K., Vergetaki, A., Makrigiannakis, A., Vanhaesebroeck, B., &Papakonstanti, E.A.High levels of p110 PI3K expression in solid tumor cells suppress PTEN activity, generating cellular sensitivity to p110 inhibitors through PTEN activation. *FASEB J*. **26**, 2498-24508 (2012).

54. Downes, C. P., Leslie, N. R., Batty, I. H., & van der Kaay, J. Metabolic switching of PI3K-dependent lipid signals. *Biochem Soc Trans*.**35**, 188 (2007).

55. Li, J., Yen, C., Liaw, D., Podsypanina, K., Bose, S., Wang, S. I., Puc, J., Miliaresis, C., Rodgers, L., McCombie, R., Bigner, S.H., Giovanella, B.C., Ittmann, M., Tycko, B., Hibshoosh, H., Wigler, M.H.,& Parsons, R. PTEN, a

putative protein tyrosine phosphatase gene mutated in human brain, breast, and prostate cancer.*Science*, **275**, 1943-1947 (1997).

56. McConnachie G, Pass I, Walker SM, Downes CP. Interfacialkinetic analysis of the tumour suppressor phosphatase, PTEN: evidence for activation by anionic phospholipids. *Biochem J*. **371**, 947–955 (2003).

57.Leslie, N. R., Batty, I. H., Maccario, H., Davidson, L., & Downes, C. P. Understanding PTEN regulation: PIP2, polarity and protein stability. *Oncogene*, **27**, 5464-5476 (2008).

58. Vazquez, F., Ramaswamy, S., Nakamura, N., & Sellers, W. R. Phosphorylation of the PTEN tail regulates protein stability and function. *MolCell Biol*, **20**, 5010-5018 (2000).

59. Timsah, Z., Ahmed, Z., Lin, C.-C., Melo, F.A., Stagg, L.J., Leonard, P.G., Jeyabal, P., Berrout, J., O'Neil, R.G., Bogdanov, M& Ladbury, J.E. Competition between Grb2 and Plcγ1 for binding to FGFR2 regulates constitutive phospholipase activity and invasive response. *Nat Struc Mol Biol*, (In press)

60. Everett, K. L., Buehler, A., Bunney, T. D., Margineanu, A., Baxendale, R. W., Vatter, P., Retlich, M., Walliser, C., Manning, H. B., Neil, M. A. A., Dunsby, C., French, P. M. W., Gierschik, P. & Katan, M. Membrane environment exerts

an important influence on Rac-mediated activation of phospholipase Cγ2. *Mol. Cell. Biol.* **31**, 1240-1251 (2011).

61. Piechulek, T., Rehlen, T., Walliser, C., Vatter, P., Moepps, B. & Gierschik, P. Isozyme-specific stimulation of phospholipase C-γ2 by Rac GTPases. *J. Biol. Chem.* **280**, 38923-38931 (2005).

62. Sekiya, F., Poulin, B., Kim, Y. J. & Rhee, S. G. Mechanism of tyrosine phosphorylation and activation of phospholipase C-γ2. *J. Biol. Chem.* **279**, 32181-32190 (2004).

63. Walliser, C., Retlich, M., Harris, R., Everett, K. L., Josephs, M. B., Vatter, P., Esposito, D., Driscoll, P. C., Katan, M., Gierschik, P. & Bunney, T. D. Rac regulates its effector phospholipase Cγ2 through interaction with a split pleckstrin homology domain. *J. Biol. Chem.* **283**, 30351-30362 (2008).

64. Bunney, T. D., Opaleye, O., Roe, M. S., Vatter, P., Baxendale, R. W., Walliser, C., Everett, K. L., Josephs, M. B., Christow, C., Rodrigues-Lima, F., Gierschik, P., Pearl, L. H. & Katan, M. Structural insights into formation of an active signaling complex between Rac and phospholipase C gamma 2. *Mol. Cell* **34**, 223-233 (2009).

65. Halupa, A., Chohan, M., Stickle, N. H., Beattie, B. K., Miller, B. A. & Barber, D. L. Erythropoietin receptor Y479 couples to ERK1/2 activation via recruitment of phospholipase Cγ. *Exp. Cell Res*. **309,** 1-11 (2005).

66. Yu, H., Kiyoko, F., Toshiki, I. & Tadaomi, T. Phosphorylation of phospholipase Cγ1 on tyrosine residue 783 by platelet-derived growth factor regulates reorganization of the cytoskeleton. *Exp. Cell. Res*. **243**, 113-122 (1998).

67. Browaeys-poly, E., Broutin, I., Antoine, A. –F. Marin, M., Lescuyer, A., Vilain, J. P., Ducruix, A. Cailliau, K. A non-canonical Grb2-Plc-γ1-Sos cascade triggered by lipovitellin 1, an apolipoprotein B homologue. *Cell. Signal*. **19**, 2540-2548 (2007).

68. DeMali, K.A., Whiteford, C.C., Ulug, E.T. & Kazlauskas, A. Platelet-derived growth factor-dependent cellular transformation requires either phospholipase C gamma or phosphatidylinositol 3 kinase. *J. Biol. Chem*. **272**, 9011–9018 (1997).

69. Smith, M. R., Kim, H. K., Park, J. B., Rhee, S. G., Rhim, J. S. & Kung, H. F. Overexpression of phosphoinositide-specific phospholipase C gamma in NIH 3T3 cells promotes transformation and tumorigenicity. *Carcinogenesis* **19**, 177-185 (1998).

70. Nomoto, K., Tomito, N., Miyake, M., Xhu, D-. B., Logerfo, P.R. & Weinstein, I.B. Expression of phospholipases γ1, β1, and δ1 in primary human colon carcinomas and colon carcinoma cell lines. *Mol. Carcinog*. **12**, 146-152 (1995).

71. Arteaga, C.L., Johnson, M.D., Todderud, G., Coffey, R.J., Carpenter, G. & Page, D.L. Elevated content of the tyrosine kinase substratephoapholipase C-g1 in primary human breast carcinomas. *Proc. Natl. Acad. Sci. USA***88**, 10435-10439 (1991).

72. Soderquist, A.M., Todderud, G. & Carpenter, G. Elevated membrane association of phospholipase C-gamma 1 in MDA-468 mammary tumor cells. *Cancer Res.* **52***,* 4526-4529 (1992).

73. Zhu, X., Asa, S. L. & Ezzat, S. Genetic and epigenetic mechanisms down-regulate FGF receptor 2 to induce melanoma-associated antigen A in breast cancer. *Am. J. Pathol*. **176**, 2333-2343 (2010).

74. Rahdar, M., Inoue, T., Meyer, T., Zhang, J., Vazquez, F., & Devreotes, P. N. A phosphorylation-dependent intramolecular interaction regulates the membrane association and activity of the tumor suppressor PTEN. *Proc Natl Acad Sci.***106**, 480-485 (2009).

75. Campbell, R. B., Liu, F., & Ross, A. H. Allosteric activation of PTEN phosphatase by phosphatidylinositol 4, 5-bisphosphate. *J Biol Chem.* **278**, 33617-33620 (2003).

76. Chalhoub, N., & Baker, S. J. PTEN and the PI3-kinase pathway in cancer. *Annu Rev Pathol*, **4**, 127-150 (2009).

77.Vazquez, F. & Devreotes, P. Regulation of PTEN function as a PIP3 gatekeeper through membrane interaction. *Cell Cycle***5**, 1523–1527 (2006).

78.Minaguchi, T., Yoshikawa, H., Oda, K., Ishino, T., Yasugi, T., Onda, T., Nakagawa, S., Matsumoto, K., Kawana, K. &Taketani, Y.PTEN mutation located only outsideexons 5, 6, and 7 is an independent predictor of favorable survival in endometrial carcinomas. *Clin.CancerRes*. **7**, 2636–2642 (2001).

79. Gronbaek, K., Zeuthen, J., Guldberg, P., Ralfkiaer, E. & Hou-Jensen, K. Alterations of theMMAC1/PTEN gene in lymphoid malignancies. *Blood***91**, 4388–4390 (1998).

80. Chen, C.-H., Chen, M.-K., Jeng, K.-C. & Lung F.-D.Effects of peptidic antagonists of Grb2-SH2 on human breast cancer cells.*Protein Pept Lett*.**71**,132-140 (2010).

81. Lung, F.-D., Chang, C.-W., Chong, M.-C., Liou, C.-C., Li, P., Peach, M.L., Nicklaus, M.C., Lou, B.-S. & Roller, P.P.Small nonphosphorylated Grb2-SH2 domain antagonists evaluated by surface plasmon resonance technology.*Cancer Res*.**67**, 6012-6016 (2007).

82. Lung, F.-D. & Tsai, J.-Y.Grb2 SH2 domain-binding peptide analogs as potential anticancer agents.*Biopolymers***80**, 628-635 (2005).

83.Giubellino, A., Gao, Y., Lee, S., Lee, M.-J, Vasselli, J.R., Medepalli, S., Trepel, J.B., Burke, T.R Jr. & Bottaro, D.P. Inhibition of tumor metastasis by a growth factor receptor bound protein 2 Src homology 2 domain-binding antagonist.*Expert Opin Ther Targets.***12**,1021-1033 (2007).

84. Giubellino, A., Burke, T.R Jr. & Bottaro, D.P. Grb2 signaling in cell motility and cancer.*J Med Chem.***9**,1585-1596 (2008).

85.Song, Y.-L., Peach, M.L., Roller, P.P., Qiu, S., Wang, S. & Long, Y.-Q. Discovery of a novel nonphosphorylated pentapeptide motif displaying high affinity for Grb2-SH2 domain by the utilization of 3'-substituted tyrosine derivatives.J Med Chem. 9, 1585-1596 (2006).

86.Atabey, N., Gao, Y., Yao, Z.-J., Breckenridge, D., Soon, L., Soriano. J.V., Burke, T.R Jr. & Bottaro D.P.Potent blockade of hepatocyte growth factor-stimulated cell motility, matrix invasion and branching morphogenesis by antagonists of Grb2 Src homology 2 domain interactions.*J Biol Chem*. **27**, 14308-14314 (2001).

87.Dharmawardana, P.G., Peruzzi, B., Giubellino, A., Burke, T.R Jr. & Bottaro ,D.P .Molecular targeting of growth factor receptor-bound 2 (Grb2) as an anti-cancer strategy.*Anticancer Drugs***17**,13-20 (2006).

88. Hennessy, B. T., Smith, D. L., Ram, P. T., Lu, Y., & Mills, G. B. Exploiting the PI3K/AKT pathway for cancer drug discovery. *Nat RevDrug Discov.***4**, 988-1004 (2005).

89. Vara, J. Á. F., Casado, E., de Castro, J., Cejas, P., Belda-Iniesta, C., & González-Barón, M. PI3K/Akt signalling pathway and cancer. *Cancer TreatRev.***30**, 193-204 (2004).

90. Hu, L., Hofmann, J., Lu, Y., Mills, G.B. &Jaffe, R.B. Inhibition ofphosphatidylinositol 3-kinase increases efficacy of paclitaxelin *in vitro* and *in vivo* ovarian cancer models. *CancerRes*.**62**, 1087–1092 (2002).

91.Ng, S.S., Tsao, M.S., Chow, S. & Hedley, D.W. Inhibition ofphosphatidylinositide 3-kinase enhances gemcitabine-inducedapoptosis in human pancreatic cancer cells. *CancerRes*. **60**, 5451–5455 (2000).

92.Rosenzweig, K.E., Youmell, M.B., Palayoor, S.T. & Price, B.D. Radiosensitizationof human tumor cells by the phosphatidylinositol-3-kinase inhibitors wortmannin and LY294002correlates with inhibition of DNA-dependent protein kinaseand prolonged G2-M delay. *Clin Cancer Res*.**3**,1149–1156 (1997).

93. Sarkaria, J. N., Tibbetts, R. S., Busby, E. C., Kennedy, A. P., Hill, D. E., & Abraham, R. T. Inhibition of phosphoinositide 3-kinase related kinases by the radiosensitizing agent wortmannin. *Cancer Res.***58**, 4375-4382 (1998).

94. Kim, S. H., Um, J. H., Kim, D. W., Kwon, B. H., Kim, D. W., Chung, B. S., & Kang, C. D. Potentiation of chemosensitivity in multidrug-resistant human leukemia CEM cells by inhibition of DNA-dependent protein kinase using wortmannin. *Leuk Res*.**24**, 917-925 (2000).

95. Wang, Q., Li, N., Wang, X., Kim, M.M. & Evers, B.M. Augmentation of sodium butyrate-induced apoptosis by phosphatidylinositol 3'-kinase inhibition in the KM20 human colon cancer cell line. *Clin Cancer Res*.**8**, 1940-1947

Vita

Zahra Timsah was born in Tyr, Lebanon on October 4, 1986. Upon graduating from Al-Mayadeen High School, she pursued her bachelor degree in biology at the American University of Beirut (AUB). After receiving her B.S. degree she enrolled at the Lebanese American University (LAU) for her Masters degree in advanced molecular biology where she also worked as a researcher and lab instructor. In 2010, she enrolled at the University of Texas Health Science Center at Houston – School of Biomedical Sciences (GSBS) for her PhD in cancer biology where she joined the lab of Dr. John E. Ladbury to study the effects of Grb2 on early signaling, its potential competition with other proteins and the effects on cellular function.